Water Quality and Hydrodynamic Modeling of Tenkiller Reservoir

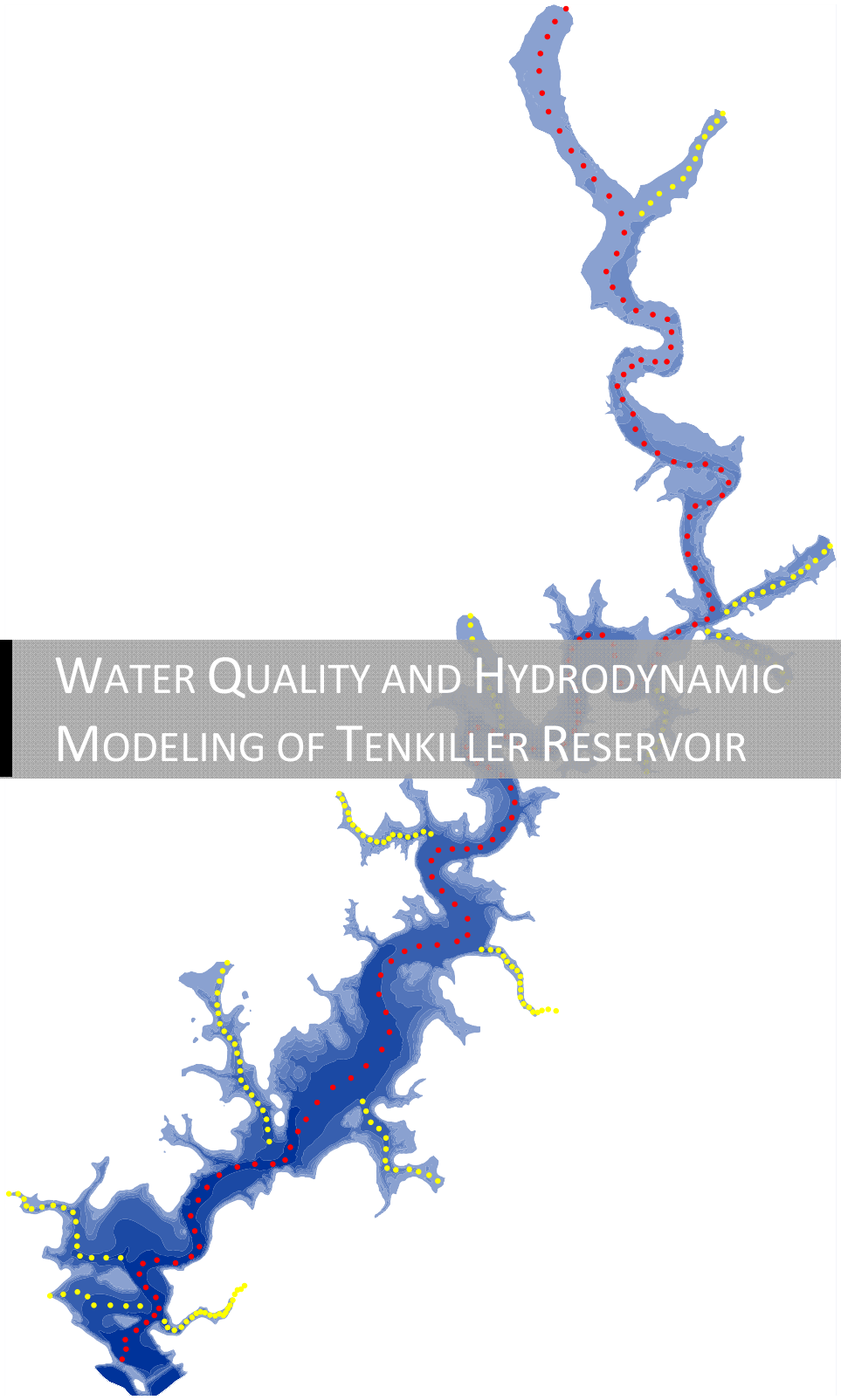

Prepared for the State of Oklahoma | S. Wells, V. Wells, and C. Berger

Water Quality and Hydrodynamic Modeling of Tenkiller Reservoir

Expert Report of S. A. Wells

V. I. Wells

and

C. J. Berger

for

State of Oklahoma

in

Case No. 05-CU-329-GKF-SAJ

State of Oklahoma v. Tyson Foods, et al.

(In the United States District Court for the Northern District of Oklahoma)

Digitally signed by Scott Wells
DN: cn=Scott Wells, o, ou, email=drswells@comcast.net, c=US
Date: 2008.05.29 23:55:15 +03'00'

May 2008

Scott Wells, PhD, PE
Professor of Civil and Environmental Engineering

Table of Contents

Table of Contents ii

List of Figures iv

List of Tables xi

Introduction 1

Previous Modeling Studies 2

Model Selection 3

Model Set-Up 8

Model Geometry 9

Bathymetry 9

Model Grid Development 10

Tenkiller Reservoir Dam and Outlet Hydraulics 15

Upstream Boundary Conditions 17

Illinois River Inflow 17

Flow 17

Temperature 18

Water Quality 20

Baron Fork Inflow 28

Flow 28

Temperature 29

Water Quality 30

Caney Creek Inflow 36

Flow 36

Temperature 37

Water Quality 38

Other Tributaries 43

Flow 43

Temperature 44

Water Quality 44

Reservoir Water Level 44

Downstream Boundary Conditions 45

Meteorological Data 45

Air and Dew Point Temperature 46

Wind Speed and Direction 52

Solar Radiation comparison between Cookson and Tulsa 54

Model Calibration 57

Water Level Calibration 58

Temperature Calibration 60

Water Quality Calibration 65

Dissolved Oxygen 73
Total Nitrogen 78
Ammonia 81
Nitrate and Nitrite 85
Total Phosphorus 93
Dissolved Ortho Phosphorus 99
Chlorophyll a 107
Light Extinction/Secchi Disk Depth 112

Analysis of Model Calibration *114*

Model Set-up for Long-term Simulation *120*

Upstream Boundary Conditions 120

Illinois River Inflow 120
Flow 120
Temperature 121
Water Quality 124
Baron Fork Inflow 126
Flow 126
Temperature 126
Water Quality 127
Caney Creek Inflow 128
Flow 128
Temperature 129
Water Quality 129
Other Tributaries 131
Flow 131
Temperature 131
Water Quality 132

Reservoir Water Level 132

Downstream Boundary Conditions 136

Meteorological Data 137

Water Quality Management Scenarios *138*

Model Scenarios 138

Estimating sediment oxygen demand reduction over time for zero order sediment model 140
Testing of 50-year model 145

Model Scenario Results 146

Surface Volume Weighted Averages 147
Time Series of Summer Surface Volume Weighted Averages 147
Frequency Distributions of Surface Volume Weighted Concentrations 156
Summary of Total P and chlorophyll a for summer volume weighted averages 161
Dissolved oxygen concentration in release from Tenkiller Reservoir 164

Dissolved Oxygen Dynamics 168
Dissolved oxygen demand from sediments 168
Dissolved oxygen water column demand from organic matter decomposition 169
Dissolved oxygen net photosynthetic production 170
Fish Habitat 171
Total P loading, export, and sediment recycling 178
Inflows 178
Outflows 181
Sediment P Flux 184

***Summary and Conclusions* 185**

Model Choice 185

Model Set Up 185

Model Calibration 186

Model Scenarios 187

***References* 193**

***Appendix A: Bathymetry in Tenkiller Reservoir* 196**

Approach 1: Sonar Elevation Data and Contour Lines – Variable Correction Factor 196

Approach 2: Sonar Elevation Data and Contour Lines - Consistent Correction factor 199

Processing of Corrected Sonar Elevation Data and Contour Line Elevation Data 200

Comparison of Approaches 1 and 2 200

***Appendix B: Estimating inflow temperatures based on meteorological conditions* 202**

The equilibrium temperature 202

The filtered equilibrium temperature 204

***Appendix C: Error statistics* 206**

***Appendix D: Temperature Profile Comparisons* 207**

***Appendix E: Dissolved Oxygen Profile Comparisons* 216**

***Appendix F: Chlorophyll a Profile Comparisons* 224**

***Appendix G: Appropriateness of Model Calibration* 232**

List of Figures

Figure 1. Model-data comparison for dissolved oxygen in forebay of Tenkiller reservoir for 1992-1993 EFDC model calibration (Craig, 2004)..... 2

Figure 2. CE-QUAL-W2 model predictions for Lake Roosevelt, WA, for temperature as a function of depth and longitudinal distance in km from the Canadian border on July 31, 2000. 4
Figure 3. Coordinate system for CE-QUAL-W2 Version 3.6. 5
Figure 4. Conceptual schematic of river-reservoir connection in CE-QUAL-W2 Version 3. 7
Figure 5. 3-D view of Tenkiller Reservoir model bathymetry. 9
Figure 6. Top view of the Tenkiller Reservoir model grid and bathymetric map. 11
Figure 7. Top view of the Tenkiller Reservoir model grid. 12
Figure 8. Side view of the Tenkiller Reservoir main branch model grid. 12
Figure 9. Side view of the Tenkiller Reservoir side branches model grid. 13
Figure 10. Slice views of the Tenkiller Reservoir main branch segments 192 (left) and 200 (right)..... 13
Figure 11. Tenkiller Reservoir volume – elevation curve. 15
Figure 12. Tenkiller Reservoir area – elevation curve. 15
Figure 13. Powerhouse (left) and 10 tainter gates and powerhouse at Tenkiller dam (right)..... 16
Figure 14. New spillway and tainter gates operational in 2006. 17
Figure 15. Illinois River discharge - USGS Gage 071965000. 18
Figure 16. Illinois River water temperature during calibration period. 19
Figure 17. Comparison of measured temperature and filtered TEQ on dates/time of measurement..... 19
Figure 18. Illinois River algae groups during calibration period. 21
Figure 19. Illinois River ammonia data during calibration period. 21
Figure 20. Illinois River dissolved oxygen during calibration period. 22
Figure 21. ISS and total phosphorus regression. 23
Figure 22. Illinois River estimated ISS during calibration period. 24
Figure 23. Illinois River organic fractions during calibration period. 25
Figure 24. Illinois River nitrate + nitrite concentration during calibration period. 26
Figure 25. Illinois River ortho phosphorus concentrations during calibration period. 27
Figure 26. Baron Fork Creek discharge - USGS Gage 07197000. 28
Figure 27. Baron Fork Creek water temperature during calibration period 29
Figure 28. Baron Fork algae groups during calibration period. 30
Figure 29. Baron Fork Creek dissolved oxygen during calibration period. 31
Figure 30. Baron Fork Creek estimated ISS during calibration period. 32
Figure 31. Illinois River organic fractions during calibration period. 33
Figure 32. Baron Fork Creek nitrate + nitrite concentration during calibration period. 34
Figure 33. Baron Fork Creek ortho phosphorus concentrations during calibration period. 35
Figure 34. Caney Creek discharge - USGS Gage 07197360. 36
Figure 35. Caney Creek water temperature during calibration period. 37
Figure 36. Caney Creek algae groups during calibration period. 38
Figure 37. Caney Creek dissolved oxygen during calibration period. 39
Figure 38. Caney Creek estimated ISS during calibration period. 40
Figure 39. Caney Creek organic fractions during calibration period. 41
Figure 40. Caney Creek nitrate + nitrite concentration during calibration period. 42
Figure 41. Caney Creek ortho phosphorus during calibration period. 42
Figure 42. Distributed tributary Inflow during calibration period. 43
Figure 43. Pool elevations at Tenkiller Dam during calibration period. 44
Figure 44. Outflows from Tenkiller Reservoir during calibration period. 45
Figure 45. Location of meteorological stations. 46
Figure 46. Air temperature at Cookson during calibration period. 47
Figure 47. Air temperature at Tulsa International Airport during calibration period. 47
Figure 48. Dew point temperature at Cookson during calibration period. 48

Figure 49. Dew point temperature at Tulsa International Airport during calibration period. 48
Figure 50. Relative humidity at Cookson during calibration period. 49
Figure 51. Relative humidity at Tulsa International Airport during calibration period..... 49
Figure 52. Tulsa vs. Cookson air temperature comparison. 50
Figure 53. Tulsa vs. Cookson dew point temperature comparison..... 50
Figure 54. Tulsa vs. Cookson relative humidity comparison. 51
Figure 55. Wind rose from Cookson during calibration period..... 52
Figure 56. Wind rose from Tulsa International Airport during calibration period..... 53
Figure 57. Cookson met data station location and wind-direction. 53
Figure 58. Comparison of daily average Cookson solar radition to computed from Tulsa cloud cover between January 1, 2005 and September 30, 2007..... 55
Figure 59. Comparison of daily average short-wave solar radiation at Cookson (measured) and Tulsa (theoretical computation based on cloud cover at Tulsa). 56
Figure 60. Calibration philosophy. 57
Figure 61. Model predicted water level compared to field data between January 1, 2005 and September 30, 2007. (Every 10th data point is shown.) 59
Figure 62. Temperature profiles of model and data for 5/18/2005..... 61
Figure 63. Temperature profiles of model and data for 6/15/2005..... 61
Figure 64. Temperature profiles of model and data for 7/12/2005..... 62
Figure 65. Temperature profiles of model and data for 8/23/2005..... 62
Figure 66. Temperature profiles of model and data for 10/4/2005..... 63
Figure 67. Sources and sinks of dissolved oxygen predicted by the model during calibration period..... 73
Figure 68. Model predictions of dissolved oxygen profiles compared to field data on 4/21/2005. 74
Figure 69. Model predictions of dissolved oxygen profiles compared to field data on 6/15/2005. 75
Figure 70. Model predictions of dissolved oxygen profiles compared to field data on 7/26/2005. 75
Figure 71. Model predictions of dissolved oxygen profiles compared to field data on 8/23/2005. 76
Figure 72. Model predictions of dissolved oxygen profiles compared to field data on 9/20/2005. 76
Figure 73. Dissolved oxygen time series - segment 89 during calibration period..... 77
Figure 74. Dissolved oxygen time series - segment 109 during calibration period..... 77
Figure 75. Total nitrogen model vs. data comparison - segment 125 during calibration period..... 78
Figure 76. Total nitrogen model vs. data comparison - segment 43 during calibration period..... 79
Figure 77. Total nitrogen model vs. data comparison - segment 46 during calibration period..... 79
Figure 78. Total nitrogen model vs. data comparison - segment 95 during calibration period..... 80
Figure 79. Total nitrogen model vs. data comparison - segment 108 during calibration period..... 80
Figure 80. Sources and sinks of ammonia predicted by the model during calibration period..... 81
Figure 81. NH_4-N concentrations predicted by the model compared to field data on 5/19/2005..... 82
Figure 82. NH_4-N concentrations predicted by the model compared to field data on 8/18/2005..... 83
Figure 83. NH_4-N concentrations predicted by the model compared to field data on 9/22/2005..... 83
Figure 84. Ammonia as nitrogen model vs. data comparison - segment 24 during calibration period. ... 84
Figure 85. Ammonia as nitrogen model vs. data comparison - segment 46 during calibration period. ... 84
Figure 86. NO_3-N concentrations predicted by the model compared to field data on 6/2/2005..... 85
Figure 87. NO_3-N concentrations predicted by the model compared to field data on 6/15/2005..... 86
Figure 88. NO_3-N concentrations predicted by the model compared to field data on 7/12/2005..... 86
Figure 89. NO_3-N concentrations predicted by the model compared to field data on 7/26/2005..... 87
Figure 90. NO_3-N concentrations predicted by the model compared to field data on 8/9/2005..... 87
Figure 91. Total nitrate + nitrite as nitrogen model vs. data comparison - segment 24 during calibration period. 88

Figure 92. Total nitrate + nitrite as nitrogen model vs. data comparison - segment 35 during calibration period. 88
Figure 93. Total nitrate + nitrite as nitrogen model vs. data comparison - segment 46 during calibration period. 89
Figure 94. Total nitrate + nitrite as nitrogen model vs. data comparison - segment 59 during calibration period. 89
Figure 95. Total nitrate + nitrite as nitrogen model vs. data comparison - segment 67 during calibration period. 90
Figure 96. Total nitrate + nitrite as nitrogen model vs. data comparison - segment 83 during calibration period. 90
Figure 97. Total nitrate + nitrite as nitrogen model vs. data comparison - segment 89 during calibration period. 91
Figure 98. Total nitrate + nitrite as nitrogen model vs. data comparison - segment 109 during calibration period. 91
Figure 99. Total nitrate + nitrite as nitrogen model vs. data comparison - segment 199 during calibration period. 92
Figure 100. Total phosphorus model vs. data comparison – segment 24 during calibration period. 93
Figure 101.Total phosphorus model vs. data comparison – segment 35 during calibration period. 94
Figure 102. Total phosphorus model vs. data comparison – segment 43 during calibration period. 94
Figure 103. Total phosphorus model vs. data comparison – segment 46 during calibration period. 95
Figure 104. Total phosphorus model vs. data comparison – segment 59 during calibration period. 95
Figure 105. Total phosphorus model vs. data comparison – segment 67 during calibration period. 96
Figure 106. Total phosphorus model vs. data comparison – segment 83 during calibration period. 96
Figure 107. Total phosphorus model vs. data comparison – segment 89 during calibration period. 97
Figure 108. Total phosphorus model vs. data comparison – segment 108 during calibration period. 97
Figure 109. Total phosphorus model vs. data comparison – segment 109 during calibration period. 98
Figure 110. Total phosphorus model vs. data comparison – segment 199 during calibration period. 98
Figure 111. Sources and sinks of dissolved PO_4-P predicted by the model during calibration period. ... 99
Figure 112. PO_4-P concentrations predicted by the model compared to field data on 5/19/2005. 100
Figure 113. PO_4-P concentrations predicted by the model compared to field data on 6/16/2005. 101
Figure 114. PO_4-P concentrations predicted by the model compared to field data on 10/3/2005. 101
Figure 115. Ortho phosphorus model vs. data comparison – segment 24 during calibration period. 102
Figure 116. Ortho phosphorus model vs. data comparison – segment 35 during calibration period. 102
Figure 117. Ortho phosphorus model vs. data comparison – segment 46 during calibration period. 103
Figure 118. Ortho phosphorus model vs. data comparison – segment 59 during calibration period. 103
Figure 119. Ortho phosphorus model vs. data comparison – segment 67 during calibration period. 104
Figure 120. Ortho phosphorus model vs. data comparison – segment 83 during calibration period. 104
Figure 121. Ortho phosphorus model vs. data comparison – segment 89 during calibration period. 105
Figure 122. Ortho phosphorus model vs. data comparison – segment 108 during calibration period. .. 105
Figure 123. Ortho phosphorus model vs. data comparison – segment 109 during calibration period. .. 106
Figure 124. Ortho phosphorus model vs. data comparison – segment 199 during calibration period. .. 106
Figure 125. Chlorophyll a model vs. data comparison – segment 35 during calibration period. 107
Figure 126. Chlorophyll a model vs. data comparison – segment 46 during calibration period. 108
Figure 127. Chlorophyll a model vs. data comparison – segment 59 during calibration period. 108
Figure 128. Chlorophyll a model vs. data comparison – segment 67 during calibration period. 109
Figure 129. Chlorophyll a model vs. data comparison – segment 83 during calibration period. 109
Figure 130. Chlorophyll a model vs. data comparison – segment 89 during calibration period. 110
Figure 131. Chlorophyll a model vs. data comparison – segment 199 during calibration period. 110

Figure 132. Chlorophyll a model vs. data comparison – segment 108/9 during calibration period. 111
Figure 133. Secchi disk data at all stations on Tenkiller Reservoir between 2005 and 2007..... 113
Figure 134. Model predictions of light extinction at the near surface compared to light extinction coefficients computed from Secchi disk depths..... 114
Figure 135. Temperature field data compared to model predictions at all locations and times. 115
Figure 136. Dissolved oxygen field data compared to model predictions at all stations and times at different depths. 116
Figure 137. NO_3-N field data compared to model predictions at all stations and times at different depths. 117
Figure 138. Model predictions of chlorophyll a compared to all field data during calibration period for all stations. 118
Figure 139. Model predicted Total P compared to field data for all stations during calibration period. 119
Figure 140. Illinois River discharge for the base 10-year period of the 50-year model scenario..... 121
Figure 141. Measured temperature compared to filtered equilibrium temperature between 1997 and 2006..... 122
Figure 142. Comparison of measured and predicted inflow temperatures between 1997 and 2006. 123
Figure 143. Illinois River algae group biomass concentrations for the base 10-year period of the 50-year model scenario. 124
Figure 144. Illinois River ammonia data for the base 10-year period of the 50-year model scenario. .. 124
Figure 145. Illinois River dissolved oxygen for the base 10-year period of the 50-year model scenario. 125
Figure 146. Illinois River nitrate + nitrite concentrations for the base 10-year period of the 50-year model scenario. 125
Figure 147. Baron Fork Creek discharge for the base 10-year period of the 50-year model scenario... 126
Figure 148. Baron Fork Creek algae group biomass concentrations for the base 10-year period of the 50-year model scenario. 127
Figure 149. Baron Fork Creek nitrate + nitrite concentrations for the base 10-year period of the 50-year model scenario. 128
Figure 150. Caney Creek discharge for the base 10-year period of the 50-year model scenario. 128
Figure 151. Caney Creek algae group biomass concentrations for the base 10-year period of the 50-year model scenario. 129
Figure 152. Caney Creek nitrate + nitrite concentrations for the base 10-year period of the 50-year model scenario. 130
Figure 153. Distributed inflow for the base 10-year period of the 50-year model scenario..... 131
Figure 154. Computed water balance flows between January 1997 and December 2006. 133
Figure 155. Water level data compared to model predictions between January 1997 and December 2006. 134
Figure 156. Distributed inflows from January 1997 to December 2006 combining the water balance flows showing the effect of smoothing..... 135
Figure 157. Minimum release flow from dam for the base 10-year period of the 50-year model scenario. 136
Figure 158. Outflows from Tenkiller Reservoir for the base 10-year period of the 50-year model scenario. 137
Figure 159. Schematic of sediment layers (after DiToro and Fitzpatrick, 1993). 140
Figure 160. CE-QUAL-W2 zero order sediment oxygen demand model. 141
Figure 161. CE-QUAL-W2 first order predictive sediment oxygen demand..... 141
Figure 162. Variation of fraction of sediment remaining without any flux of organic matter to sediments as a function of decay rate range..... 143

Figure 163. Fraction of sediment categories remaining assuming a constant sediment flux of 100 mg/m^2/day, C_{so} of 5000 g/m^2, and a burial rate of 7E-5 day^{-1}. 144
Figure 164. Water level for 50-year simulation showing no drift in water level after every 10-year period. 146
Figure 165. Volume weighted surface (5-6 m depth) average chlorophyll a at sampling site LK04, model segment 35 comparing cessation, growth and base case trends..... 148
Figure 166. Volume weighted surface (5-6 m depth) average chlorophyll a at sampling site LK03, model segment 59 comparing cessation, growth and base case trends..... 149
Figure 167. Volume weighted surface (5-6 m depth) average chlorophyll a at sampling site LK02, model segment 83 comparing cessation, growth and base case trends..... 149
Figure 168. Volume weighted surface (5-6 m depth) average chlorophyll a at sampling site LK01, model segment 199 comparing cessation, growth and base case trends..... 150
Figure 169. Volume weighted surface (5-6 m depth) average chlorophyll a at sampling site LK04, model segment 35 for historical and natural cases. 150
Figure 170. Volume weighted surface (5-6 m depth) average chlorophyll a at sampling site LK03, model segment 59 for historical and natural cases. 151
Figure 171. Volume weighted surface (5-6 m depth) average chlorophyll a at sampling site LK02, model segment 83 for historical and natural cases. 151
Figure 172. Volume weighted surface (5-6 m depth) average chlorophyll a at sampling site LK01, model segment 109 for historical and natural cases. 152
Figure 173. Volume weighted surface (5-6 m depth) average Total P at sampling site LK04, model segment 35 comparing cessation and base case trends. 152
Figure 174. Volume weighted surface (5-6 m depth) average Total P at sampling site LK03, model segment 59 comparing cessation and base case trends. 153
Figure 175. Volume weighted surface (5-6 m depth) average Total P at sampling site LK02, model segment 83 comparing cessation and base case trends. 153
Figure 176. Volume weighted surface (5-6 m depth) average Total P at sampling site LK01, model segment 199 comparing cessation, growth and base case trends..... 154
Figure 177. Volume weighted surface (5-6 m depth) average Total P at sampling site LK04, model segment 35 for historical and natural cases. 154
Figure 178. Volume weighted surface (5-6 m depth) average Total P at sampling site LK03, model segment 59 for historical and natural cases. 155
Figure 179. Volume weighted surface (5-6 m depth) average Total P at sampling site LK02, model segment 83 for historical and natural cases. 155
Figure 180. Volume weighted surface (5-6 m depth) average Total P at sampling site LK01, model segment 109(199) for growth, historical, and natural cases compared to base case. 156
Figure 181. Frequency distribution for LK04 (segment 35) for chlorophyll a for summer surface layer over 50-year period. 157
Figure 182. Frequency distribution for LK03 (segment 59) for chlorophyll a for summer surface layer over 50-year period. 157
Figure 183. Frequency distribution for LK02 (segment 83) for chlorophyll a for summer surface layer over 50-year period. 158
Figure 184. Frequency distribution for LK01 (segment 109) for chlorophyll a for summer surface layer over 50-year period. 158
Figure 185. Frequency distribution for LK04 (segment 35) for Total P for summer surface layer over 50-year period. 159
Figure 186. Frequency distribution for LK03 (segment 59) for Total P for summer surface layer over 50-year period. 159

Figure 187. Frequency distribution for LK02 (segment 83) for Total P for summer surface layer over 50-year period. 160
Figure 188. Frequency distribution for LK01 (segment 109) for Total P for summer surface layer over 50-year period. 160
Figure 189. Average dissolved oxygen between May 1 and October 31 of each year for the base case and the cessation with SOD declining to 0.1 g/m^2/d. Running average is over 11 years. 165
Figure 190. Historical scenario for summer outlet dissolved oxygen concentration each year for 50 years. 166
Figure 191. Growth scenario for summer outlet dissolved oxygen concentration each year for 50 years. 167
Figure 192. Difference between dissolved oxygen demand from zero order and first order sediment demand between base and cessation with SOD set to 0.1 g/m^2/d scenarios including linear trend lines over the 50-year period. 168
Figure 193. Dissolved oxygen demand from particulate and dissolved organic matter in the water column between base and cessation with SOD set to 0.1 g/m^2/d scenarios including linear trend lines over the 50-year period. 169
Figure 194. Dissolved oxygen net photosynthetic production from algae and periphyton between base and cessation scenarios with SOD set to 0.1 g/m^2/d including linear trend lines over the 50-year period. 170
Figure 195. Smallmouth bass suboptimal habitat volume and fraction of volume over the last 5 years of the 50-year period. 173
Figure 196. Smallmouth bass suboptimal habitat volume and fraction of volume over one of the last years of the 50-year period. 174
Figure 197. Walleye suboptimal habitat volume and fraction of volume over the last 5 years of the 50-year period. 175
Figure 198. Walleye habitat volume and fraction of volume over one of the last years in the 50-year period. 176
Figure 199: Total phosphorus inflow, two scenarios. 178
Figure 200. Yearly Total P inflow load to Tenkiller reservoir for the cessation scenario including linear trend line over 50-year period. 179
Figure 201. Yearly Total P inflow load to Tenkiller reservoir over for the growth scenario including linear trend line over 50-year period. 180
Figure 202. Yearly Total P inflow load to Tenkiller reservoir for the historical scenario including linear trend line over 50-year period. 181
Figure 203. Total P outflow from Tenkiller reservoir for base and cessation scenarios, including linear cessation trend line over the 50-year period. 182
Figure 204. Total P outflow from Tenkiller reservoir for natural and growth scenarios, including linear growth trend line over the 50-year period. 183
Figure 205. Total P outflow from Tenkiller reservoir for historical case, including linear historical trend line over the 50-year period. 183
Figure 206. Sonar elevation vs. contour line comparison 196
Figure 207. Plot of difference between sonar elevation and contour lines 198
Figure 208. Consistent sonar elevation error scenario. 200
Figure 209. Volume-elevation curve for approaches 1 and 2. 201
Figure 210. Surface area-elevation curve for approaches 1 and 2. 201
Figure 211. The definition of equilibrium temperature. 204
Figure 212. Temperature profiles segment 35 Part 1. 207
Figure 213. Temperature profiles segment 35 Parts 2 & 3. 208

Figure 214. Temperature profiles segment 59 Parts 1 & 2. 209
Figure 215. Temperature profiles segment 59 Parts 3 & 4. 210
Figure 216. Temperature profiles segment 83 Parts 1 & 2. 211
Figure 217. Temperature profiles segment 83 Parts 3 & 4. 212
Figure 218. Temperature profiles segment 109. 213
Figure 219. Temperature profiles segment 199 Part 1. 213
Figure 220. Temperature profiles segment 199 Parts 2 & 3. 214
Figure 221. Temperature profiles segment 199 Part 4. 215
Figure 222. Dissolved oxygen profiles segment 35 Part 1. 216
Figure 223. Dissolved oxygen profiles segment 35 Parts 2 & 3. 217
Figure 224. Dissolved oxygen profiles segment 43. 218
Figure 225. Dissolved oxygen profiles segment 46. 218
Figure 226. Dissolved oxygen profiles segment 67. 219
Figure 227. Dissolved oxygen profiles segment 83 Part 1. 219
Figure 228. Dissolved oxygen profiles segment 83 Parts 2 & 3. 220
Figure 229. Dissolved oxygen profiles segment 83 Part 4. 221
Figure 230. Dissolved oxygen profiles segment 199 Part 1. 221
Figure 231. Dissolved oxygen profiles segment 199 Parts 2 & 3. 222
Figure 232. Dissolved oxygen profiles segment 199 Part 4. 223
Figure 233. Chlorophyll a model vs. data profile – segment 46 during calibration period. 224
Figure 234. Chlorophyll a model vs. data profile – segment 59 Parts 1 & 2 during calibration period. 225
Figure 235. Chlorophyll a model vs. data profile – segment 59 Parts 3 & 4 during calibration period. 226
Figure 236. Chlorophyll a model vs. data profile – segment 67 during calibration period. 227
Figure 237. Chlorophyll a model vs. data profile – segment 83, Part 1 during calibration period..... 227
Figure 238. Chlorophyll a model vs. data profile – segment 83 Parts 2 & 3 during calibration period. 228
Figure 239. Chlorophyll a model vs. data profile – segment 83 Part 4 during calibration period..... 229
Figure 240. Chlorophyll a model vs. data profile – segment 89 during calibration period. 229
Figure 241. Chlorophyll a model vs. data profile – segment 199 Parts 1 & 2 during calibration period. 230
Figure 242. Chlorophyll a model vs. data profile – segment 199 Parts 3 & 4 during calibration period. 231

List of Tables

Table 1. CE-QUAL-W2 applications between 2000-2006. 5
Table 2. Data needs for modeling Tenkiller Reservoir. 8
Table 3. Tenkiller Reservoir model grid specifications. 14
Table 4. Features of Tenkiller Reservoir dam. 16
Table 5. Model-data error statistics for water level. 58
Table 6. Model-data error statistics for temperature. 60
Table 7. CE-QUAL-W2 model parameters affecting hydrodynamics and temperature. 64
Table 8. CE-QUAL-W2 model water quality parameters 65
Table 9. Model-data error statistics for dissolved oxygen. 74
Table 10. Water level errors between January 1997 and December 2006. 132

Table 11. Minimum base flows over time. 136
Table 12. Management scenarios considered with the Tenkiller Reservoir model. 138
Table 13. Sediment decay rates and assumed fraction sediment based on sediment type (DiToro and Fitzpatrick, 1993, and Cerco and Cole, 1994). 142
Table 14. Time averages of the Total P between model runs over the 50-year period. 161
Table 15. Median of the Total P between model runs over the 50-year period. 161
Table 16. Time averages of the Total P between model runs over the last 10-year period. 162
Table 17. Median of the Total P between model runs over the last 10-year period. 162
Table 18. Time averages of the chlorophyll a between model runs over the 50-year period. 162
Table 19. Median of the chlorophyll a between model runs over the 50-year period. 163
Table 20. Time averages of the chlorophyll a between model runs over the last 10-year period. 163
Table 21. Median of the chlorophyll a between model runs over the last 10-year period. 163
Table 22. Average of May-October outlet dissolved oxygen concentrations. 164
Table 23. Fish habitat temperature and dissolved oxygen preferences (Cooke and Welch, 2008). 171
Table 24. Fish habitat temperature and dissolved oxygen preferences used in the CE-QUAL-W2 model. 171
Table 25. Habitat volume for small mouth bass and walleye for summer (June 15 through September 15) over the 50-year simulation. 177
Table 26: Detailed summary of phosphorus inflows. 179
Table 27: Summary of Total P outflow from Tenkiller Reservoir. 181
Table 28: Summary of Total P sediment flux. 184
Table 29. Change in chlorophyll a over time during the 50-year period for the cessation, growth, and historical runs. Trends are only for summer periods between June 1 and September 30. 190
Table 30. Change in Total P over time during the 50-year period for the cessation, growth, and historical runs. Trends are only for summer periods between June 1 and September 30. 190
Table 31. Change in outlet dissolved oxygen over time during the 50-year period for the base, cessation, growth, and historical runs between June 1 and September 30. 191
Table 32. Sonar elevation vs. contour line comparison 197
Table 33. Variable sonar elevation corrections. 198
Table 34. Water level on days of sonar survey. 199
Table 35. Typical model-data calibration errors. 232

Introduction

Tenkiller Reservoir, sometimes called Tenkiller Ferry Lake, is a Corps of Engineers facility operated by the Tulsa District located in Oklahoma (see Figure 1). Tenkiller Reservoir is on the Illinois River, which originates in Arkansas, and eventually drains into the Arkansas River. The State of Oklahoma has designated the Illinois River as a scenic river.

Because of the issues associated with impacts of poultry waste applied to agriculture lands in the basin, a hydrodynamic and water quality model of Tenkiller Reservoir was constructed to evaluate how the reservoir would respond to future changes in nutrient loading from the watershed and has responded to past changes in nutrient loading from the watershed.

The objective of this project is to produce a hydrodynamic and water quality model of Tenkiller Reservoir that is calibrated to field data and that can predict the impacts of various nutrient loading scenarios. In order to meet that objective, the following steps were performed and described in this report:

1. Compile data for the modeling effort
2. Set-up a model for Tenkiller Reservoir for the following parameters: water surface elevation, velocities, temperature, dissolved oxygen, labile/refractory dissolved organic matter, labile/refractory particulate organic matter, algae, PO_4-P, NH_3-N, NO_3-N + NO_2-N, suspended solids.
3. Calibrate the model to field data
4. Evaluate management scenarios

This report contains the following sections:

1. Previous model studies
2. Model selection
3. Model set-up
4. Model calibration
5. Model alternatives
6. Summary and Conclusions

Previous Modeling Studies

A previous model application to Tenkiller Reservoir was the application of the 3D model, EFDC (Craig, 2004; Park et al., 1995), by Dynamic Solutions. This model was set up and compared to field data between January 1992 and December 1993. Some of the reasons why this particular model was not used for this study are itemized below:

1. Model data comparisons were made of minimum, mean, and maximum predicted values of water quality parameters (dissolved oxygen, chlorophyll a, Total P) at several reservoir locations (hence over depth) to field data (see for example, Figure 1). No instantaneous data-model comparisons were made at the time and location of the field data. No model error statistics were presented for instantaneous model-data comparisons. In general, though the overall range of the model prediction seemed to be within the overall range of the data.

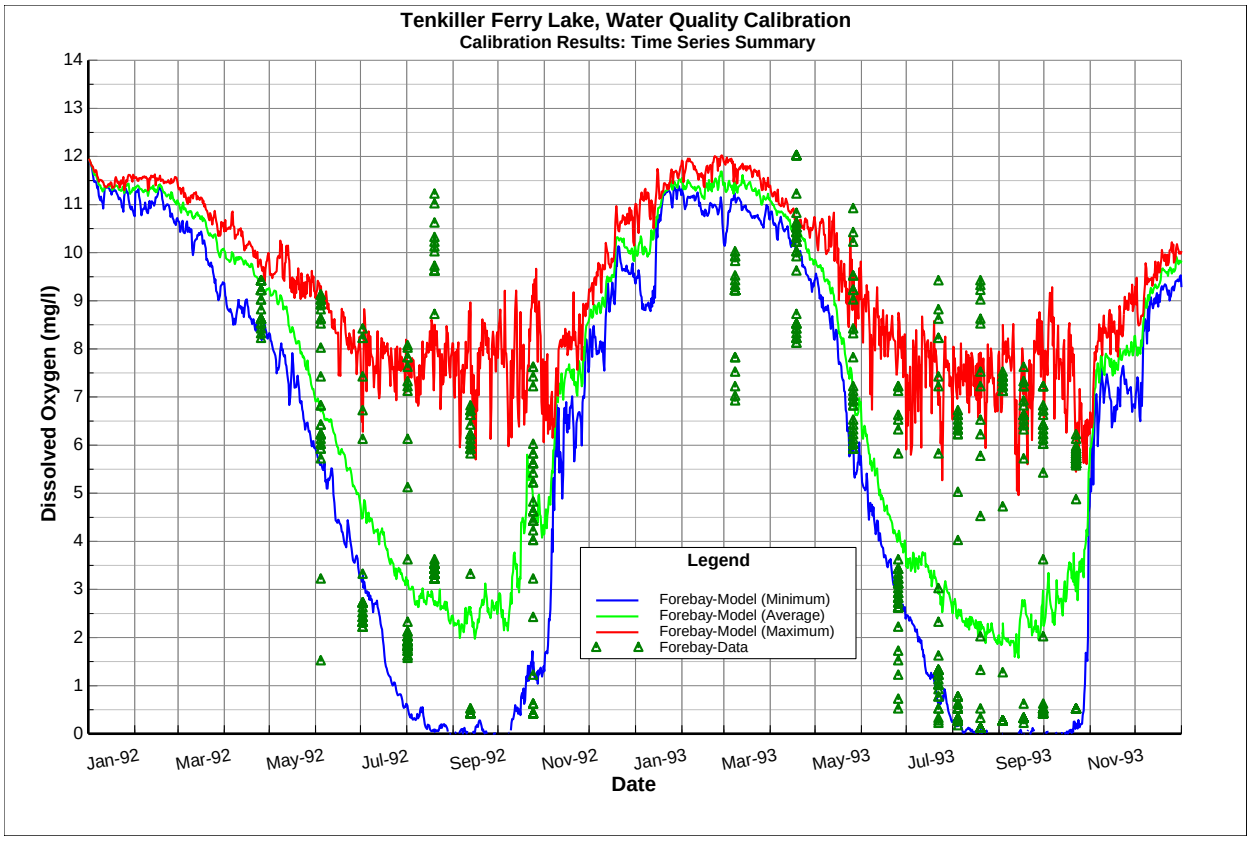

Figure 1. Model-data comparison for dissolved oxygen in forebay of Tenkiller reservoir for 1992-1993 EFDC model calibration (Craig, 2004).

2. No model-data comparisons of vertical profiles of temperature or dissolved oxygen were provided for review. Hence, the correct thermal and oxygen structure of the reservoir was not verifiable.

3. No comparisons were provided that showed model water level in the reservoir agreed with field data.
4. Computational time for the 3D model to run a 50-year model simulation may have been excessive.

Because of these limitations, a model based on more current field data was decided to be constructed, one that could reproduce the structure and trends of the system and could be run for long-term simulations.

Model Selection

Selection of the appropriate water quality model is a function of properly identifying the water quality problem ("conceptualization") and selecting a model which appropriately describes the water quality changes in the water body, is theoretically valid, and can be easily adapted to site-specific physical characteristics of the water body.

The performance of a mathematical model in predicting the existing and future water quality dynamics of a system is dependent on the following steps:

i. identification of the problem
ii. selection of model type and relationship of model to the problem
iii. computational representation
iv. model response studies or model sensitivity analyses
v. model calibration
vi. application of model to evaluate management strategies

Because there are many water quality models available, a choice of the appropriate model would be made after considering the following questions: What physical processes are represented in the model and which are ignored? How are physical processes included in the model? What processes are represented by model coefficients? For example in defining the problem, the following questions could be asked:

What are the dominant physical processes at work and can the chosen model represent those processes? (such as, how does the water move? Is there stratification, wind-driven currents, and/or selective withdrawal?)

What are the spatial and temporal scales of these processes and can the model represent them? (such as, is steady-state representation adequate, is 1-D, 2-D, or 3-D spatial discretization necessary?)

The choice of the proper model is also based on answering

1. Site specific questions (physical characteristics of the each system component - river or reservoir reach, water quality cycles, algal types),
2. Management objectives (required accuracy, use for future studies),
3. Project resources (data availability, staff constraints, time limitations).

The model proposed for Tenkiller Reservoir is the public domain model, CE-QUAL-W2 (Cole and Wells, 2008). This model is a 2-dimensional (longitudinal-vertical) hydrodynamic and water quality model capable of predicting water surface, velocity, temperature, nutrients, multiple algae, zooplankton, periphyton, and macrophyte groups/species, dissolved oxygen, pH, alkalinity, multiple CBOD groups, multiple suspended solids groups, multiple generic constituents (such as tracer, bacteria, toxics), and multiple organic matter groups, both dissolved and particulate. The model is set up to predict these state variables at longitudinal segments and vertical layers (see Figure 1).

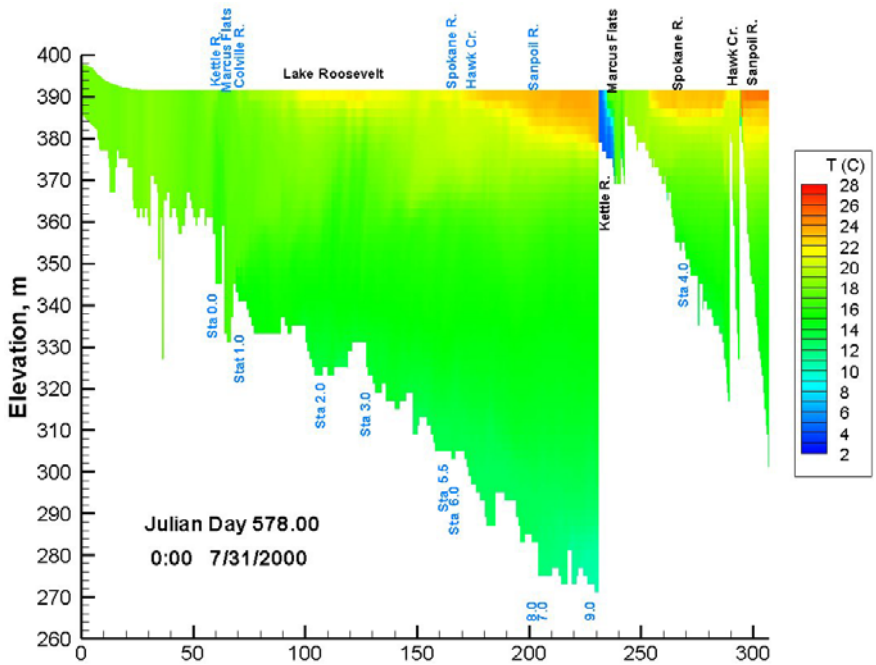

Figure 2. CE-QUAL-W2 model predictions for Lake Roosevelt, WA, for temperature as a function of depth and longitudinal distance in km from the Canadian border on July 31, 2000.

This model is a Corps of Engineers model that was originally developed as a modification of the Laterally Averaged Reservoir Model (Edinger and Buchak 1978). CE-QUAL-W2 consists of directly coupled hydrodynamic and water quality transport models. A typical model grid or schematization is shown in Figure 3. Hydrodynamic computations are influenced by variable water density caused by temperature, salinity, and dissolved and suspended solids. Developed for reservoirs and narrow, stratified estuaries, CE-QUAL-W2 can handle a branched and/or looped system with flow and/or head boundary conditions. With two dimensions depicted, point and non-point loading can be spatially distributed. Relative to other 2-D models, CE-QUAL-W2 is numerically accurate, efficient and cost effective to use.

Typical model longitudinal resolution is between 100-1000 m; vertical resolution is usually between 0.5 m and 2 m. The model can also be used in quasi-3-D mode, where embayments are treated as separate model branches off the main stem of the reservoir. The user manual and documentation can be found at

the following website: http://www.cee.pdx.edu/w2. Since 2000, this model has been used extensively throughout the world in 116 different countries (see Table 1). Over the last 10 years, Dr. Wells and his research group at Portland State University have been working with the Corps of Engineer's Waterways Experiment Station in the development of the CE-QUAL-W2 model.

Table 1. CE-QUAL-W2 applications between 2000-2006.

Water body	Known Number of Applications
Reservoirs	319+
Lakes	287+
Rivers	436+
Estuaries	82+
Pit Lakes	10+

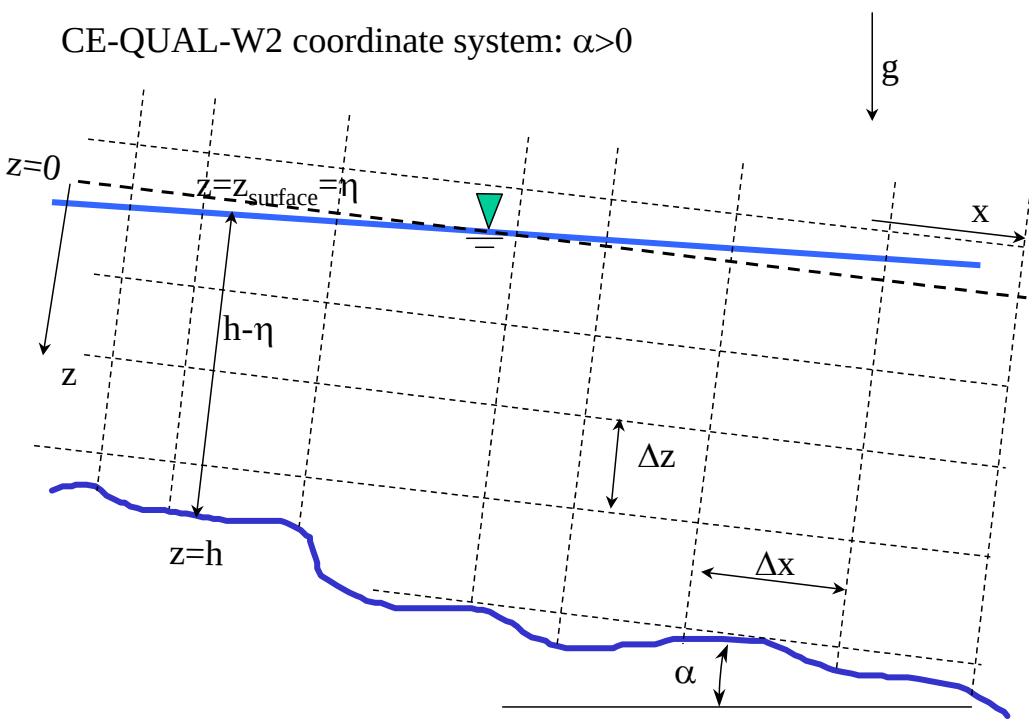

Figure 3. Coordinate system for CE-QUAL-W2 Version 3.6.

Models, such as WQRSS (Smith 1978), HEC-5Q (Corps of Engineers 1986), and HSPF (Donigian, et al. 1984), have been developed for river basin modeling but have serious limitations. One issue is that the HEC-5Q (similar to WQRSS) and HSPF models incorporate a one-dimensional, longitudinal river model with a one-dimensional, vertical reservoir model (one-dimensional for temperature and water quality and zero dimensional for hydrodynamics). The modeler must choose the location of the transition from 1-D longitudinal to 1-D vertical. Besides the limitation of not solving for the velocity field in the

stratified, reservoir system, any point source inputs to the reservoir section are spread over the entire horizontal area of the reservoir.

Also, other one-dimensional reservoir models, such as the HEC WQRRS (Water Quality River-Reservoir Simulation) model and the Corps's CE-QUAL-R1, are also not adequate to compute 2-D circulation within pool areas. These models conceptualize a pool as well mixed in each horizontal slab, i.e., over the length and the width of the system. By making this assumption, the vertical and longitudinal circulation patterns within a pool cannot be resolved.

A one-dimensional reservoir model would not be adequate for the Tenkiller Reservoir because of longitudinal and vertical gradients in water quality.

Would a 3-D model be more appropriate? Even though in the future all models may eventually be 3-D, currently the added complexity of 3D models does not always justify its use in this system for the following reasons:

- There are inadequate water quality field data to assess the importance of lateral variations. Field data show clear evidence of strong gradients vertically and longitudinally.
- Wells and Gordon (1982) showed that often 3D variations in temperature, conductivity, dissolved oxygen and pH were negligible in many deep-density stratified reservoirs.
- Current work on 3D models compared to 2D models in Lake Sammamish (DeGasperi, 2007), Lake Erie (Boegman, 2006, Boegman, et al., 2001), and the Dead Sea (Gavrieli et al., 2006) show that often 2D models are more predictive of water quality processes than more complex 3D models.

For this project, the CE-QUAL-W2 River Basin Model Version 3.6 (Cole and Wells, 2008), as schematized in Figure 4, was the most appropriate for modeling the Tenkiller Reservoir since it contains the following elements:

- Two-dimensional, dynamic hydrodynamics and water quality capable of replicating temperature and water quality in a density stratified waterbody
- The model is a state-of-the-art tool with features not found in other models
- CE-QUAL-W2 has a proven track-record of being capable of modeling complex dendritic reservoir systems in the US and abroad
- The code is open source and is readily available for peer-review
- The code is maintained by the Corps of Engineers, Waterways Experiment Station, and has been used by other Federal Agencies (such as the EPA, Bureau of Reclamation, USGS) extensively
- The model code is easily modified for custom output features such as fish habitat volumes and statistics of water quality variables
- Depending on model set-up and complexity, the model can be run for long-term simulations within a reasonable time period

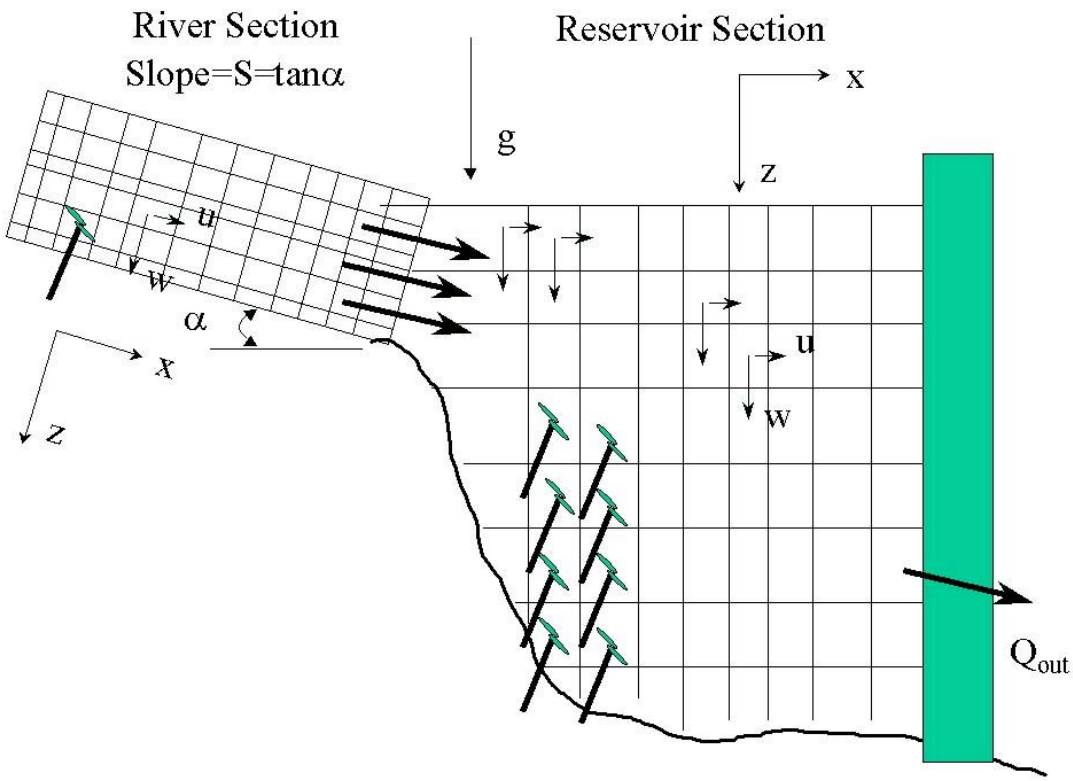

Figure 4. Conceptual schematic of river-reservoir connection in CE-QUAL-W2 Version 3.

Model Set-Up

In order to set up this model, specific data are required to provide the forcing functions to the reservoir system. In addition, data are required for comparison to model predictions. A list of these data is shown in Table 2.

Table 2. Data needs for modeling Tenkiller Reservoir.

#	Data Type	Why necessary?
1	Bathymetric x-y-z data of the reservoir	Construct model segments and layers
2	Flow rates (Q), temperatures (T), and concentrations for all inflows	These are the model boundary conditions; continuous data are preferable, otherwise the model can use any temporal resolution available
3	Outlet structure details for the power house and spillways, including rating curves for the spillways	The centerline elevation of the outlets and the weir crest elevations are of importance in predicting the vertical stratification in the reservoir system and the correct outflow during spill events (unless these are measured and known)
4	Flow rates and locations of outflows from the system, including the dam outlet, irrigation withdrawals, and water withdrawals	These are model boundary conditions.
5	Meteorological data such as air temperature, dew point temperature (or relative humidity), wind speed and direction, solar radiation and cloud cover; hourly data are preferred	These are model boundary conditions.
6	Water surface elevation data (continuous)	Matching these data with model predictions is an important part of verifying that the water balance for the system is accurate.
7	In-reservoir data of temperature and water quality (nutrients, algae, DO)	These data would be used to verify that the model predictions are reasonable.
8	Measured kinetic or estimated model coefficients from field data	Measured field kinetic values would be used as model coefficients.

Model Geometry

Bathymetry

Bathymetry data for Tenkiller Reservoir were gathered from two sources: (1) contour line elevation data provided by Fishing Hot Spots Inc. and (2) sonar depth measurements collected by Global Remote Sensing LLC. The sonar depth measurements were either "depth-from-water-surface" or "depth-from-sonar-tow fish." In order to address these two possible situations, separate approaches were used to process the sonar data. The two different approaches for processing the sonar data were detailed in Appendix A. Once this issue was resolved, the sonar elevation data and contour lines were combined to create a composite Tenkiller Reservoir bathymetry dataset. Using SURFER software, the bathymetry dataset was processed and an elevation grid was created to form the basis for 3-D bathymetry maps of Tenkiller Reservoir. These 3D topographical maps were then broken into model longitudinal segments (or polygons) and the model grid was then developed.

The final 3-D bathymetry map used as the basis for W2-model bathymetry files is shown in Figure 5.

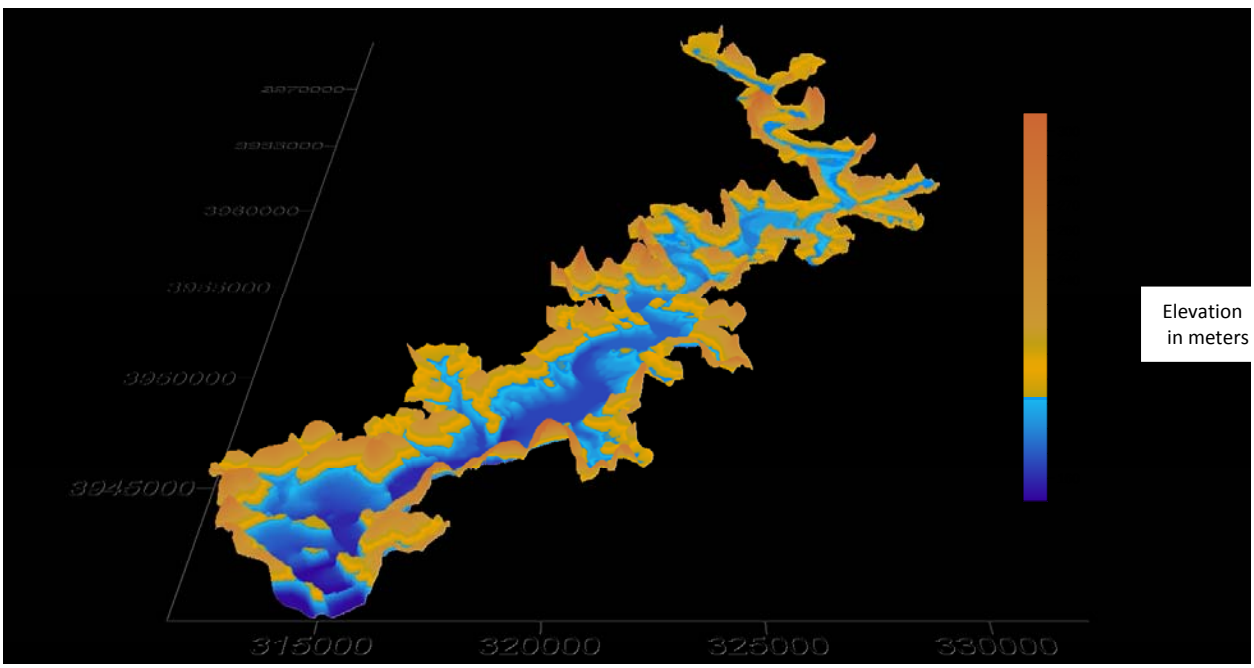

Figure 5. 3-D view of Tenkiller Reservoir model bathymetry.

Model Grid Development

Tenkiller Reservoir was divided into almost 200 discreet computational model segments and 13 separate model branches, allowing for quasi-3D approach to the model domain. A top view of the model grid overlaid on the bathymetric map of Tenkiller Reservoir is shown in Figure 6. Figure 7, Figure 8, Figure 9, and Figure 10 show the top, side, and vertical views of the final CE-QUAL-W2 model grid configuration, respectively.

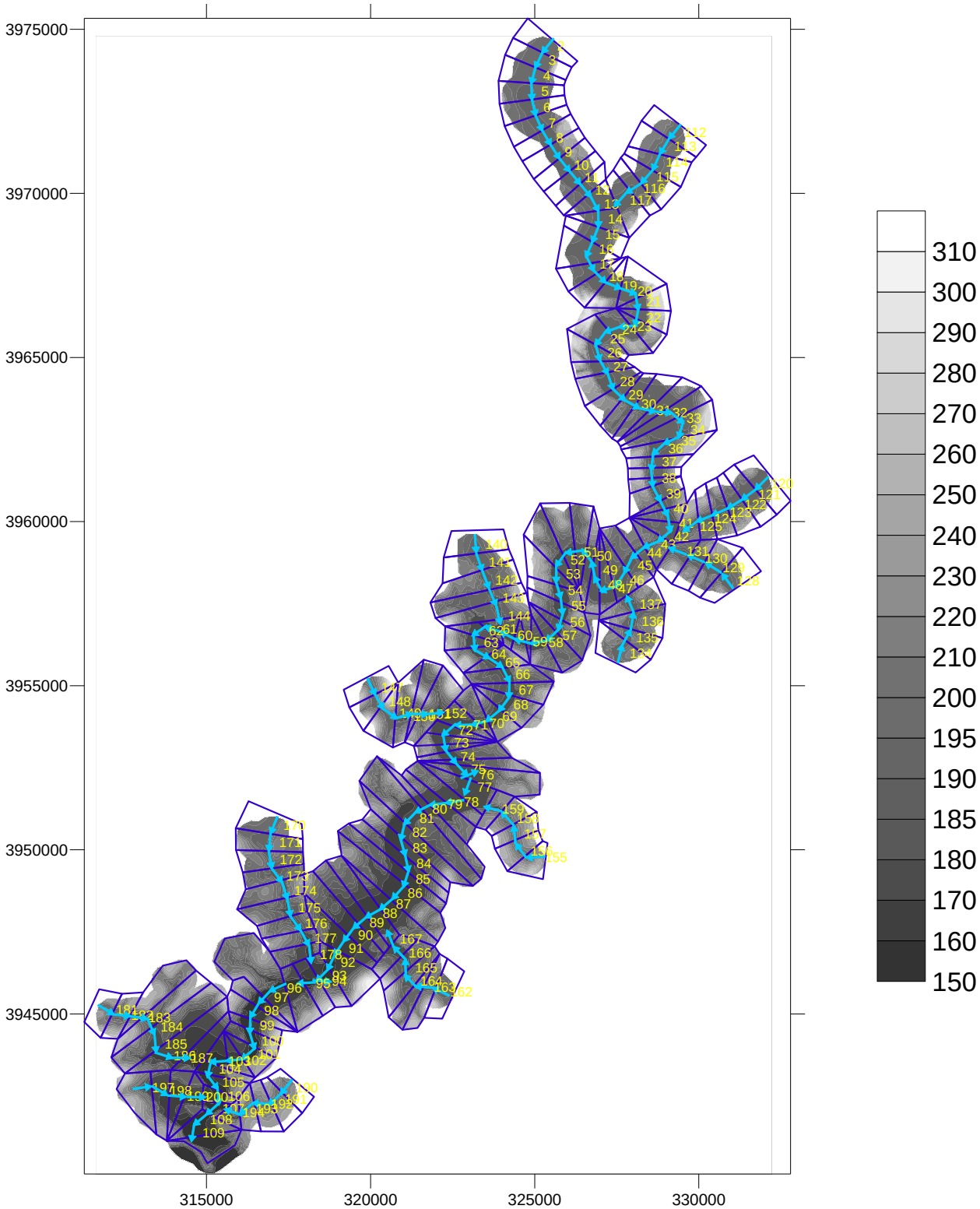

Figure 6. Top view of the Tenkiller Reservoir model grid and bathymetric map.

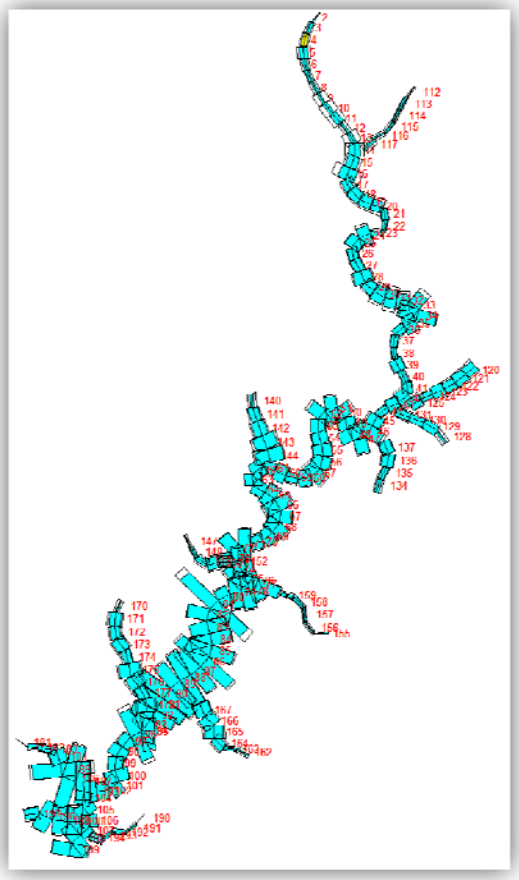

Figure 7. Top view of the Tenkiller Reservoir model grid.

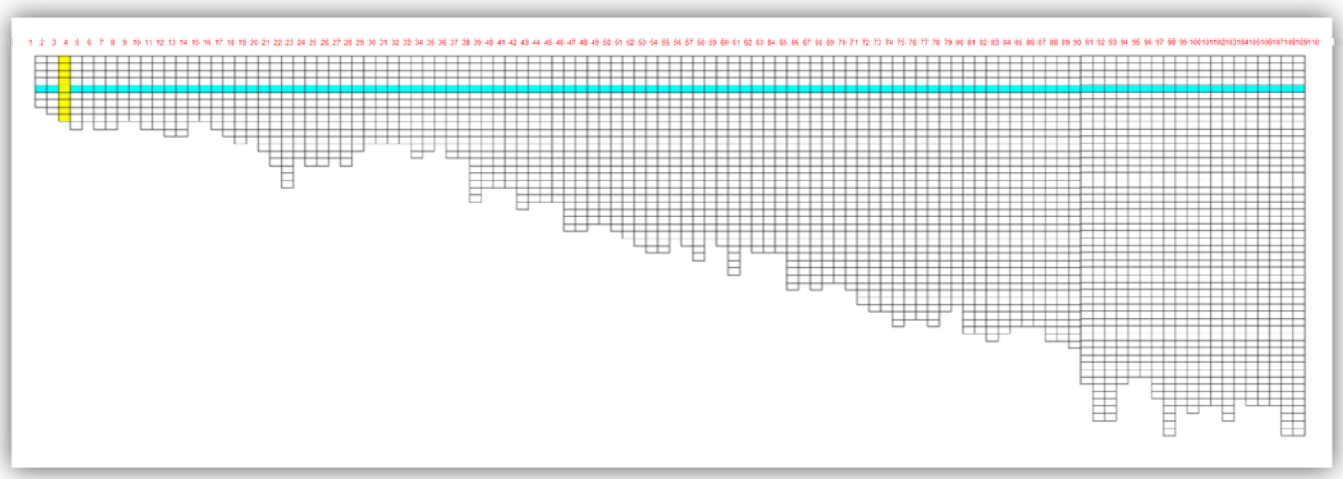

Figure 8. Side view of the Tenkiller Reservoir main branch model grid.

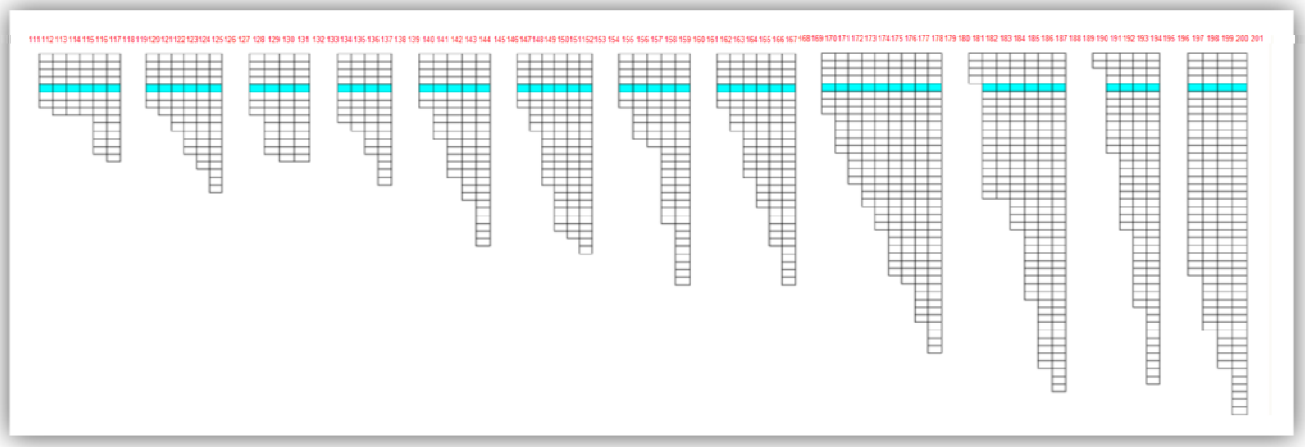

Figure 9. Side view of the Tenkiller Reservoir side branches model grid.

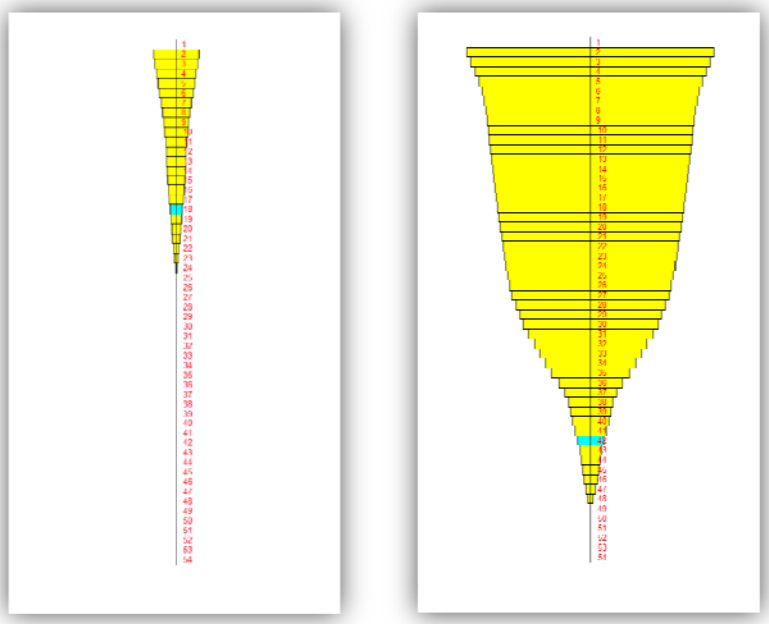

Figure 10. Slice views of the Tenkiller Reservoir main branch segments 192 (left) and 200 (right).

Table 3. Tenkiller Reservoir model grid specifications.

Branch #	Start Segment	End Segment	# segments	Grid spacing, Δx, m	Centerline distance, m
1 (Illinois River, Main Branch)	2	109	108	500.86	54093.3
2 (Baron Fork Creek)	112	117	6	545.16	3271.0
3 (Caney Creek)	120	125	6	513.02	3078.1
4	128	131	4	606.13	2424.5
5	134	137	4	547.67	2190.7
6	140	144	5	577.34	2886.7
7	147	152	6	507.97	3047.8
8	155	159	5	576.22	2881.1
9	162	167	6	531.03	3186.2
10	170	178	9	537.13	4834.2
11	181	187	7	563.20	3942.4
12	190	194	5	539.97	2699.8
13	197	200	4	594.53	2378.1

The volume-elevation curves from the surface contour plot of the reservoir (SURFER) and the model grid were compared with the known rating curve from Corps of Engineers. Figure 11 shows the volume elevation curves for the contour plot, the model grid, and the rating curve from the Corps of Engineers. The figure indicates there is close agreement between the model grid and known rating curve which means the appropriate volume over elevation was preserved. The discrepancy between the Corps rating curve points and the model grid could be a result of using newer field data to construct the volume-elevation curve. One would expect that over time due to sedimentation that the reservoir volume would slightly decrease. Other reasons for the discrepancy could be (1) errors in original computation of the volume-elevation curve, or (2) errors in the sonar data or processing of the sonar data in construction of the current bathymetric map. Figure 12 shows a surface area-elevation curve for the contour plot and the model grid.

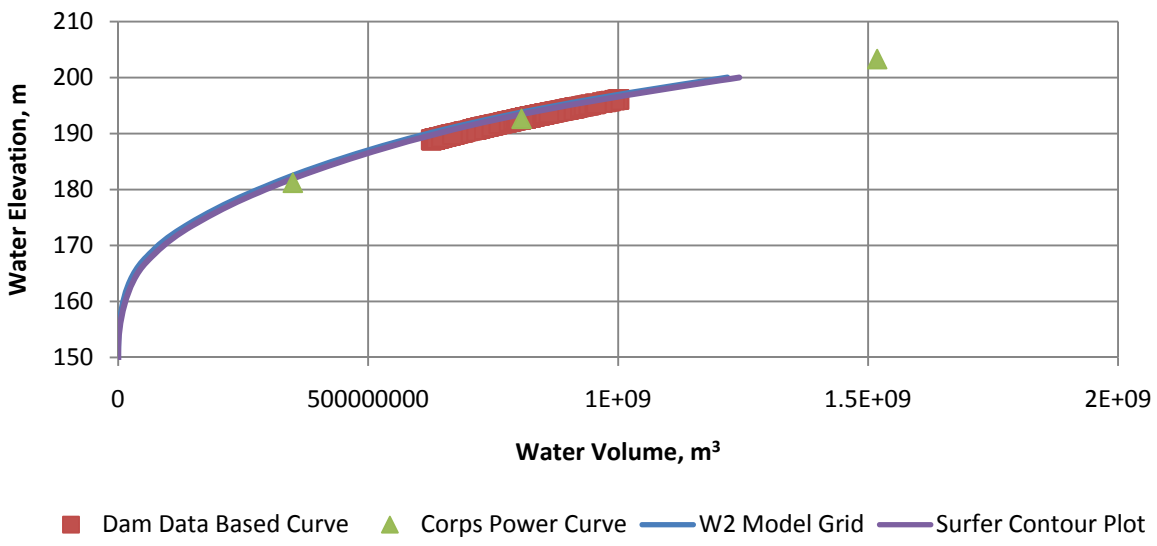

Figure 11. Tenkiller Reservoir volume – elevation curve.

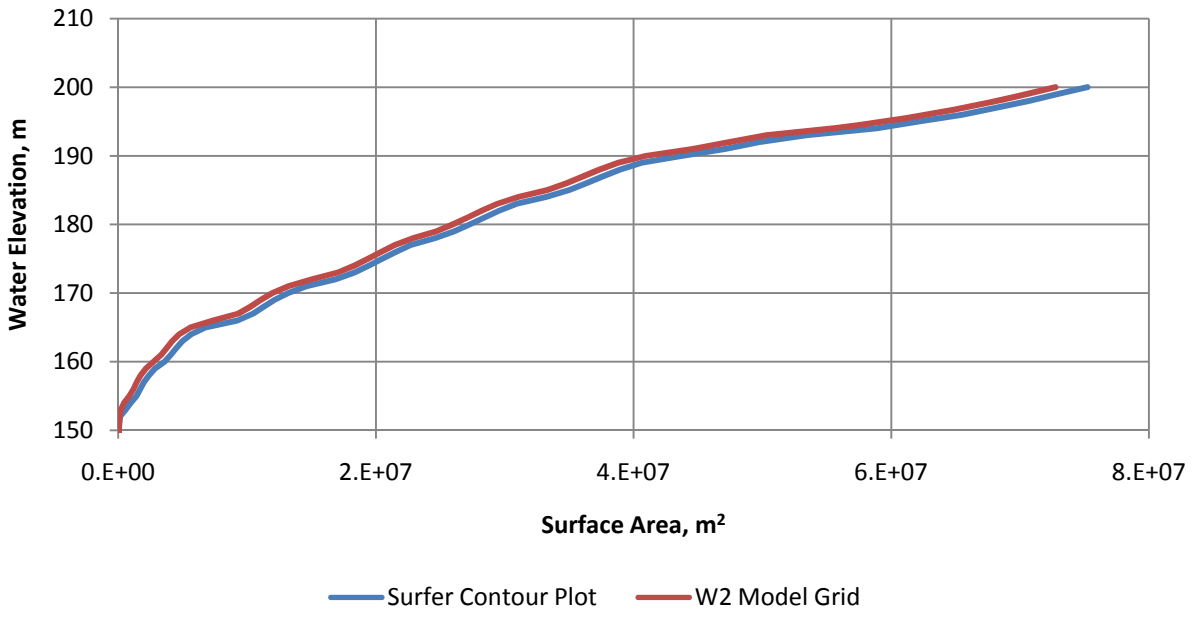

Figure 12. Tenkiller Reservoir area – elevation curve.

Tenkiller Reservoir Dam and Outlet Hydraulics

Table 4 contains an overview of important features of the dam outlets and structure. The Corps (2008) reports the following basic information on the dam itself: The dam construction was started in 1947, and by 1953 the dam was ready for operation for flood control and power generation. Next to the powerhouse (see Figure 13) a 590 ft width gravity spillway is located at the maximum water surface

elevation of 672.2 ft which is controlled by 10 50 ft X 25 ft tainter gates. By 2006, 5 new tainter gates (50 ft X 35 ft) were installed to allow passage of larger floods (see Figure 14). A 19 ft diameter penstock is the entrance conduit to the powerhouse at the base of the dam which is near the elevation of the old riverbed.

Table 4. Features of Tenkiller Reservoir dam.

Feature	Elev., ft, NGVD29	Elev., m, NGVD29	Comments
Top of dam elevation	677.2	206.4	
Maximum high water level	672.2	204.9	
Flood control pool top	667	203.3	
Flood control pool bottom	632	192.6	
Inactive pool	594.5	181.2	
Powerhouse intake centerline elevation	509	154.8	Centerline of the powerhouse intake used in the CE-QUAL-W2 model
Crest elevation of spillways	632	192.6	Crest of spillways used in the CE-QUAL-W2 model

Figure 13. Powerhouse (left) and 10 tainter gates and powerhouse at Tenkiller dam (right).

Figure 14. New spillway and tainter gates operational in 2006.

Upstream Boundary Conditions

Illinois River Inflow

Flow

Daily average discharge data were available for the Illinois River upstream of Tenkiller Reservoir from USGS Gage Station 071965000. Figure 15 shows river discharge over the model calibration period.

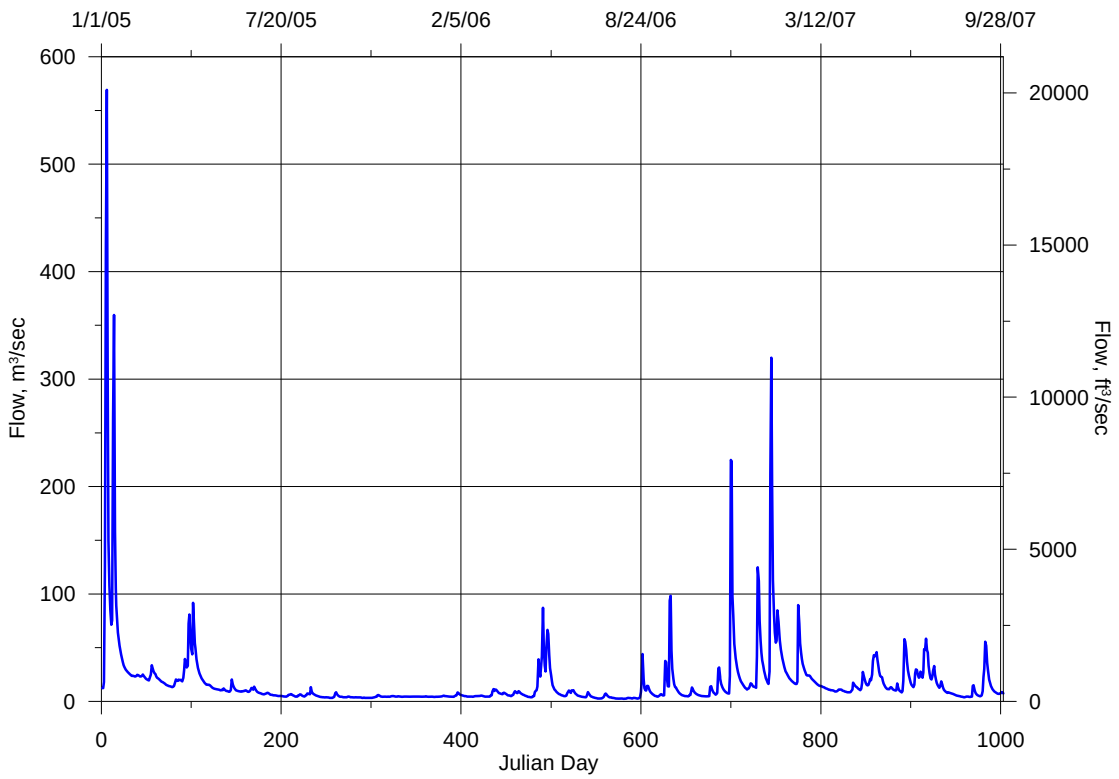

Figure 15**. Illinois River discharge - USGS Gage 071965000.**

Temperature

The inflow temperature data for Illinois River were sparse over the calibration period. A filtered equilibrium approach was used to estimate the daily inflow temperature. This approach is discussed in Appendix B.

Figure 16 shows a comparison of the theoretical inflow temperature compared to measurements. Figure 17 shows another comparison of field data compared to the filtered equilibrium approaching showing that the mean error was 0.3^{o}C and the absolute mean error was about 1.2^{o}C. This approach was deemed much better than using linear interpolation between data points.

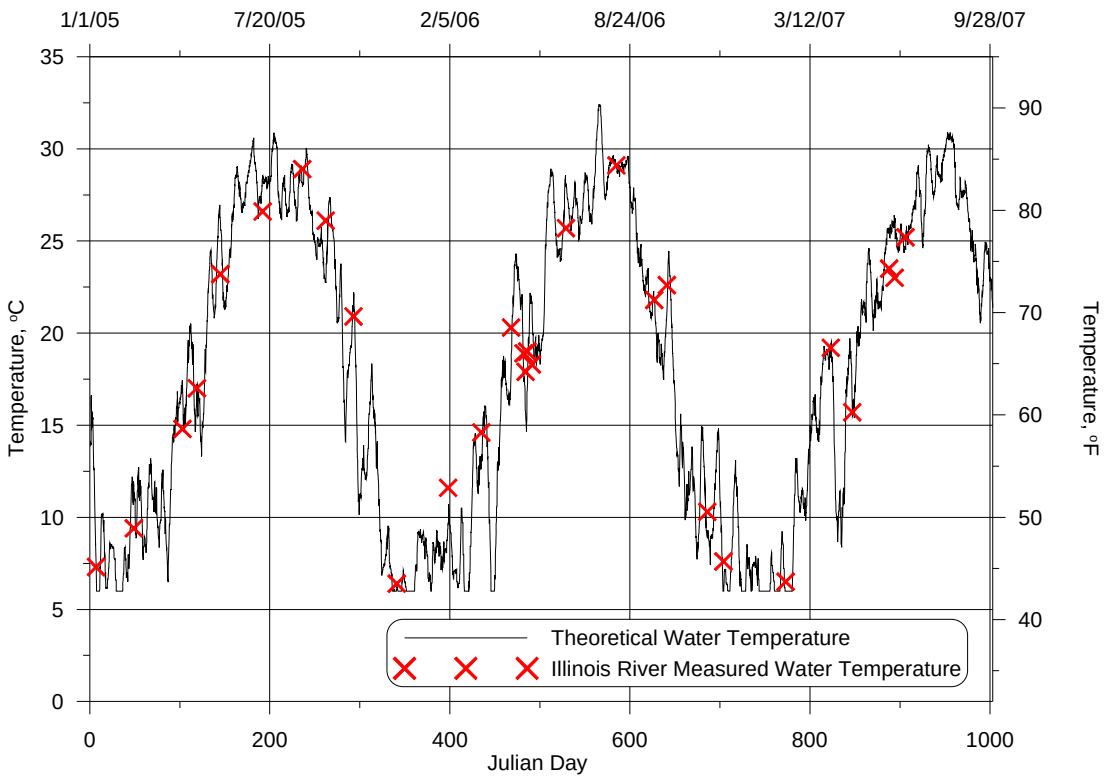

Figure 16. Illinois River water temperature during calibration period.

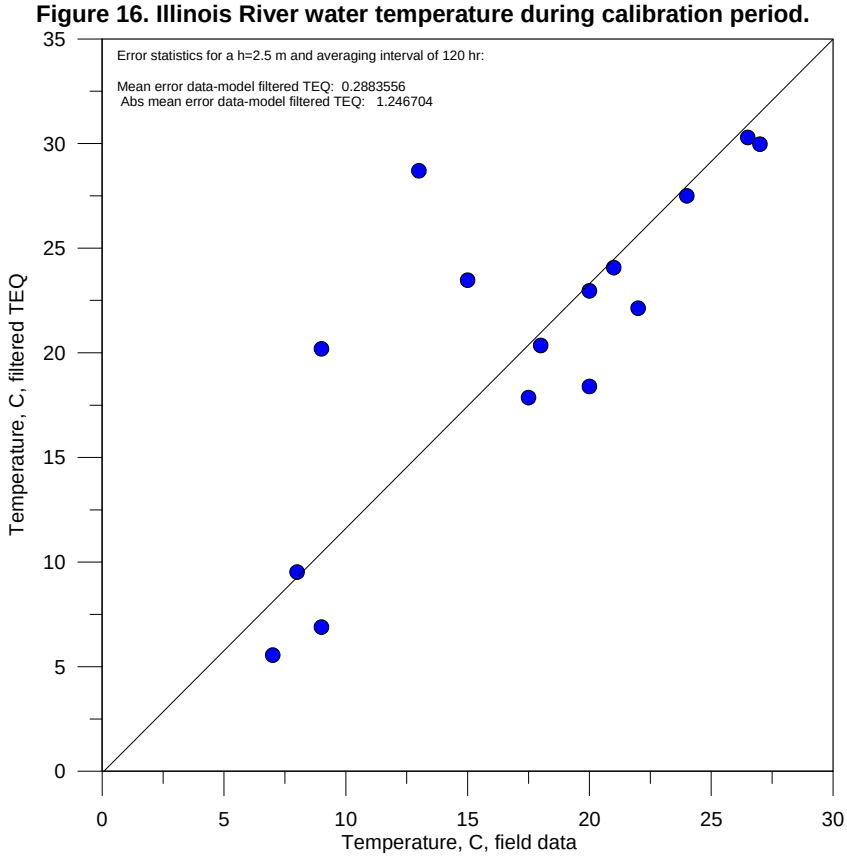

Figure 17. Comparison of measured temperature and filtered TEQ on dates/time of measurement.

Water Quality

Algae – Linear interpolation was used to estimate total chlorophyll a inflow concentrations between available measured chlorophyll a data. Since the model used dry weight algae biomass as the state variable, the inflow dry weight was estimated from chlorophyll a values. A fixed chlorophyll a to biomass ratio of 25 microgram/mg was used to calculate total algae concentrations. The total algae concentration was then divided between three algae groups using the following approach:

Between the months of June and September (based on algae field data):

ALG 1 = 0.41*(ALG TOT)

ALG 2 = 0.28*(ALG TOT)

ALG 3 = 0.31*(ALG TOT)

All other months of the year:

If ALG TOT >= 0.03 mg/L

ALG 1 = (ALG TOT) – 0.02 mg/L

ALG 2 = 0.01 mg/L

ALG 3 = 0.01 mg/L

If ALG TOT <0.03 mg/L

ALG 1 = 0.01 mg/L

ALG 2 = (ALG TOT – ALG 1)/2

ALG 3 = (ALG TOT – ALG 1)/2

Each algae group was assigned the following classification:

ALG 1: Diatoms

ALG 2: Greens and other kinds

ALG 3: Cyanobacteria

Figure 18 shows the three algae groups as calculated from chlorophyll a data available for the Illinois River.

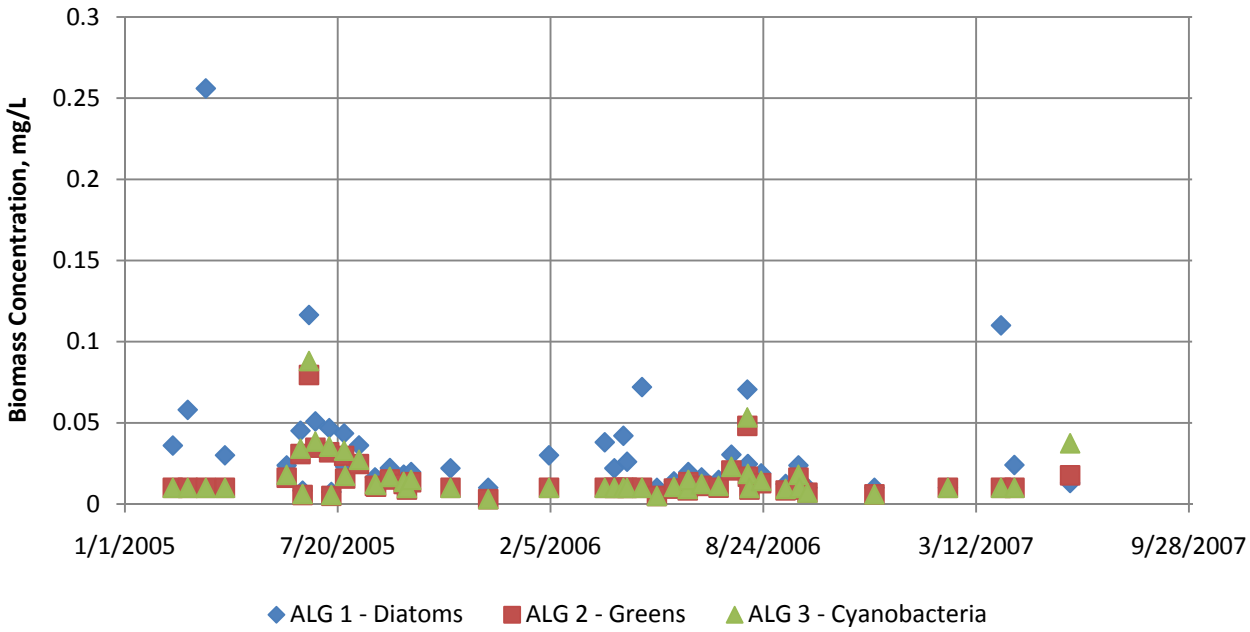

Figure 18. Illinois River algae groups during calibration period.

Ammonia (NH_4) – Linear interpolation was used to estimate ammonia concentrations between available measured data. Figure 19 shows available ammonia data for the calibration period.

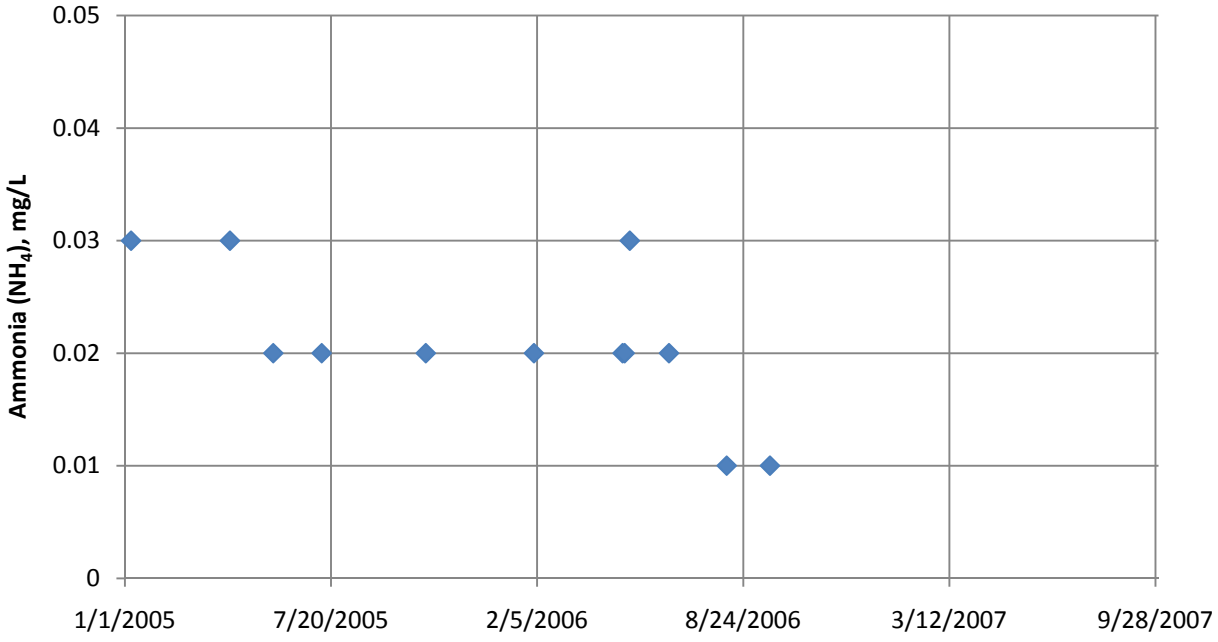

Figure 19. Illinois River ammonia data during calibration period.

Dissolved Oxygen – When available, direct measurements where used for inflow DO concentrations. In order to more accurately fill in data gaps, dissolved oxygen saturation values were calculated based upon water temperature and atmospheric pressure (elevation) using the following equation:

$$C_{sat}, \frac{mg}{l} = \exp[7.7117 - 1.31403 * (\log(Temp^{o}C + 45.93))] * P$$

$$where\ P = \left[1.0 - \frac{(Elev\ above\ sea\ level, m)}{1000} / 44.3\right]^{5.25}$$

Equation 1. Dissolved oxygen saturation value calculation.

These theoretical saturation values were then used to fill in gaps between existing dissolved oxygen data as illustrated in Figure 20. The final dissolved oxygen in the inflow boundary condition included the measured field data and interpolated between these data using the theoretical dissolved oxygen saturation. The measured data were integrated with the theoretical saturation values using a simple averaging technique within a 5 day window before and after the date of data collection.

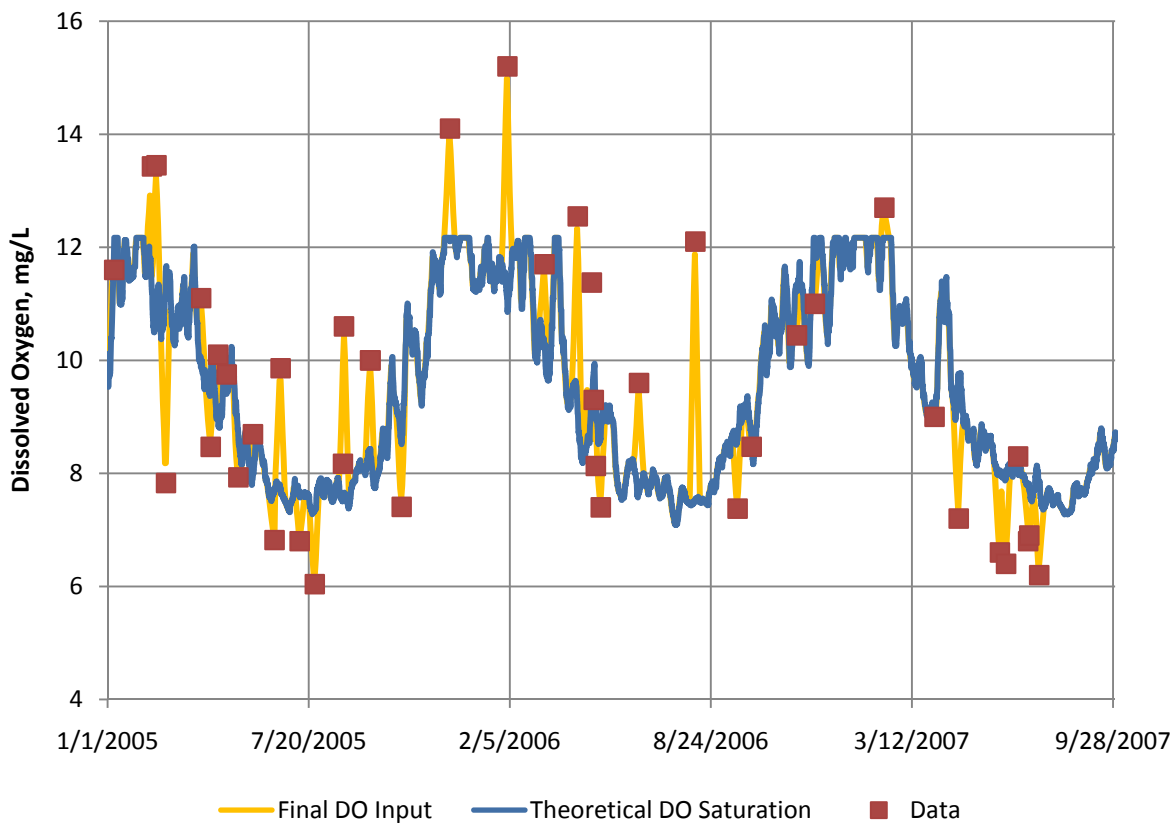

Figure 20. Illinois River dissolved oxygen during calibration period.

Inorganic Suspended Solids (ISS) – ISS was calculated based upon the following relationship to total phosphorus:

$$ISS = 956.83 * (Total\ P)^{1.8079}$$

Note: This calculation was based upon the total phosphorus regression data only.

Equation 2. Inorganic suspended solids calculation.

This relationship is based upon the regression shown in Figure 21.

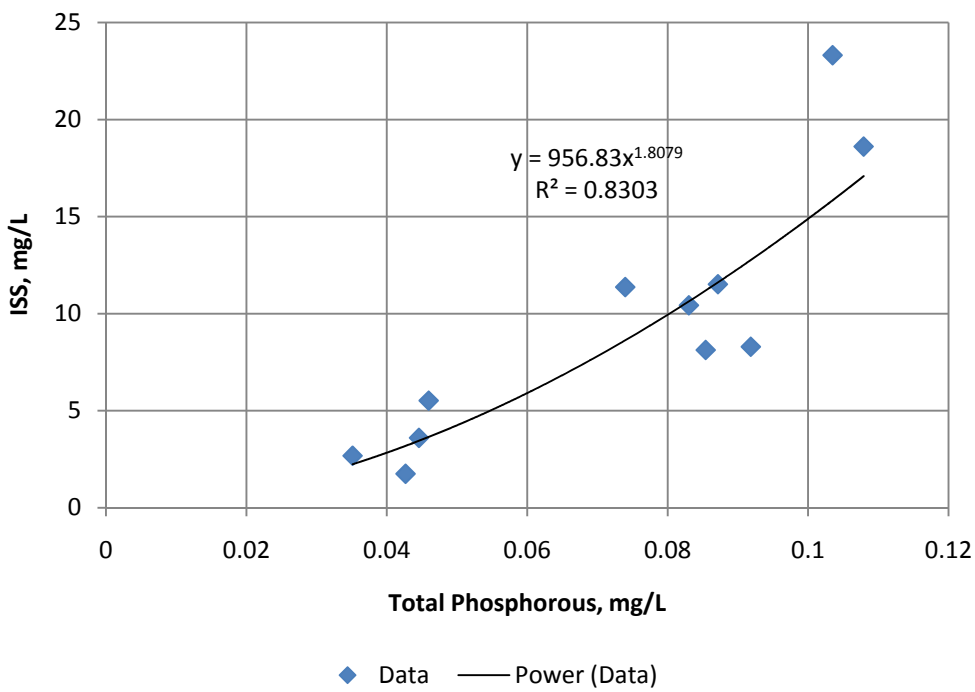

Figure 21. ISS and total phosphorus regression.

Figure 22 shows the resulting estimated ISS values for the Illinois River over the model calibration period.

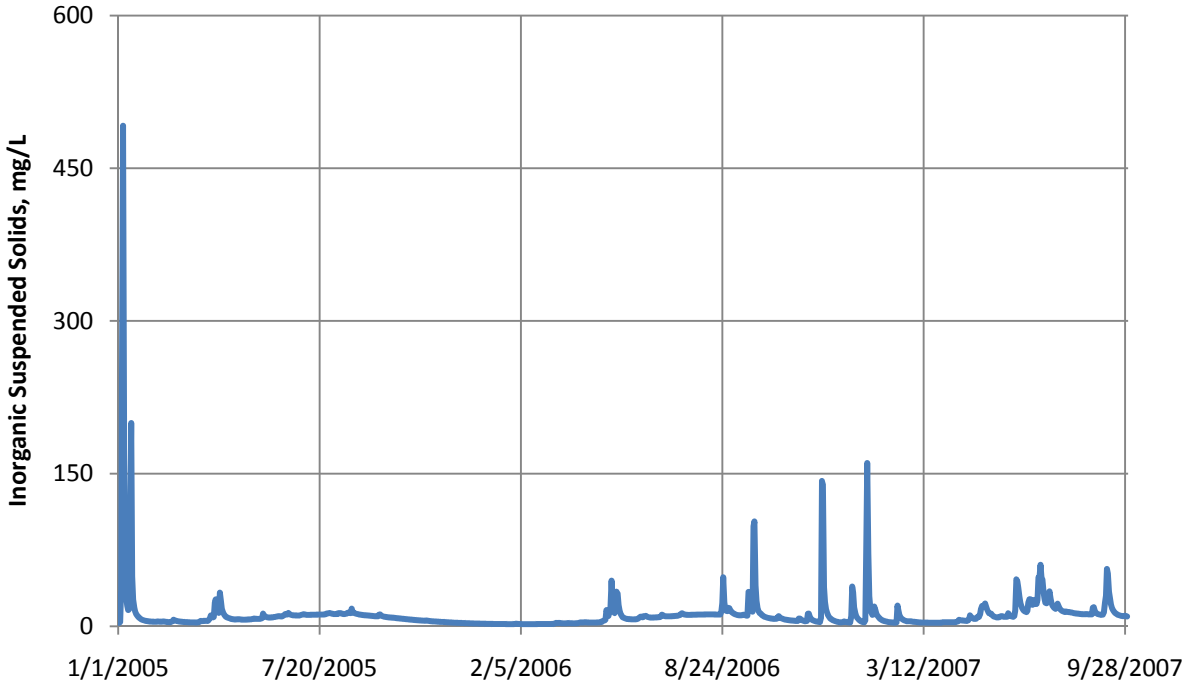

Figure 22. Illinois River estimated ISS during calibration period.

Organic Dissolved and Particulate Fractions – No direct measurements of dissolved and particulate organic fractions were available for the Illinois River. In order to estimate organic phosphorus the following equation was used:

$$Max\ Organic\ Phosphorous\ (Total\ P - Ortho\ P) - Algae\ (1.0\%\ P\ by\ weight) = Total\ Organic\ Phosphorous$$

Equation 3. Total organic phosphorus calculation.

The following ratios were assumed to relate organic phosphorus to total organics and organic nitrogen:

$$Total\ Organics : ORG\ Nitrogen : ORG\ Phosphorous\ (100:8:1)$$

These were then divided into labile dissolved (LDOM), refractory dissolved (RDOM), labile particulate (LPOM), and refractory particulate (RPOM) fractions by assuming the following ratios:

$$Total\ Organics : LDOM : RDOM : LPOM : RPOM\ (4:1:1:1:1)$$

Note: The above ratios were assumed for total, nitrogen, and phosphorus organic fractions.

Figure 23 shows the resulting organic fractions values for the model calibration period for the Illinois River. Only one of the four representative fractions was plotted for total nitrogen and total phosphorus organics.

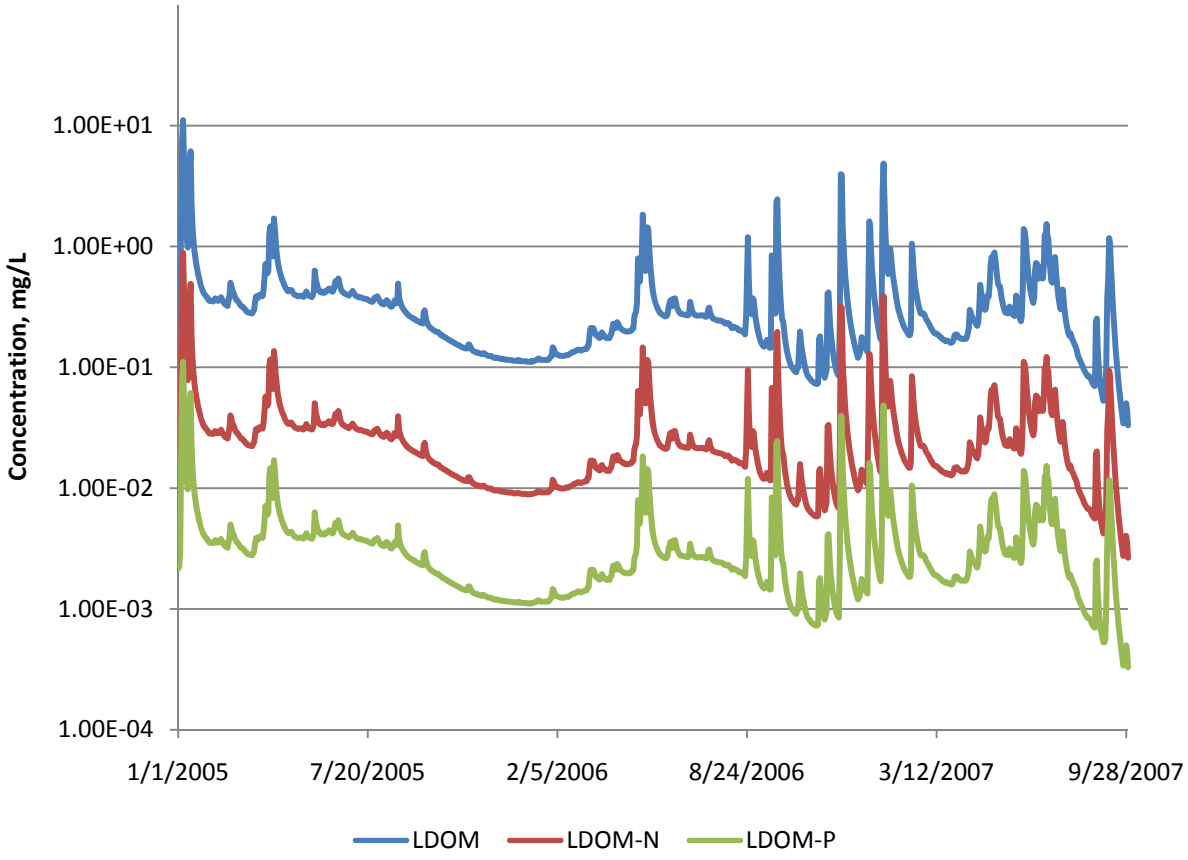

Figure 23. Illinois River organic fractions during calibration period.
Note: Y-axis is displayed as a log scale. LDOM: Labile dissolved organic matter

Nitrate/Nitrites – Linear interpolation was used to estimate nitrate+ nitrite concentrations between available measured data. Figure 24 shows available Illinois River nitrate + nitrite data for the model calibration period.

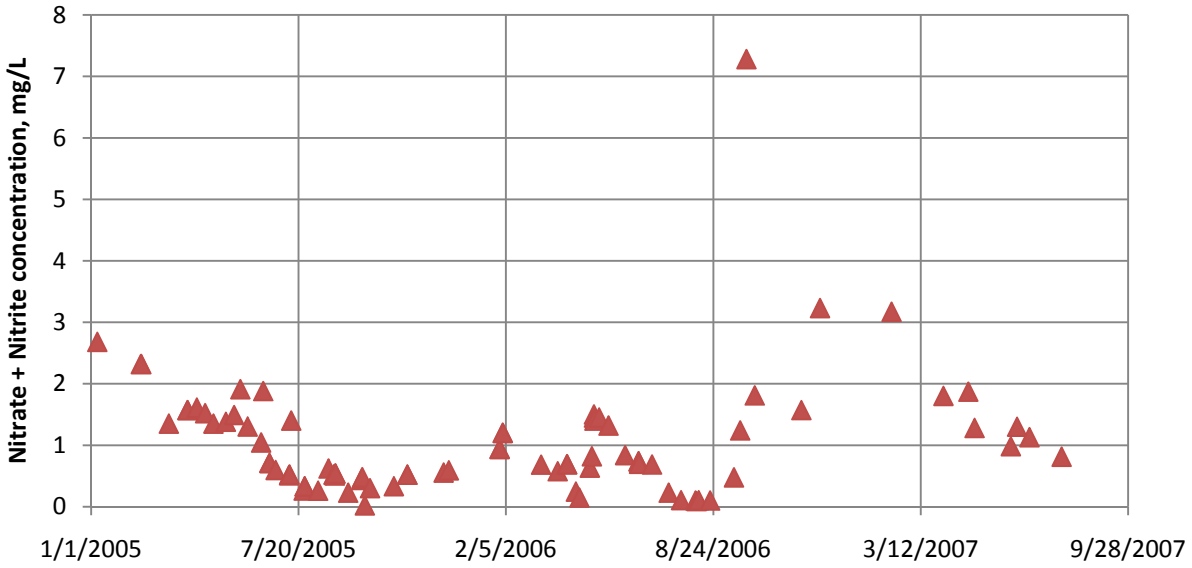

Figure 24. Illinois River nitrate + nitrite concentration during calibration period.

Ortho Phosphorus (PO_4) – When available, direct measurements were used for inflow dissolved PO_4 concentrations. When data were unavailable, ortho P correlations based on LOADEST USGS model (Pickup, et. al, 2003; Tortorelli and Pickup, 2006) to time of year and flow rate were used. Figure 25 shows the available data and final input file Illinois River ortho P concentrations. The solid blue line represents the daily inflow dissolved ortho-P used in the model, while the USGS and OWEB measured field data are shown as discrete points.

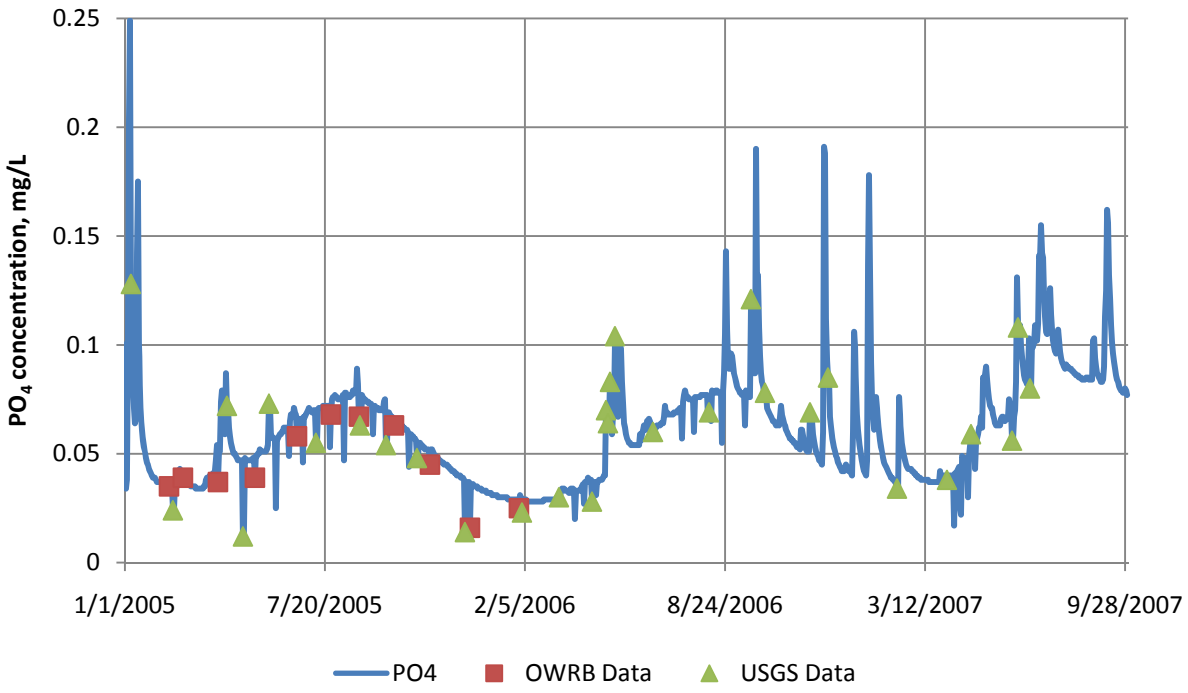

Figure 25. Illinois River ortho phosphorus concentrations during calibration period.

Baron Fork Inflow

Flow

Daily average discharge data were available for Baron Fork Creek at Eldon, OK from USGS Gage Station 07197000. Figure 26 shows stream discharge over the calibration period.

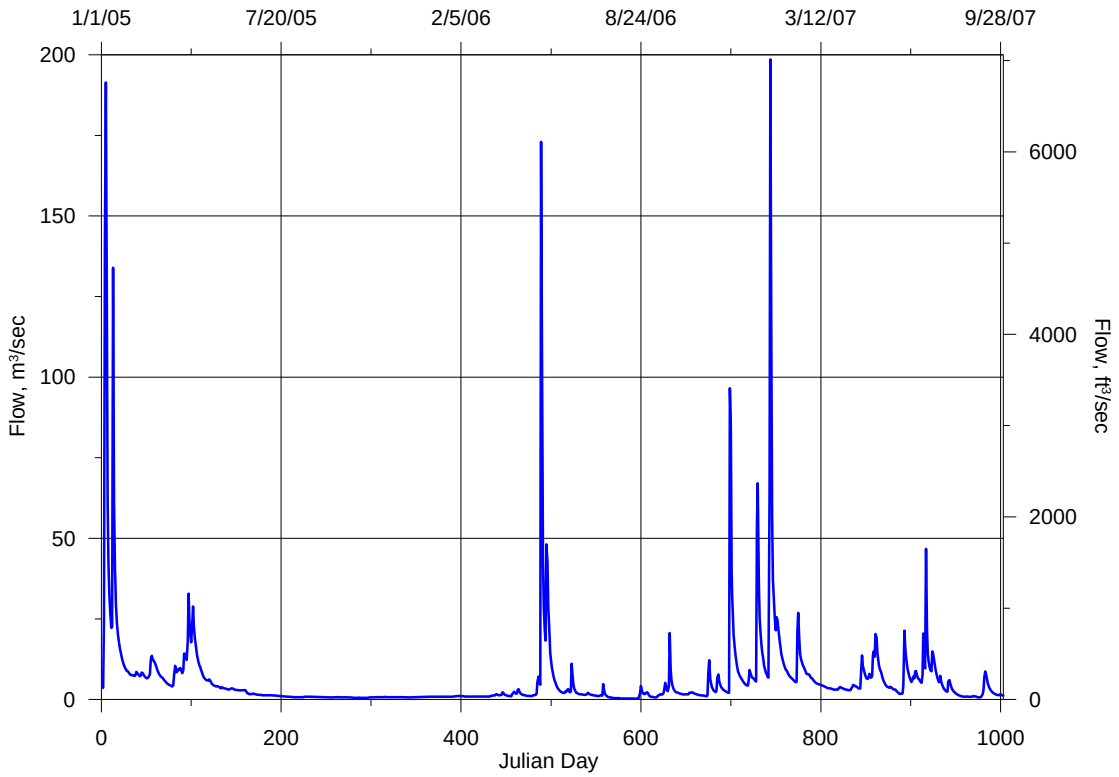

Figure 26. Baron Fork Creek discharge - USGS Gage 07197000.

Temperature

The filtered equilibrium temperature approach (see Appendix B) for the Illinois River was also used for Baron Fork. A comparison of measured temperatures and synthetic temperatures for Baron Fork are shown in Figure 27.

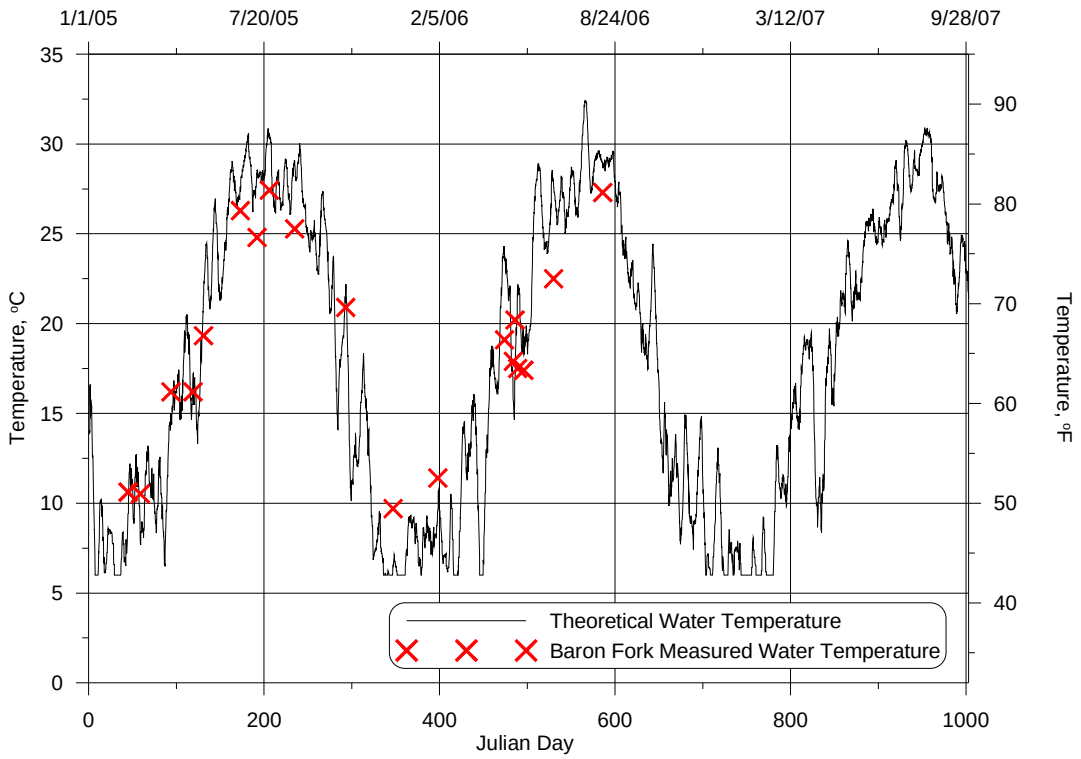

Figure 27. Baron Fork Creek water temperature during calibration period

Water Quality

Algae – Linear interpolation was used to estimate total chlorophyll a inflow concentrations between available measured chlorophyll a data for Baron Fork Creek. A fixed chlorophyll a to biomass ratio of 25 microgram/mg was used to calculate total algae concentrations. The total algae concentration was then divided between three algae groups using the conditions explained on page 20 for the Illinois River.

Figure 28 shows the three algae groups as calculated from chlorophyll a data available for Baron Fork Creek.

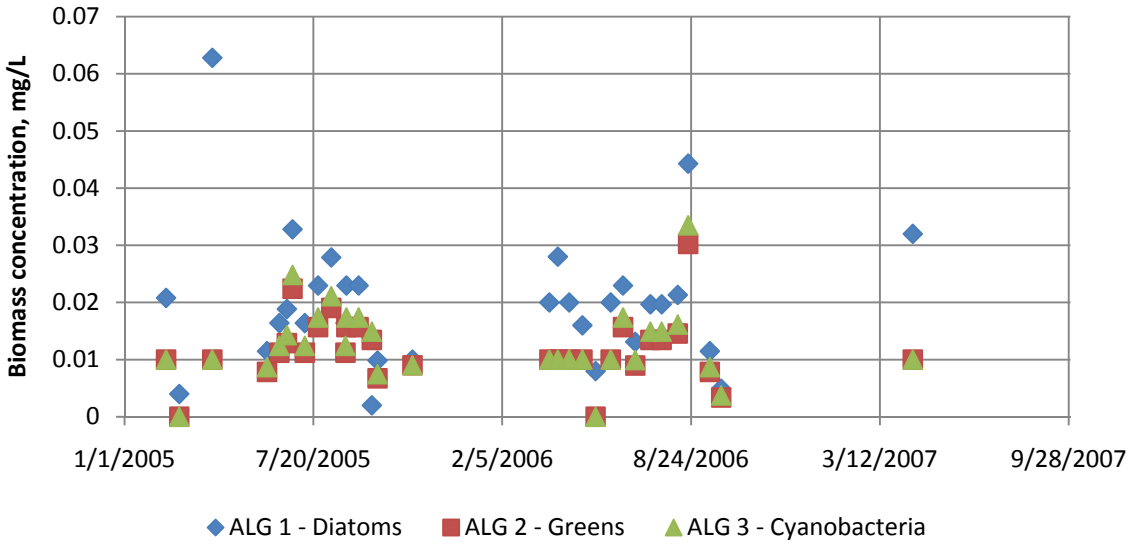

Figure 28. Baron Fork algae groups during calibration period.

Ammonia (NH_4) – All NH_4 data collected from Baron Fork Creek were measured below the detection limit of 0.05 mg/L. Hence, a constant value of 0.05 mg/l was used for the Baron Fork inflow.

Dissolved Oxygen – When available, direct measurements where used for inflow DO concentrations. In order to fill in data gaps, dissolved oxygen saturation values were calculated based upon water temperature and atmospheric pressure using Equation 1 (see page 22). Figure 29 shows the available DO data as discrete points, theoretical saturation values (solid blue line), and the final DO input combining these two data sets (the blue line + the gold line).

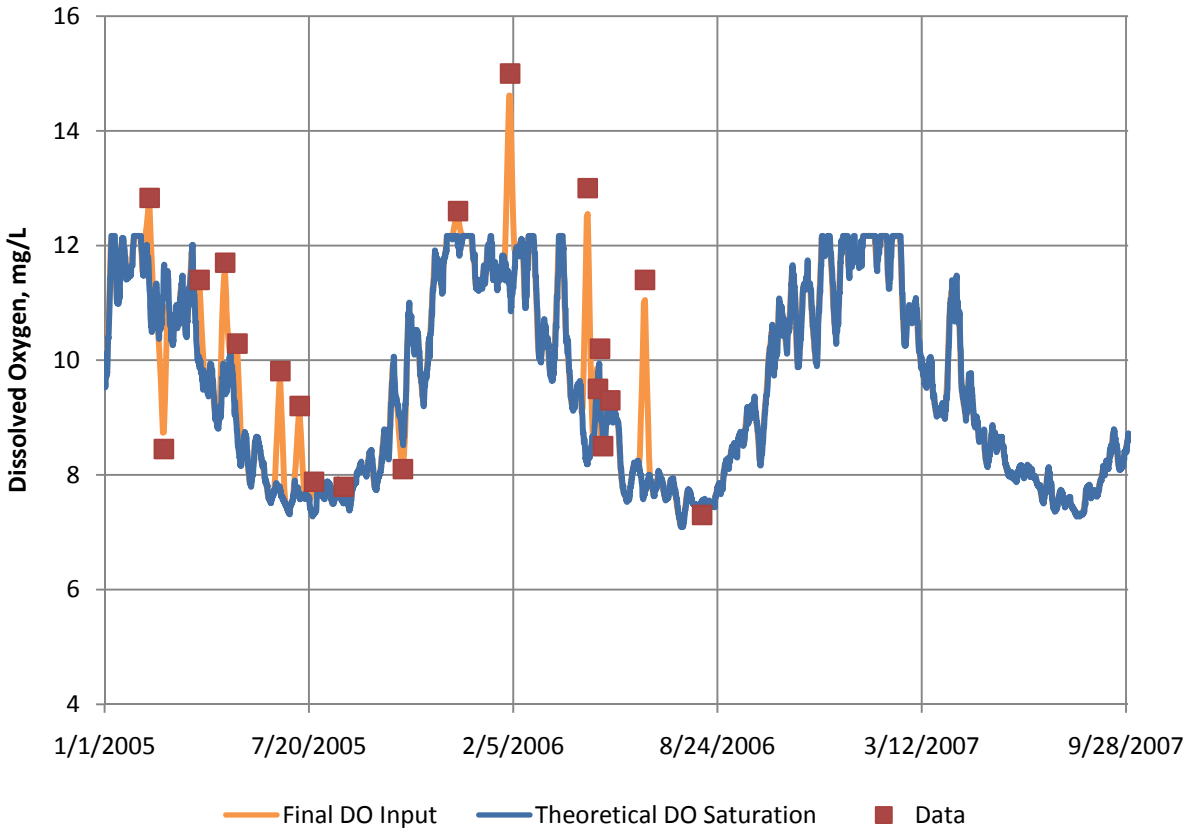

Figure 29. Baron Fork Creek dissolved oxygen during calibration period.

Inorganic Suspended Solids (ISS) – ISS was calculated based upon its relationship to total phosphorus shown in Equation 2 on page 23. Figure 30 shows the estimated ISS for Baron Fork Creek over the calibration period.

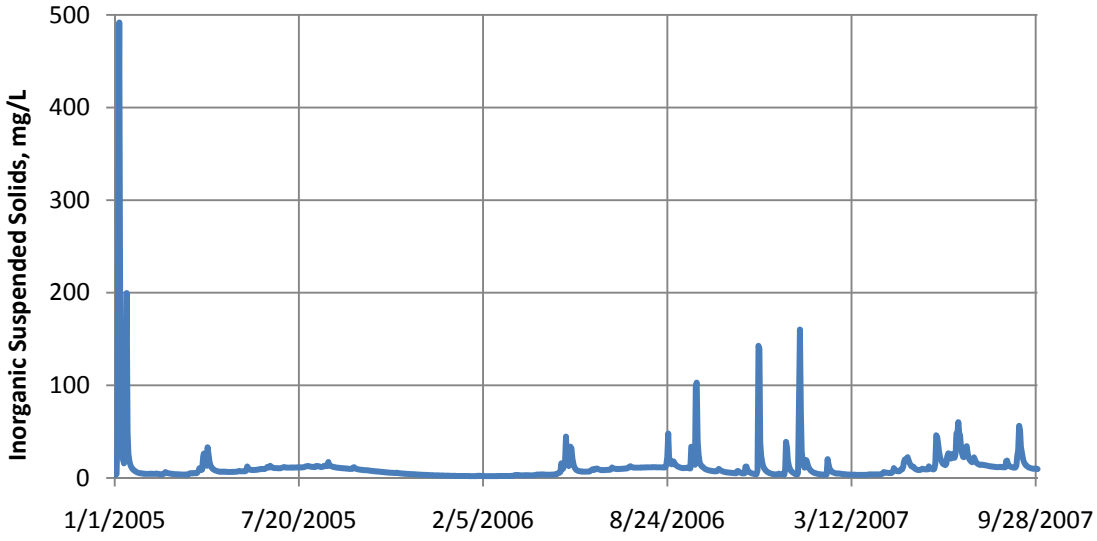

Figure 30. Baron Fork Creek estimated ISS during calibration period.

Organic Dissolved and Particulate Fractions – As was the case with the Illinois River, no direct measurements of dissolved and particulate organic fractions were available for Baron Fork Creek. In order to estimate organic phosphorus the same approach was used as had been used for the Illinois River.

Figure 31 shows the resulting organic fractions values for the model calibration period for Baron Fork Creek. Only one of the four representative fractions was plotted for total, nitrogen, and phosphorus organics.

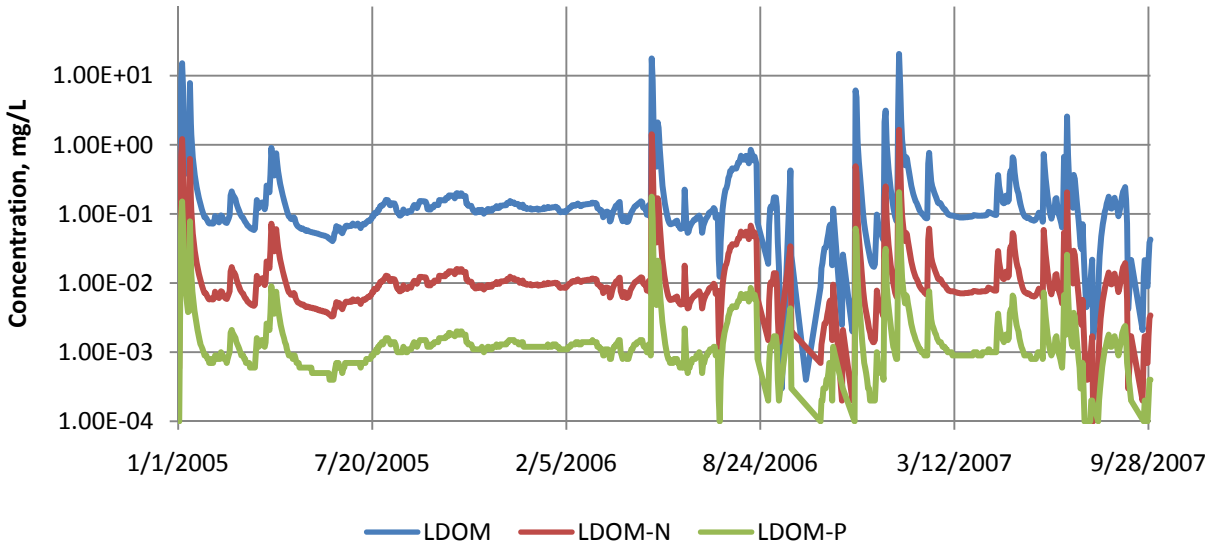

Figure 31. Illinois River organic fractions during calibration period.
Note: Y-axis is displayed as a log scale. LDOM: labile dissolved organic matter

Nitrate/Nitrites – Linear interpolation was used to estimate nitrate+ nitrite concentrations between available measured data. Figure 24 shows available Illinois River nitrate + nitrite data for the model calibration period.

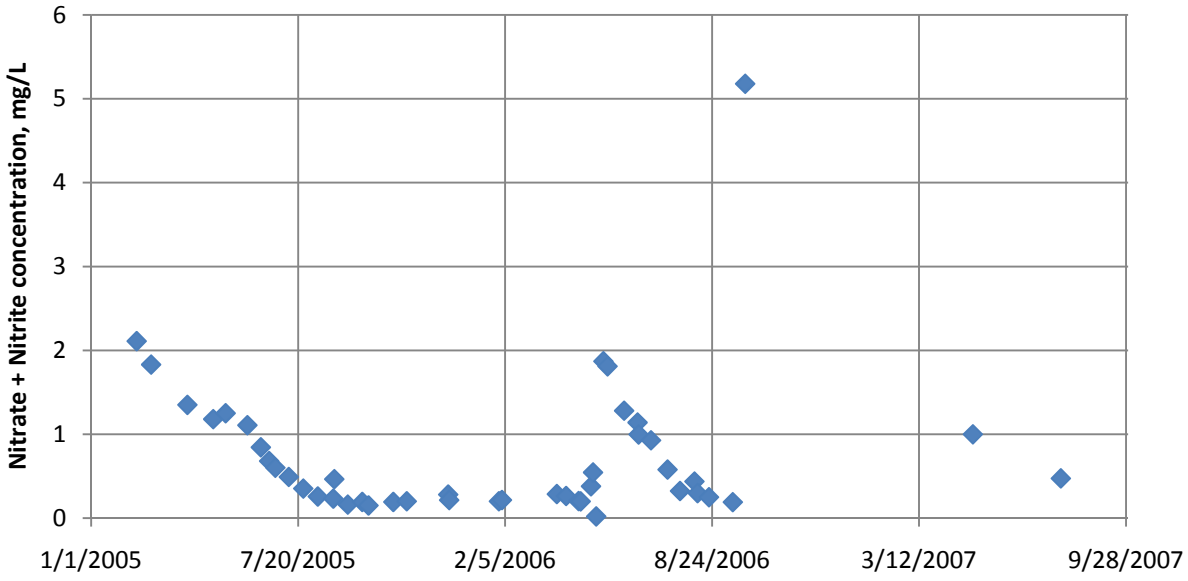

Figure 32. Baron Fork Creek nitrate + nitrite concentration during calibration period.

Ortho Phosphorus (PO_4) – When available, direct measurements were used for inflow PO_4 concentrations. When data were unavailable, ortho P correlations based on LOADEST USGS model (Pickup, et. al, 2003; Tortorelli and Pickup, 2006) to time of year and flow rate were used. Figure 33 shows the available data as discrete points and daily average value used for the inflow Baron Fork Creek ortho P concentrations as a blue continuous line.

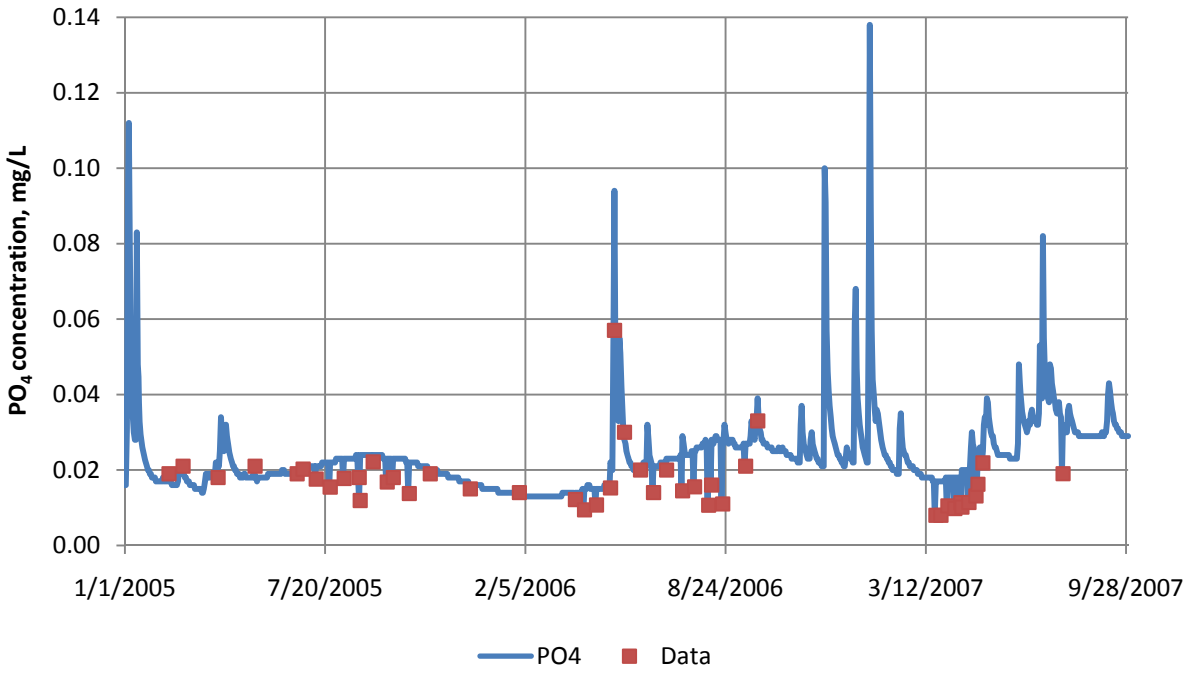

Figure 33. Baron Fork Creek ortho phosphorus concentrations during calibration period.

Caney Creek Inflow

Flow

Daily average discharge data were available for Caney Creek from USGS Gage Station 07197360. Figure 34 shows stream discharge over the calibration period.

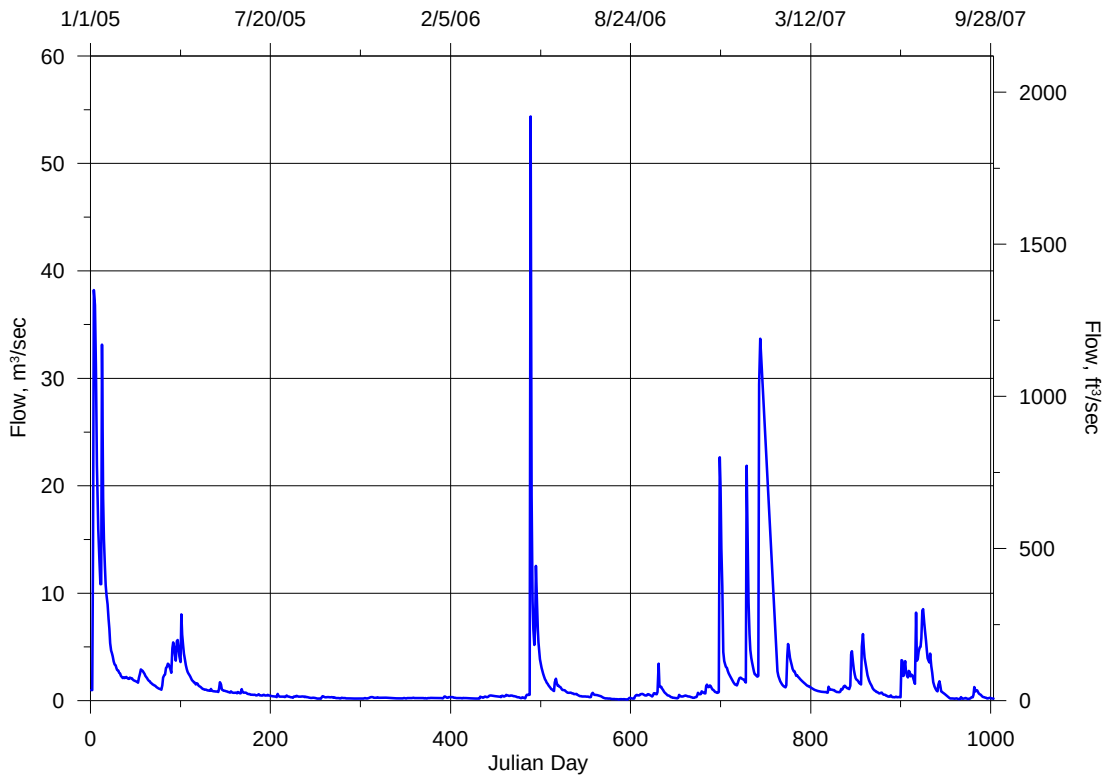

Figure 34. Caney Creek discharge - USGS Gage 07197360.

Temperature

The filtered equilibrium temperature approach (see Appendix B) for the Illinois River was also used for Caney Creek. A comparison of measured temperatures and synthetic temperatures for Caney Creek are shown in Figure 35.

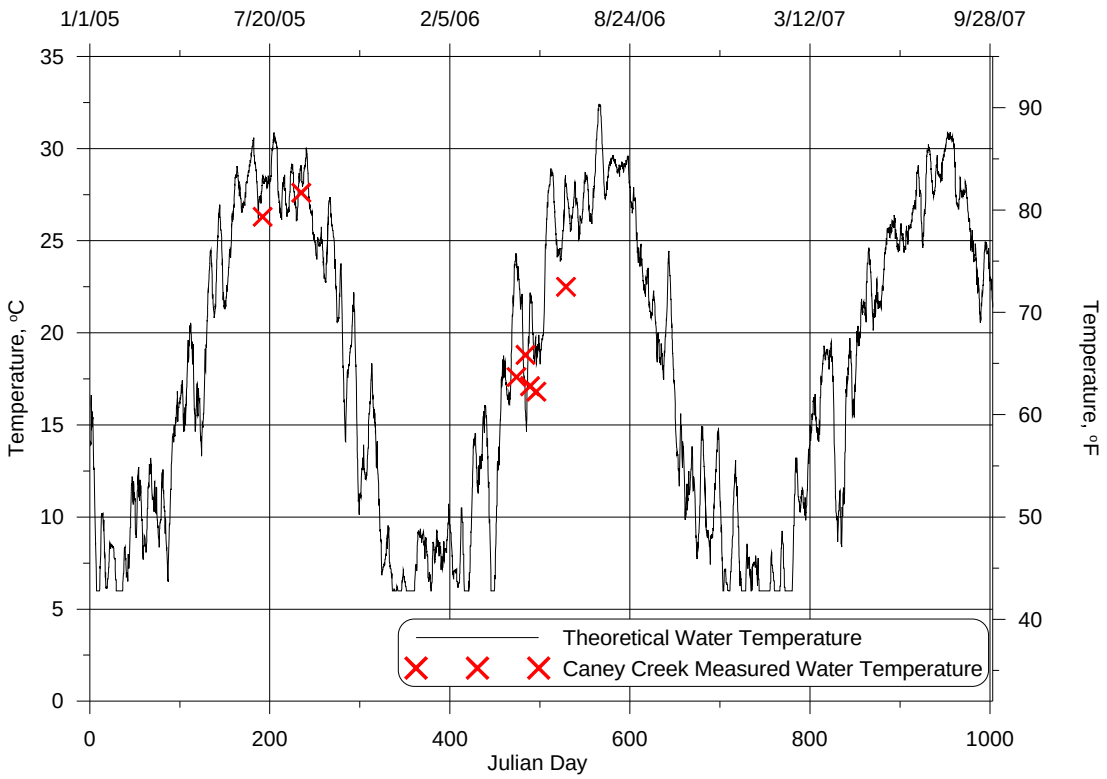

Figure 35. Caney Creek water temperature during calibration period.

Water Quality

Algae – Linear interpolation was used to estimate total chlorophyll a inflow concentrations between available measured chlorophyll a data for Caney Creek. A fixed chlorophyll a to biomass ratio of 25 microgram/mg was used to calculate total algae concentrations. The total algae concentration was then divided between three algae groups using the conditions explained on page 20 for the Illinois River. Figure 36 shows the three algae groups as calculated from chlorophyll a data available for Caney Creek.

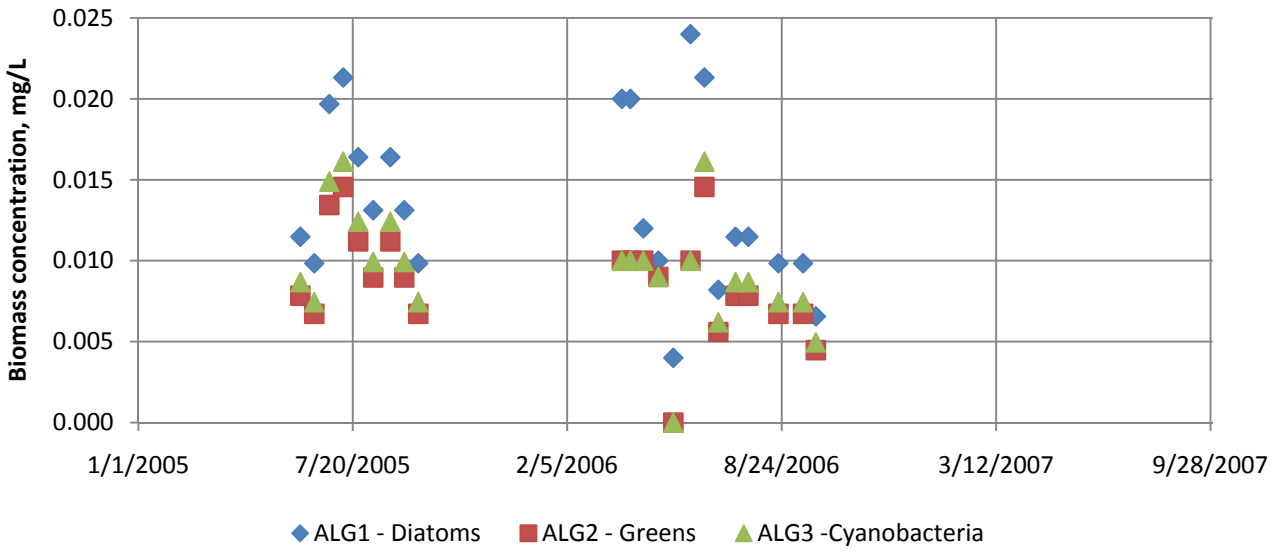

Figure 36. Caney Creek algae groups during calibration period.

Ammonia (NH_4) – No NH_4 data were available for Caney Creek. An average value of 0.05 mg/L was assumed for the duration of the calibration period.

Dissolved Oxygen – When available, direct measurements from Caney Creek where used for inflow DO concentrations. In order to more accurately fill in data gaps, dissolved oxygen saturation values were calculated based upon water temperature and pressure using Equation 1 (See page 22). Figure 37 shows the available DO data as discrete points, theoretical saturation values as a continuous blue line, and the DO used for the Caney Creek inflow combining the data and estimated saturation values (the blue line + the gold line).

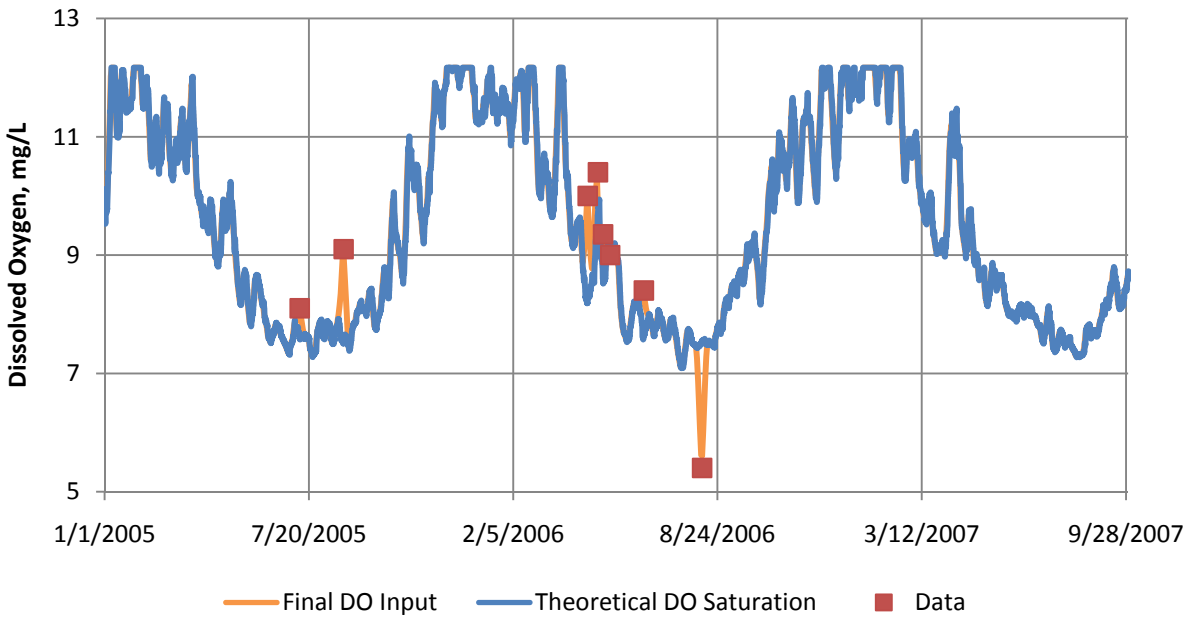

Figure 37. Caney Creek dissolved oxygen during calibration period.

Inorganic Suspended Solids (ISS) – ISS was calculated based upon its relationship to total phosphorus shown in Equation 2 on page 23. Figure 38 shows the estimated ISS for Caney Creek over the calibration period.

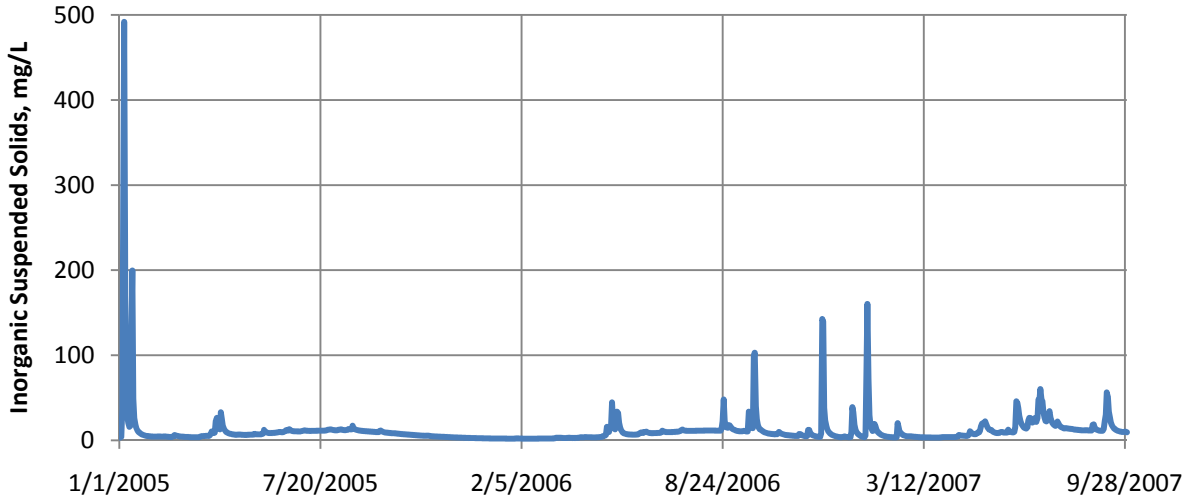

Figure 38. Caney Creek estimated ISS during calibration period.

Organic Dissolved and Particulate Fractions – As was the case with the Illinois River, no direct measurements of dissolved and particulate organic fractions were available for Caney Creek. In order to estimate organic phosphorus the same approach was used as had been used for the Illinois River (see page 23.)

Figure 39 shows the resulting dissolved labile organic matter (LDOM) fractions values for the model calibration period for Caney Creek. A similar approach was used for the particulate and refractory fractions.

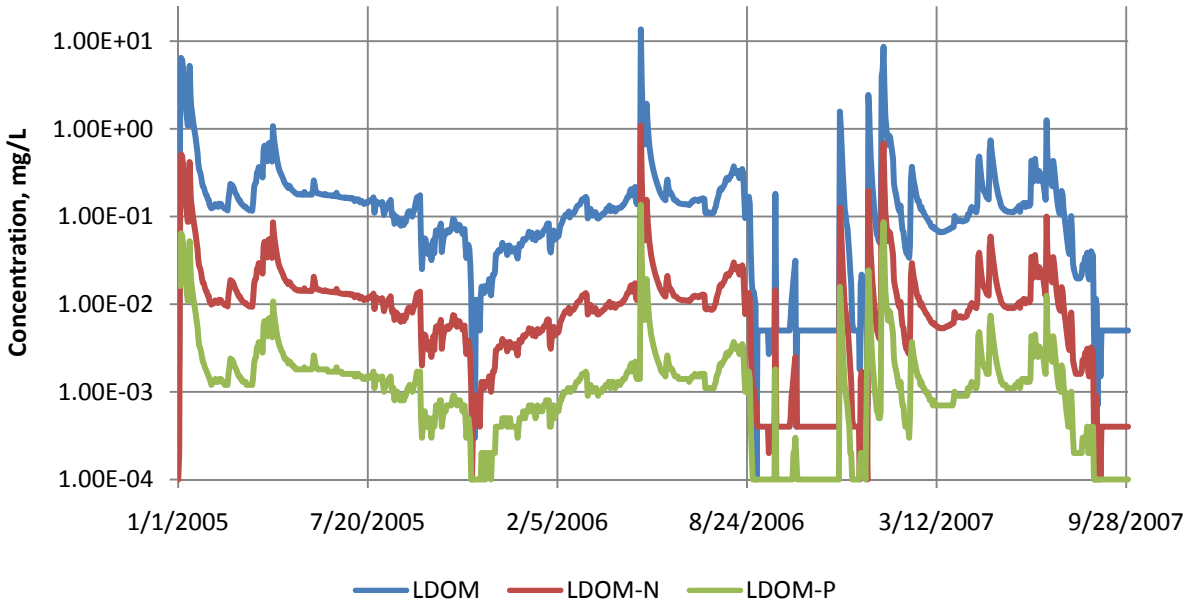

Figure 39. Caney Creek organic fractions during calibration period.
Note: Y-axis is displayed as a log scale. LDOM: labile dissolved organic matter

Nitrate/Nitrites – Linear interpolation was used to estimate nitrate+ nitrite concentrations between available measured data. Figure 40 shows available Illinois River nitrate + nitrite data for the model calibration period.

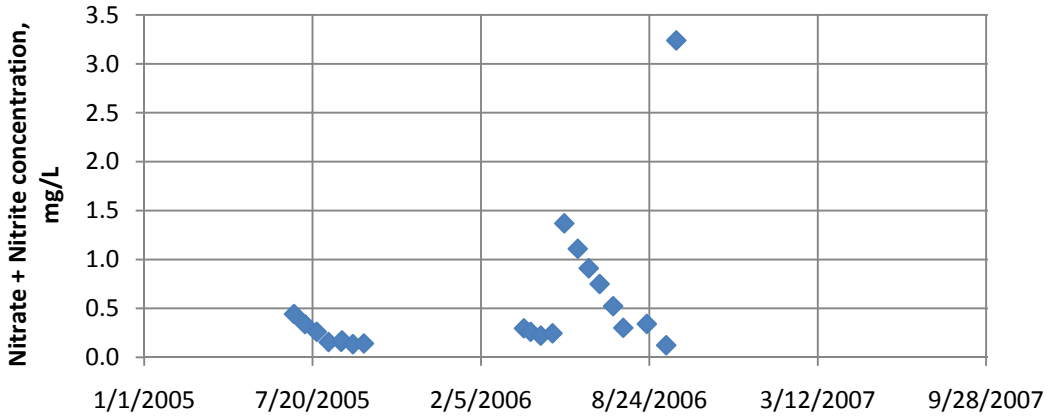

Figure 40. Caney Creek nitrate + nitrite concentration during calibration period.

Ortho Phosphorus (PO_4) – When available, direct measurements were used for inflow PO_4 concentrations. When data were unavailable, ortho P correlations based on LOADEST USGS model (Pickup, et. al, 2003; Tortorelli and Pickup, 2006) to time of year and flow rate were used. Figure 41 shows the data as discrete points and concentrations used for Caney Creek as the blue solid line. As shown in the figure, whenever measured data were available, field data were used in the inflow to the model.

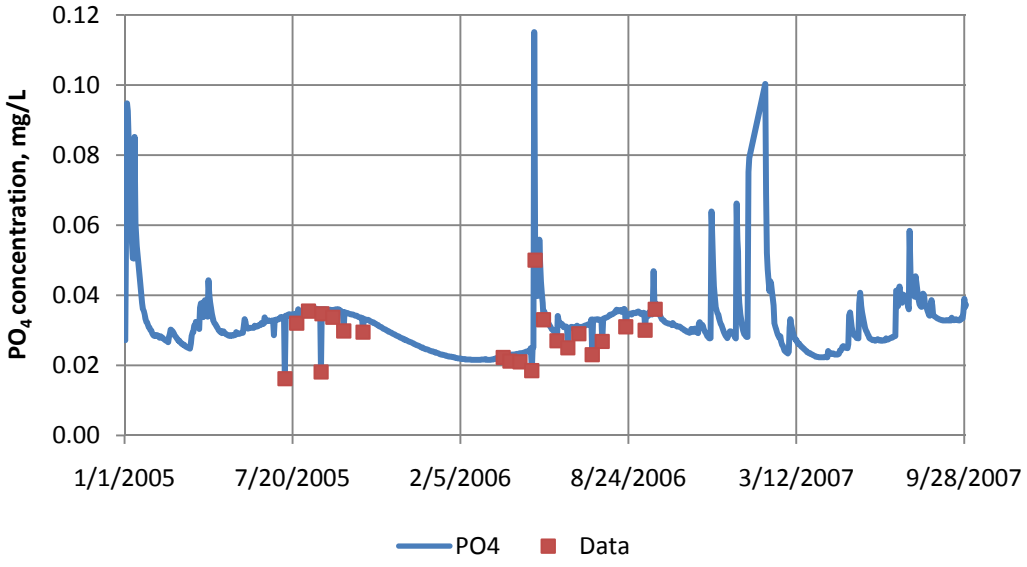

.

Figure 41. Caney Creek ortho phosphorus during calibration period.

Other Tributaries

Flow

Tenkiller Reservoir is fed by a number of smaller ungaged streams in addition to the Illinois, Baron Fork and Caney Creek. Because no flow data were available for these smaller tributaries, it was necessary to estimate their combined flow by using a flow balance. Also, there are water withdrawals along Tenkiller reservoir that are for municipal and agricultural use. Since these withdrawals were not always clearly known, these withdrawals were also included the in overall distributed inflow (or outflow).

The total inflow to the reservoir was estimated using water levels at the dam and gauged outflow data. The known (gauged) inflows were then subtracted from the total inflow to estimate the combined inflow (or outflow) of the ungaged streams and water withdrawals. This flow was classified as a distributed flow and dispersed evenly over the surface of the lake and was both positive and negative.

After the four inflow files were created, a water balance was conducted to determine if all the inflows and outflows had been properly accounted for and if the model was reproducing measured water levels.

The Inflow corrections were averaged over periods of one month and added to the distributed inflow file. The distributed tributary flow file was then smoothed to reduce large negative or positive flows. Figure 42 shows the final distributed tributary flow before and after smoothing.

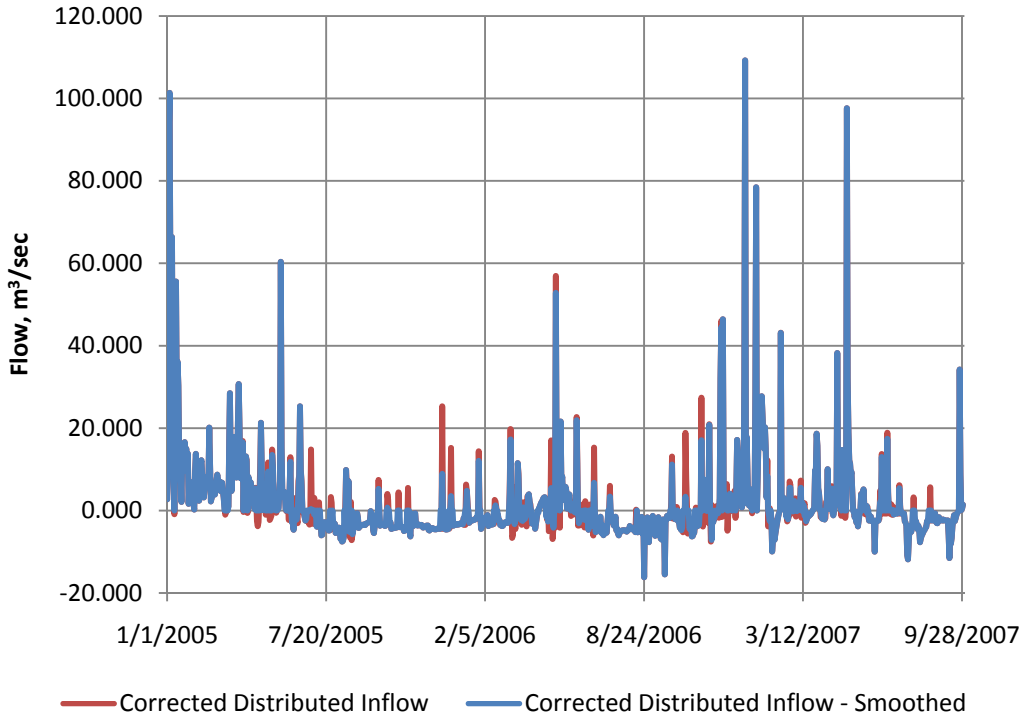

Figure 42. Distributed tributary Inflow during calibration period.

Temperature

Temperature data from the Illinois River were used to estimate water temperature for the distributed tributary inflow. (See page 18.)

Water Quality

Water quality data from Caney Creek were used to estimate water quality parameters for the distributed tributary inflow. (See page 38.)

Reservoir Water Level

Water level data were measured at the dam at midnight and 8 am over the study period. A plot of these water levels over time in Figure 43 show little difference between the midnight and 8 am reading. The midnight water level data were used as a comparison to model predictions (see Calibration section).

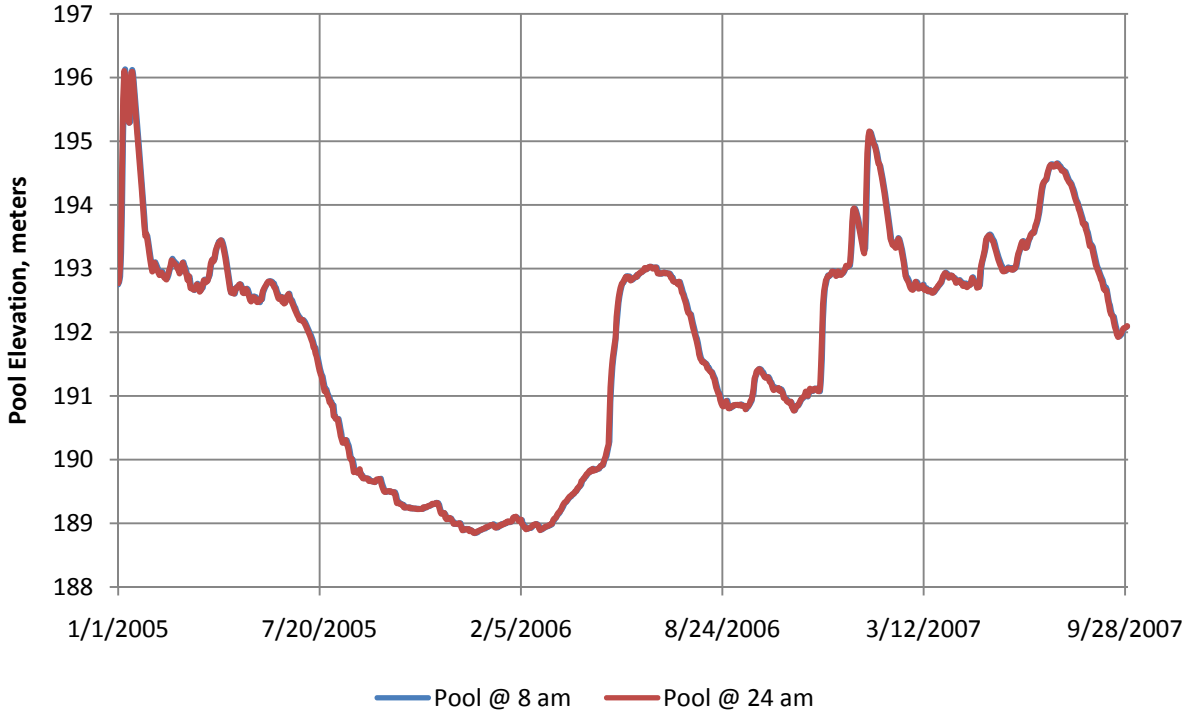

Figure 43. Pool elevations at Tenkiller Dam during calibration period.

Downstream Boundary Conditions

The downstream boundary conditions for the reservoir model consist of outflows from the dam water flow. Records are available for total outflow and water released through the powerhouse. There are also 2 spillway structures and a release for downstream minimum or base flows. "Seepage" or minimum release flows were based upon observed minimum values in the total outflow data provided by the Army Corps of Engineers. For the 2005 to 2007 period the maximum base flow was about 2.5 cubic meters per second.

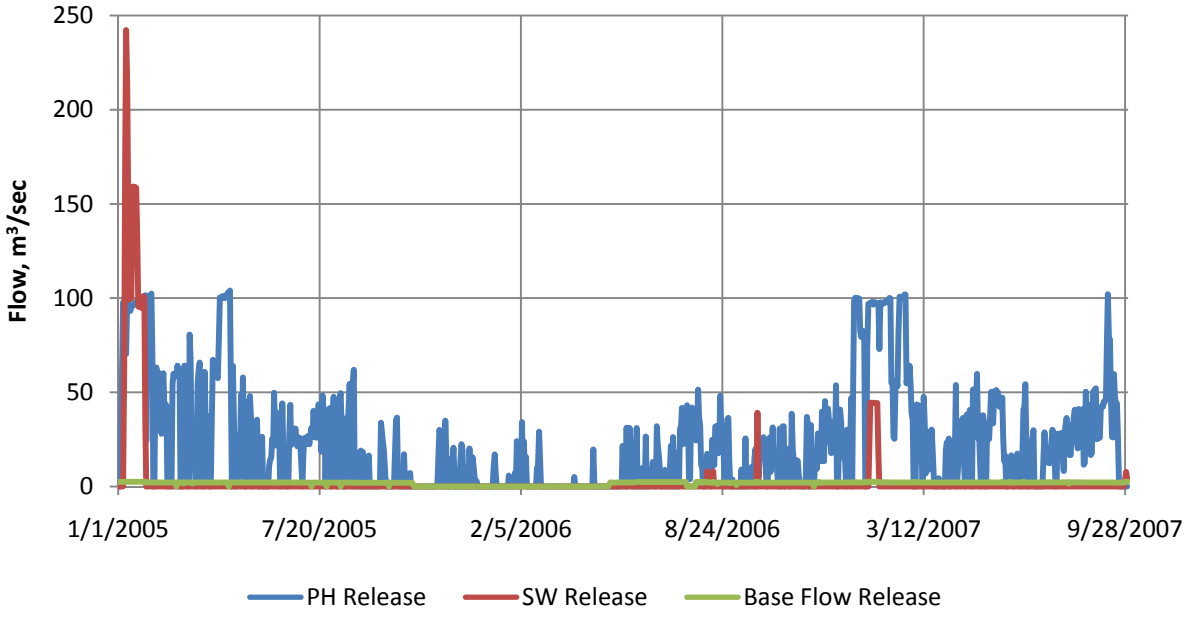

Figure 44. Outflows from Tenkiller Reservoir during calibration period.

Meteorological Data

The CE-QUAL-W2 model requires meteorological inputs such as air temperature, dew point temperature, wind speed and direction, cloud cover, and solar radiation. Two meteorological stations, located at Cookson, OK and at the Tulsa International Airport, OK, were used to estimate conditions on Tenkiller Reservoir. Figure 45 shows the locations of these two sites in relation to Tenkiller Reservoir.

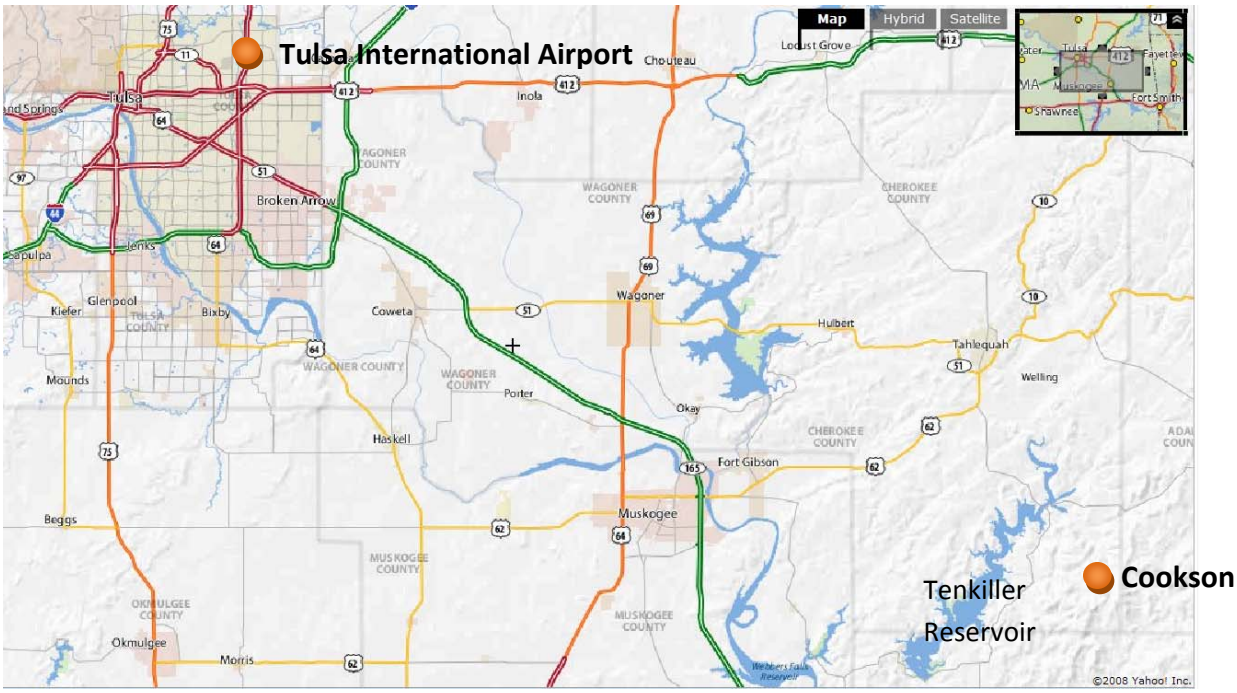

Figure 45. Location of meteorological stations.

Map from Yahoo! Inc.

Air and Dew Point Temperature

Figure 46 and Figure 47 show air temperature at Cookson, OK and Tulsa International Airport, respectively, for the duration of the calibration period. Figure 48 and Figure 49 show dew point temperature at Cookson, OK and Tulsa International Airport, respectively, for the duration of the calibration period. Figure 50 and Figure 51 show relative humidity at Cookson, OK and Tulsa International Airport, respectively, for the duration of the calibration period. The proximity of Cookson to Tenkiller Reservoir suggests that temperature, dew point, and relative humidity data from this site are likely to be a better estimate of conditions on the lake than that collected at Tulsa International Airport. However, due to the limited time of record for meteorological data at Cookson (available for this three year period only) it was necessary to compare and create correlations between the two concurrent data sets to allow for more extended model runs. Figure 52, Figure 53, and Figure 54 show the best fit linear correlations between data collected at Cookson and Tulsa International Airport for air temperature, dew point temperature, and relative humidity respectively.

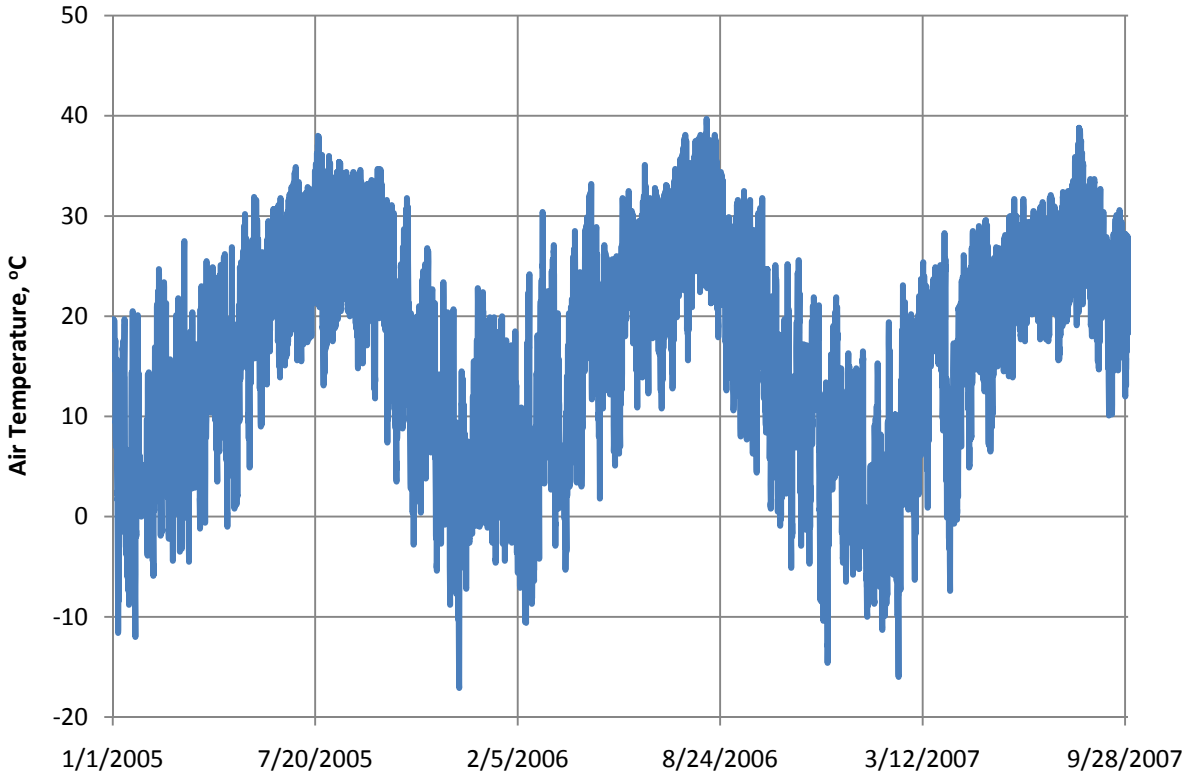

Figure 46. Air temperature at Cookson during calibration period.

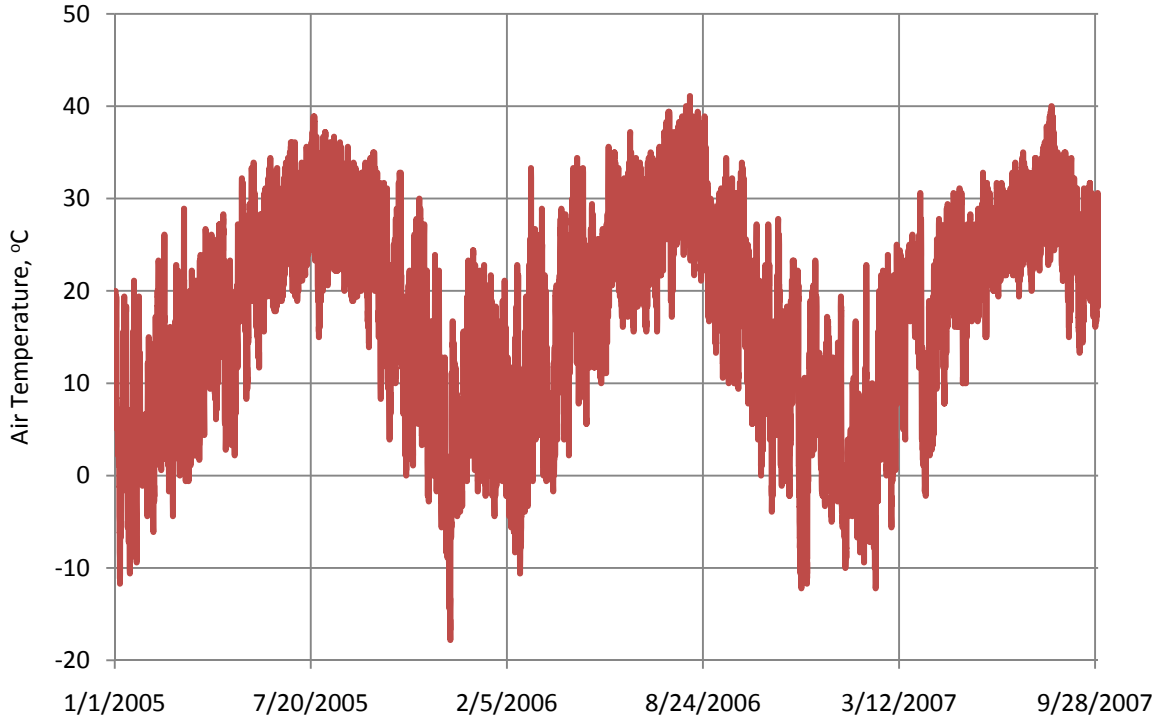

Figure 47. Air temperature at Tulsa International Airport during calibration period.

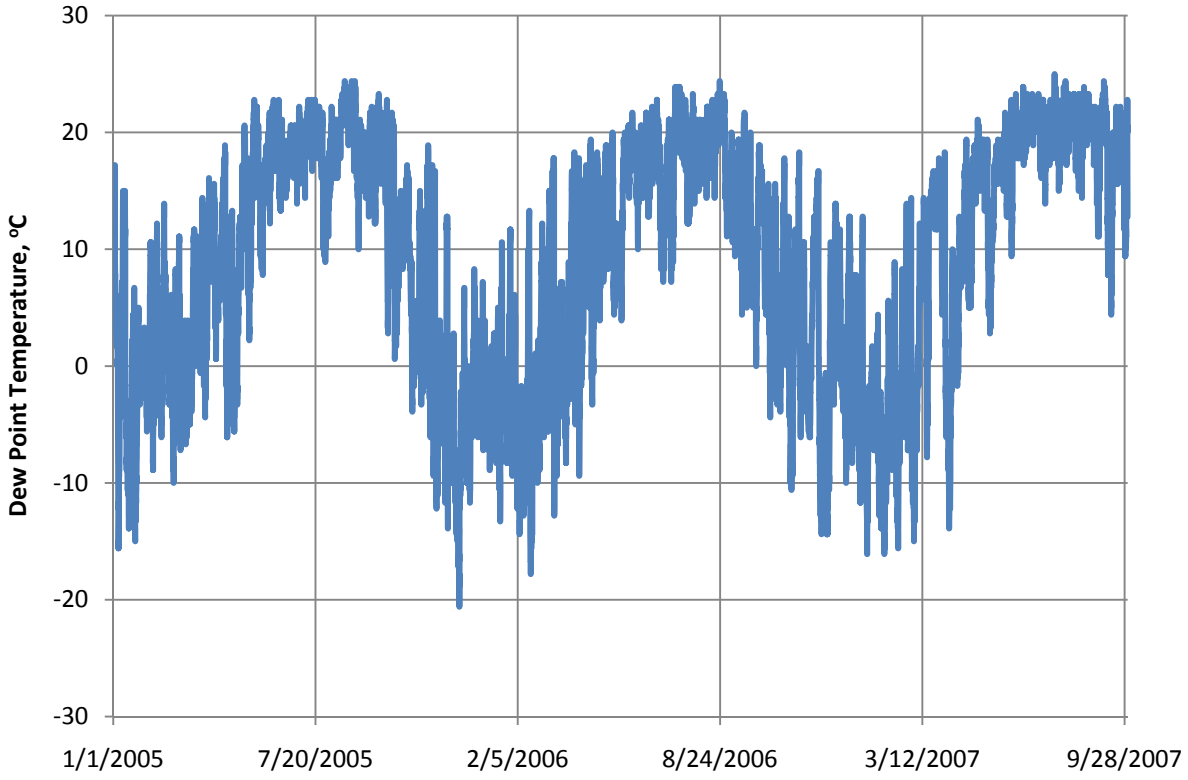

Figure 48. Dew point temperature at Cookson during calibration period.

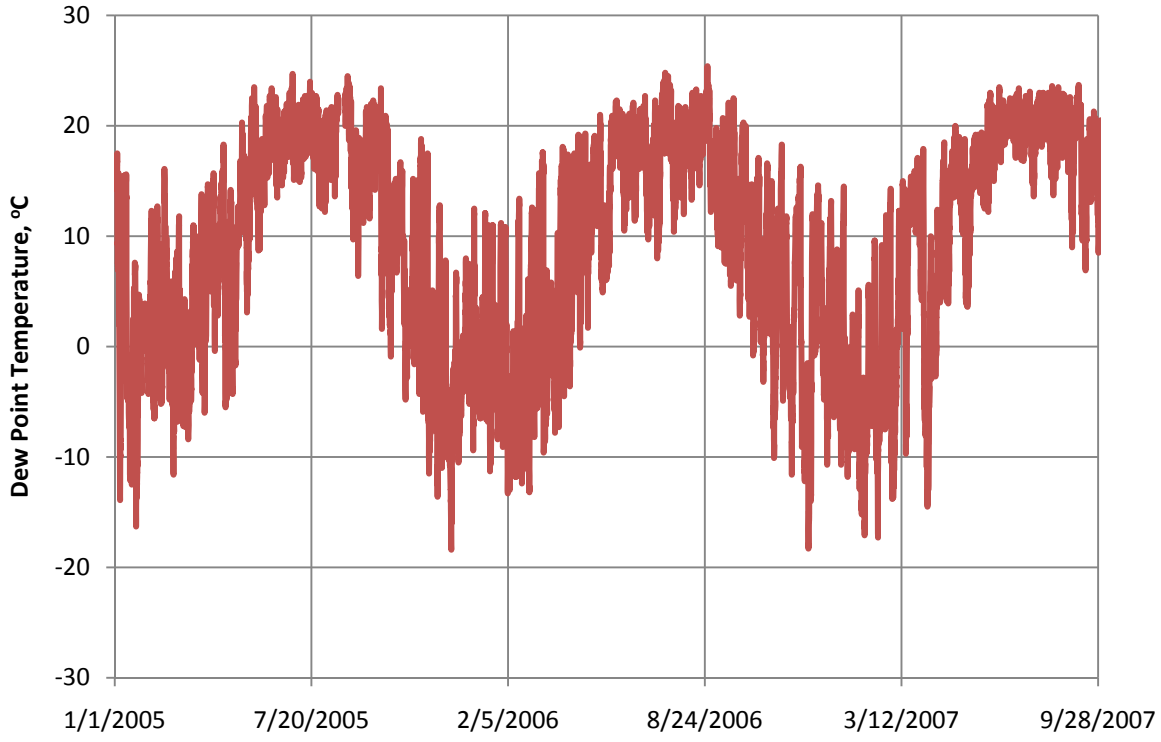

Figure 49. Dew point temperature at Tulsa International Airport during calibration period.

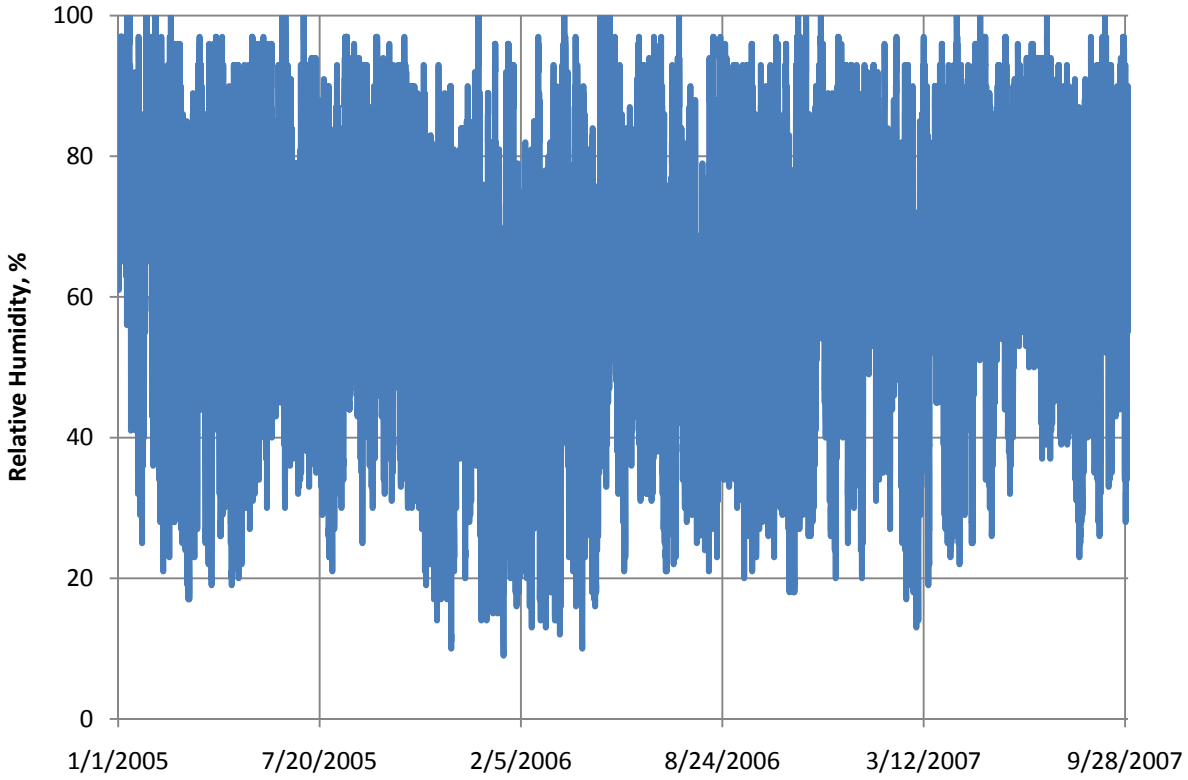

Figure 50. Relative humidity at Cookson during calibration period.

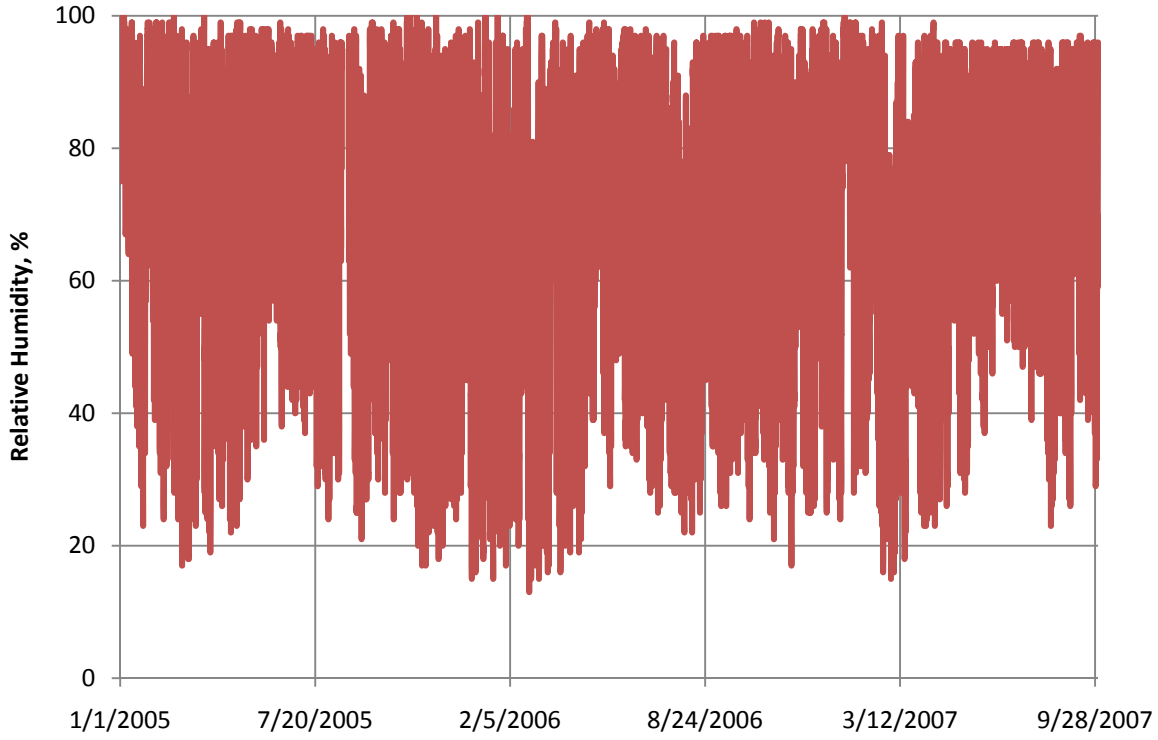

Figure 51. Relative humidity at Tulsa International Airport during calibration period.

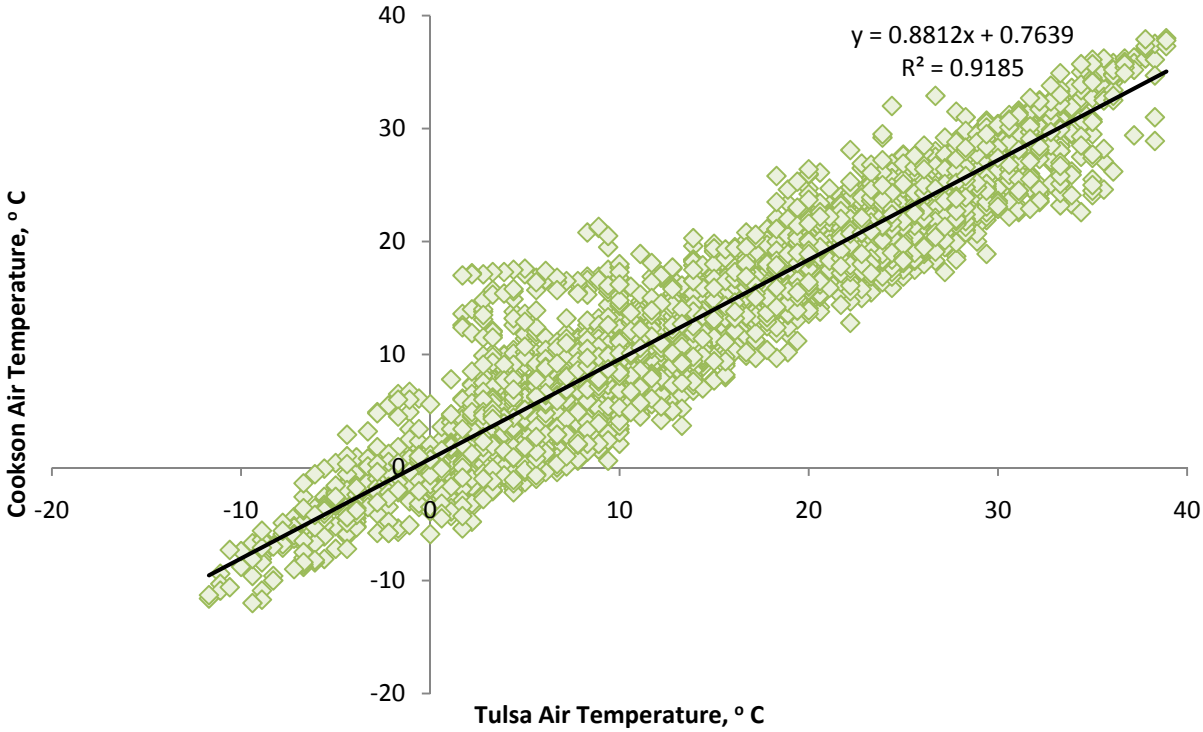

Figure 52. Tulsa vs. Cookson air temperature comparison.

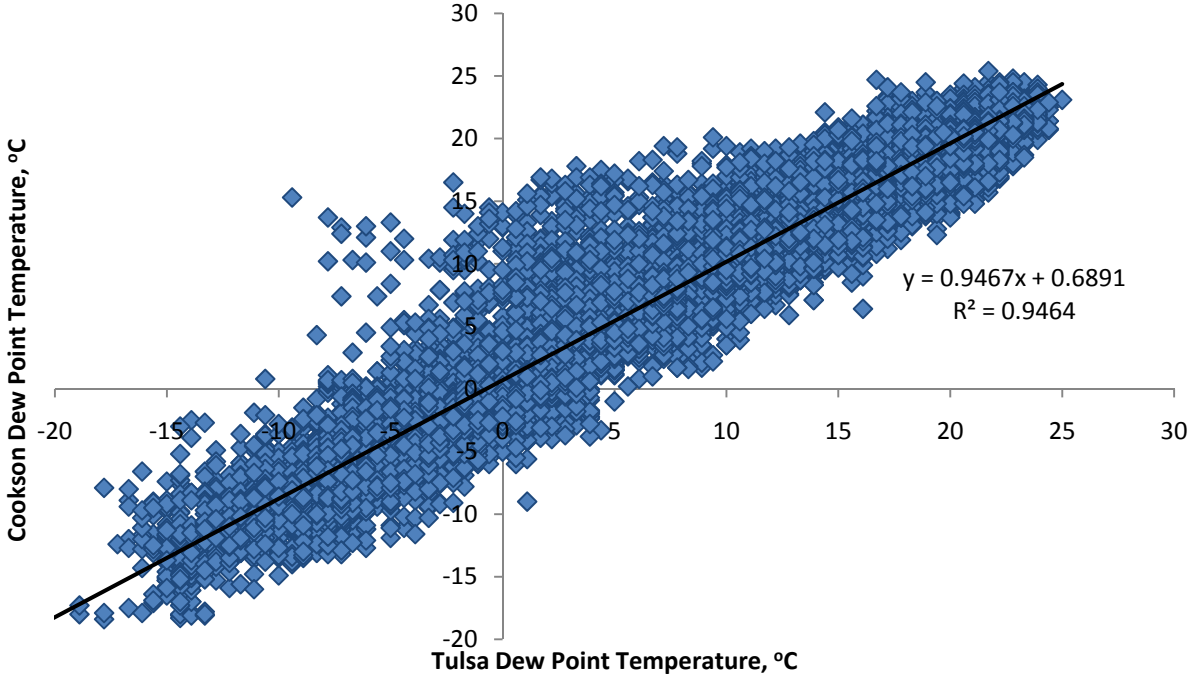

Figure 53. Tulsa vs. Cookson dew point temperature comparison.

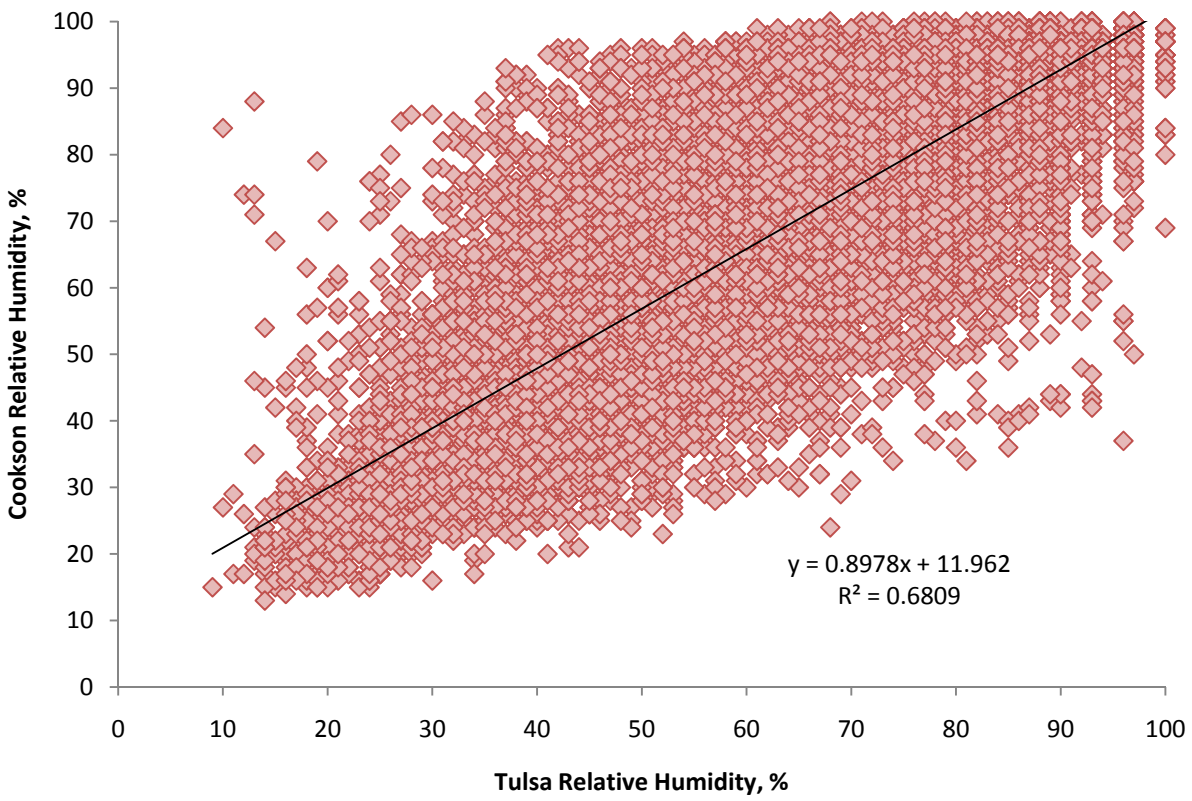

Figure 54. Tulsa vs. Cookson relative humidity comparison.

Wind Speed and Direction

Wind speed and direction data were available from Cookson, OK and Tulsa International Airport. Figure 55 shows the wind rose for Cookson over the calibration period. Figure 56 shows the wind rose for Tulsa International Airport over the same period. As can be seen from these charts, the principle axis of the wind direction measured at the two locations varied by over 20 degrees. A likely reason for the wind direction seen at Cookson, OK is shown in Figure 57. The Cookson met station is located in a valley, the orientation of which corresponds exactly to the principle axis of wind direction data taken at the site. This "funnel" effect is a local phenomenon, not representative of wind conditions over the whole lake. Hence, wind speed and direction data from Tulsa were used in the Tenkiller model. Wind speeds at Cookson were on average 40% lower than speeds measured at Tulsa.

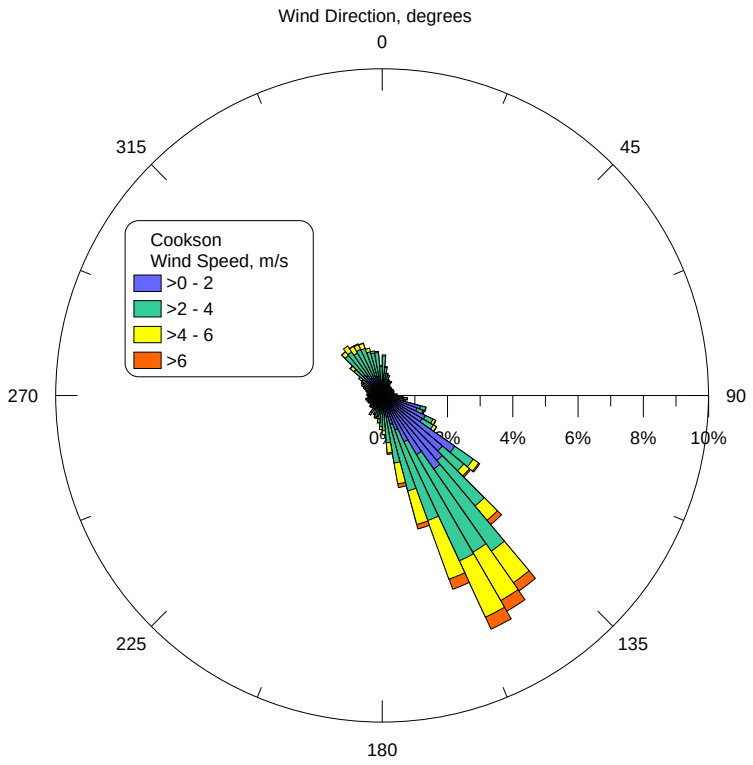

Figure 55. Wind rose from Cookson during calibration period.

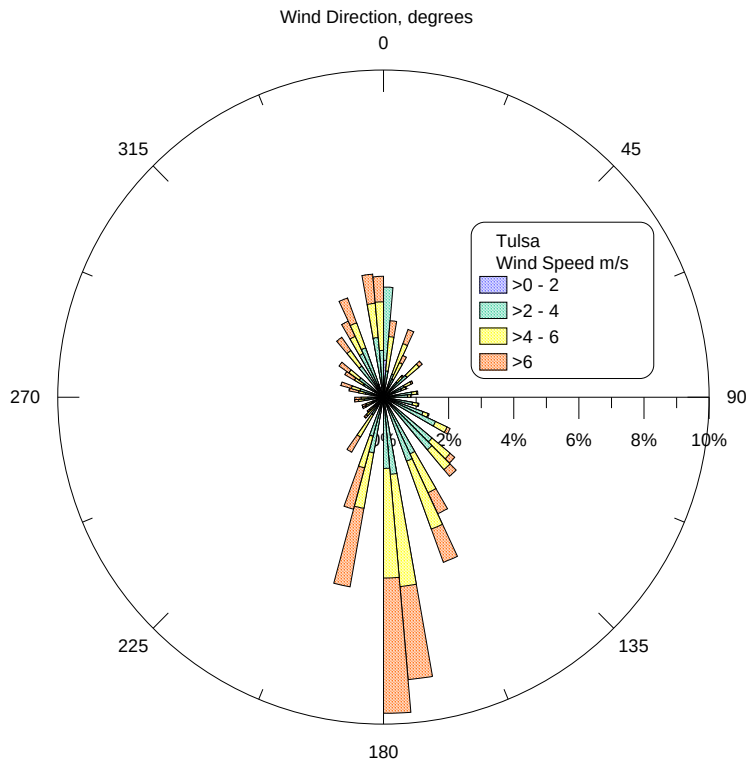

Figure 56. Wind rose from Tulsa International Airport during calibration period.

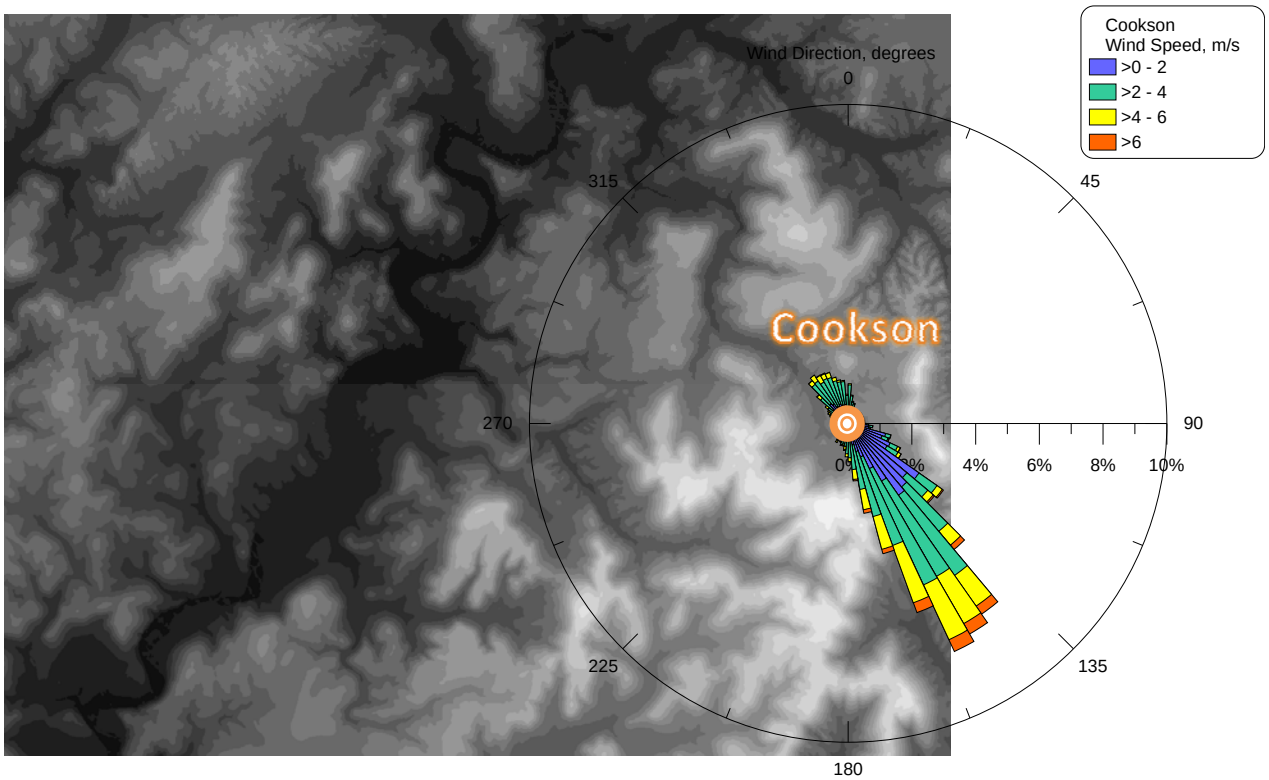

Figure 57. Cookson met data station location and wind-direction.

Solar Radiation comparison between Cookson and Tulsa

The Cookson site had measured short-wave solar, while the Tulsa site only had measured cloud cover. Using the formula used in CE-QUAL-W2 for estimating the theoretical short-wave solar radiation (see Annear and Wells, 2007), the theoretical solar based on Tulsa cloud cover was computed and compared to the measured Cookson data between January 1, 2005 and September 30, 2007.

The Cookson solar radiation measurement was 16.3 W/m^2 higher than the computed Tulsa meteorological data on a mean basis. Since often a difference occurs when the theoretical model of sunrise/sunset is off by an hour from the field data. This can occur to a slight difference in local time versus computed time based on the standard meridian and when one data set is in daylight savings time and the other in standard time.

In order to eliminate the issue of the timing of hourly comparisons of solar radiation, a daily-average of the total solar radiation was computed. A comparison of these between January 1, 2005 and September 30, 2007 is shown in Figure 58. On a daily average basis, the Cookson solar radiation measurement was also on average 16.3 W/m^2 more than the computed Tulsa meteorological data. A comparison of these daily averages is shown in Figure 59.

Hence, the 10-year simulation since it is using Tulsa cloud cover to compute solar radiation must be adjusted to account for that difference to have a similar data set as used during the calibration period. This difference is likely due to inaccuracies in measuring cloud cover or in computing the impact of cloud cover on short wave solar radiation.

The cloud cover correction for short-wave solar is based on the following relationship

$$\varphi_s = \varphi_{cs}(1 - \alpha C^2)$$

Where φ_s is the solar radiation, φ_{cs} is the clear-sky solar radiation, C is the cloud cover between 1-10, and α is the correction factor for cloud cover on solar radiation. In general the value of α is 0.0065, but can vary based on the type of cloud cover and the measurement technique.

In order to eliminate the bias between the Tulsa computed solar radiation and the measured Cookson solar, a value of α of 0.0046 was required for the period from 2005 to 2007. The average Tulsa cloud cover was about 4.4 between January 2005 and September 2007. For the period of record between January 1997 and December 2006 for the scenario runs, the average cloud cover was about 4.9.

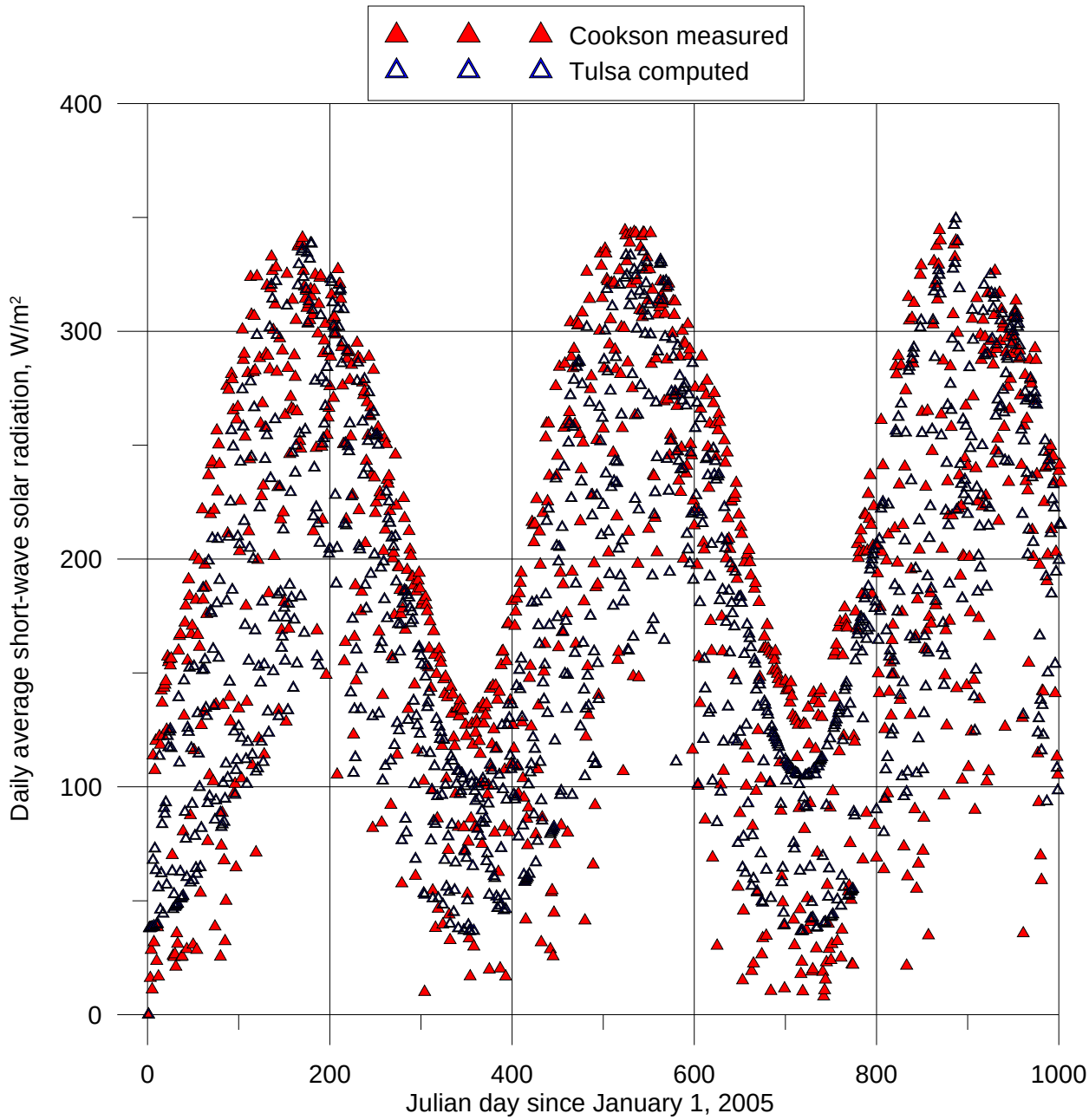

Figure 58. Comparison of daily average Cookson solar radition to computed from Tulsa cloud cover between January 1, 2005 and September 30, 2007.

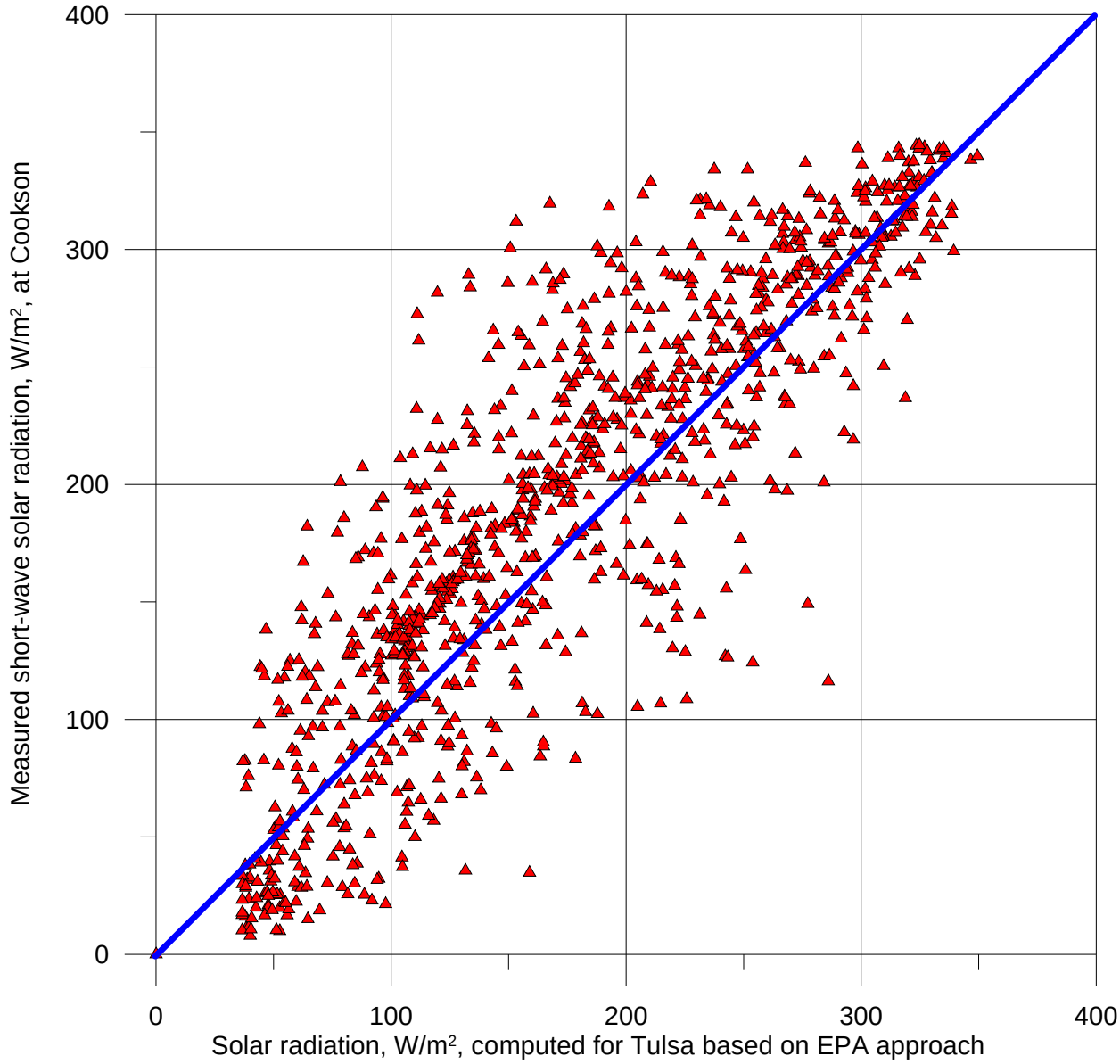

Figure 59. Comparison of daily average short-wave solar radiation at Cookson (measured) and Tulsa (theoretical computation based on cloud cover at Tulsa).

Model Calibration

The process of model calibration was to ensure agreement that model predictions reasonably agreed with field data for the period from January 1, 2005 [Julian day 1] through September 30, 2007 [Julian day 1003]. The National Research Council (2001) showed that evaluation of model calibration usually depends on a comparison of model predictions with observations including statistical evaluation of the model errors. A reasonable prediction of field data during the calibration period provides confidence in model results when the model is run for different water quality management scenarios. The process of model calibration is shown in Figure 60. Model calibration proceeded in the following steps:

1. Water level agreement
2. Basic thermal structure agreement – since the temperature profiles change with the water quality calibration as a result of suspended solids and algae growth, the temperature calibration was re-evaluated after the water quality calibration
3. Water quality calibration

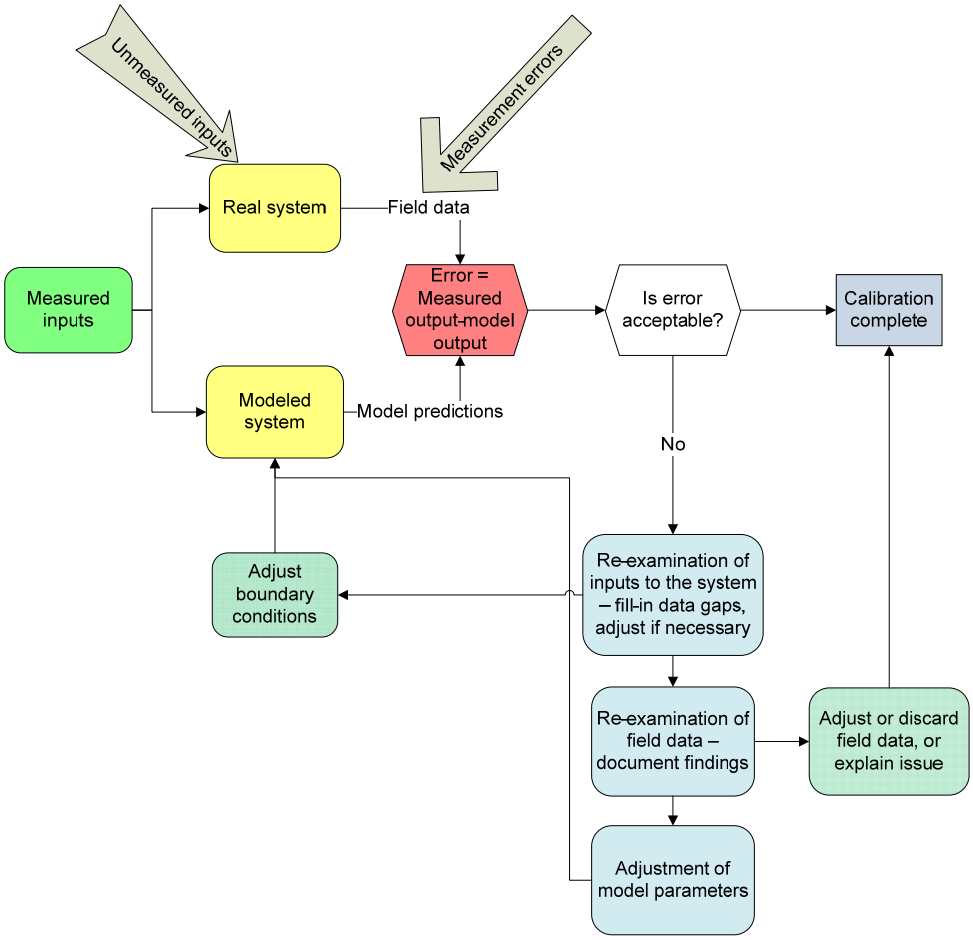

Figure 60. Calibration philosophy.

Water Level Calibration

Water level data were measured at the dam at 2 times during the day – 8 am and 12 midnight. Essentially there was little difference comparing the measurement at 8 am and at midnight over the time frame of the calibration. A comparison of the water level predicted by the model and the field data are shown in Figure 61. The Corps of Engineers provided measurements of outflow and change in water level from which they estimated total inflow including evaporation. Subtracting the total inflow from measured flow at Caney Creek, Baron Fork and the Illinois River, the residual inflow (either positive or negative) was used as a distributed inflow/outflow for the model. After running the model with these flows, the program 'waterbalance.exe' was used to estimate additional flows (either positive or negative) to match measured water levels.

The water balance flows averaged a net outflow of -1.47 m^3/s or about 50 cfs. This could be a result of dam leakage, improperly gaged inflows/outflows, and/or imprecision in the reservoir volume-elevation curve in estimating inflows or as used in the model. It is not uncommon for flow gages to have errors of 5-10%. This net outflow of 1.47 m^3/s is 5% of the average outflow from the reservoir. Since the Corps water balance estimate included evaporation, predicted evaporation was not used as a water loss in the CE-QUAL-W2 model.

Statistics for the water level error (data-model) are shown in Table 5 indicating excellent model-data agreement.

Table 5. Model-data error statistics for water level.

Location	# of comparisons, N	Mean error, m	Absolute mean error, m	RMS error, m
Segment 109 at Tenkiller dam	1002	0.00	0.02	0.04

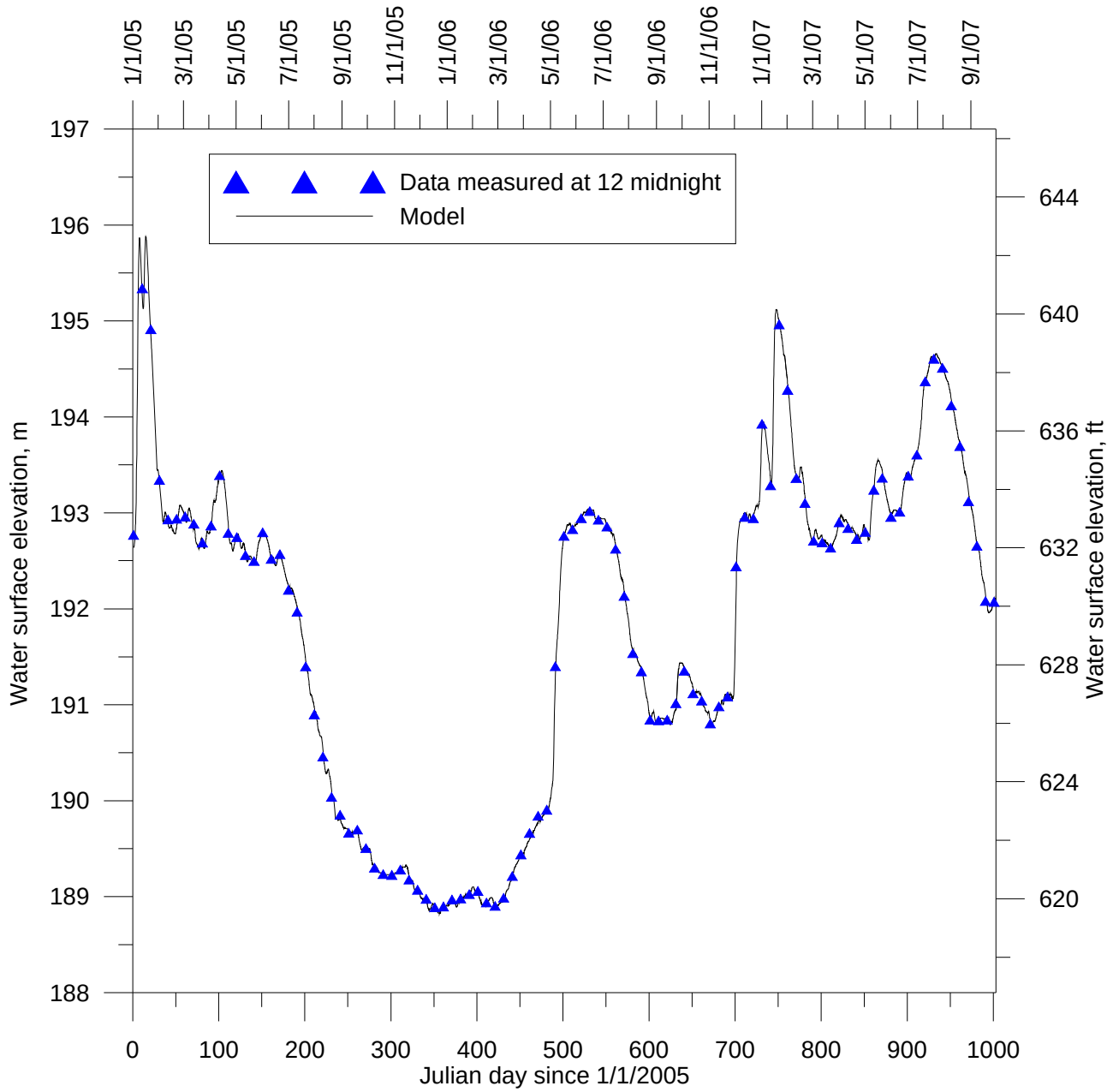

Figure 61. Model predicted water level compared to field data between January 1, 2005 and September 30, 2007. (Every 10th data point is shown.)

Temperature Calibration

The predicted model temperatures were very sensitive to the inflow temperatures, the wind field (which affects the evaporation rate), light extinction, and outflow hydraulics. The final temperature calibration was affected significantly by inflow suspended solids (both organic and inorganic) and algae growth. Since the wind data at Cookson were influenced by the topography, the Tulsa wind data were used and adjusted after comparing temperature data to predicted temperature profiles. The final model data errors for temperature are shown in Table 6. A discussion of the calibration results is shown in the next section, Analysis of Model Calibration. Representative temperature profiles for the first part of 2005 for 5/18/2005, 6/15/2005, 7/12/2005, 8/23/2005, and 10/4/2005 are shown in Figure 62, Figure 63, Figure 64, Figure 65, Figure 66, respectively. Appendix D shows all the model-data temperature profile comparisons. Model parameters that affect the temperature calibration are shown in Table 7. These parameters are part of the model input file, w2_con.npt, and include parameters such as light extinction and evaporation coefficients that can affect the model's prediction of temperature.

Table 6. Model-data error statistics for temperature.

Model segment #	Lake sampling station	# of profiles	ME, ^{o}C*	AME, ^{o}C*	RMS error, ^{o}C*
35	LK04	24	-0.57	1.04	1.14
59	LK03	30	-0.04	0.58	0.69
83	LK02	30	0.16	0.75	0.88
109	LK05	3	-0.68	0.70	0.86
199	LK01	30	0.23	0.75	0.90
Weighted average of all observations			-0.05	0.76	0.89

* For definitions of ME: mean error, AME: absolute mean error, and RMS: root mean squared error, see Appendix C.

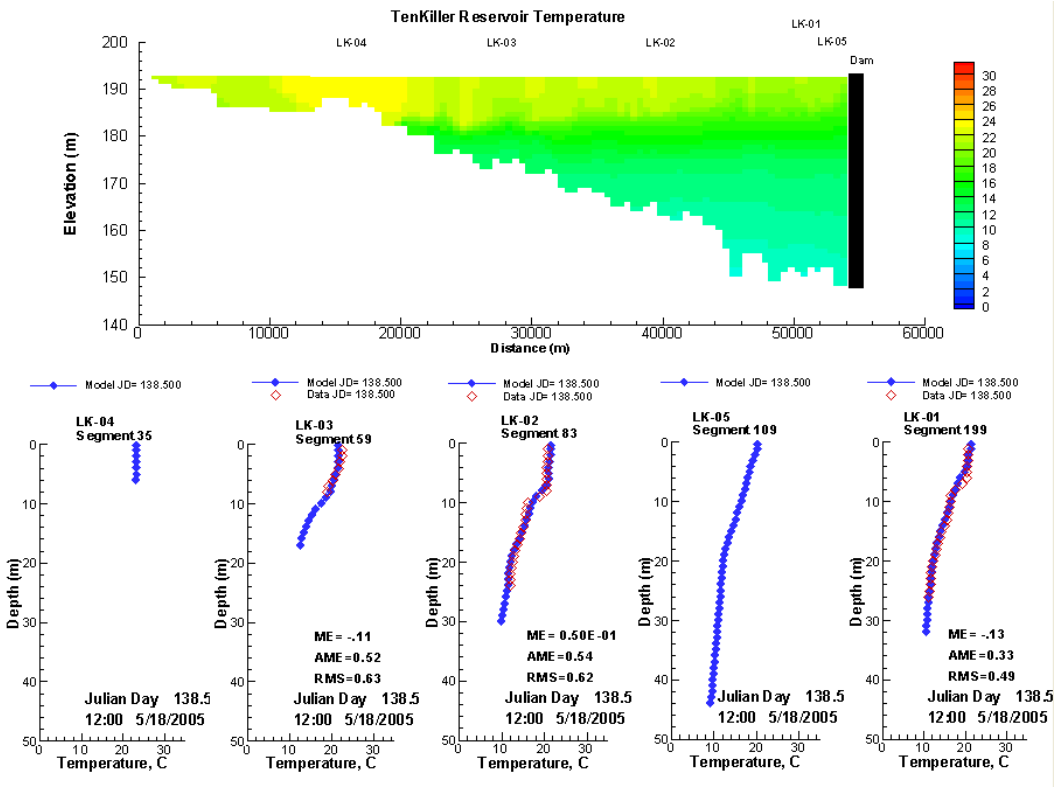

Figure 62. Temperature profiles of model and data for 5/18/2005.

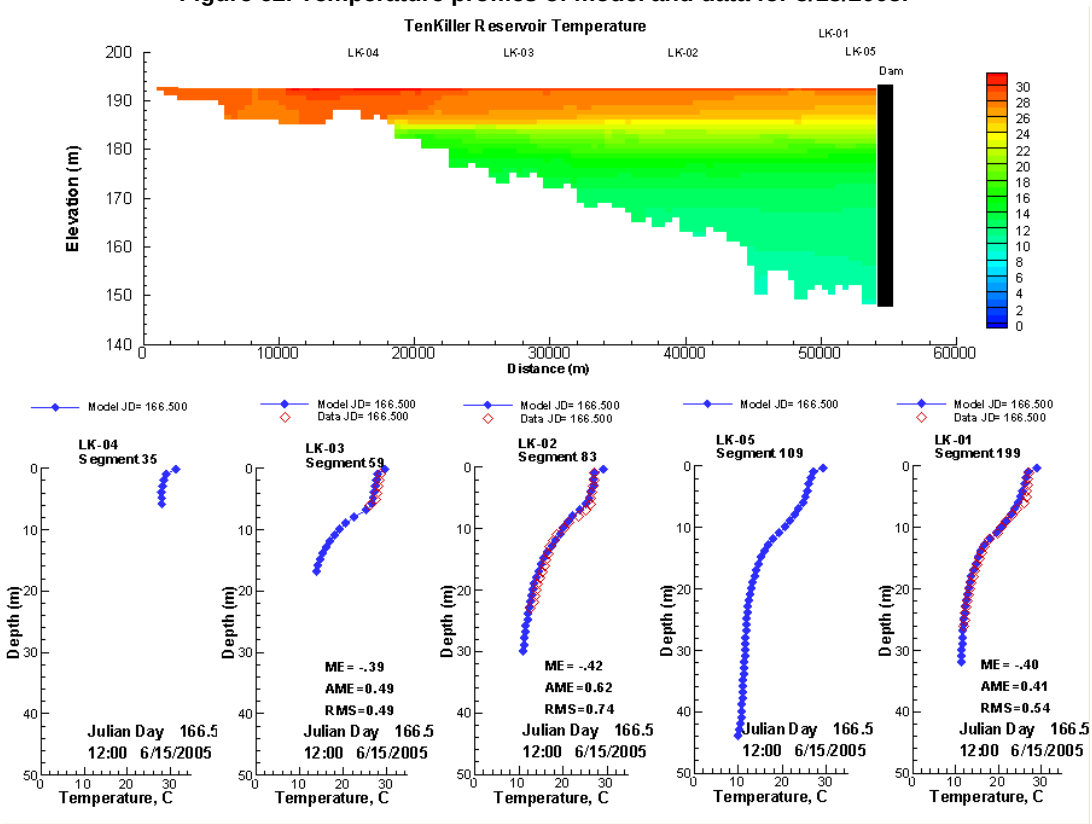

Figure 63. Temperature profiles of model and data for 6/15/2005.

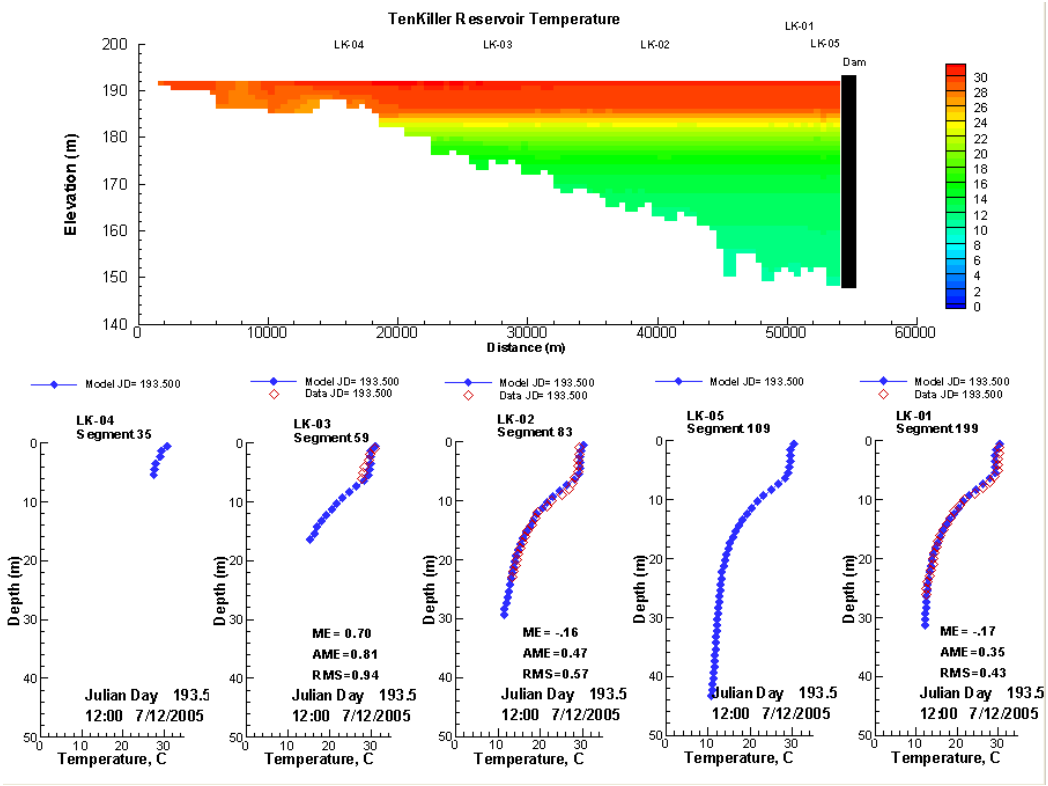

Figure 64. Temperature profiles of model and data for 7/12/2005.

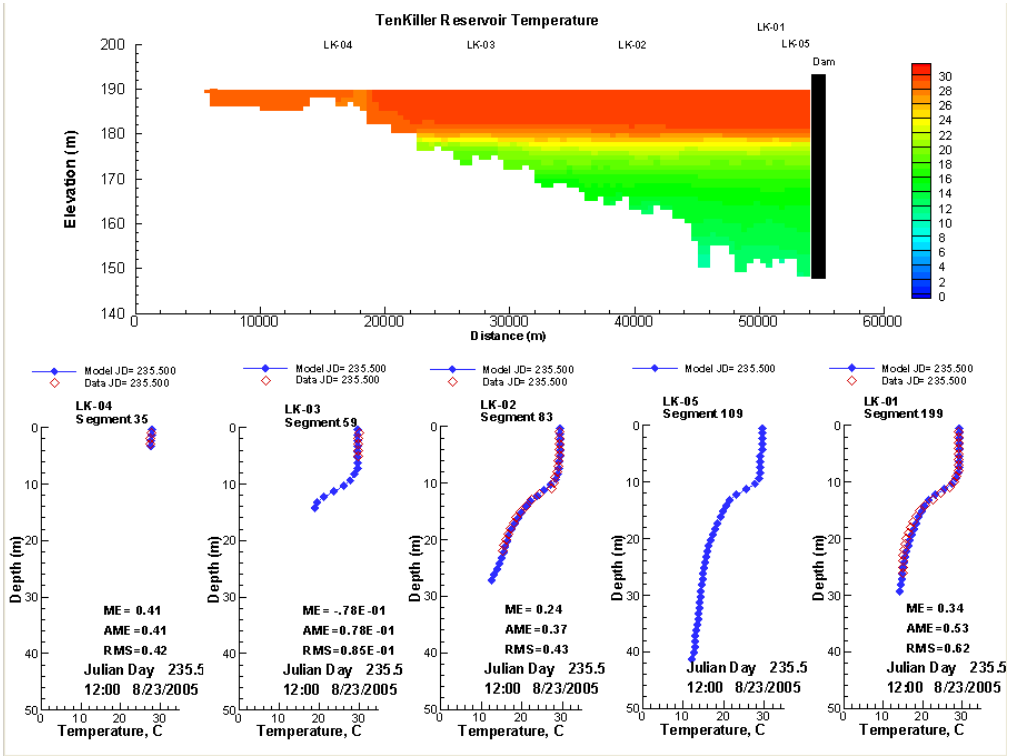

Figure 65. Temperature profiles of model and data for 8/23/2005.

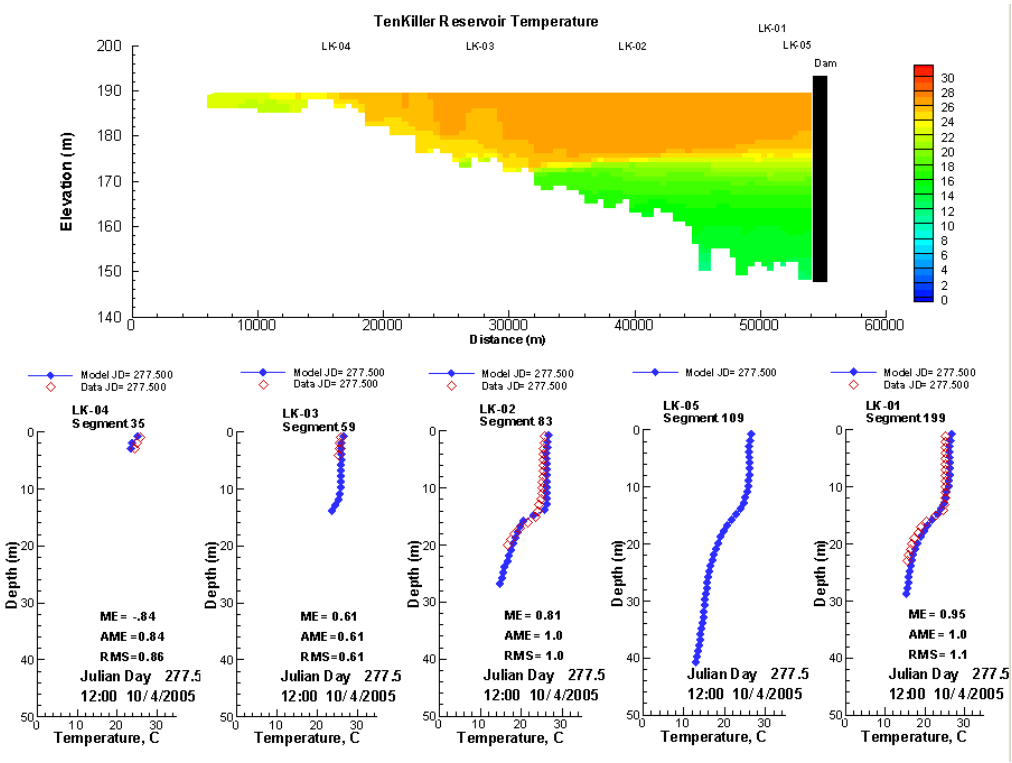

Figure 66. Temperature profiles of model and data for 10/4/2005.

Table 7. CE-QUAL-W2 model parameters affecting hydrodynamics and temperature.

Variable	Description	Units	Typical values*	Calibration Values
Hydrodynamics and Longitudinal Transport				
AX	Longitudinal eddy viscosity (for momentum dispersion)	m^2/sec	1	1
DX	Longitudinal eddy diffusivity (for dispersion of heat and constituents)	m^2/sec	1	1
Temperature				
CBHE	Coefficient of bottom heat exchange	Wm^2/sec	0.30	0.30
TSED	Sediment (ground) temperature	^oC	10-12	11.5
WSC	Wind sheltering coefficient	[-]	0.85	0.7 to 1.25
BETA	Fraction of incident solar radiation absorbed at the water surface	[-]	0.45	0.45
EXH2O	Light extinction for pure water	1/m	0.25-0.45	0.25
EXALG	Light extinction for algae	1/(m mg/l)	0.2	0.2
EXOM	Light extinction for particulate organic matter	1/(m mg/l)		0.05
EXSS	Light extinction for inorganic suspended solids	1/(m mg/l)	0.1	0.1
AFW	Evaporation coefficient		9.2	7.5
BFW	Evaporation coefficient		0.46	0.2
CFW	Evaporation coefficient	[-]	2.0	2.0

Water Quality Calibration

The water quality parameters used for the model calibration are shown below in Table 8. These represent parameters included in the model input file w2_con.npt. This file is used by the model in setting all the model water quality kinetic parameters for algae, periphyton, organic matter, nutrients, and sediment model compartments. For algae these parameters include algae growth rates, settling rates, respiration rates, C:N:P stoichiometry, light saturation, and temperature preferences. Most of the parameters used in the Tenkiller model are typical values used in many other reservoir eutrophication studies. The rest of this section goes through the statistics and model-data comparisons for dissolved oxygen, nutrients, algae, and light transparency. An analysis of the calibration is included in the following section, Analysis of Model Calibration.

Table 8. CE-QUAL-W2 model water quality parameters

Variable	Description	Units	Typical values*	Calibration values
Inorganic suspended solids				
SSS	Suspended solids settling rate	m/day	2	2.5
Algae group 1				
AG1	Algal growth rate for algal type 1	/day	2.0	1.75
AM1	Algal mortality rate for algal type 1	/day	0.1	0.1
AE1	Algal excretion rate for algal type 1	/day	0.04	0.04
AR1	Algal dark respiration rate for algal type 1	/day	0.04	0.1
AS1	Algal settling rate for algal type 1	/day	0.1	0.3
ASAT1	Saturation intensity at maximum photosynthetic rate for algal type 1	W/m^2	75-150	150
APOM1	Fraction of algal biomass lost by mortality to detritus for algal type 1		0.8	0.8
AT11	Lower temperature for algal growth for algal type 1	^oC	5	5
AT21	Lower temperature for maximum algal growth for algal type 1	^oC	25	15

Variable	Description	Units	Typical values*	Calibration values
AT31	Upper temperature for maximum algal growth for algal type 1	^{o}C	35	20
AT41	Upper temperature for algal growth for algal type 1	^{o}C	40	30
AK11	Fraction of algal growth rate at ALGT1 for algal type 1		0.1	0.1
AK21	Fraction of maximum algal growth rate at ALGT2 for algal type 1		0.99	0.5
AK31	Fraction of maximum algal growth rate at ALGT3 for algal type 1		0.99	0.99
AK41	Fraction of algal growth rate at ALGT4 for algal type 1		0.1	0.1
ALGP-A1	Stoichiometric equivalent between organic matter and phosphorus for algal type 1		0.005	0.005
ALGN-A1	Stoichiometric equivalent between organic matter and nitrogen for algal type 1		0.08	0.08
ALGC-A1	Stoichiometric equivalent between organic matter and carbon for algal type 1		0.45	0.45
Algae group 2				
AG2	Algal growth rate for algal type 2	/day	2.0	1.9
AM2	Algal mortality rate for algal type 2	/day	0.1	0.1
AE2	Algal excretion rate for algal type 2	/day	0.04	0.04
AR2	Algal dark respiration rate for algal type 2	/day	0.04	0.1
AS2	Algal settling rate for algal type 2	/day	0.1	0.1
ASAT2	Saturation intensity at maximum photosynthetic rate for algal type 2	W/m^2	75-150	125
APOM2	Fraction of algal biomass lost by mortality to detritus for algal type 2		0.8	0.8
AT12	Lower temperature for algal growth for algal type 2	^{o}C	5	10

Variable	Description	Units	Typical values*	Calibration values
AT22	Lower temperature for maximum algal growth for algal type 2	^{o}C	25	20
AT32	Upper temperature for maximum algal growth for algal type 2	^{o}C	35	26
AT42	Upper temperature for algal growth for algal type 2	^{o}C	40	35
AK12	Fraction of algal growth rate at AT1 for algal type 2		0.1	0.1
AK22	Fraction of maximum algal growth rate at AT2 for algal type 2		0.99	0.8
AK32	Fraction of maximum algal growth rate at AT3 for algal type 2		0.99	0.99
AK42	Fraction of algal growth rate at AT4 for algal type 2		0.1	0.1
ALGP-A2	Stoichiometric equivalent between organic matter and phosphorus for algal type 2		0.005	0.005
ALGN-A2	Stoichiometric equivalent between organic matter and nitrogen for algal type 2		0.08	0.07
ALGC-A2	Stoichiometric equivalent between organic matter and carbon for algal type 2		0.45	0.50
Algal group 3				
AG3	Algal growth rate for algal type 3	/day	2.0	2.5
AM3	Algal mortality rate for algal type 3	/day	0.1	0.1
AE3	Algal excretion rate for algal type 3	/day	0.04	0.04
AR3	Algal dark respiration rate for algal type 3	/day	0.04	0.1
AS3	Algal settling rate for algal type 3	/day	0.1	0.0
ASAT3	Saturation intensity at maximum photosynthetic rate for algal type 3	W/m^2	75-150	145

Variable	Description	Units	Typical values*	Calibration values
APOM3	Fraction of algal biomass lost by mortality to detritus for algal type 3		0.8	0.8
AT13	Lower temperature for algal growth for algal type 3	^{o}C	5	15
AT23	Lower temperature for maximum algal growth for algal type 3	^{o}C	25	28
AT33	Upper temperature for maximum algal growth for algal type 3	^{o}C	35	35
AT43	Upper temperature for algal growth for algal type 3	^{o}C	40	40
AK13	Fraction of algal growth rate at AT1 for algal type 3		0.1	0.1
AK23	Fraction of maximum algal growth rate at AT2 for algal type 3		0.99	0.99
AK33	Fraction of maximum algal growth rate at AT3 for algal type 3		0.99	0.99
AK43	Fraction of algal growth rate at AT4 for algal type 3		0.1	0.1
ALGP-A3	Stoichiometric equivalent between organic matter and phosphorus for algal type 3		0.005	0.005
ALGN-A3	Stoichiometric equivalent between organic matter and nitrogen for algal type 3		0.08	0.08
ALGC-A3	Stoichiometric equivalent between organic matter and carbon for algal type 3		0.45	0.45
Epiphyton/Periphyton				
EG1	Periphyton growth rate for periphyton type 1	/day	2.0	1.0
EM1	Periphyton mortality rate for periphyton type 1	/day	0.1	0.1
EE1	Periphyton excretion rate for periphyton type 1	/day	0.04	0.04
ER1	Periphyton dark respiration rate for periphyton type 1	/day	0.04	0.1
EB1	Periphyton burial rate for a periphyton type 1	m/day	0.1	0.01

Variable	Description	Units	Typical values*	Calibration values
ESAT1	Saturation intensity at maximum photosynthetic rate for periphyton type 1	W/m^2	75-150	125
EPOM1	Fraction of periphyton biomass lost by mortality to detritus for periphyton type 1		0.8	0.8
EHS1	Biomass limitation factor for periphyton type 1			
ET11	Lower temperature for algal growth for periphyton type 1	^oC	5	5
ET21	Lower temperature for maximum algal growth for periphyton type 1	^oC	25	12
ET31	Upper temperature for maximum algal growth for periphyton type 1	^oC	35	20
ET41	Upper temperature for algal growth for periphyton type 1	^oC	40	35
EK11	Fraction of algal growth rate at ET1 for periphyton type 1		0.1	0.15
EK21	Fraction of maximum algal growth rate at ET2 for periphyton type 1		0.99	0.5
EK31	Fraction of maximum algal growth rate at ET3 for periphyton type 1		0.99	0.99
EK41	Fraction of algal growth rate at ET4 for periphyton type 1		0.1	0.2
EP-1	Stoichiometric equivalent between organic matter and phosphorus for periphyton type 1		0.005	0.005
EN-1	Stoichiometric equivalent between organic matter and nitrogen for periphyton type 1		0.08	0.08
EC-1	Stoichiometric equivalent between organic matter and carbon for periphyton type 1		0.45	0.45
Organic Matter				
LDOMDK	Labile DOM decay rate	/day	0.1	0.1

Variable	Description	Units	Typical values*	Calibration values
LRDDK	Labile to refractory decay rate	/day	0.01	0.005
RDOMDK	Maximum refractory decay rate	/day	0.01	0.001
LPOMDK	Labile Detritus decay rate	/day	0.08	0.08
POMS	Detritus settling rate	m/day	0.1	1.0
RPOMDK	Refractory POM or detritus decay rate	/day	0.001	0.001
LRPDK	Labile to refractory POM decay rate	/day	0.01	0.005
OMT1	Lower temperature for organic matter decay	^{o}C	4	4
OMT2	Lower temperature for maximum organic matter decay	^{o}C	20	20
OMK1	Fraction of organic matter decay rate at OMT1		0.1	0.1
OMK2	Fraction of organic matter decay rate at OMT2		0.99	0.99
Phosphorus				
PARTP	Phosphorus partitioning coefficient for suspended solids		0.0	0.0
AHSP1	Algal half-saturation constant for phosphorus – algae 1	g/m^3	0.003	0.002
AHSP2	Algal half-saturation constant for phosphorus – algae 2	g/m^3	0.003	0.002
AHSP3	Algal half-saturation constant for phosphorus –algae 3	g/m^3	0.003	0.002
EHSP1	Periphyton half-saturation constant for phosphorus – periphyton 1	g/m^3	0.003	0.004
ORGP	Stoichiometric equivalent between organic matter and phosphorus		0.005	0.005
Nitrogen				
NH4DK	Ammonia decay rate (nitrification rate)	/day	0.12	0.05
AHSN1	Algal half-saturation constant for ammonia-algae 1	g/m^3	0.014	0.014
AHSN2	Algal half-saturation constant for ammonia-algae 2	g/m^3	0.014	0.035
AHSN3	Algal half-saturation constant for ammonia-algae 3	g/m^3	0.014	0.001

Variable	Description	Units	Typical values*	Calibration values
EHSN1	Algal half-saturation constant for ammonia-periphyton type 1	g/m^3	0.014	0.015
NH4T1	Lower temperature for ammonia decay	^oC	5	5
NH4T2	Lower temperature for maximum ammonia decay	^oC	20	25
NH4K1	Fraction of nitrification rate at NH4T1		0.1	0.1
NH4K2	Fraction of nitrification rate at NH4T2		0.99	0.99
NO3DK	Nitrate decay rate (denitrification rate)	/day	0.03	0.05
NO3T1	Lower temperature for nitrate decay	^oC	5	5
NO3T2	Lower temperature for maximum nitrate decay	^oC	25	25
NO3K1	Fraction of denitrification rate at NO3T1		0.1	0.1
NO3K2	Fraction of denitrification rate at NO3T2		0.99	0.99
ORGN	Stoichiometric equivalent between organic matter and nitrogen		0.08	0.08
Oxygen				
O2NH4	Oxygen stoichiometric equivalent for ammonia decay		4.57	4.2
O2OM	Oxygen stoichiometric equivalent for organic matter decay		1.4	1.2
O2AR	Oxygen stoichiometric equivalent for dark respiration		1.1	1.1
O2AG	Oxygen stoichiometric equivalent for algal growth		1.4	1.6
O2ER	Oxygen stoichiometric equivalent for periphyton respiration		1.1	1.1
O2EG	Oxygen stoichiometric equivalent for periphyton growth		1.4	1.6
O2LIM	Dissolved oxygen concentration half saturation constant	g/m^3	0.1	0.1
Sediment organic matter and SOD				

Variable	Description	Units	Typical values*	Calibration values
SEDK	Sediment decay rate	/day	0.1	0.015
SEDS	Sediment focusing velocity	m/day	0.1	0.05
SEDBR	Sediment burial rate	/day	0.01	0.0005
SOD	Maximum sediment oxygen demand at SODT2 (also adjusted by FSOD)	g/m^2/ day		1.0
SODT1	Sediment temperature	^oC	4	5
SODT2	Upper temperature for sediment decay	^oC	25	25
SODK1	Fraction of SOD at SODT1		0.1	0.1
SODK2	Fraction fo SOD at SODT2		0.99	0.99
Organic matter and carbon				
ORGC	Stoichiometric equivalent between organic matter and carbon		0.45	0.45
* Cole and Wells (2007)				

Dissolved Oxygen

The dissolved oxygen profiles were sensitive to inflow boundary conditions and algae and organic matter internal processes, including sediment oxygen demand. The sources and sinks of dissolved oxygen during the simulation period are shown in Figure 67 where DOAP: algae production, DOAR: algae respiration, DOEP: ephiphyton/periphyton production, DOER: Epiphyton/periphyton respiration, DOPOM: particulate organic matter oxygen demand, DODOM: dissolved organic matter oxygen demand, DOOM: total organic matter oxygen consumption, DONITR: nitrification, DOREAER: reaeration, DOSED: first order sediment oxygen demand, DOSOD: zero order sediment oxygen demand. Primary sources/sinks for dissolved oxygen include algal and epiphyton production, organic matter decay, total sediment oxygen demand and reaeration. During the summer algal production is highest and reaeration acts as a sink of dissolved oxygen allowing supersaturated dissolved oxygen to evolve from the epilimnion to the atmosphere. Organic matter decay and total sediment oxygen demand are highest in the summer when water temperatures are warm.

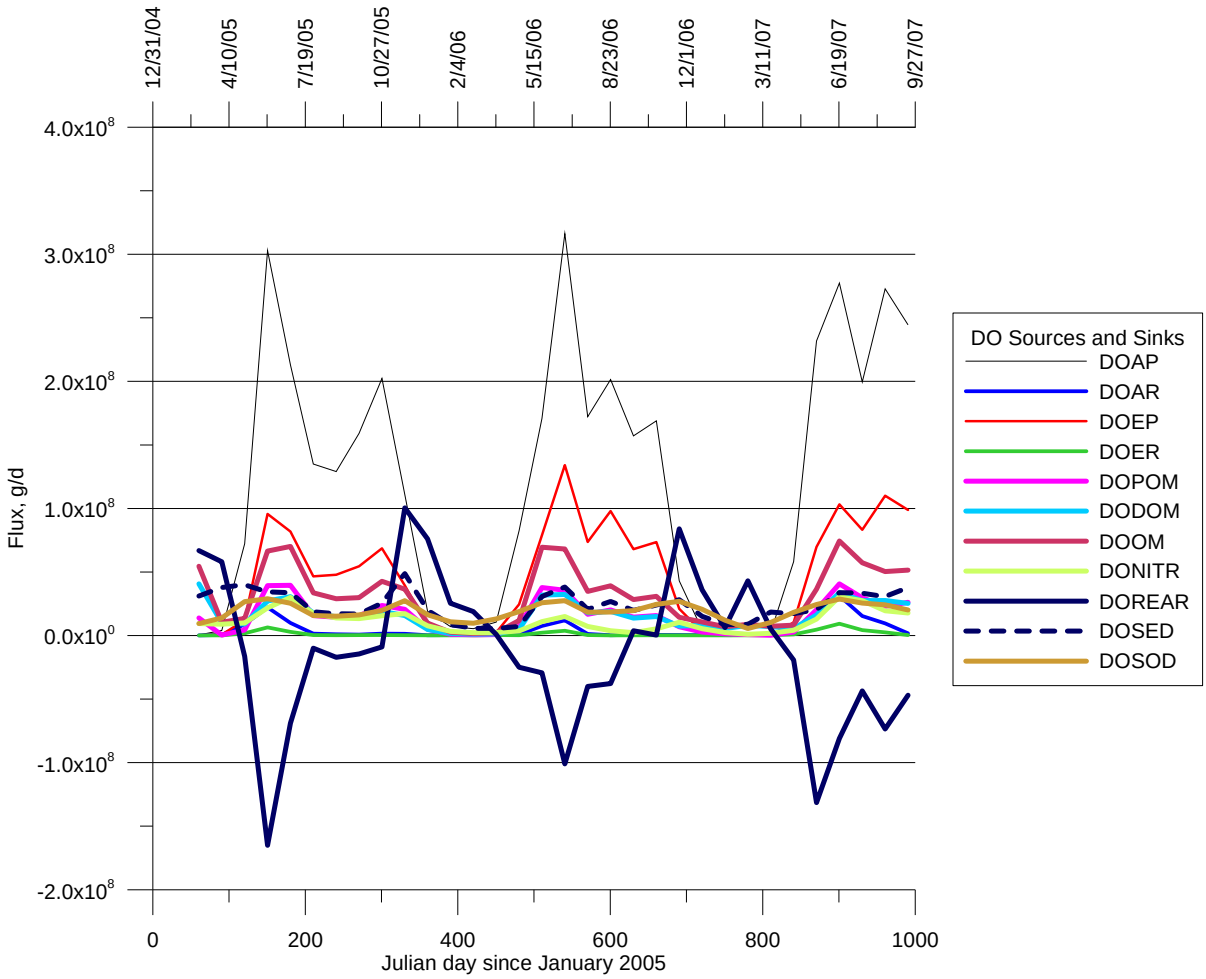

Figure 67. Sources and sinks of dissolved oxygen predicted by the model during calibration period.

Several representative profiles throughout the lake are shown in Figure 68, Figure 69, Figure 70, Figure 71, and Figure 72 for 4/21/05, 6/15/05, 7/26/05, 8/23/05, and 9/20/05, respectively. These profiles show the progression from well-mixed conditions where dissolved oxygen is at saturation in the early spring to profiles that exhibit both metalimnetic minima and hypolimnetic depletion as the summer progresses. Ultimately, the hypolimnion approaches zero dissolved oxygen until fall overturn when the water column eventually approaches fully-saturated conditions again.

Model–data error statistics are shown in Table 9 for dissolved oxygen profiles between January 2005 and September 2007.

Table 9. Model-data error statistics for dissolved oxygen.

Model segment #	Lake sampling station	# of profiles	ME, mg/l *	AME, mg/l*	RMS error, mg/l*
35	LK04	25	-0.48	1.95	2.21
59	LK03	31	-0.94	1.74	2.00
83	LK02	30	-0.06	1.17	1.60
109	LK05	8	0.38	1.43	1.66
199	LK01	30	-0.12	1.16	1.48
		Weighted averages	-0.35	1.48	1.80

* For definitions of ME: mean error, AME: absolute mean error, and RMS: root mean squared error, see Appendix C

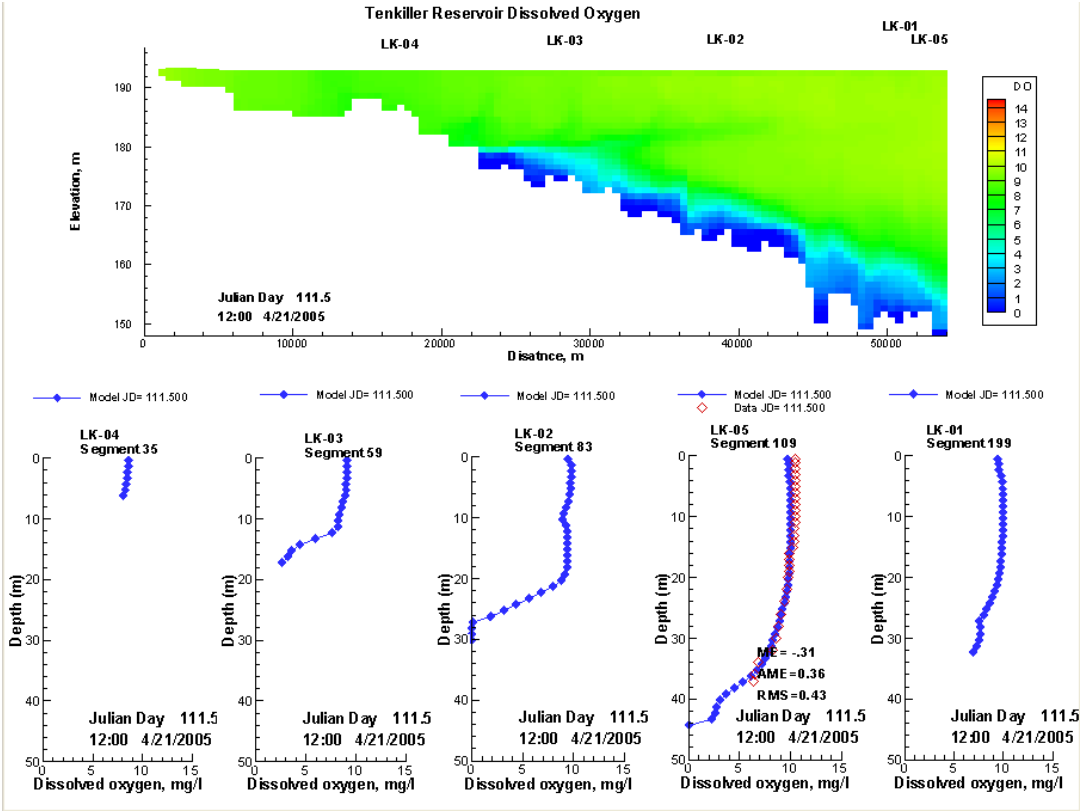

Figure 68. Model predictions of dissolved oxygen profiles compared to field data on 4/21/2005.

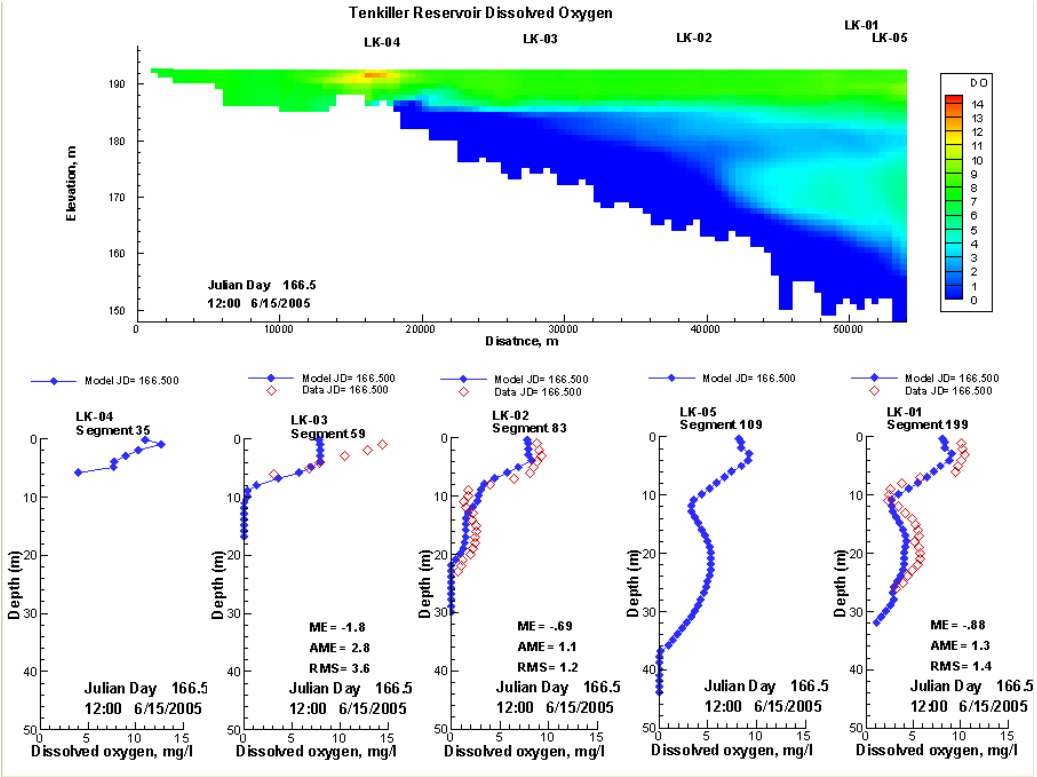

Figure 69. Model predictions of dissolved oxygen profiles compared to field data on 6/15/2005.

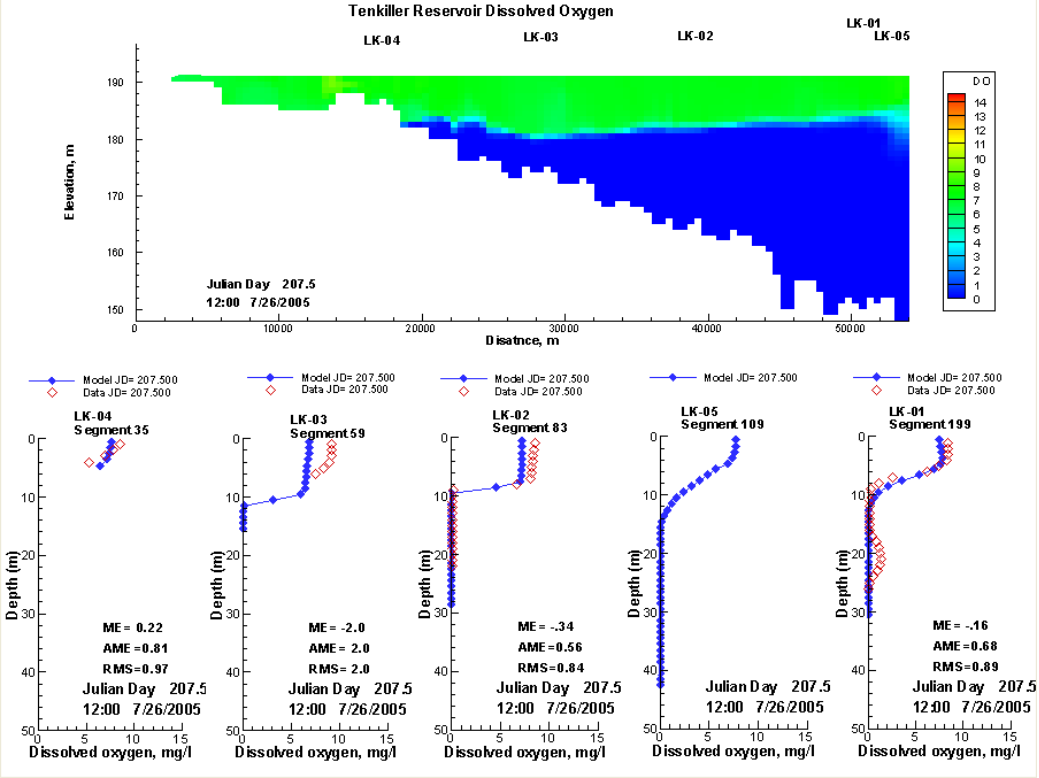

Figure 70. Model predictions of dissolved oxygen profiles compared to field data on 7/26/2005.

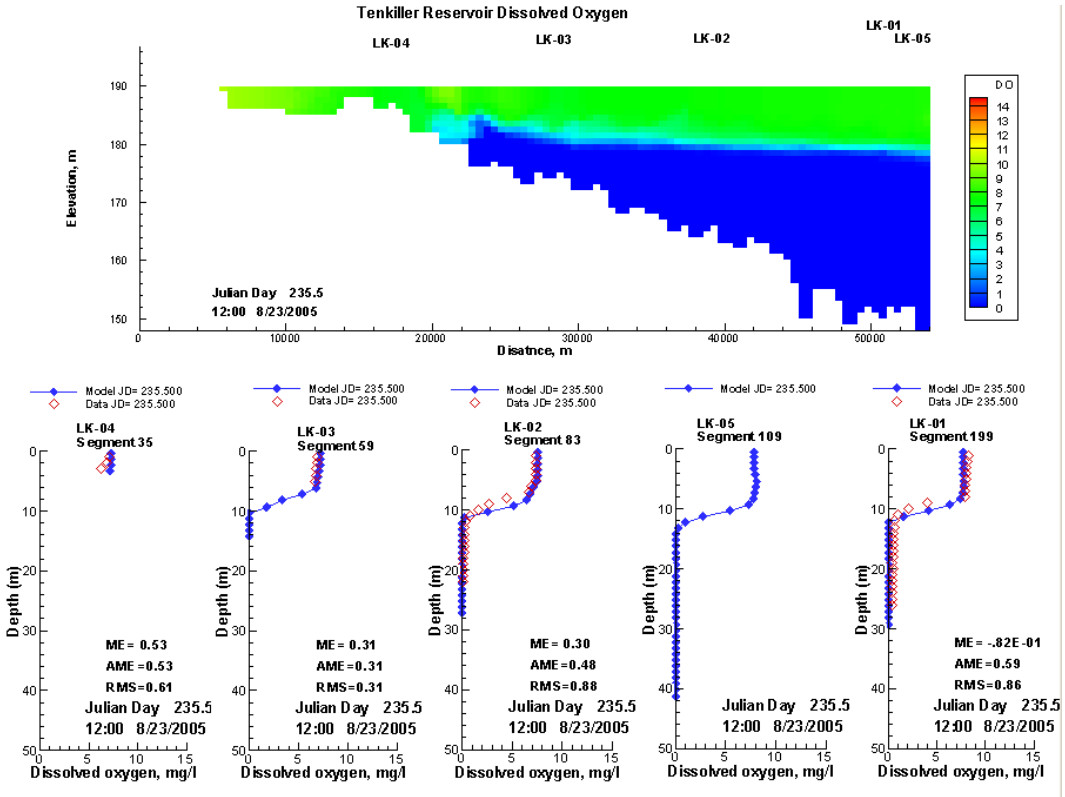

Figure 71. Model predictions of dissolved oxygen profiles compared to field data on 8/23/2005.

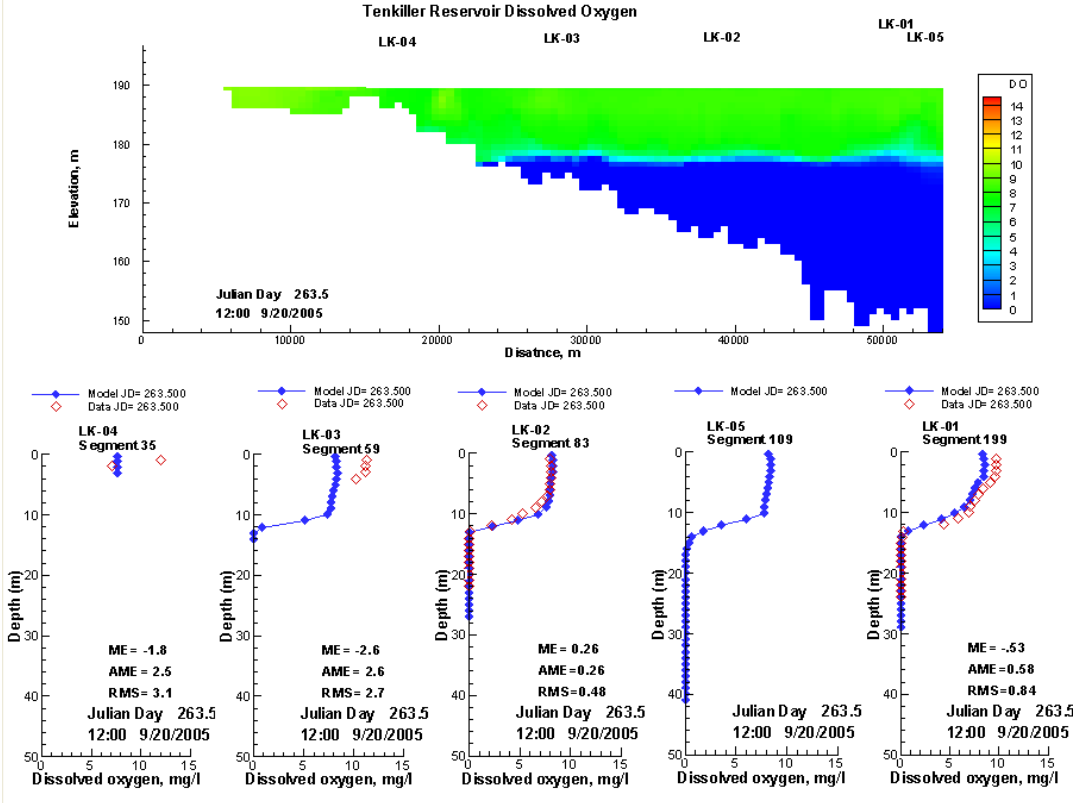

Figure 72. Model predictions of dissolved oxygen profiles compared to field data on 9/20/2005.

Model-data profile comparisons are shown in Appendix E. In order to also obtain an idea of the model prediction of dissolved oxygen temporally, representative time series of dissolved oxygen for model segment 89 and 109 are shown in Figure 73 and Figure 74, respectively. In these figures, the smooth line is the model prediction at the stated depth, and the crosses are the measured field data at the depth shown on the figure.

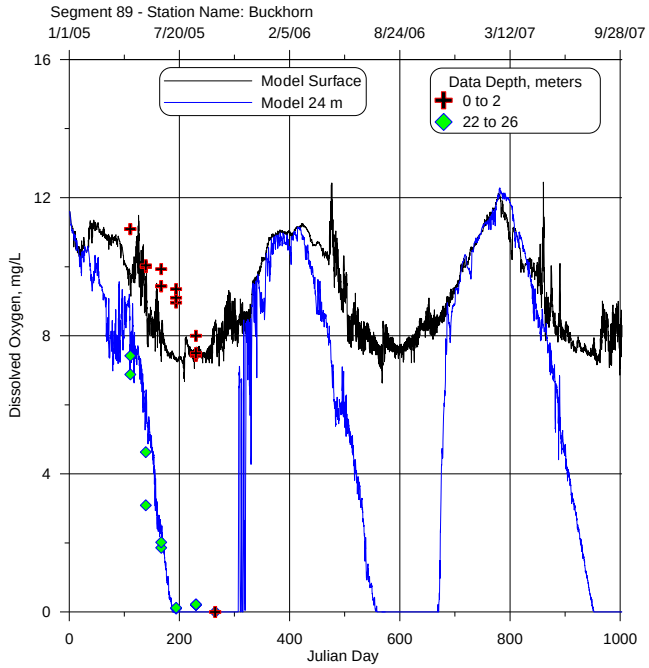

Figure 73. Dissolved oxygen time series - segment 89 during calibration period.

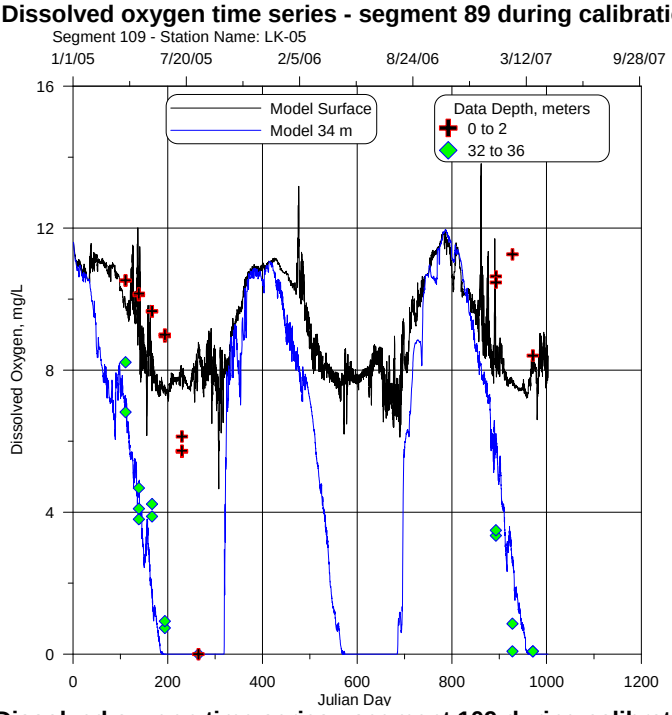

Figure 74. Dissolved oxygen time series - segment 109 during calibration period.

Total Nitrogen

The model computes Total N as a derived variable based on the following state variables:

$$TotalN = NH_{4_} + NO_3 + \sum ALGN * C_{algae} + \sum ORGN * C_{organicmatter}$$

Where C_{algae} is the concentration of algae on a dry weight basis, ALGN is the stoichiometric coefficient for each algae group, Corganic_matter is the concentration of LPOM, RPOM, LDOM, RDOM, and ORGN is the stoichiometric coefficient for organic matter:N, NO_3 is the nitrate-N, NH_4 is the ammonia-N.

Figure 75, Figure 76, Figure 77, Figure 78, and Figure 79 display a time series model vs. data comparisons of total nitrogen for various model segments. In these figures, the smooth line is the model prediction at the stated depth, and the crosses are the measured field data at the depth shown on the figure.

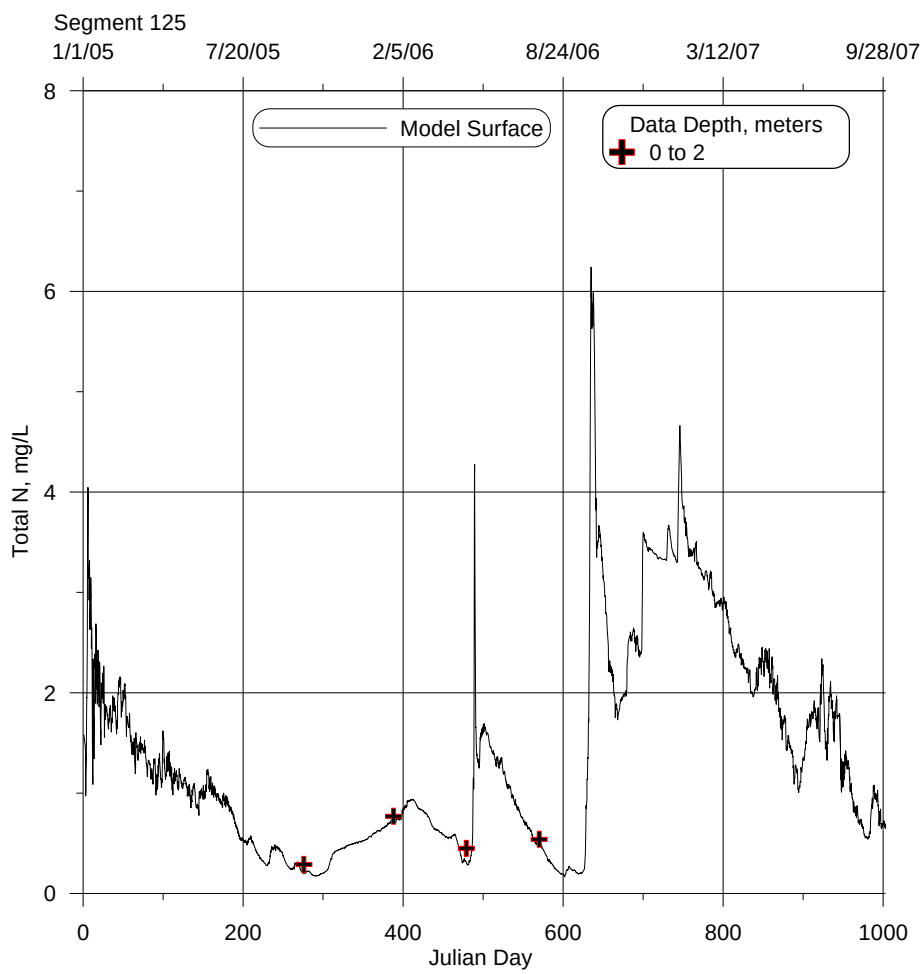

Figure 75. Total nitrogen model vs. data comparison - segment 125 during calibration period.

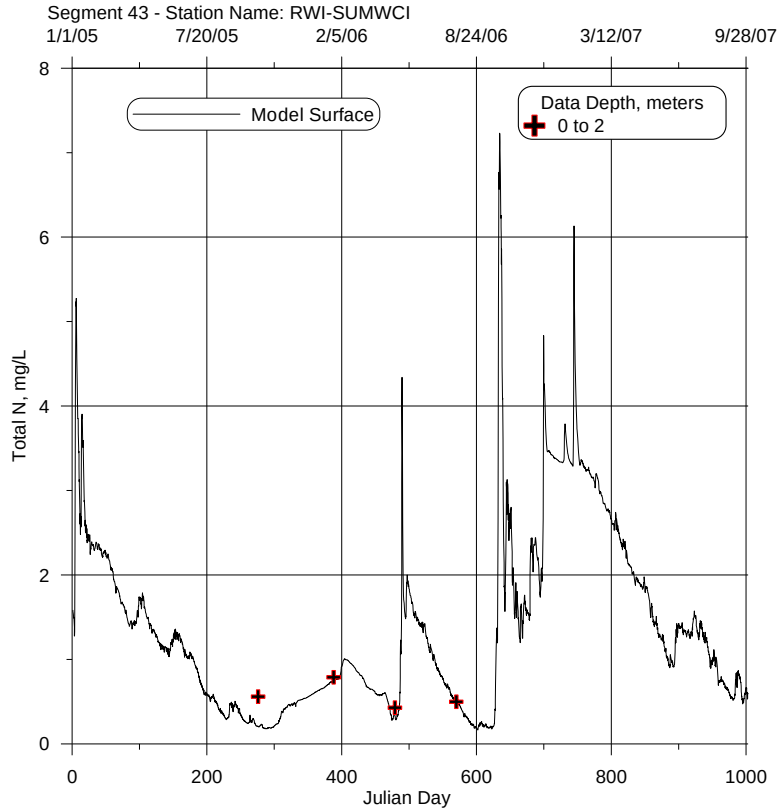

Figure 76. Total nitrogen model vs. data comparison - segment 43 during calibration period.

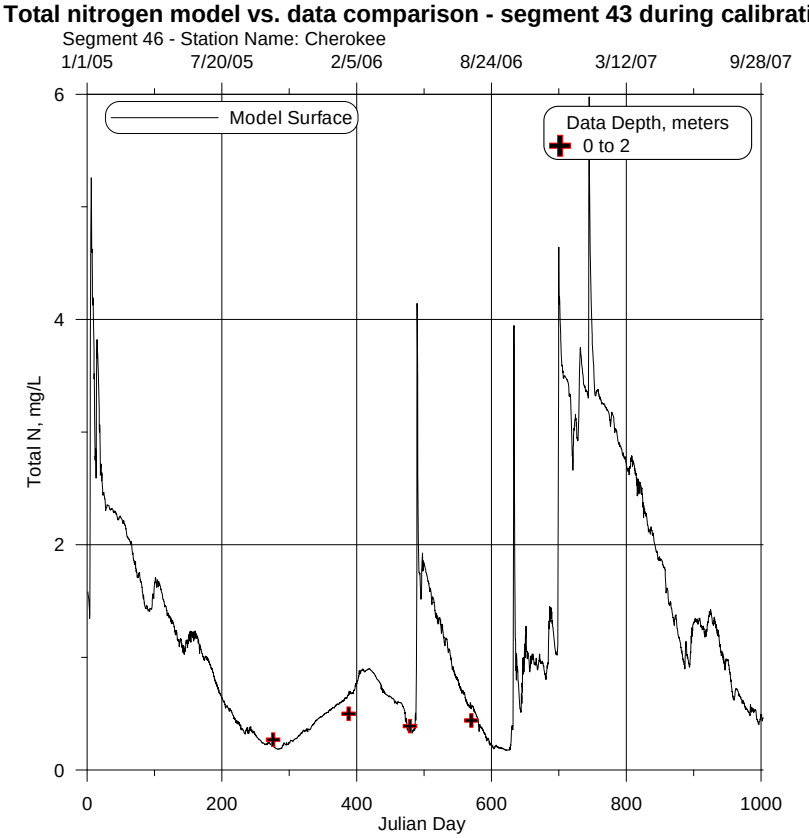

Figure 77. Total nitrogen model vs. data comparison - segment 46 during calibration period.

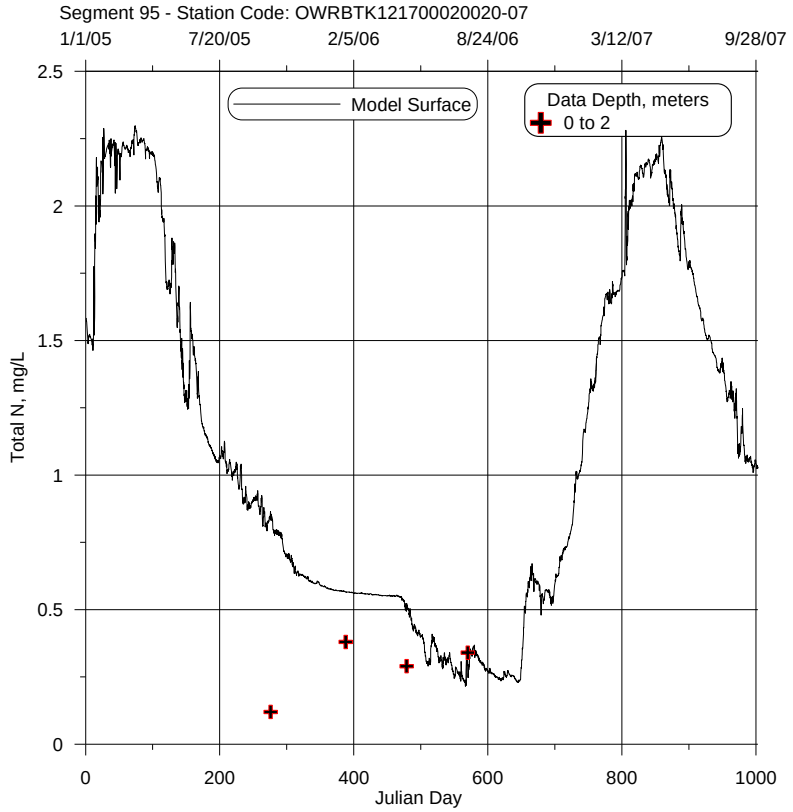

Figure 78. Total nitrogen model vs. data comparison - segment 95 during calibration period.

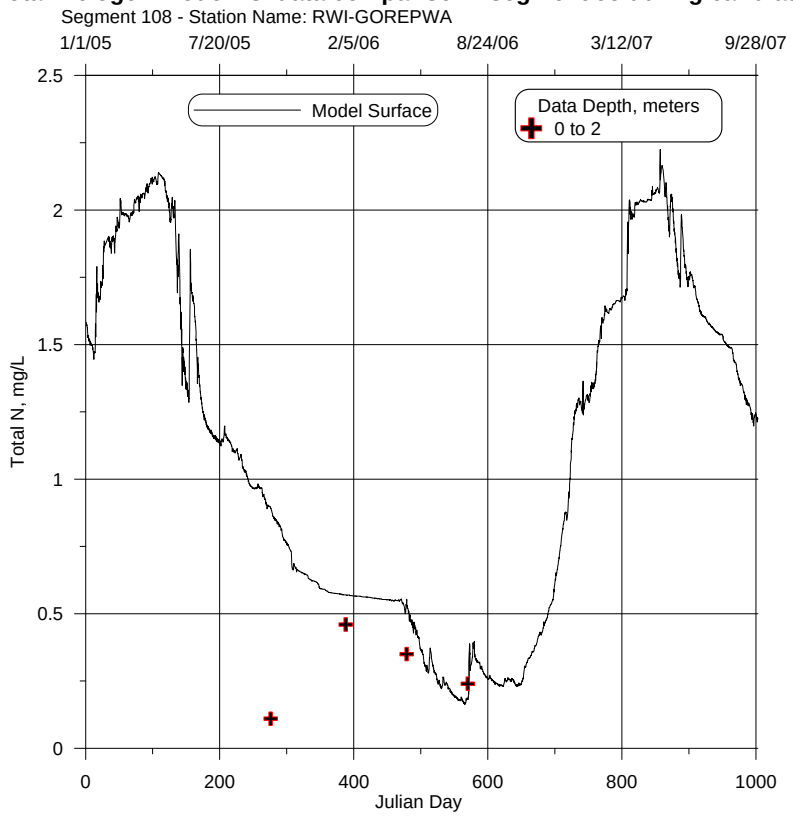

Figure 79. Total nitrogen model vs. data comparison - segment 108 during calibration period.

Ammonia

The ammonia levels in the reservoir were sensitive to inflow boundary conditions and algae, nitrification and organic matter internal processes. The sources and sinks of ammonia during the simulation period are shown in Figure 80 where NH4NITR: nitrification, NH4AR: algae respiration release, NH4AG: algae growth uptake, NH4AP: overall net algae production, NH4ER: epiphyton/periphyton respiration release, NH4EG: epiphyton/periphyton growth uptake, NH4EP: overall net ephiphyton/periphyton production, NH4POM: particulate organic matter oxygen demand, NH4DOM: dissolved organic matter oxygen demand, NH4OM: total organic matter oxygen consumption, NH4SED: first order sediment oxygen demand, NH4SOD: zero order sediment oxygen demand. Principle mechanisms for ammonia uptake/release are algae growth and respiration, nitrification, and organic matter decay. Even though for the entire reservoir SOD and SED release are not large compared to other sources/sinks, their impact on the hypolimnion is large because of the hypolimnion's small volume compared to the upper reservoir. In some cases the algae release of ammonia is greater than uptake during the summer. This can occur as a result of algae favoring nitrate as a N source.

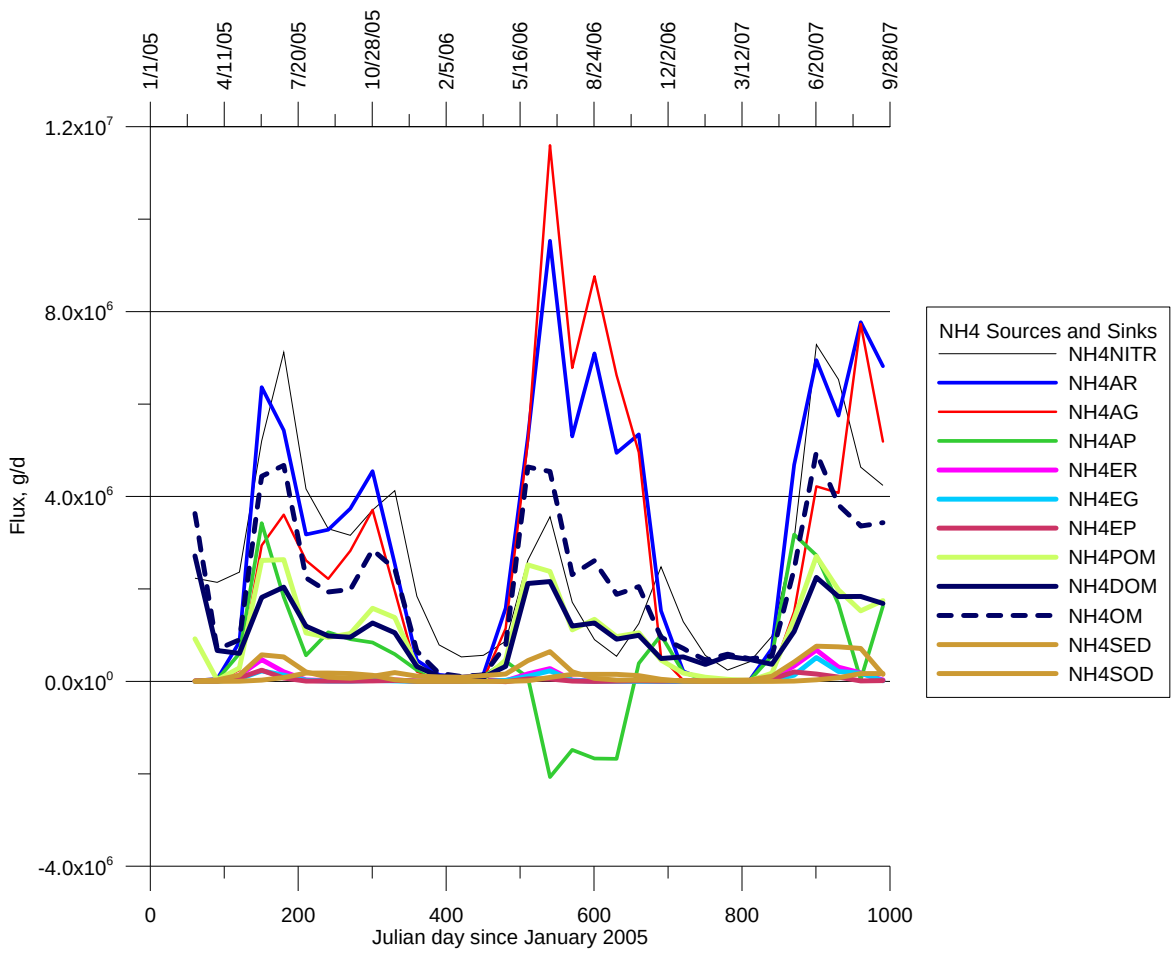

Figure 80. Sources and sinks of ammonia predicted by the model during calibration period.

Ammonia-N concentrations were affected significantly by high inflow events (compare 2005 moderate inflows to 2006 low inflows), algal/periphyton uptake, nitrification dynamics, and sediment release during oxic and anoxic decomposition.. A snapshot of ammonia dynamics in Tenkiller is shown in model-data comparisons in Figure 81, Figure 86, Figure 82, and Figure 83 for the dates 5/19/2005, 8/18/2005, and 9/22/2005, respectively. Generally, during the summer ammonia was depleted in the epilimnion as a result of algae uptake and increased in the hypolimnion due to sediment ammonia release. There were few ammonia field measurements with most comparisons (usually only a near surface and bottom) occurring at segment 109 at the dam. Note that the model results are all shown at 12 noon even though there can be uptake and release depending on the time of day.

Time series model vs. data comparisons of NH_4 are shown for segments 24 and 46 in Figure 84 and Figure 85, respectively. In these figures, the smooth line is the model prediction at the stated depth, and the crosses are the measured field data at the depth shown on the figure.

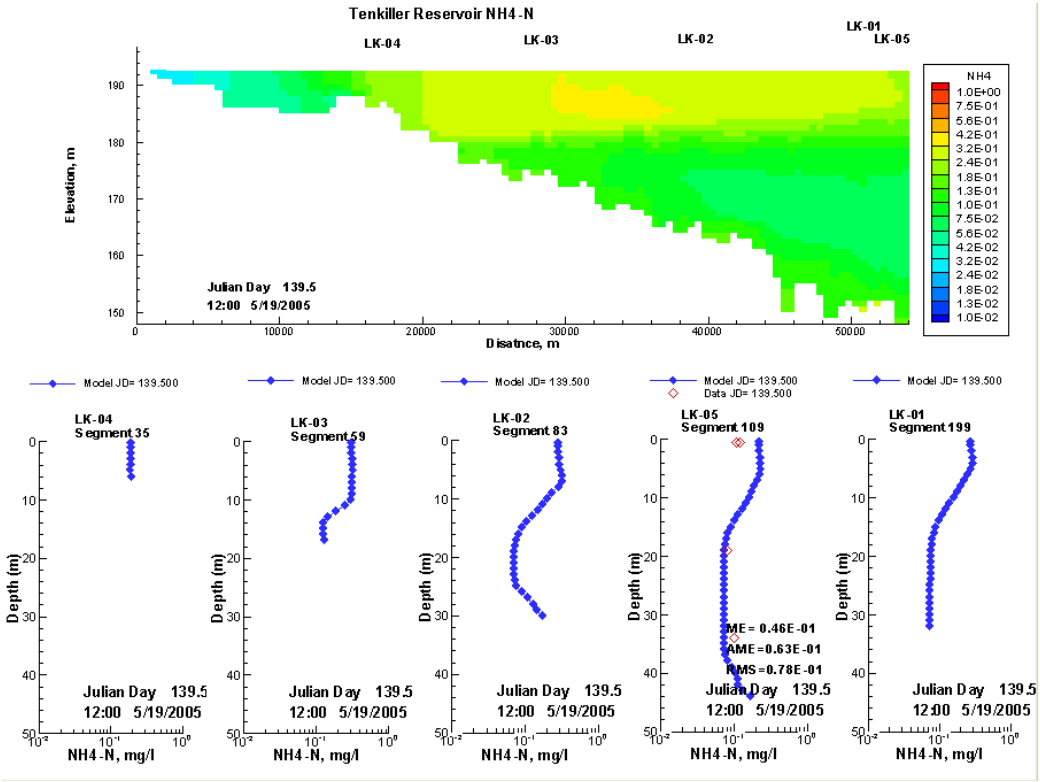

Figure 81. NH_4-N concentrations predicted by the model compared to field data on 5/19/2005.

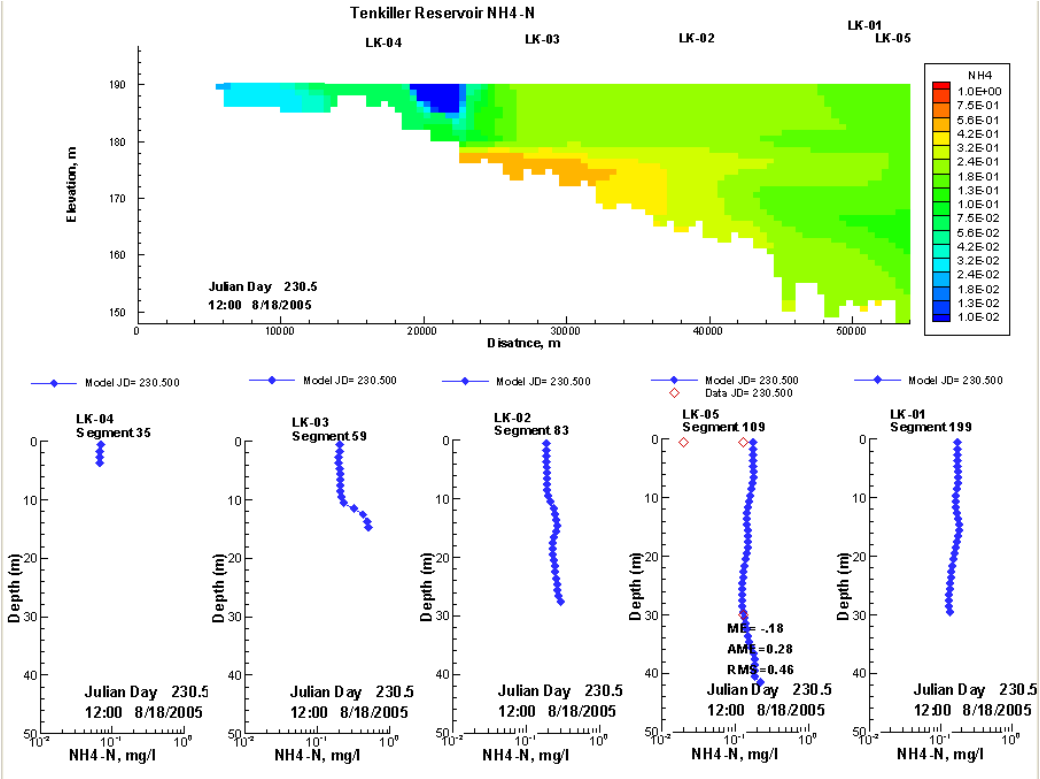

Figure 82. NH_4-N concentrations predicted by the model compared to field data on 8/18/2005.

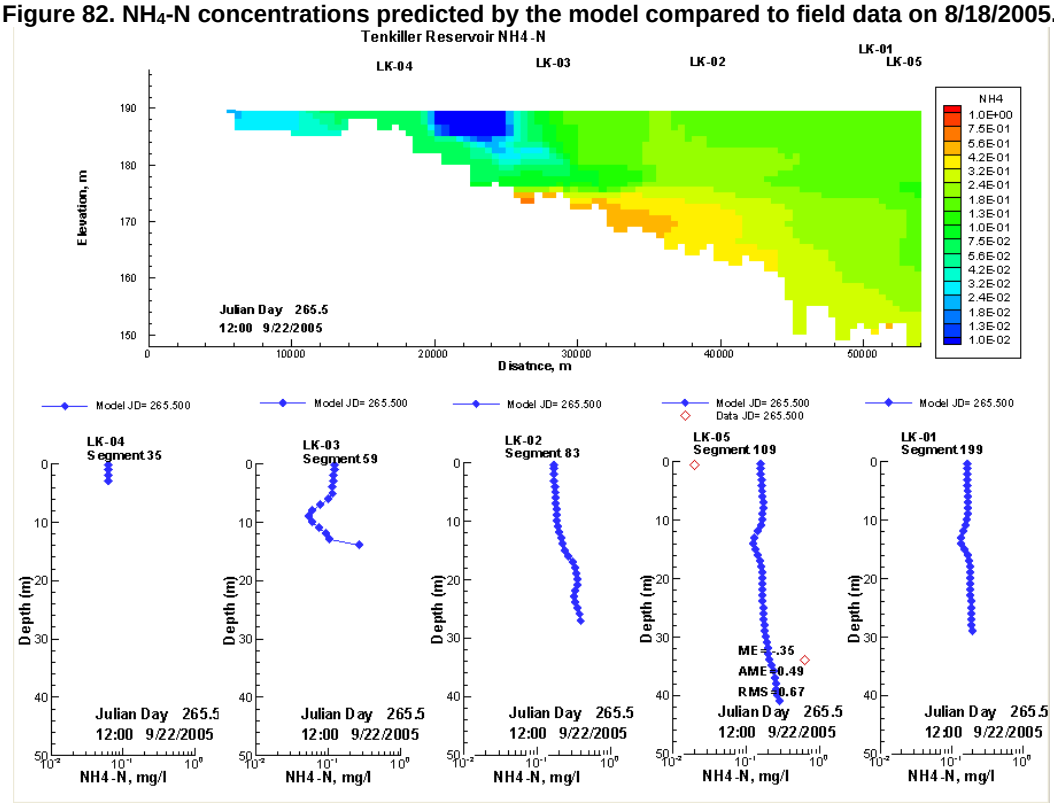

Figure 83. NH_4-N concentrations predicted by the model compared to field data on 9/22/2005.

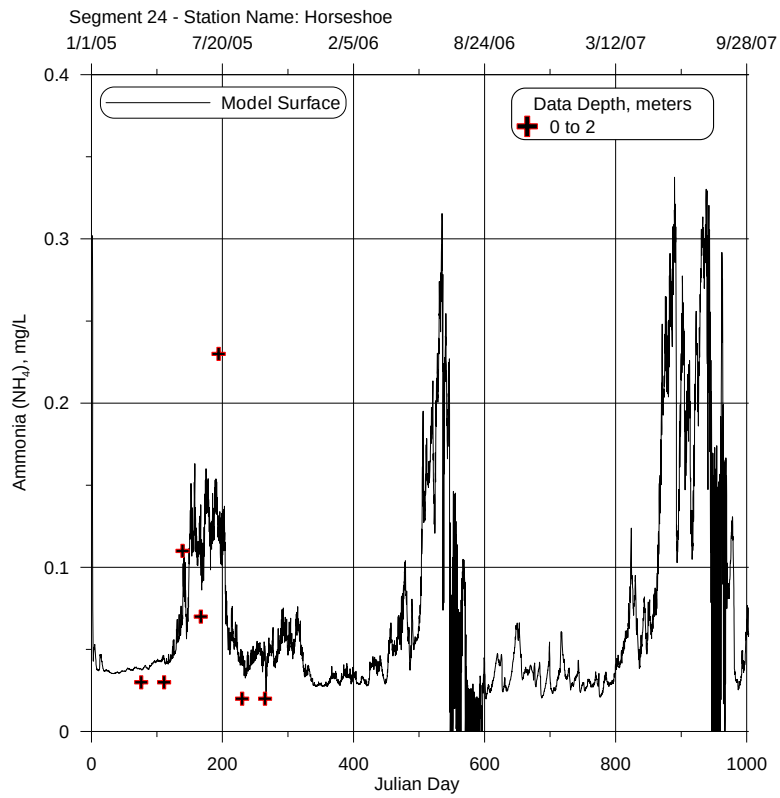

Figure 84. Ammonia as nitrogen model vs. data comparison - segment 24 during calibration period.

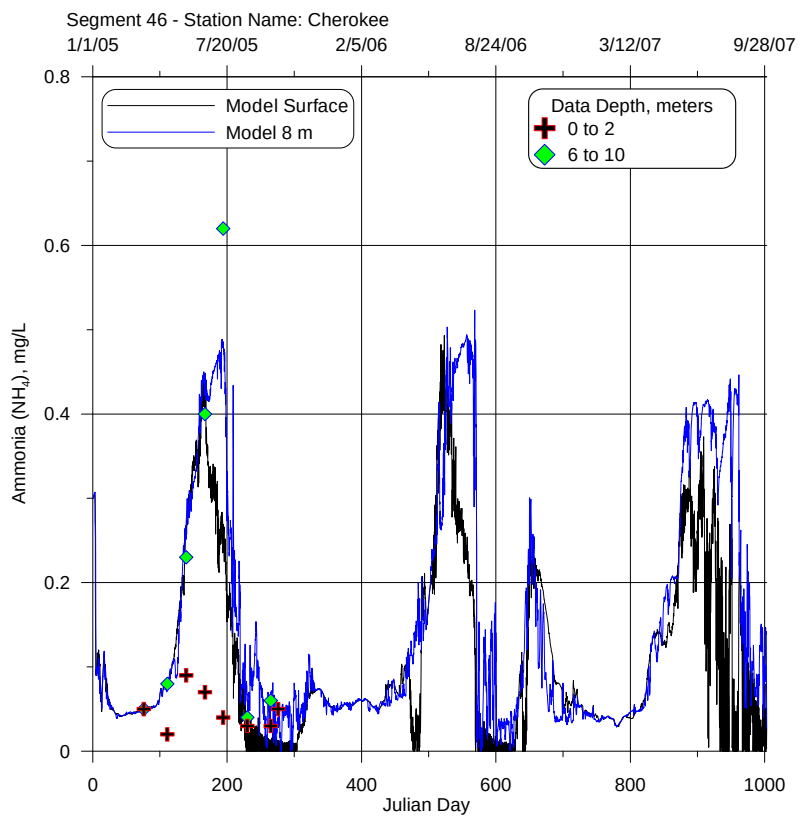

Figure 85. Ammonia as nitrogen model vs. data comparison - segment 46 during calibration period.

Nitrate and Nitrite

Significant nitrate+nitrite sources/sinks included inflow events (compare 2005 moderate inflows to 2006 low inflows), algal/periphyton uptake, and nitrification dynamics. A snapshot of nitrate dynamics in Tenkiller is shown in model-data comparisons in Figure 86, Figure 87, Figure 88, Figure 89, and Figure 90 for the dates 6/2/2005, 6/15/2005, 7/12/2005, 7/26/2005, and 8/9/2005, respectively. The typical pattern is that nitrate is depeted from the epilimnion as a result of algae uptake.

Time series model vs. data comparisons of total nitrate + nitrite are shown in Figure 91, Figure 92, Figure 93, Figure 94, Figure 95, Figure 96, Figure 97, Figure 98, and Figure 99 at various model segments. In these figures, the smooth line is the model prediction at the stated depth, and the crosses are the measured field data at the depth shown on the figure.

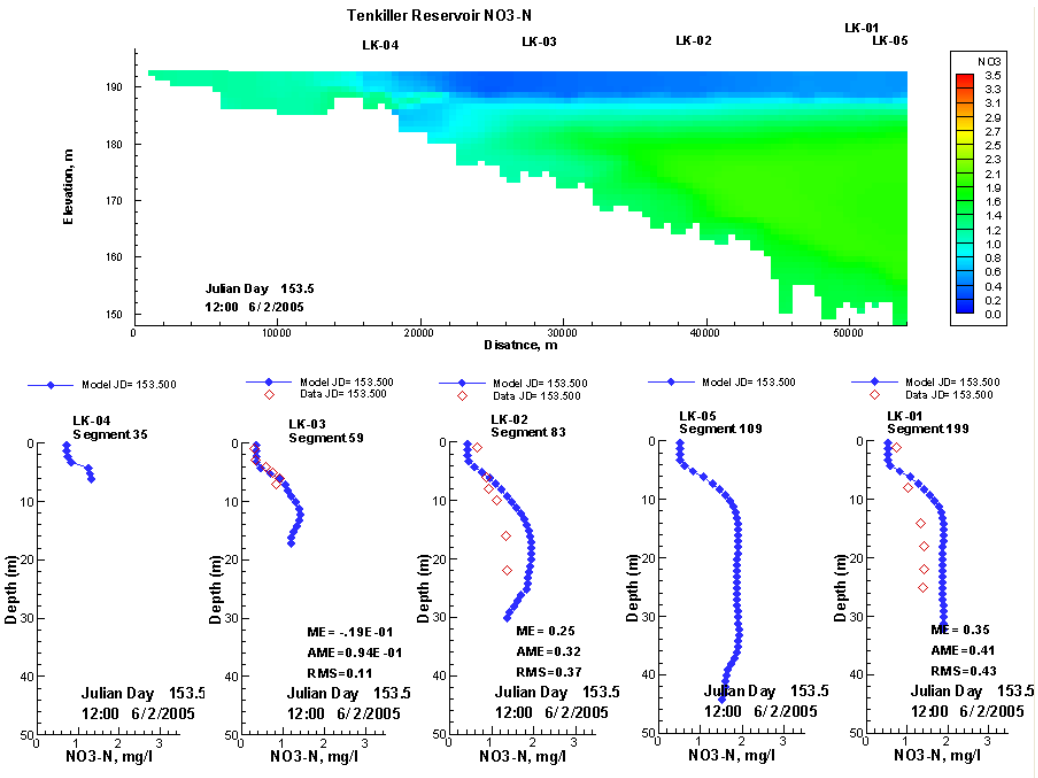

Figure 86. NO_3-N concentrations predicted by the model compared to field data on 6/2/2005.

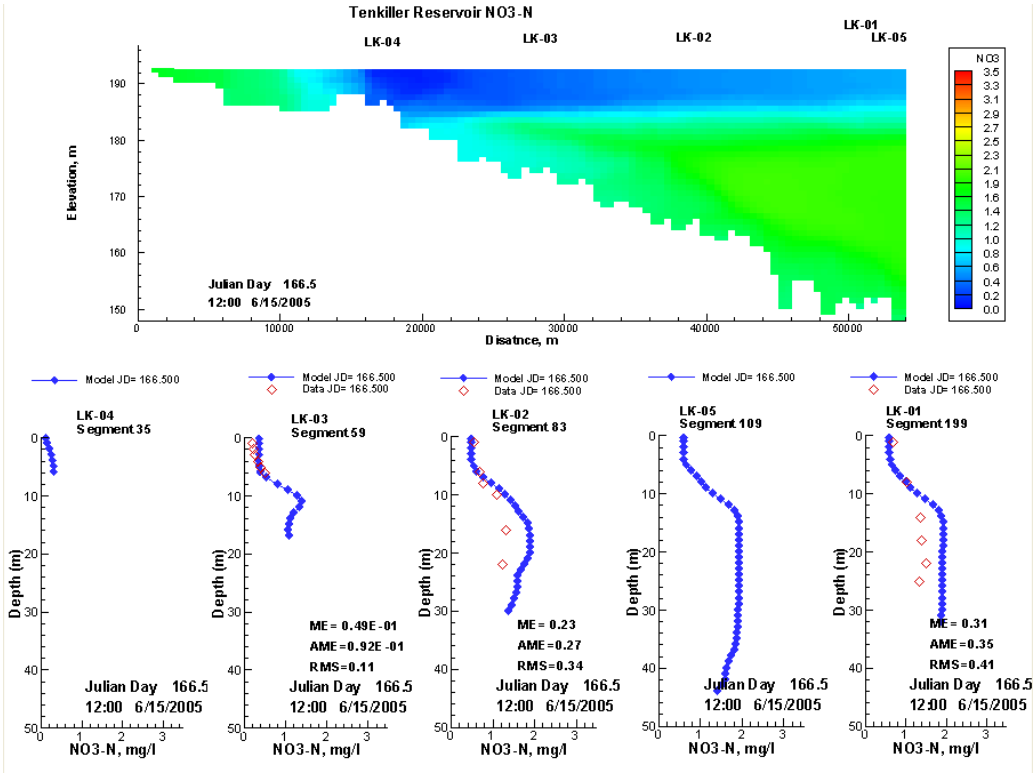

Figure 87. NO_3-N concentrations predicted by the model compared to field data on 6/15/2005.

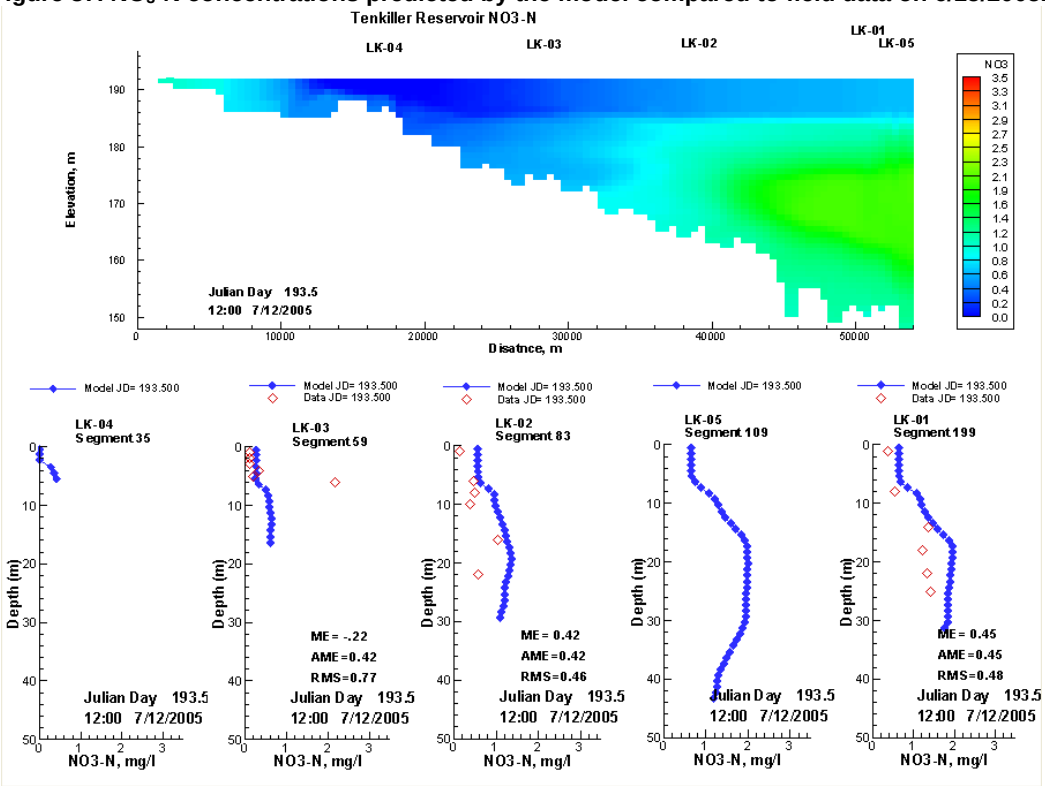

Figure 88. NO_3-N concentrations predicted by the model compared to field data on 7/12/2005.

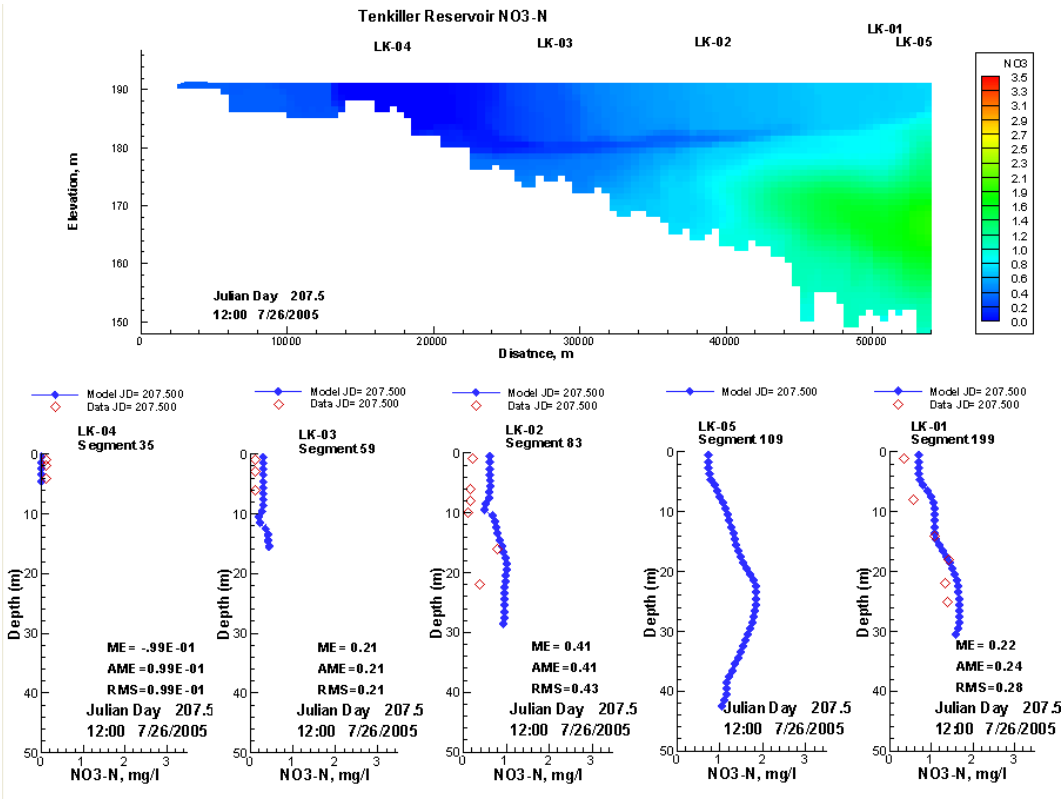

Figure 89. NO_3-N concentrations predicted by the model compared to field data on 7/26/2005.

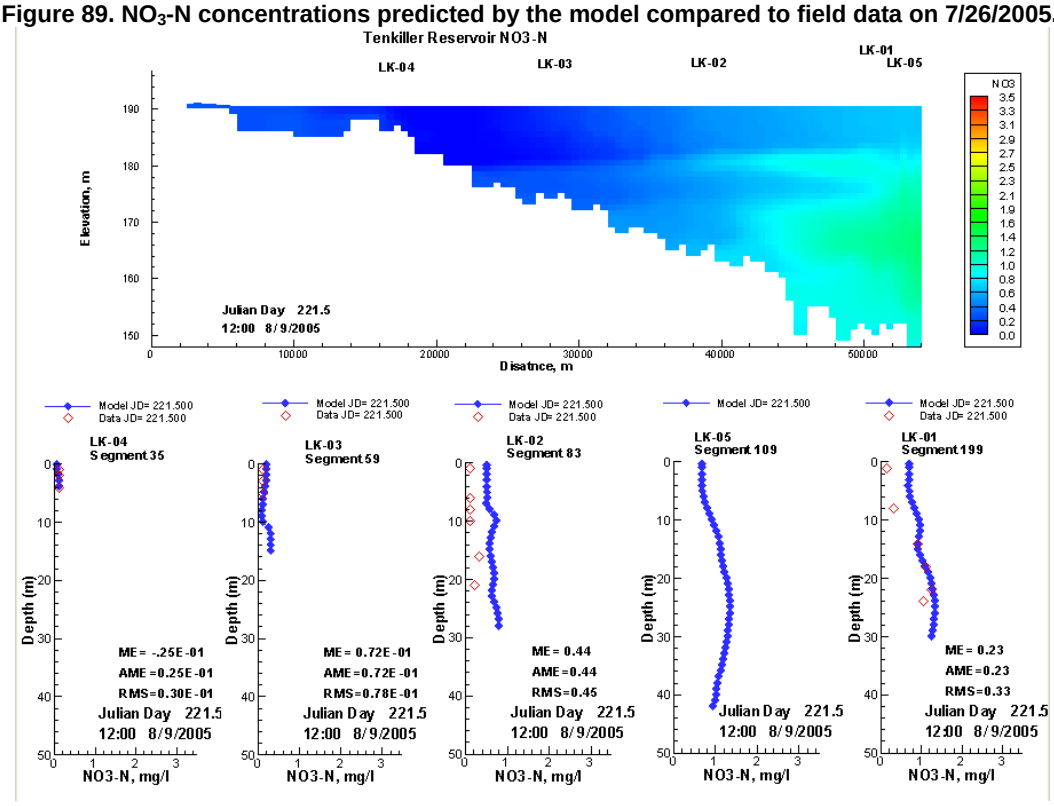

Figure 90. NO_3-N concentrations predicted by the model compared to field data on 8/9/2005.

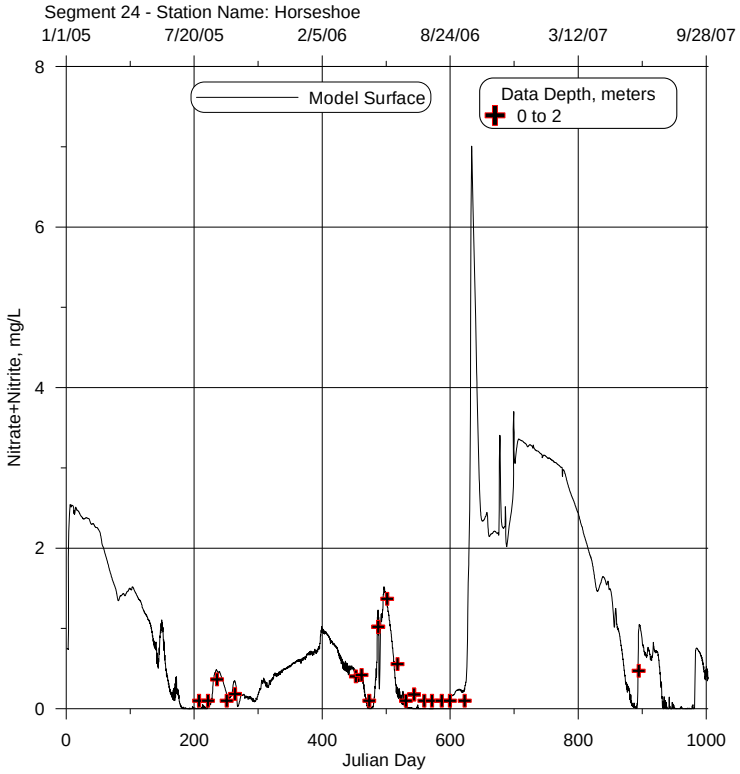

Figure 91. Total nitrate + nitrite as nitrogen model vs. data comparison - segment 24 during calibration period.

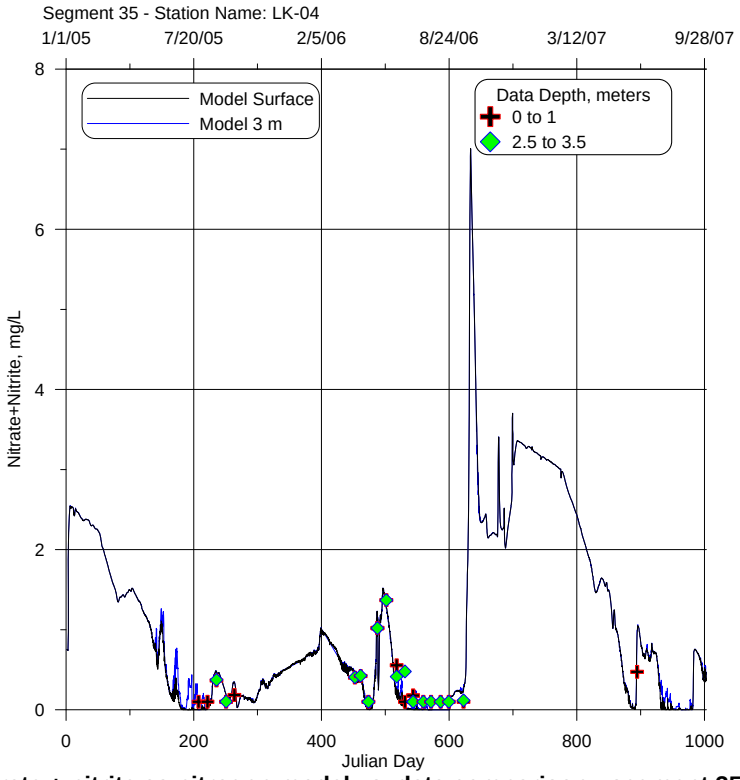

Figure 92. Total nitrate + nitrite as nitrogen model vs. data comparison - segment 35 during calibration period.

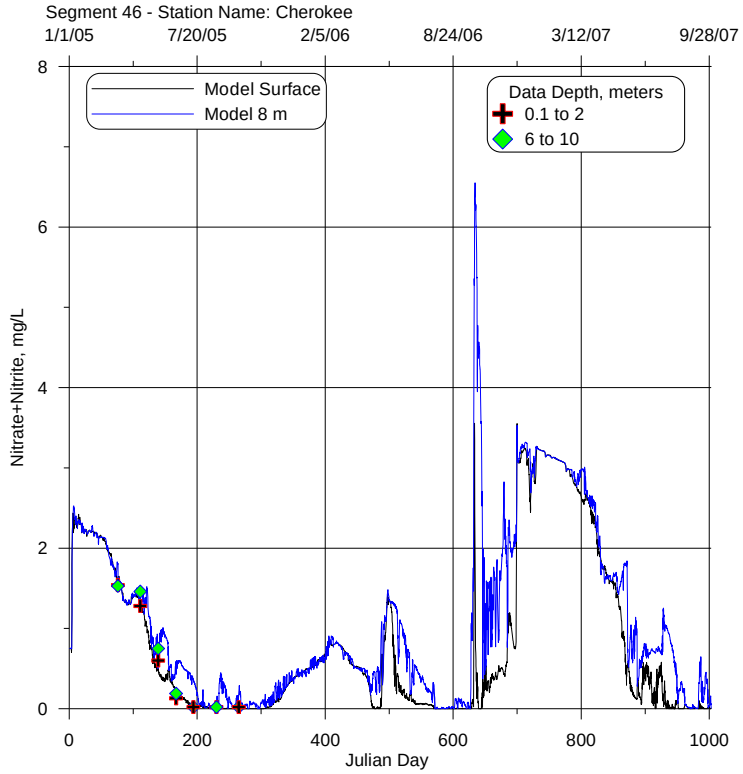

Figure 93. Total nitrate + nitrite as nitrogen model vs. data comparison - segment 46 during calibration period.

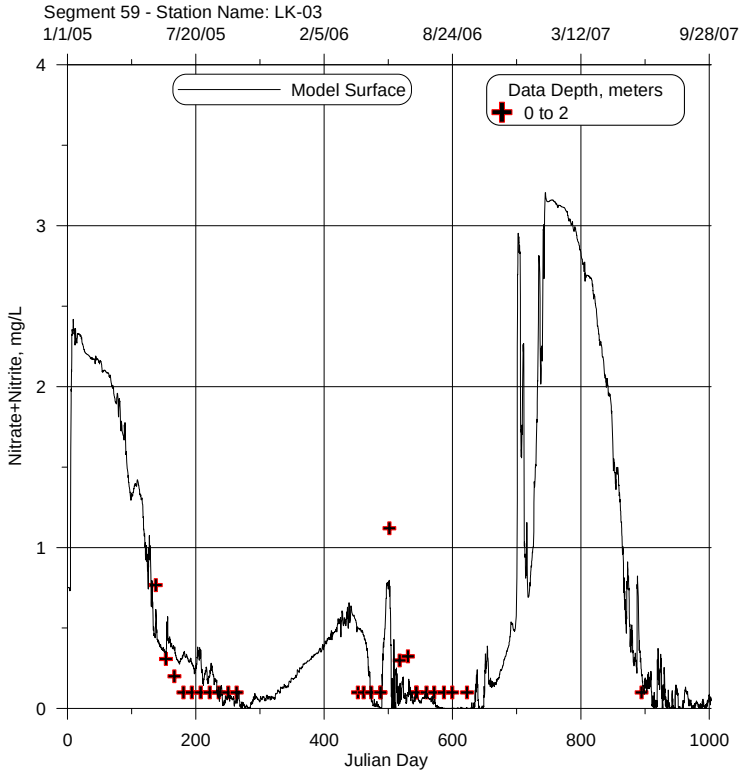

Figure 94. Total nitrate + nitrite as nitrogen model vs. data comparison - segment 59 during calibration period.

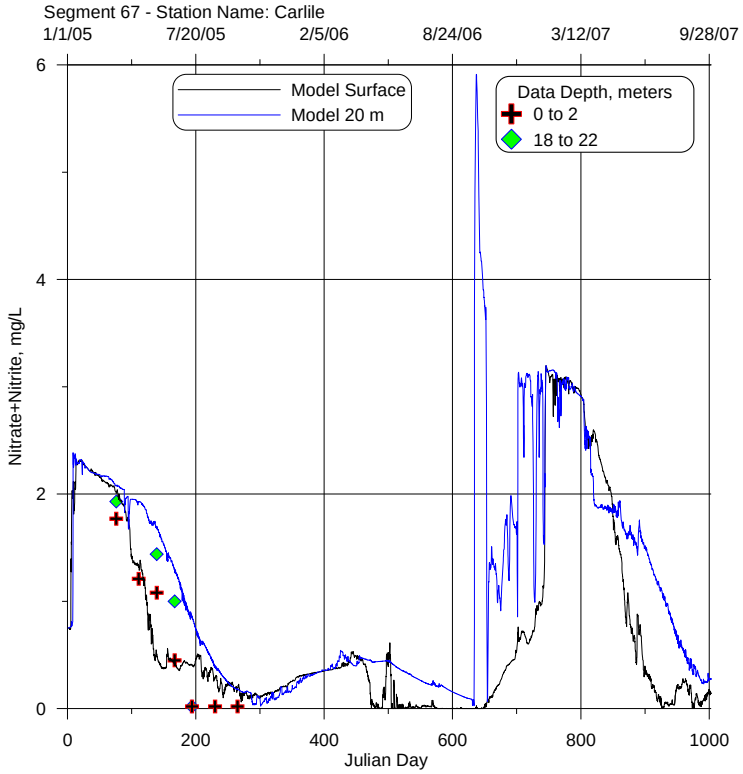

Figure 95. Total nitrate + nitrite as nitrogen model vs. data comparison - segment 67 during calibration period.

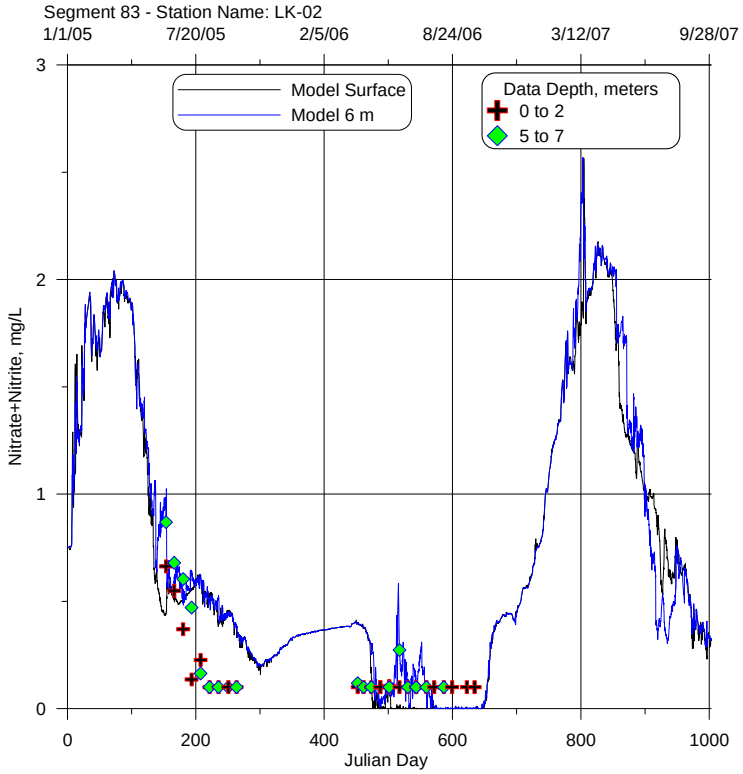

Figure 96. Total nitrate + nitrite as nitrogen model vs. data comparison - segment 83 during calibration period.

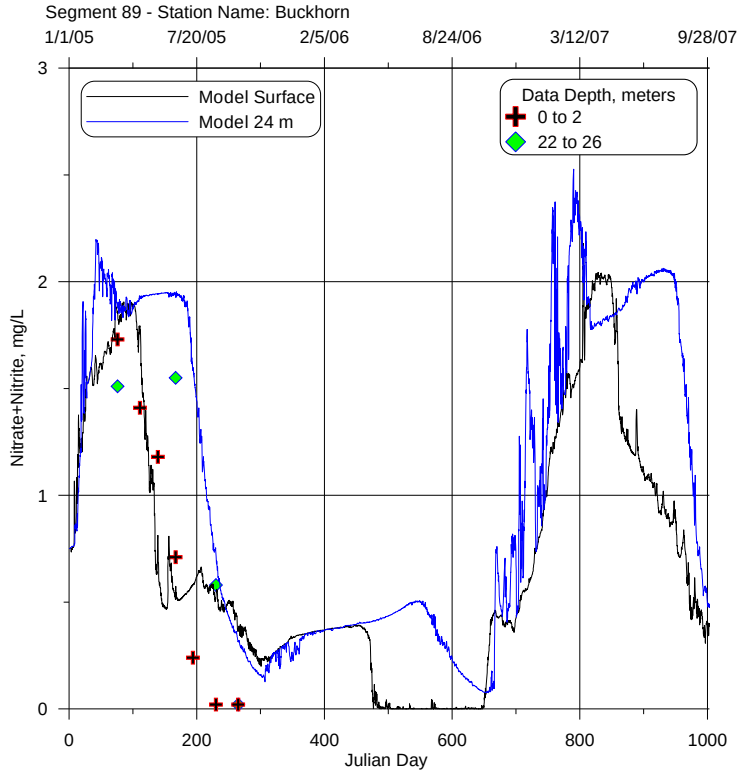

Figure 97. Total nitrate + nitrite as nitrogen model vs. data comparison - segment 89 during calibration period.

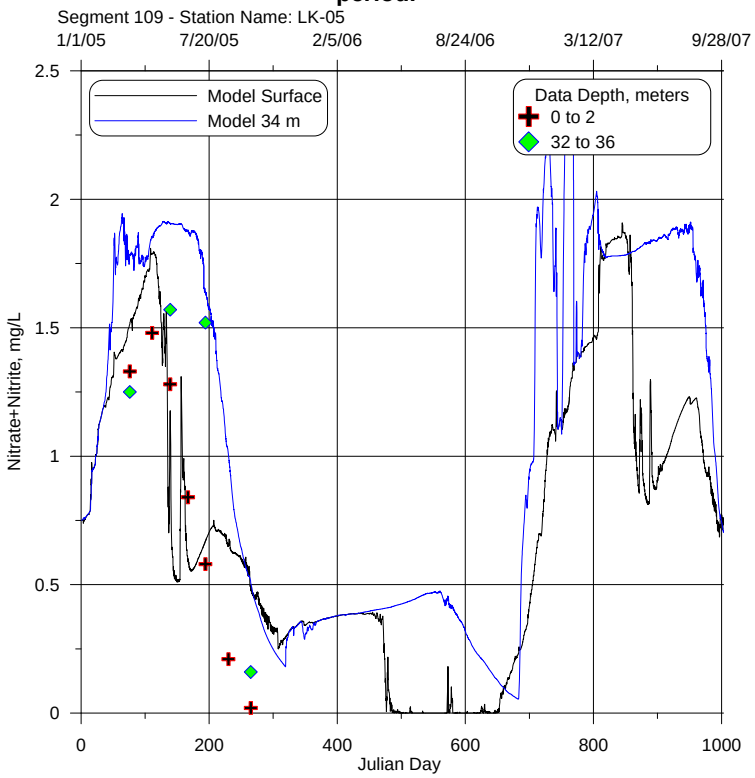

Figure 98. Total nitrate + nitrite as nitrogen model vs. data comparison - segment 109 during calibration period.

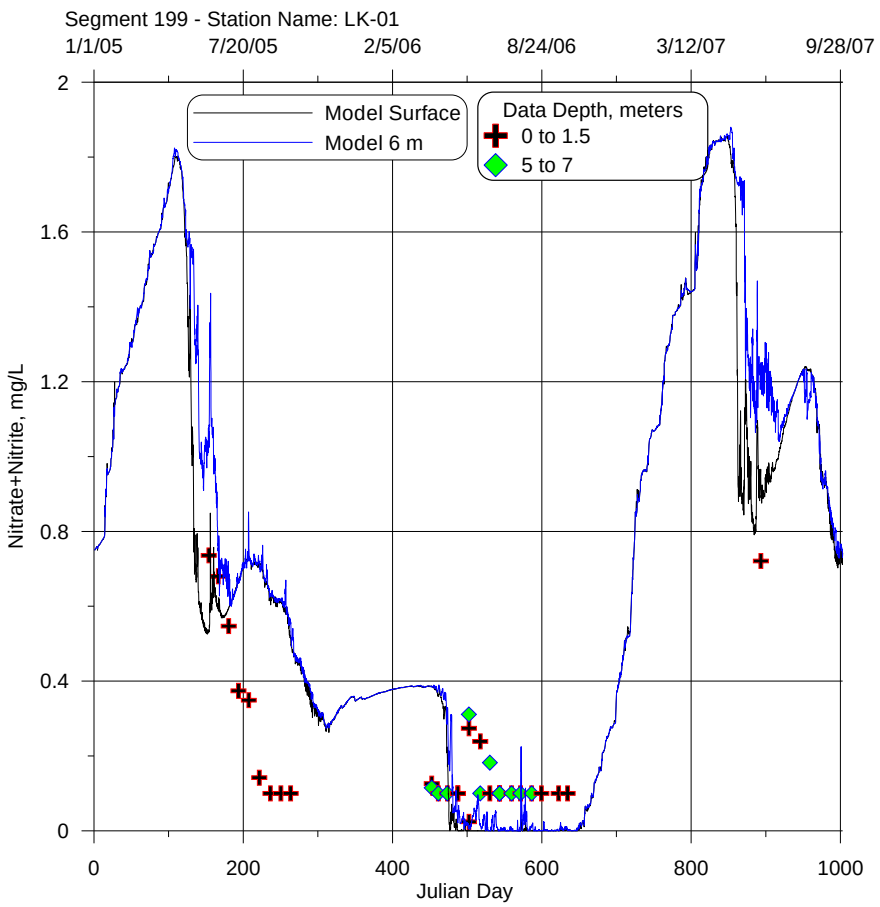

Figure 99. Total nitrate + nitrite as nitrogen model vs. data comparison - segment 199 during calibration period.

Total Phosphorus

Total Phosphorus is a computed derived variable in CE-QUAL-W2. Total P in mg/l is computed using the following state variables:

$$Total\ P = PO_4 - P + \sum ALGP * C_{algae} + \sum ORGP * C_{organicmatter}$$

where PO_4-P is dissolved ortho-phosphorus, C_{algae} is the concentration of algae on a dry weight basis, ALGP is the stoichiometric coefficient for each algae group, $C_{organic_matter}$ is the concentration of LPOM+ RPOM+ LDOM+ RDOM, and ORGP is the stoichiometric coefficient for organic matter:P.

Time series comparisons of Total P at model segments 24, 35, 43, 46, 59, 67, 83, 89, 108, and 109 is shown in Figure 100, Figure 101, Figure 102, Figure 103, Figure 104, Figure 105, Figure 106, Figure 107, Figure 108, Figure 109, and Figure 110 respectively. In these figures, the smooth line is the model prediction at the stated depth, and the discrete points are the measured field data at the depth shown on the figure. Most field data shown were taken in 2005, with fewer measurements in the later 2 years. Some of the stations show near surface and hypolimnetic samples.

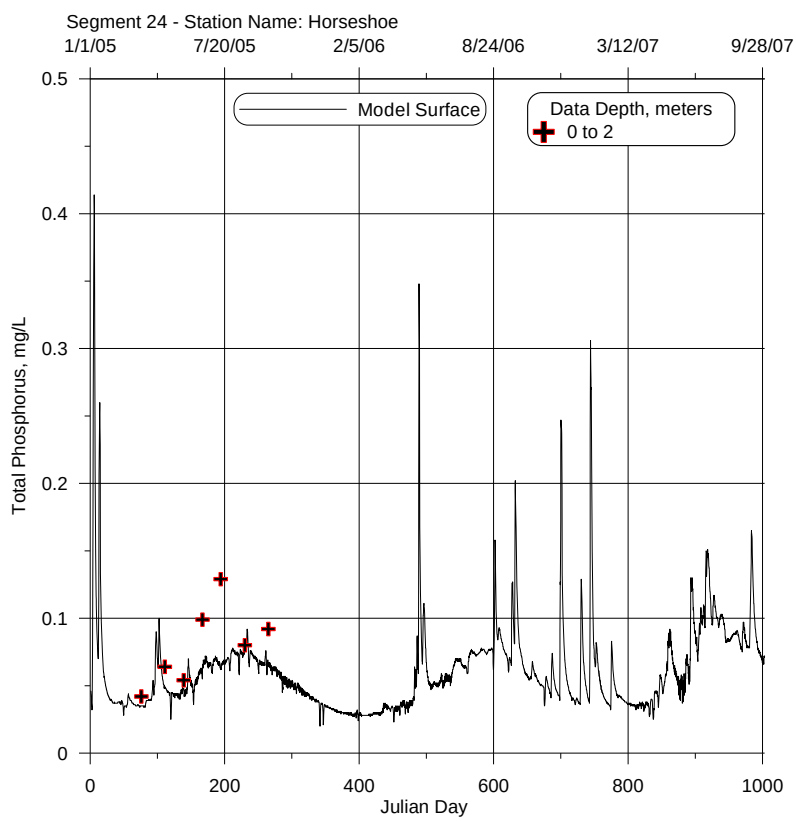

Figure 100. Total phosphorus model vs. data comparison – segment 24 during calibration period.

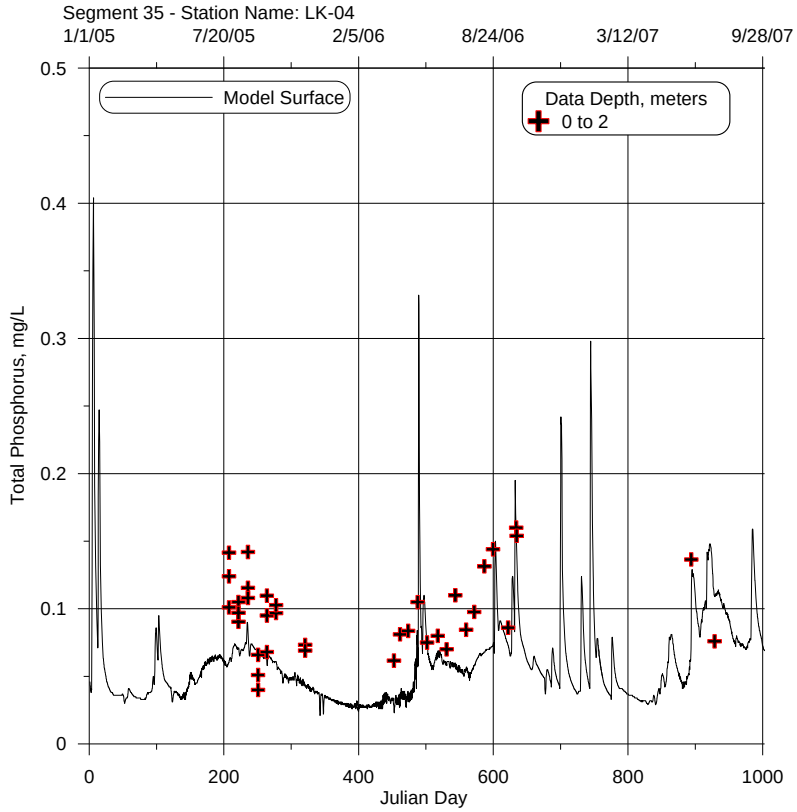

Figure 101.Total phosphorus model vs. data comparison – segment 35 during calibration period.

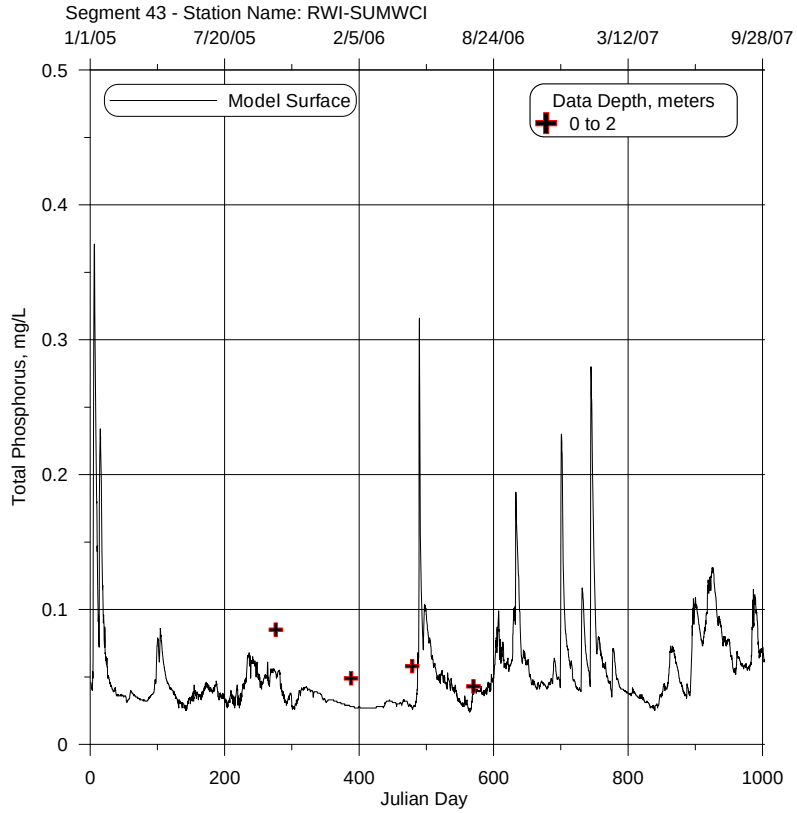

Figure 102. Total phosphorus model vs. data comparison – segment 43 during calibration period.

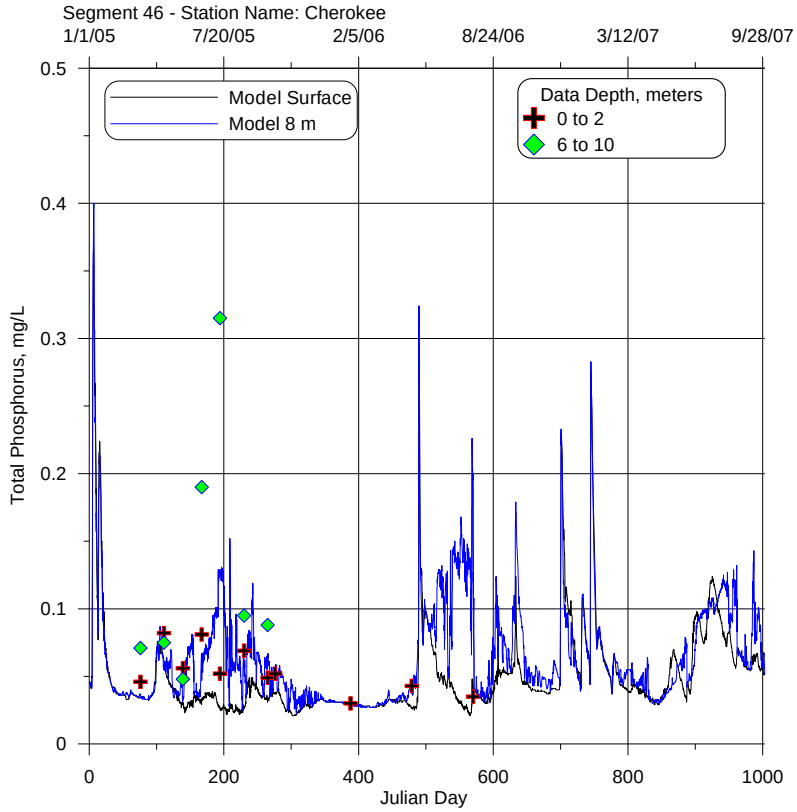

Figure 103. Total phosphorus model vs. data comparison – segment 46 during calibration period.

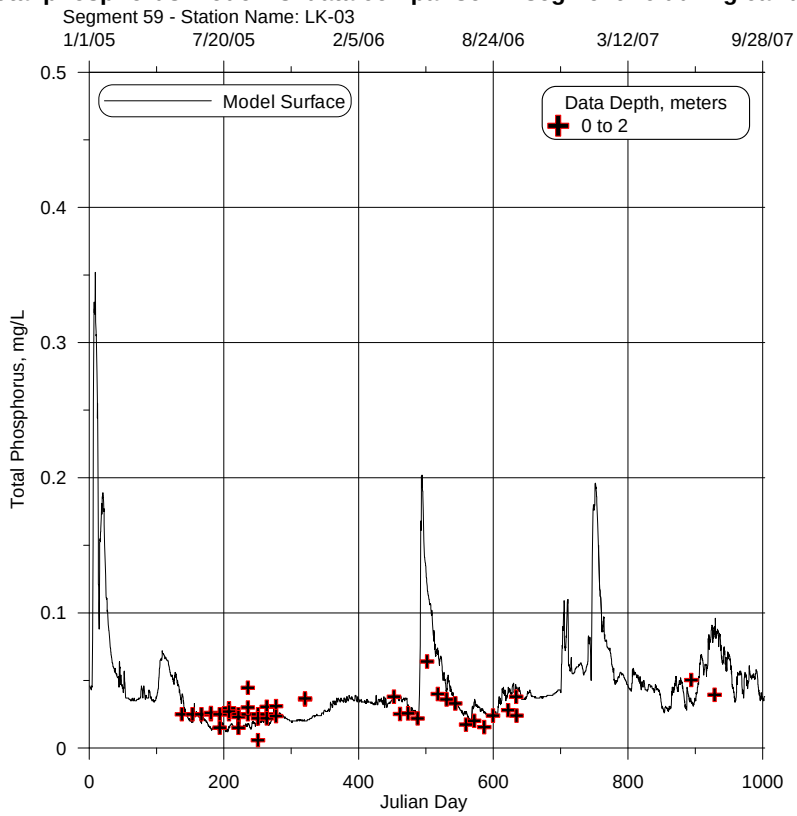

Figure 104. Total phosphorus model vs. data comparison – segment 59 during calibration period.

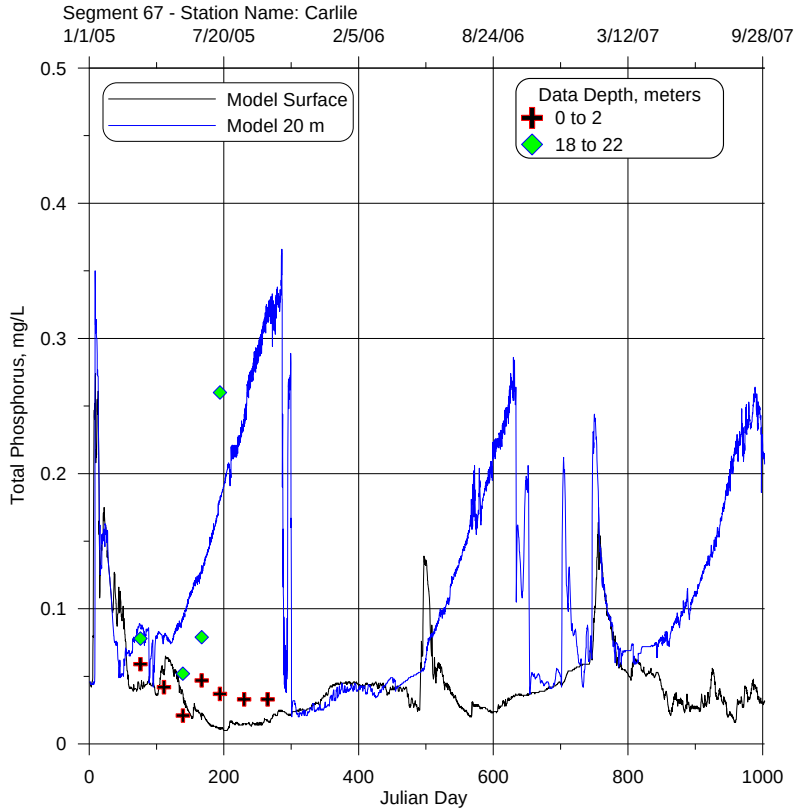

Figure 105. Total phosphorus model vs. data comparison – segment 67 during calibration period.

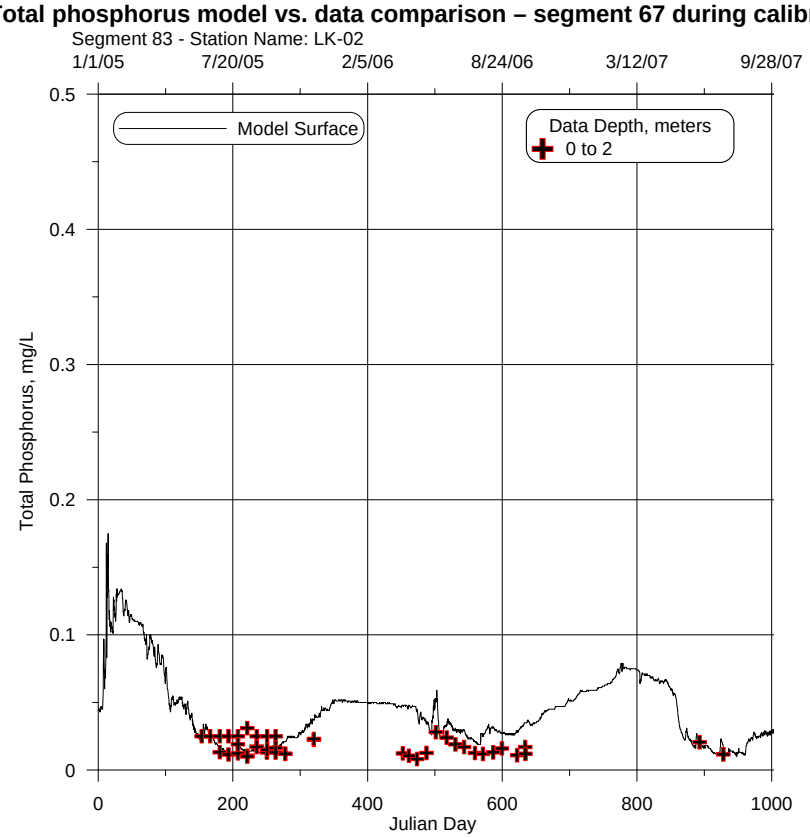

Figure 106. Total phosphorus model vs. data comparison – segment 83 during calibration period.

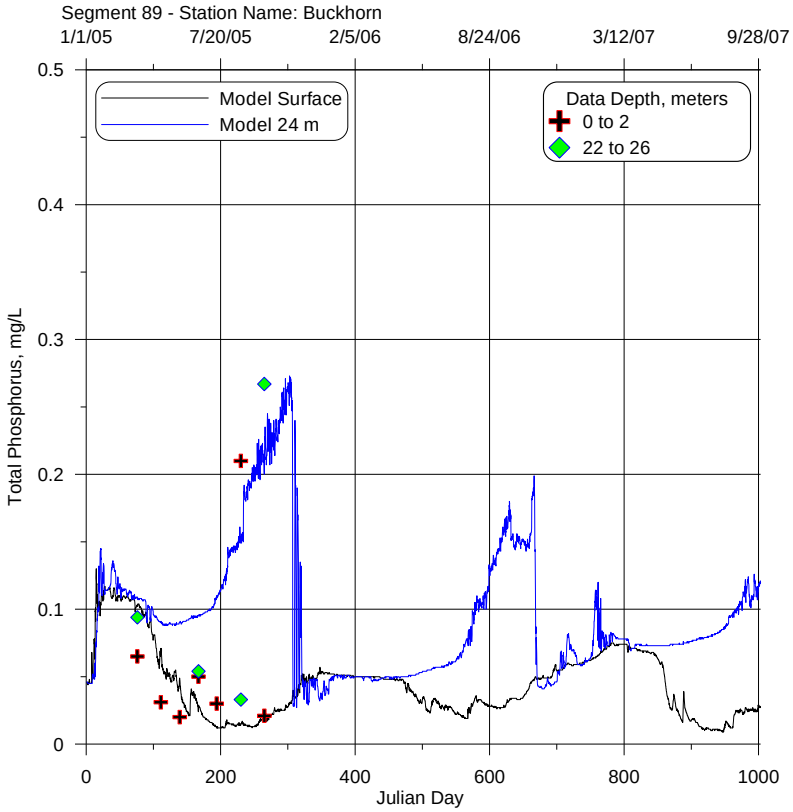

Figure 107. Total phosphorus model vs. data comparison – segment 89 during calibration period.

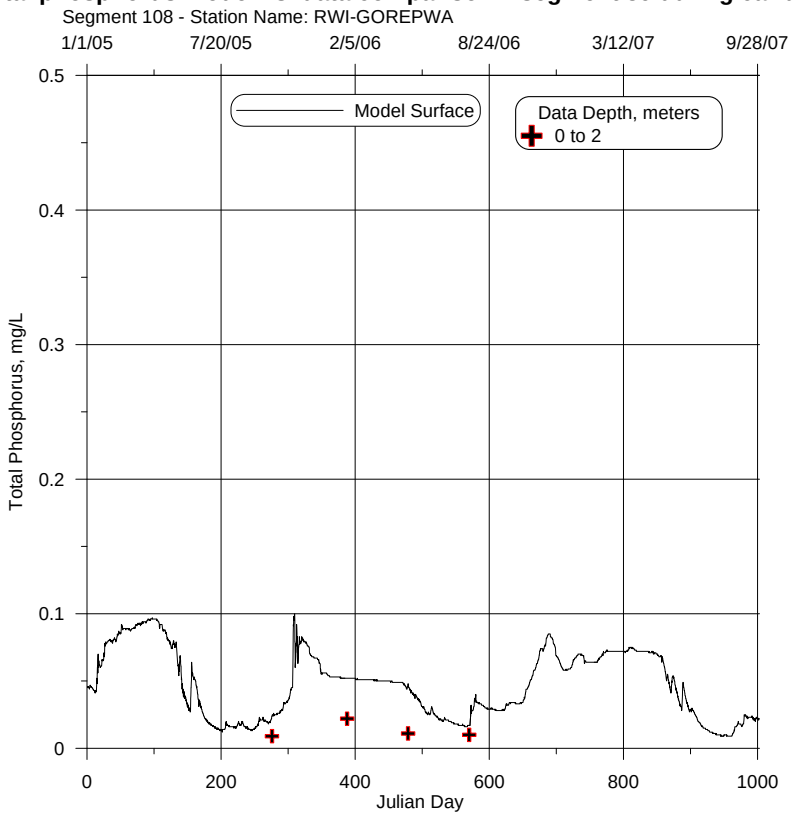

Figure 108. Total phosphorus model vs. data comparison – segment 108 during calibration period.

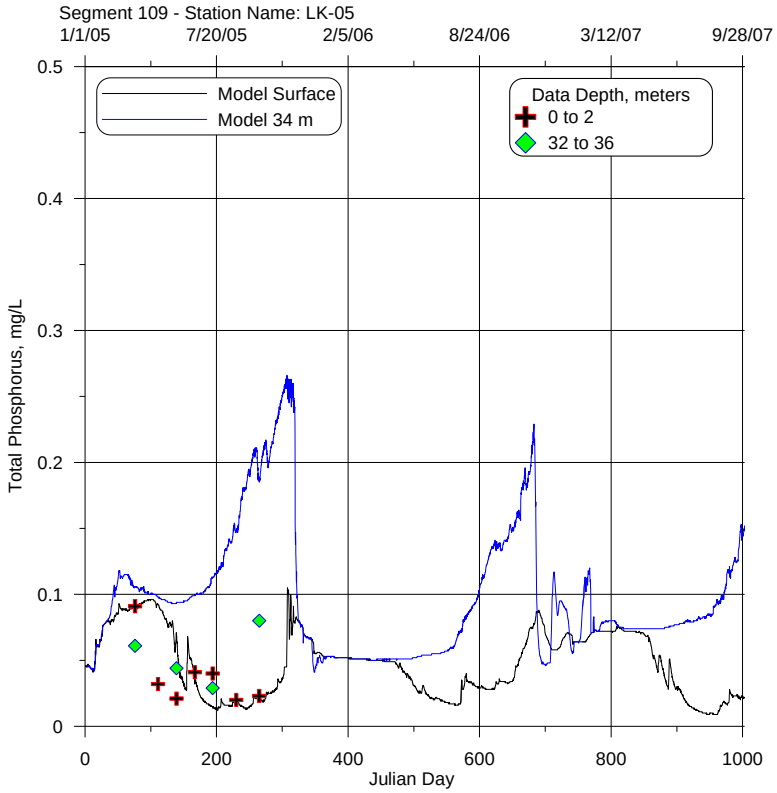

Figure 109. Total phosphorus model vs. data comparison – segment 109 during calibration period.

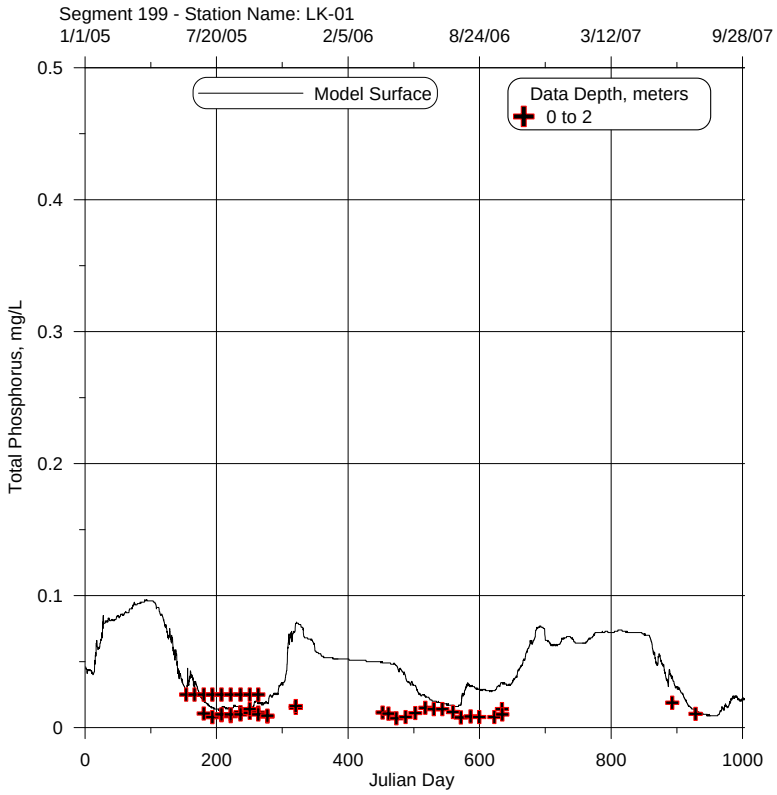

Figure 110. Total phosphorus model vs. data comparison – segment 199 during calibration period.

Dissolved Ortho Phosphorus

The dissolved PO_4-P levels in the reservoir were sensitive to inflow boundary conditions and algae, sediment and organic matter internal processes. The sources and sinks of PO_4-P during the simulation period are shown in Figure 111 where PO4AR: algae respiration PO_4 release, PO4AG: algae growth PO_4 uptake, PO4AP: overall net algae PO_4 release(uptake), PO4ER: epiphyton/periphyton respiration release, PO4EG: epiphyton/periphyton growth PO_4 uptake, PO4EP: overall net ephiphyton/periphyton PO_4 release (uptake), PO4POM: particulate organic matter PO_4 release, PO4DOM: dissolved organic matter PO_4 release, PO4OM: total organic matter PO_4 release, PO4SED: first order sediment PO_4 release, PO4SOD: zero order sediment PO_4 release. During the summer, algal uptake was the largest sink of PO_4. Release of PO_4 from organic matter decay from the water column and release of PO_4 from the sediment were also large sources of PO_4 when water temperatures were high.

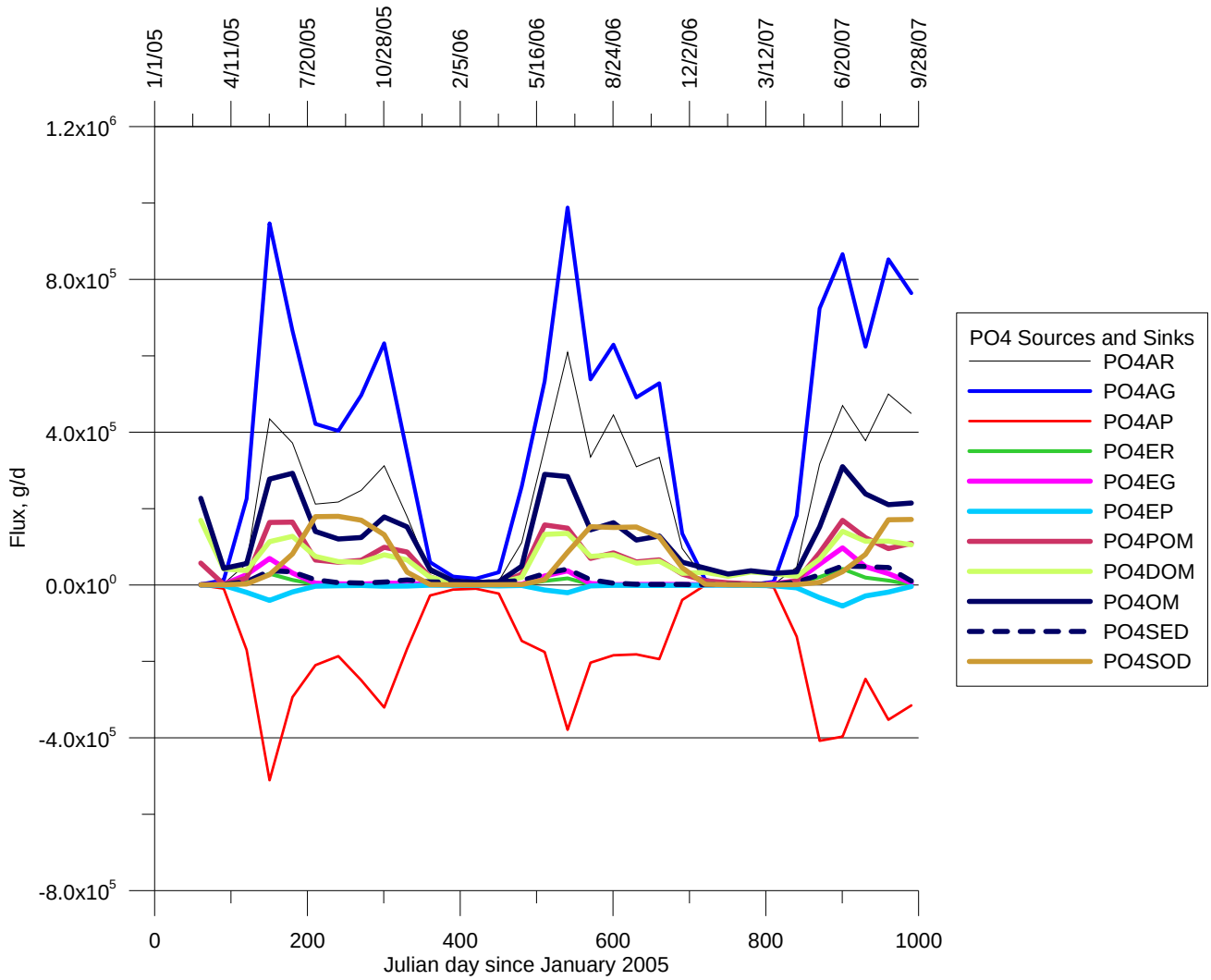

Figure 111. Sources and sinks of dissolved PO_4-P predicted by the model during calibration period.

PO_4-P concentrations were affected significantly by inflow events, algal/periphyton dynamics, organic matter decay, and sediment release during oxic and anoxic decomposition.. A snapshot of dissolved ortho-P dynamics in Tenkiller is shown in model-data comparisons in Figure 112, Figure 113, and Figure 114 for the dates 5/19/2005, 6/16/2005, and 10/3/2005, respectively. Many of the measurements were at the detection limits in the epilimnion during the summer. This means that the measured concentration is at the detection limit or is less than the detection limit. Hence many of the model-data comparisons at the surface show data at the detection limit while the model result is lower than the detection limit. The model usually predicts very low concentrations of PO_4 at the surface during the summer because of algal uptake, and increased concentrations in the hypolimnion during the summer as PO_4 is released from the anoxic sediments.

Figure 115, Figure 116, Figure 117, Figure 118, Figure 119, Figure 120, Figure 121, Figure 122, Figure 123, and Figure 124 show model predictions of ortho phosphorus compared to measured field data for the calibration period for model segments 24, 35, 46, 59 [LK03], 67, 83, 89 [LK02], 108 [LK01], 109, and 199 [LK05], respectively. The solid line represents model predictions and the discrete points represent field measurements.

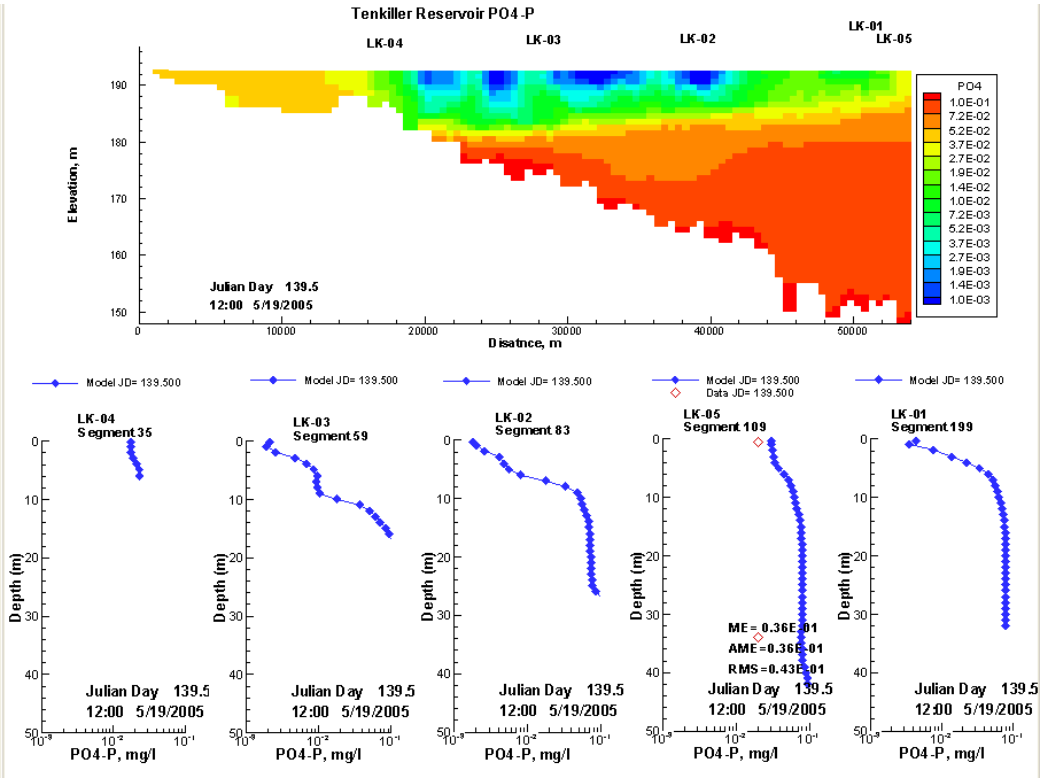

Figure 112. PO_4-P concentrations predicted by the model compared to field data on 5/19/2005.

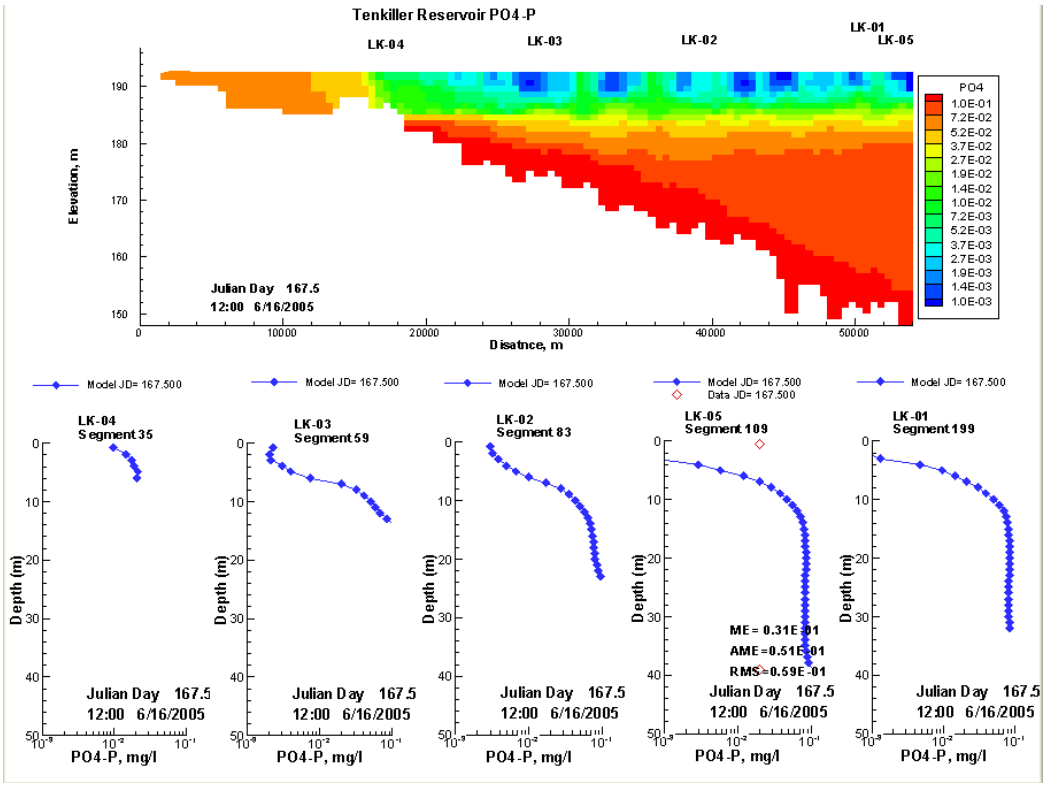

Figure 113. PO_4-P concentrations predicted by the model compared to field data on 6/16/2005.

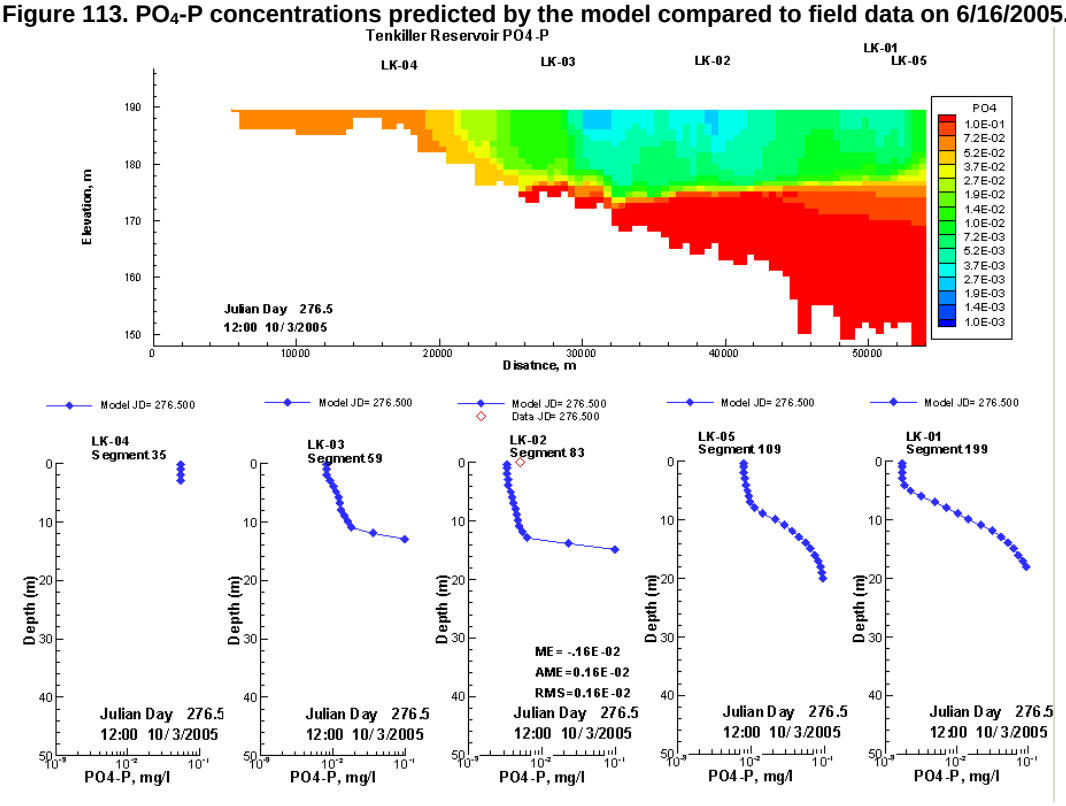

Figure 114. PO_4-P concentrations predicted by the model compared to field data on 10/3/2005.

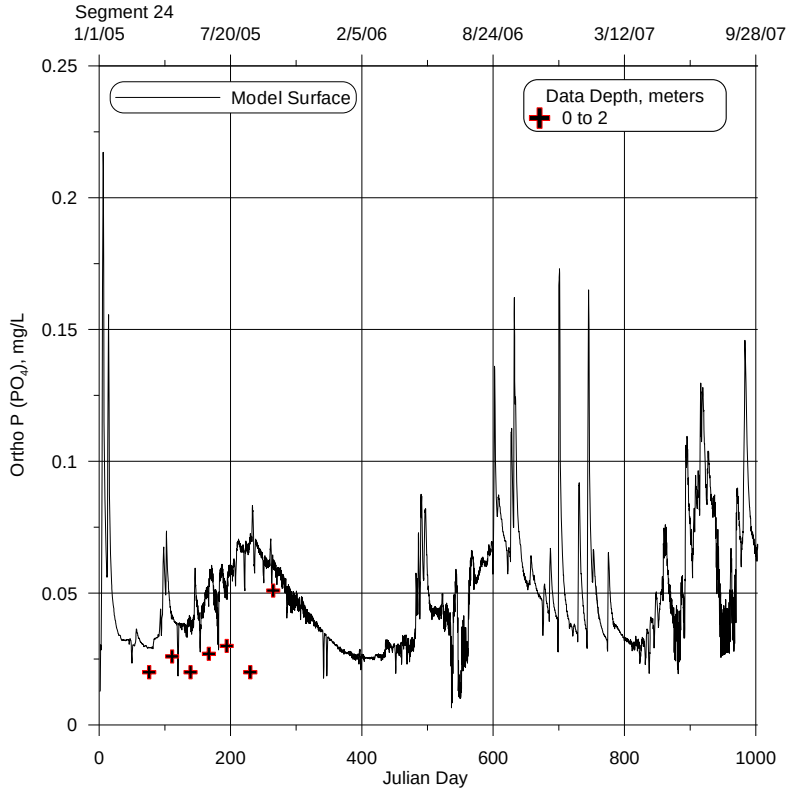

Figure 115. Ortho phosphorus model vs. data comparison – segment 24 during calibration period.

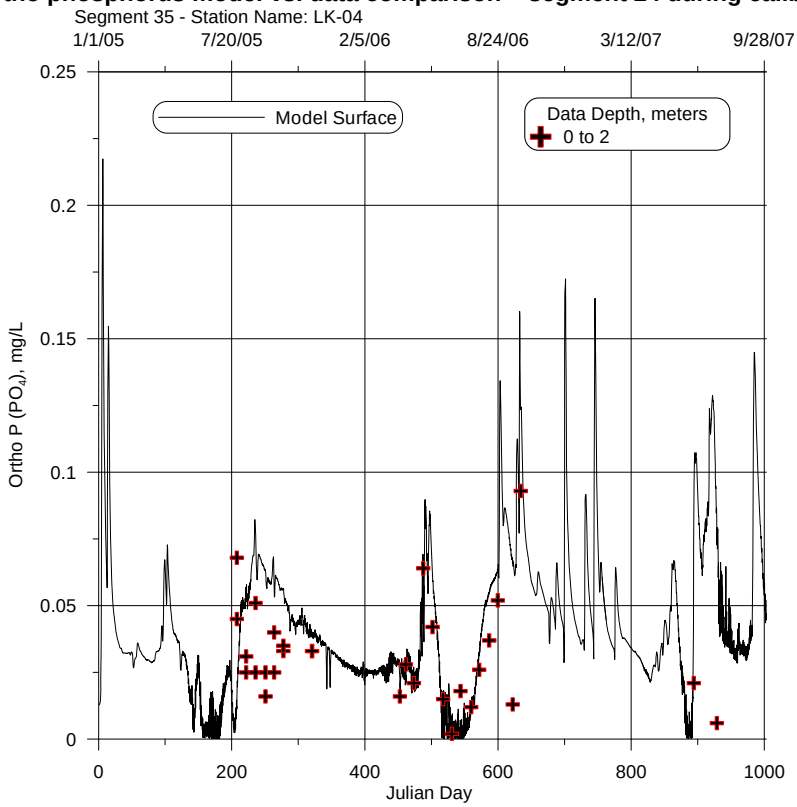

Figure 116. Ortho phosphorus model vs. data comparison – segment 35 during calibration period.

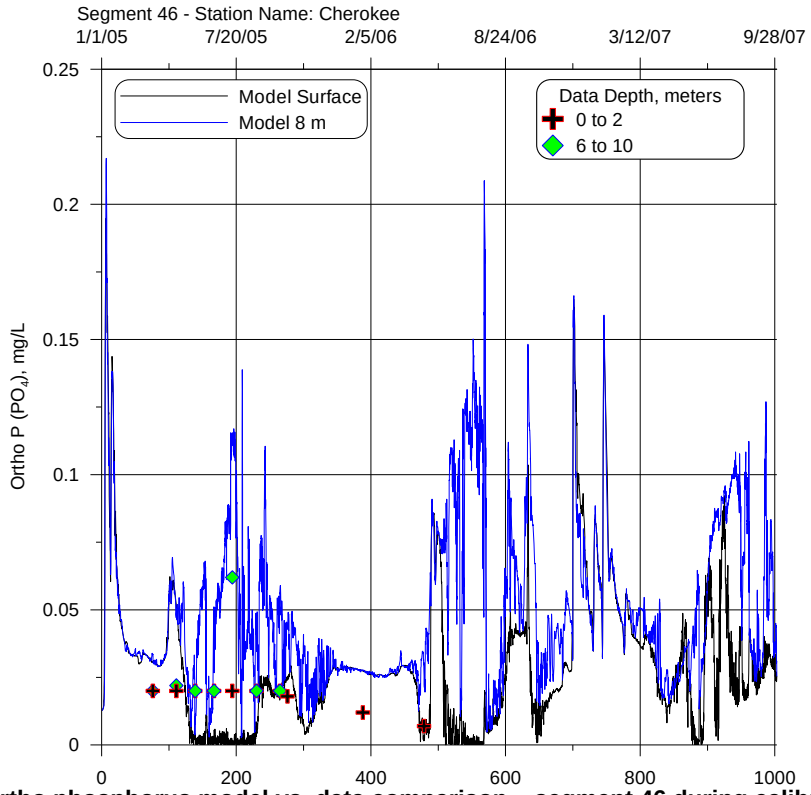

Figure 117. Ortho phosphorus model vs. data comparison – segment 46 during calibration period.

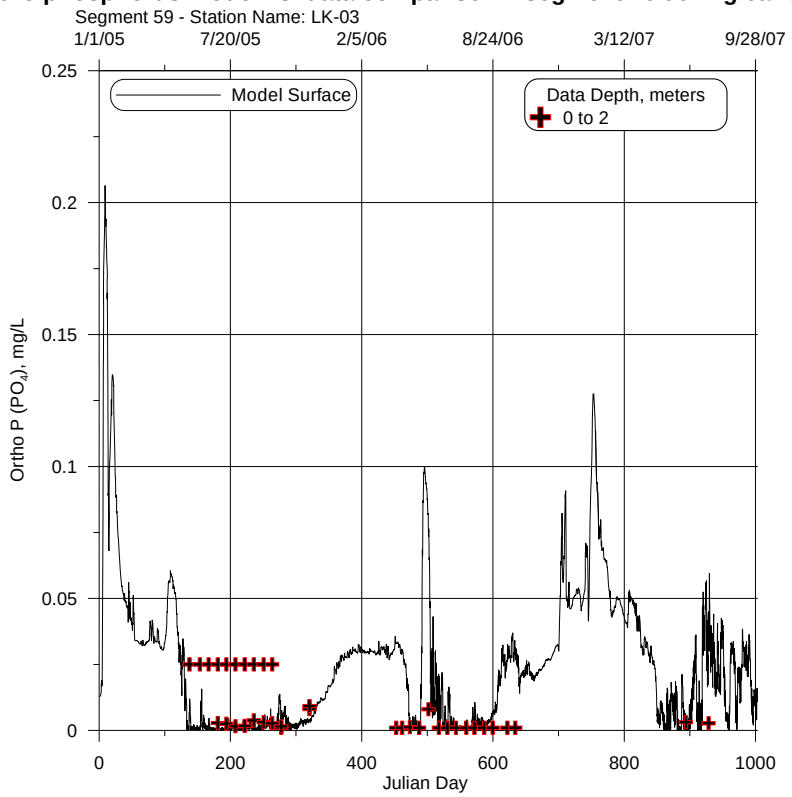

Figure 118. Ortho phosphorus model vs. data comparison – segment 59 during calibration period.

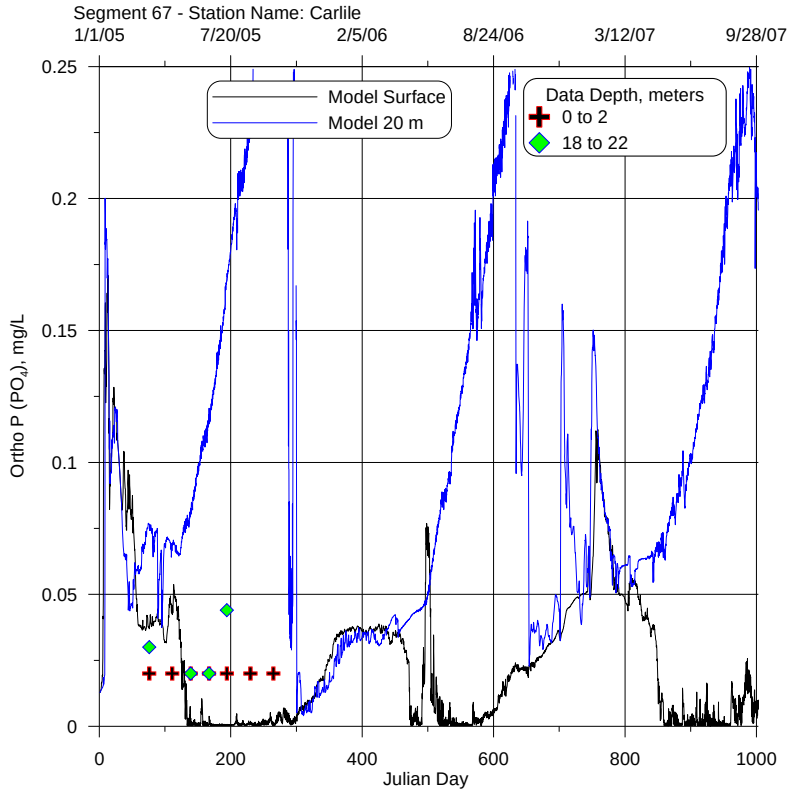

Figure 119. Ortho phosphorus model vs. data comparison – segment 67 during calibration period.

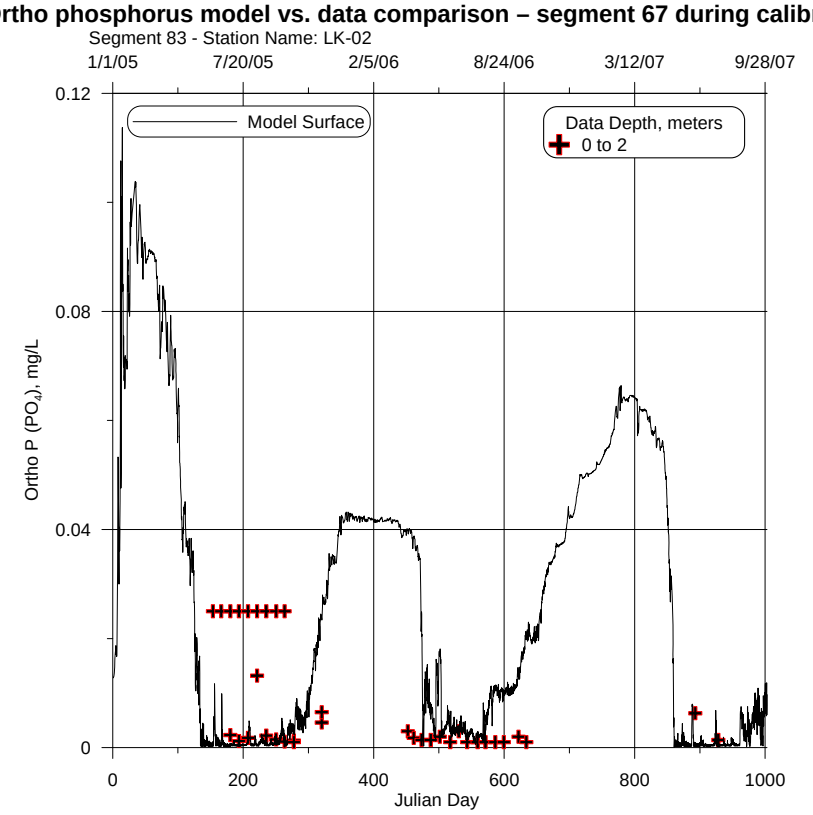

Figure 120. Ortho phosphorus model vs. data comparison – segment 83 during calibration period.

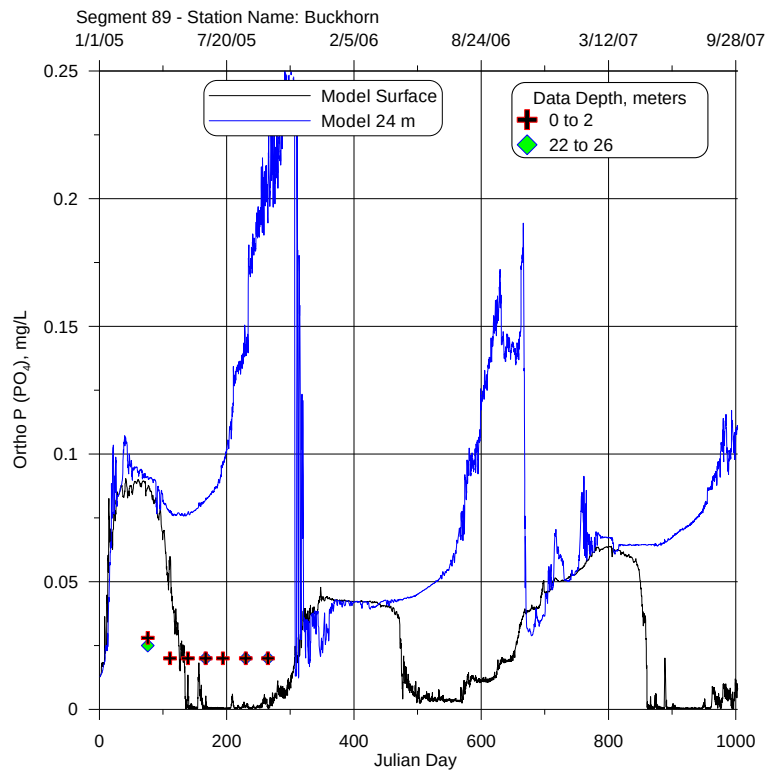

Figure 121. Ortho phosphorus model vs. data comparison – segment 89 during calibration period.

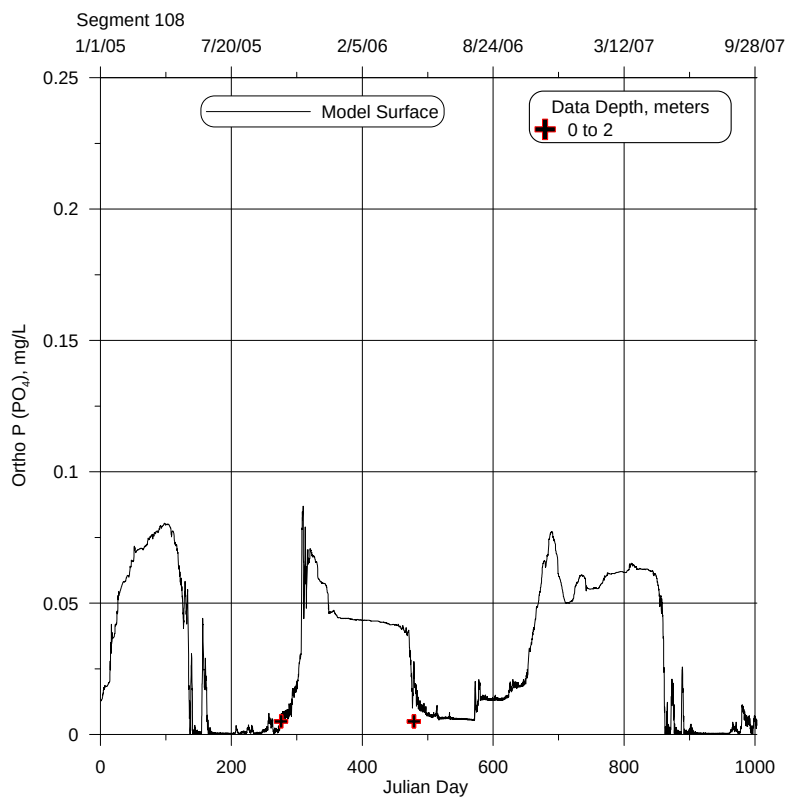

Figure 122. Ortho phosphorus model vs. data comparison – segment 108 during calibration period.

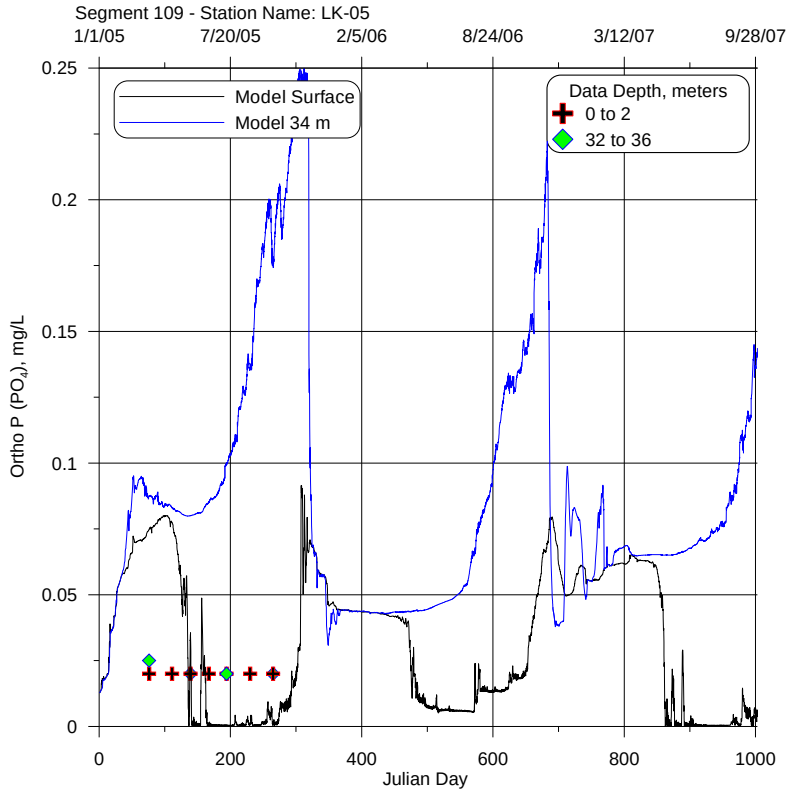

Figure 123. Ortho phosphorus model vs. data comparison – segment 109 during calibration period.

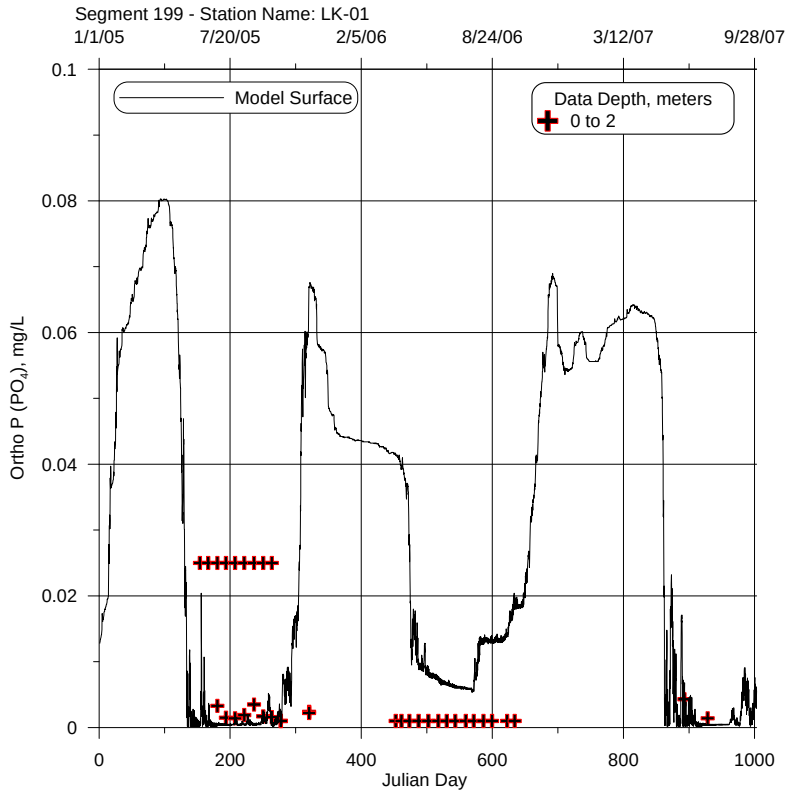

Figure 124. Ortho phosphorus model vs. data comparison – segment 199 during calibration period.

Chlorophyll a

The CE-QUAL-W2 model tracks dry weight biomass of algae rather than chlorophyll a. Chlorophyll a is a derived variable in the CE-QUAL-W2 model and values are computed from dry weight biomass using the chlorophyll a to algae ratio. The chlorophyll a to algae ratio can be thought of as a linear scaling factor for the biomass data.

Time series model vs. data comparisons of chlorophyll a concentrations are shown in Figure 125, Figure 126, Figure 128, Figure 129, Figure 130, Figure 131, and Figure 132 for model segments 35, 46, 67, 83, 89, 199, and 108/109, respectively. In these figures, the smooth line is the model prediction at the stated depth, and the crosses are the measured field data at the depth shown on the figure.

Profiles of chlorophyll a field data compared to profiles of model predictions are shown in Appendix F.

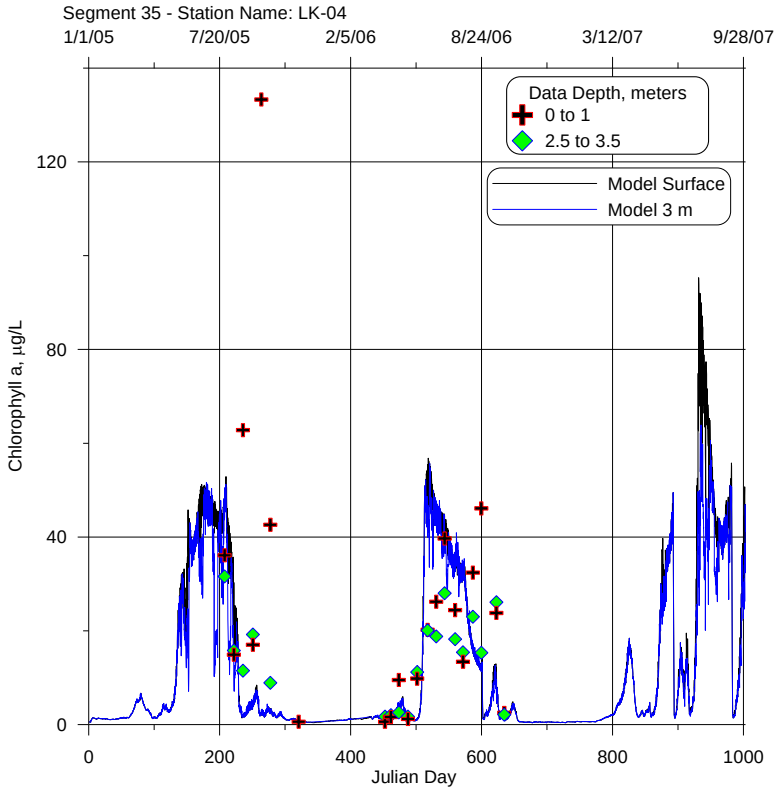

Figure 125. Chlorophyll a model vs. data comparison – segment 35 during calibration period.

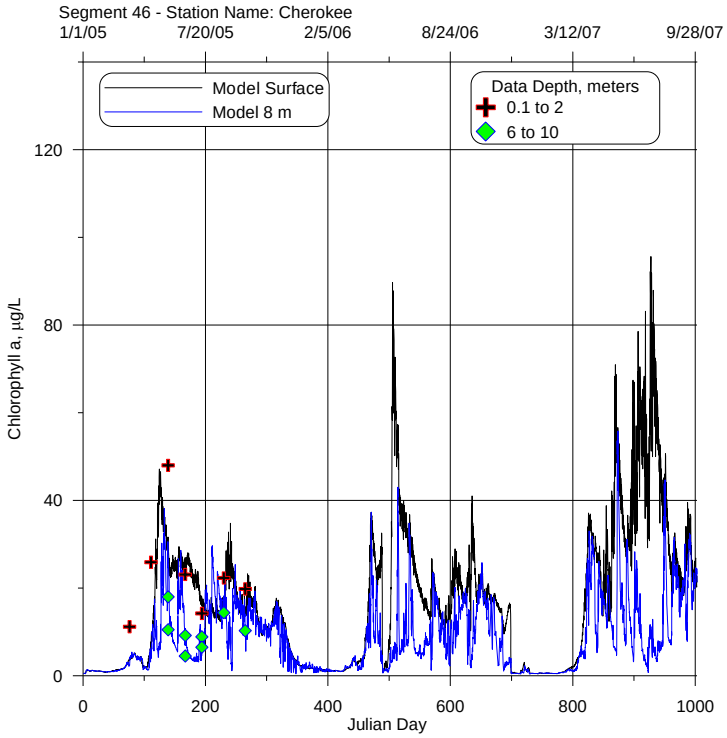

Figure 126. Chlorophyll a model vs. data comparison – segment 46 during calibration period.

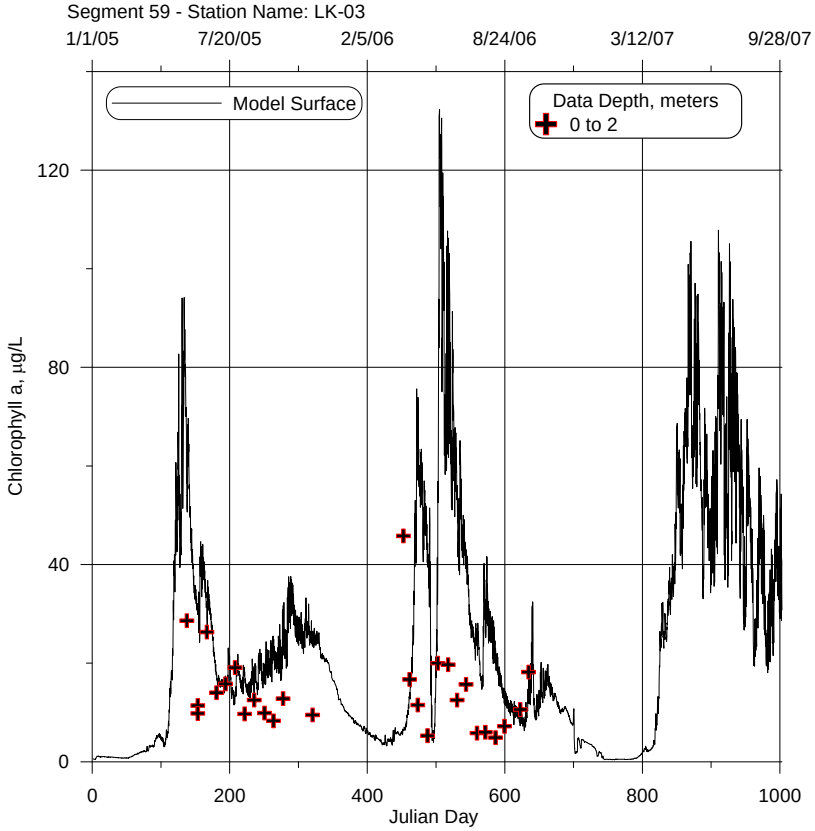

Figure 127. Chlorophyll a model vs. data comparison – segment 59 during calibration period.

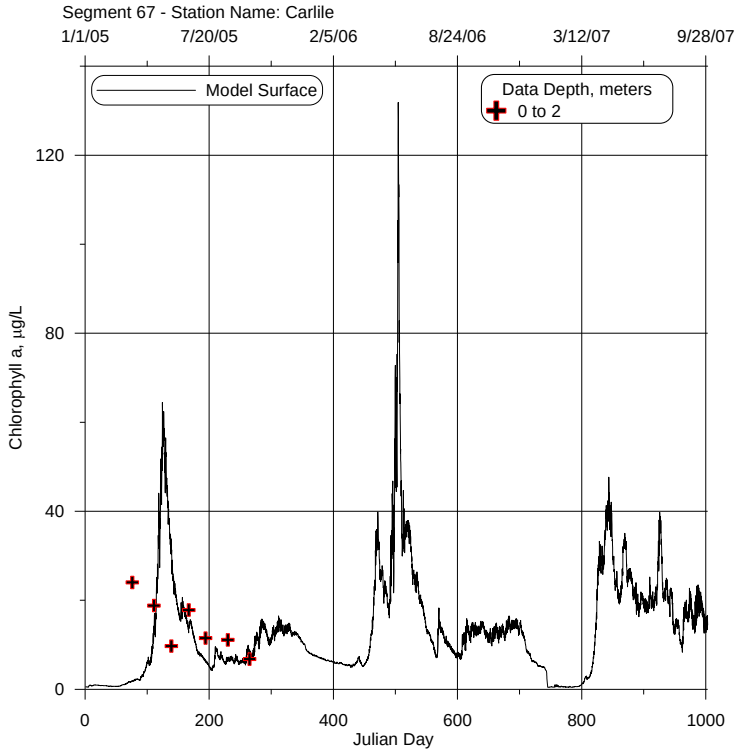

Figure 128. Chlorophyll a model vs. data comparison – segment 67 during calibration period.

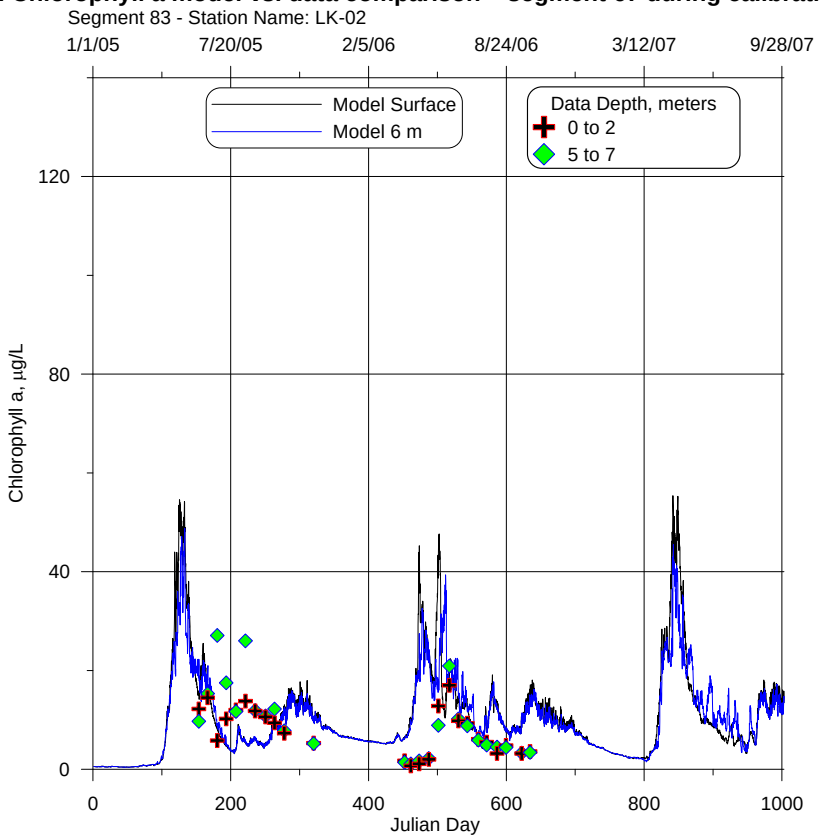

Figure 129. Chlorophyll a model vs. data comparison – segment 83 during calibration period.

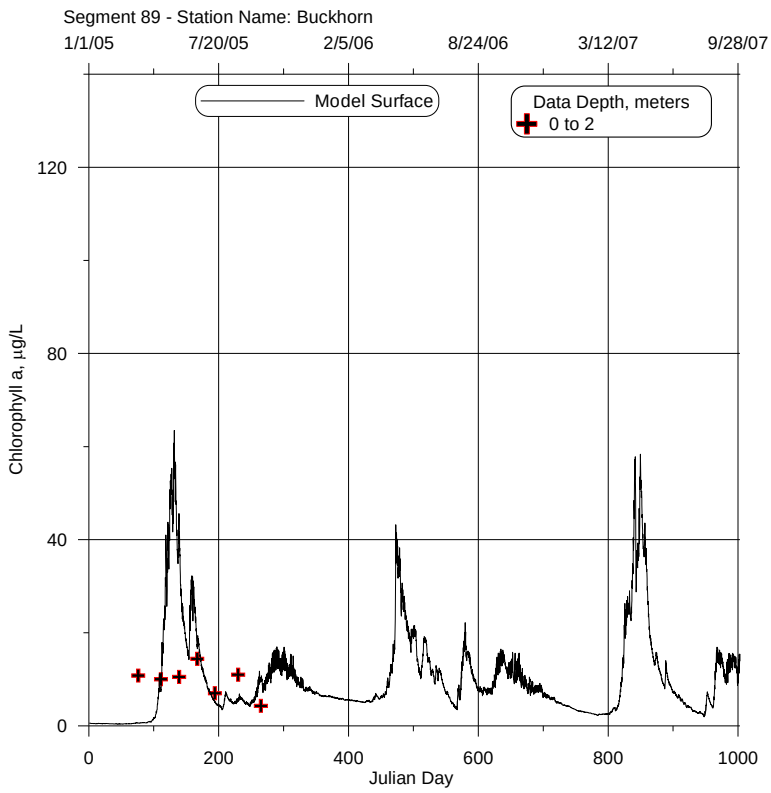

Figure 130. Chlorophyll a model vs. data comparison – segment 89 during calibration period.

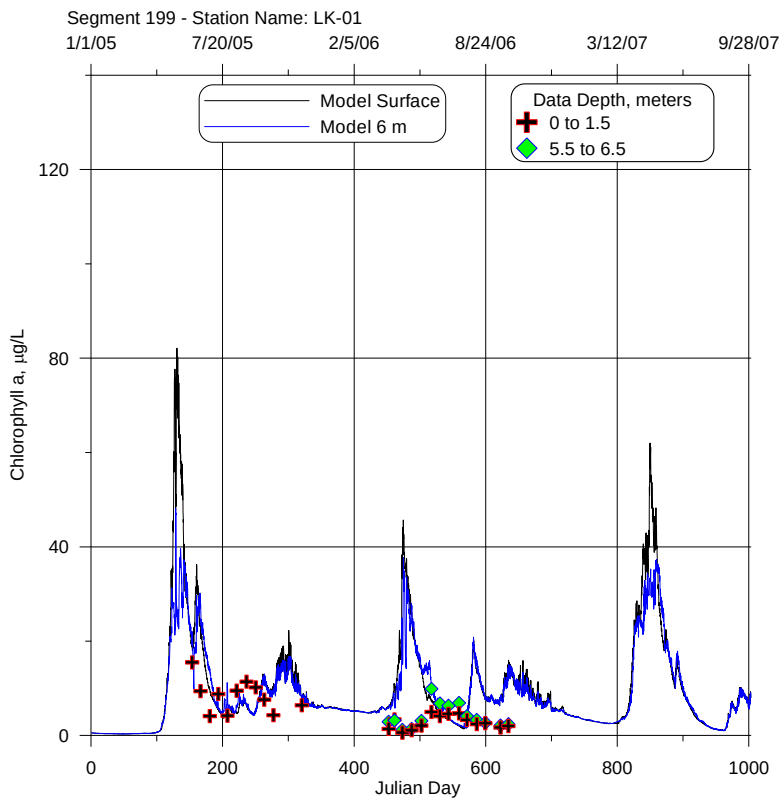

Figure 131. Chlorophyll a model vs. data comparison – segment 199 during calibration period.

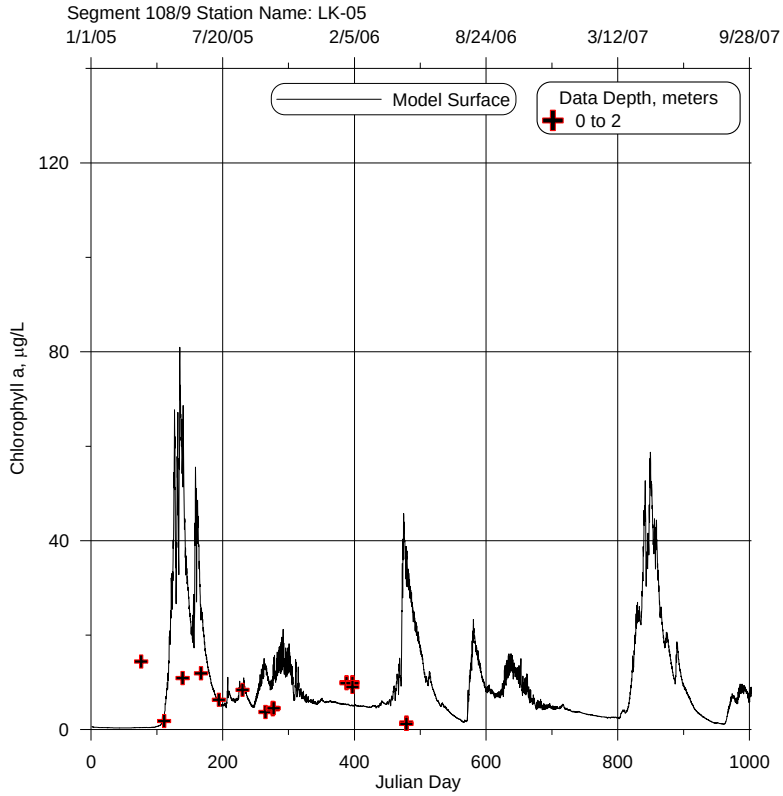

Figure 132. Chlorophyll a model vs. data comparison – segment 108/9 during calibration period.

Light Extinction/Secchi Disk Depth

The CE-QUAL-W2 model computes the light extinction coefficient, λ [m^{-1}], dynamically based on the following relationship:

$$\lambda = \lambda_{H2O} + \lambda_{ISS} + \lambda_{POM} + \lambda_a + \lambda_{macro} + \lambda_{zoo}$$

where:

$$\lambda_{ISS} = \varepsilon_{ISS} \sum_{\#ISS} \Phi_{ISS}$$

ε_{ISS} = extinction parameter for inorganic suspended solids, $m^{-1}/(g\ m^{-3})$ - user supplied parameter

Φ_{ISS} = inorganic suspended solids concentration for each size fraction

$$\lambda_{POM} = \varepsilon_{POM} \sum \Phi_{POM}$$

ε_{POM} = extinction parameter for particulate organic matter, $m^{-1}/g\ m^{-3}$) - user supplied parameter

Φ_{POM} = particulate organic matter concentration = particulate labile + particulate refractory organic matter concentration

$$\lambda_a = \sum \varepsilon_a \Phi_a$$

$$\lambda_{zoo} = \sum \varepsilon_{zoo} \Phi_{zoo}$$

$$\lambda_{macro} = \sum \varepsilon_{macro} \Phi_{macro}$$

ε_a = extinction coefficient for each algal group, $m^{-1}/g\ m^{-3}$ - user supplied parameter

Φ_a = algal concentration for each algal group, $g\ m^{-3}$

ε_{zoo} = extinction coefficient for each zooplankton group, $m^{-1}/g\ m^{-3}$ - user supplied parameter

Φ_{zoo} = zooplankton concentration for each zooplankton group, $g\ m^{-3}$

ε_{macro} = extinction coefficient for each macrophyte group, $m^{-1}/g\ m^{-3}$ - user supplied parameter

Φ_{macro} = macrophyte concentration for each macrophyte group, $g\ m^{-3}$

λ_{H2O} = extinction coefficient for water (for a wavelength of between 0.5 and 0.6μm, the absorption coefficient for *pure water* is about 0.1 m^{-1}). Note that λ_{H2O} can also vary greatly depending upon the dissolved substances in the water.

In the Tenkiller model, zooplankton and macrophytes have not been simulated; hence light extinction is a function of inflow inorganic suspended solids, particulate organic matter, and algae biomass, as well as the background value for pure water. Because of the dynamic nature of the inflow and high solids loading during rainfall events, the goal for matching Secchi disk data was to make sure the model predicted the approximate range of the field data. Secchi disk data shown in Figure 133 was obtained during the calibration period and varies significantly from 0.25 m to 6 m. This figure illustrates the wide variability in Secchi disk depth throughout the lake. In many cases it is difficult to model this variability. There are different expressions for converting Secchi disk depth, z_{Secchi} in m, to a light extinction coefficient in m^{-1}, some of these include

- $\lambda = \frac{\alpha}{z_{Secchi}}$ (Chapra, 2006) where α varies from 1.4 to 1.9
- $\lambda = \frac{1.11}{z_{Secchi}{}^{0.73}}$ (Williams et al., 1980)

- $\lambda = \frac{1.36}{z_{Secchi}{}^{0.86}}$

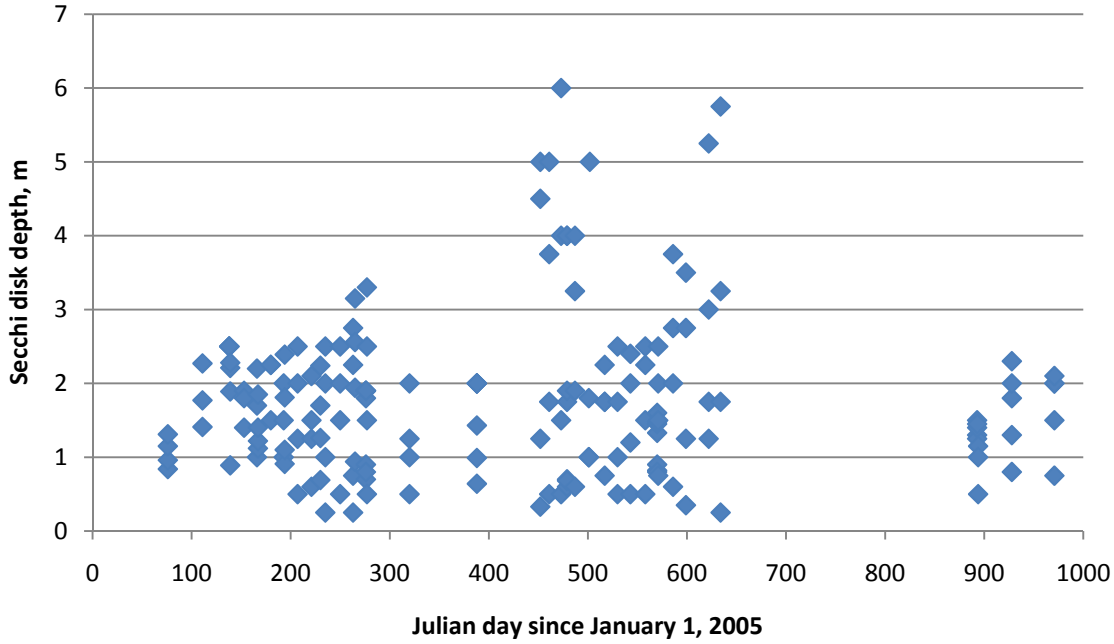

Figure 133. Secchi disk data at all stations on Tenkiller Reservoir between 2005 and 2007.

Using the Williams et al. (1980) relationship above, secchi disk depths were converted to light extinction coefficients and compared to predicted model light extinction coefficients at the surface (within 1 m of the surface) in Figure 134. Generally the model compares well with the magnitude of the field data, except for missing an algae event in the late summer/fall of 2005.

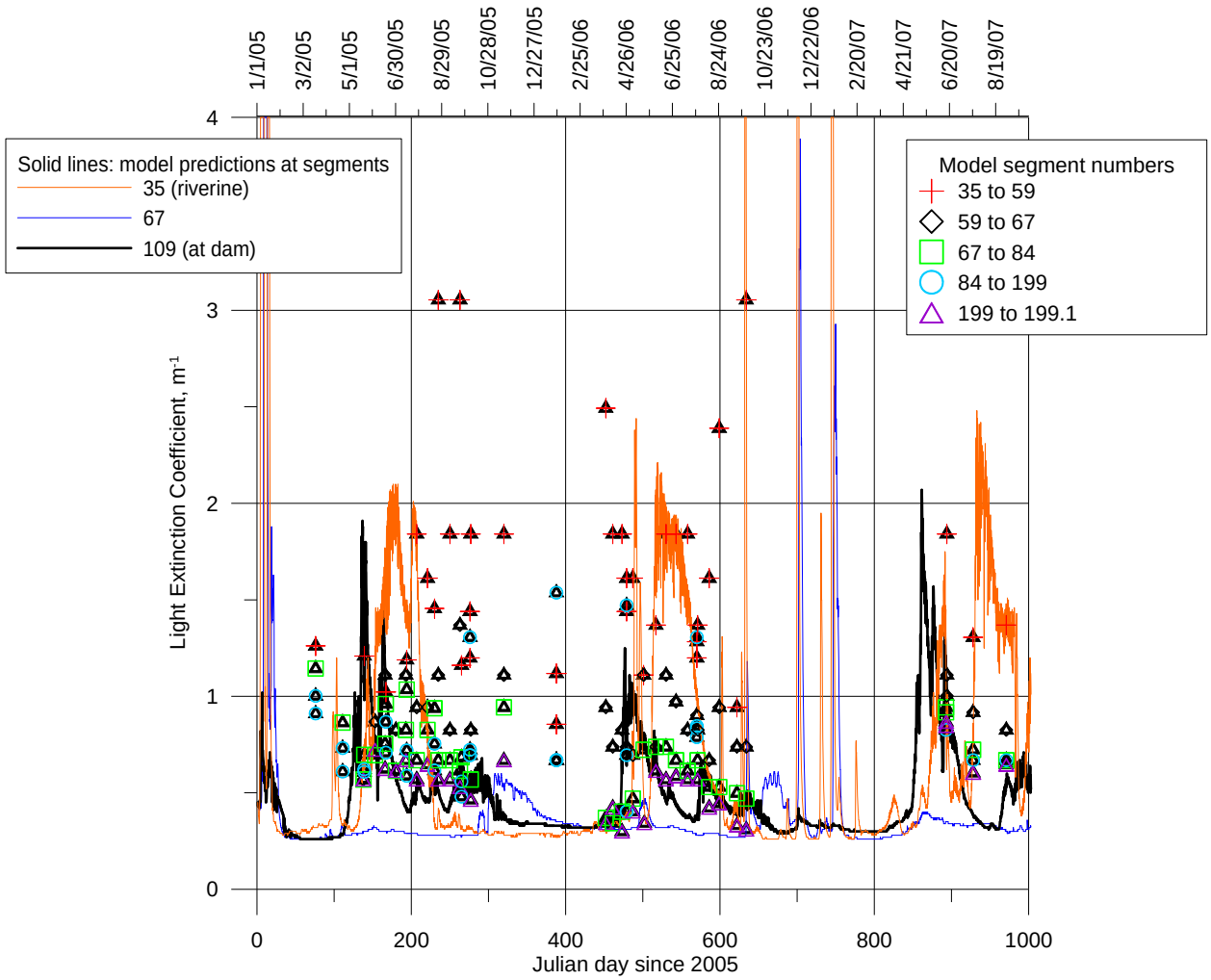

Figure 134. Model predictions of light extinction at the near surface compared to light extinction coefficients computed from Secchi disk depths.

Analysis of Model Calibration

This section is an analysis of the model's ability to predict the internal state variables of the CE-QUAL-W2 model. The state variables include water level, temperature, dissolved oxygen, algae concentration in dry weight biomass, and nutrient concentrations. Criteria to evaluate if a model calibration is appropriate are shown in Appendix G.

Water level. The water level calibration is excellent with no mean error and an absolute mean error of 2 cm. The model accurately reproduces the fluctuations/trends in water level during the calibration period. This is an essential first step in model calibration.

Temperature. The overall model absolute mean error of 0.76°C is well below the typically acceptable value of 1°C for an acceptable temperature calibration The higher model absolute mean error at segment 35 [sampling station LK04 station] is a result of not having measured inflow temperatures. Neglecting the model data comparisons at Segment 35 (sampling station LK04), the temperature AME error statistics are about 0.7°C. This error could be reduced further by fine-tuning the wind (measured at Tulsa) and re-evaluating the difference between dew point temperature measured at Cookson and that over the lake. To improve the temperature calibration, an on-site meteorological station and continuous inflow temperatures for the primary river inflows would be recommended. Nevertheless, the overall model-data error is quite good as shown in a comparison of all temperature profile data and model predictions in Figure 135.

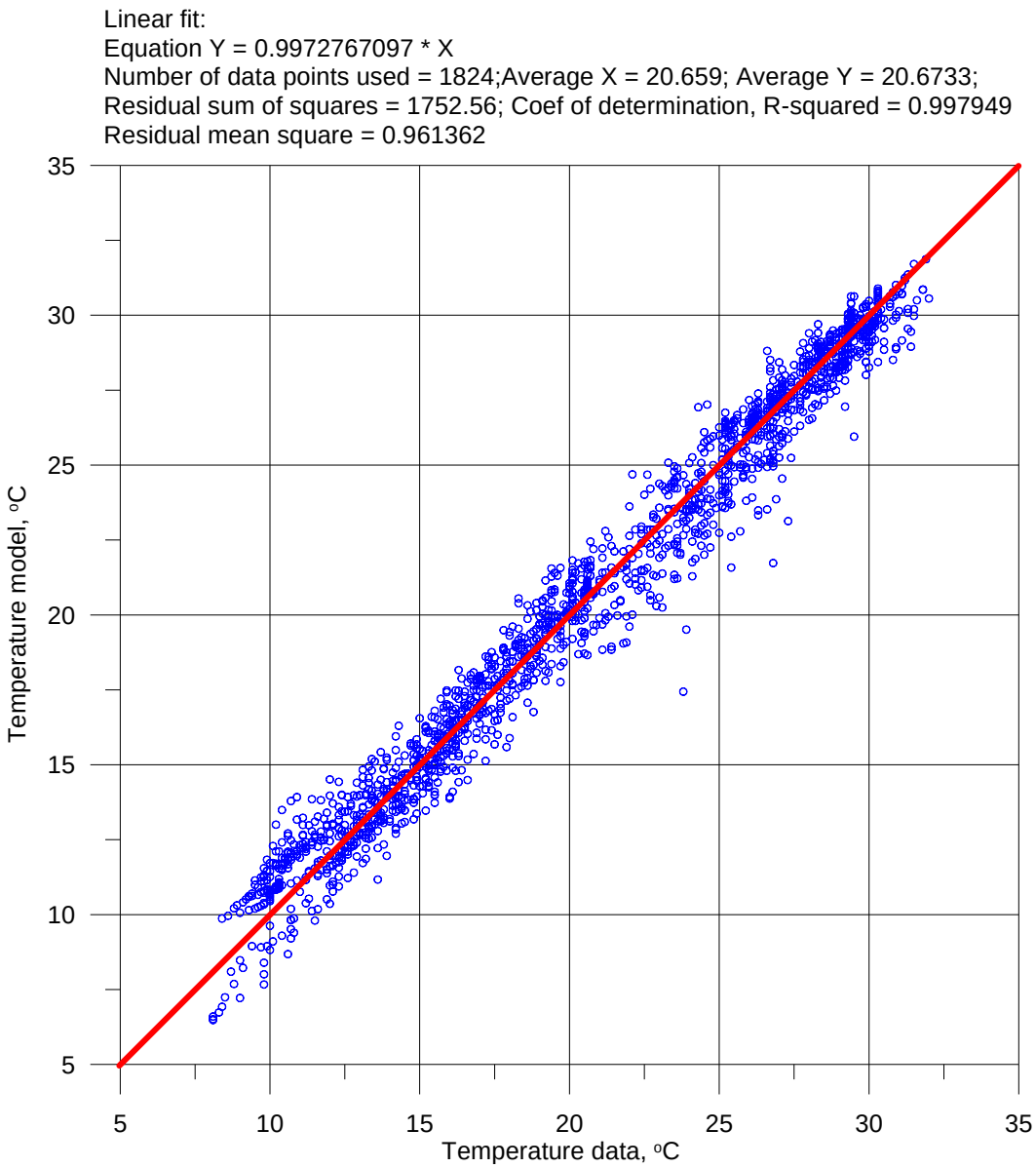

Figure 135. Temperature field data compared to model predictions at all locations and times.

Dissolved oxygen. Figure 136 shows a comparison of all dissolved oxygen data to model predictions separated as to depth of the measurement. For the near-surface data, one can note that there is a slight bias in the model not predicting super-saturation near the surface. Of more importance though is the prediction of the seasonal decline in dissolved oxygen below the epilimnion and fall overturn. The lake station profile comparisons shown in Table 9 at segments 83, 109, 199 all had very good model-data error statistics, approaching 1.2 mg/l in absolute mean error (AME). Also, the zero order SOD was kept constant for all 3 years of the calibration period. It was clear that organic matter deposition during storm events was important to obtaining good model–data comparisons going from a well-mixed to a fully anoxic hypolimnion in the summer. Sometimes the model captured well the trend of the dissolved oxygen profile shape, but did not match exactly the measured concentrations. In general a dissolved oxygen calibration below an AME of 2 mg/l is a reasonable calibration in a eutrophic system where measured dissolved oxygen values range from 0 to over 20 mg/l.

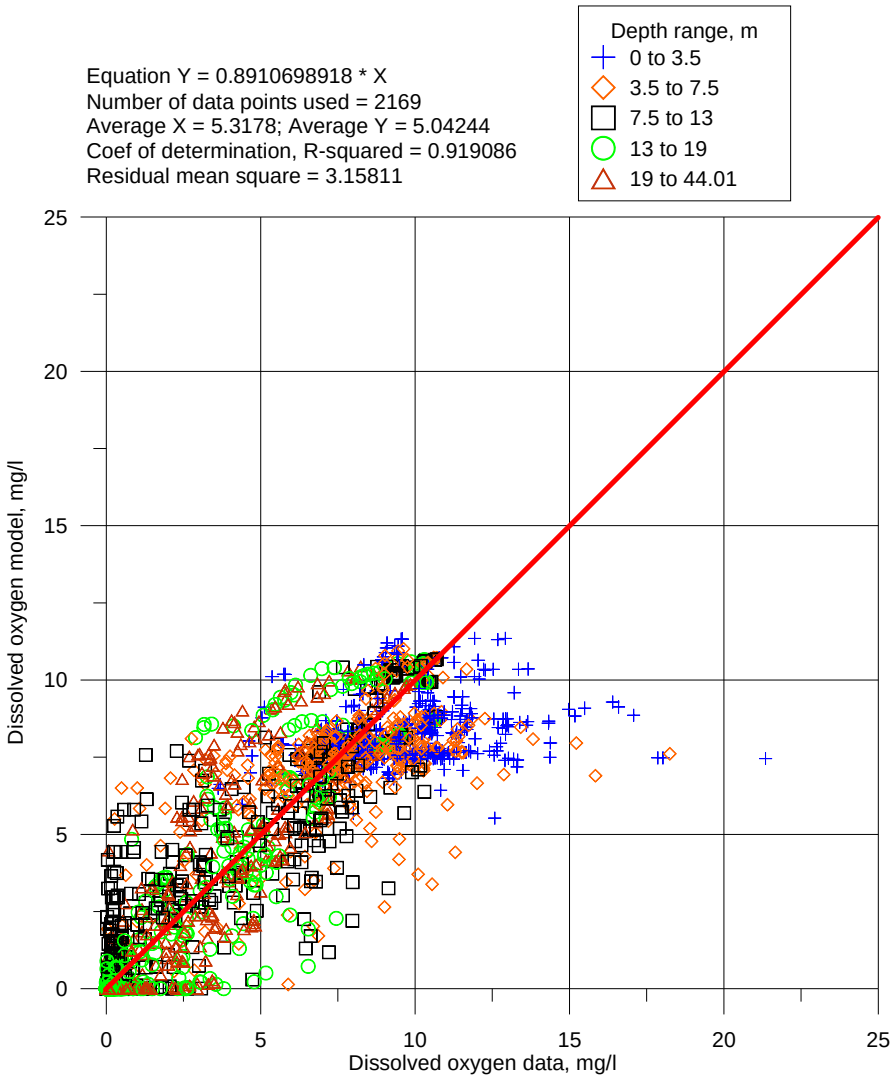

Figure 136. Dissolved oxygen field data compared to model predictions at all stations and times at different depths.

Nitrate. Nitrate model predictions compared well to field data as shown in Figure 137. The typical model error for NO_3-N was less than 0.16 mg/l (absolute mean error using 195 model-data comparisons) as NO_3-N even though concentrations measured during this period were as high as 2.2 mg/l and the standard deviation in the field data was 0.46 mg/l. For ammonia, model errors were less than 0.15 mg/l even though concentrations measured were as high as 1.4 mg/l NH_4-N and the standard deviation in the field data was 0.27 mg/l.

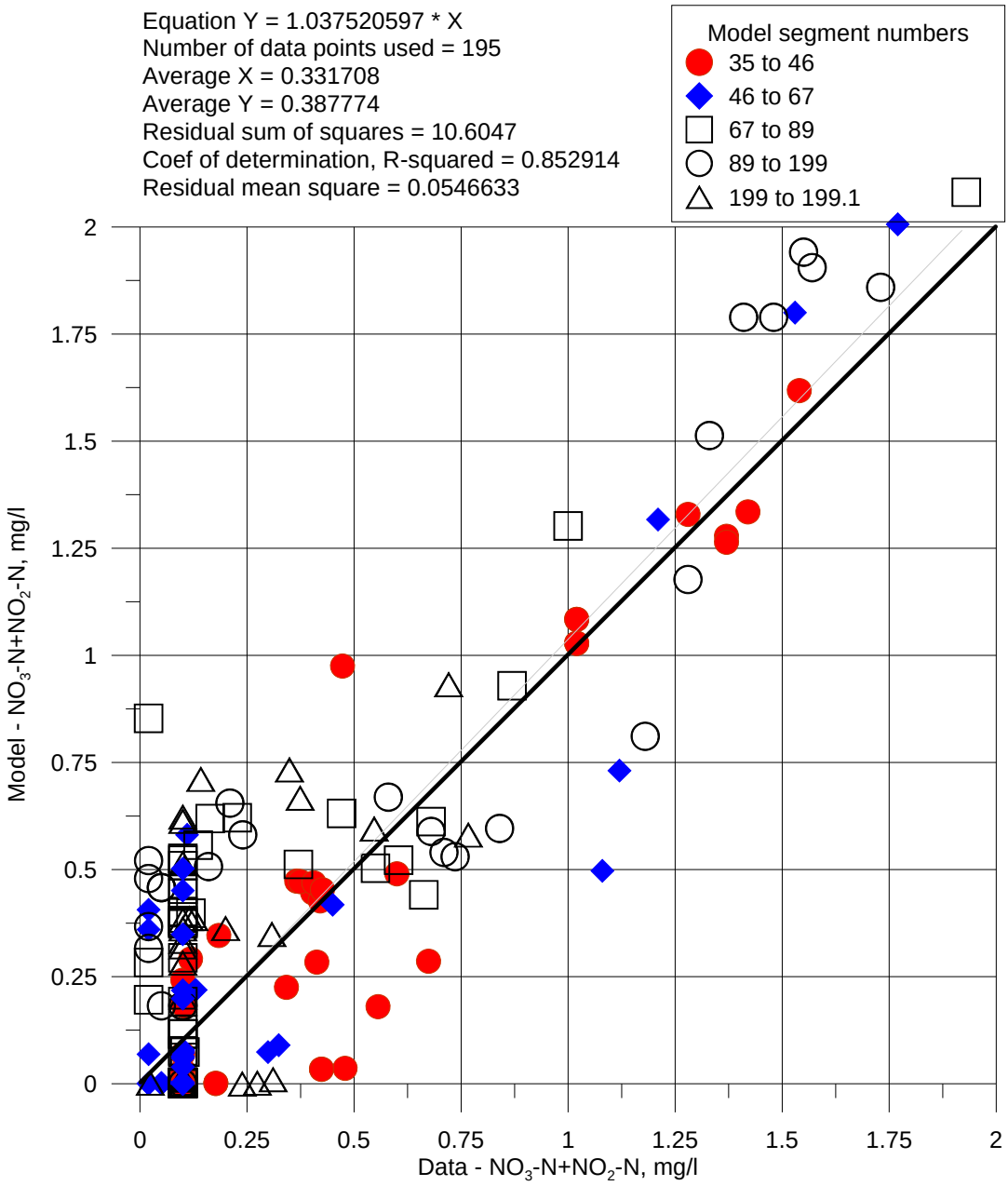

Figure 137. NO_3-N field data compared to model predictions at all stations and times at different depths.

Chlorophyll a. Comparisons of chlorophyll a field data to all the model predictions are shown in Figure 138. This is a comparison of measured chlorophyll a to model predicted chlorophyll a. Different sampling stations are differentiated by different symbols so that any bias along the length of the reservoir can be seen. There are several high chlorophyll a readings at Segment 35 that were not captured by the sparse Illinois River boundary condition. Oftentimes, if sampling was conducted on a monthly or twice monthly basis at the upstream model boundary of the Illinois River, the conditions at Segment 35 were reflective of conditions that occurred perhaps a week or less depending on the incoming flow rate. Hence, some of the peaks can be difficult to capture without more frequent boundary conditions. The CE-QUAL-W2 model uses dry weight algae biomass and a constant chlorophyll a to algae ratio. In reality, these ratios can change not only between algae groups, but over time as lake conditions change. Measurements of chlorophyll a were as high as 133 µg/l with a standard deviation of the field data of 11 µg/l.

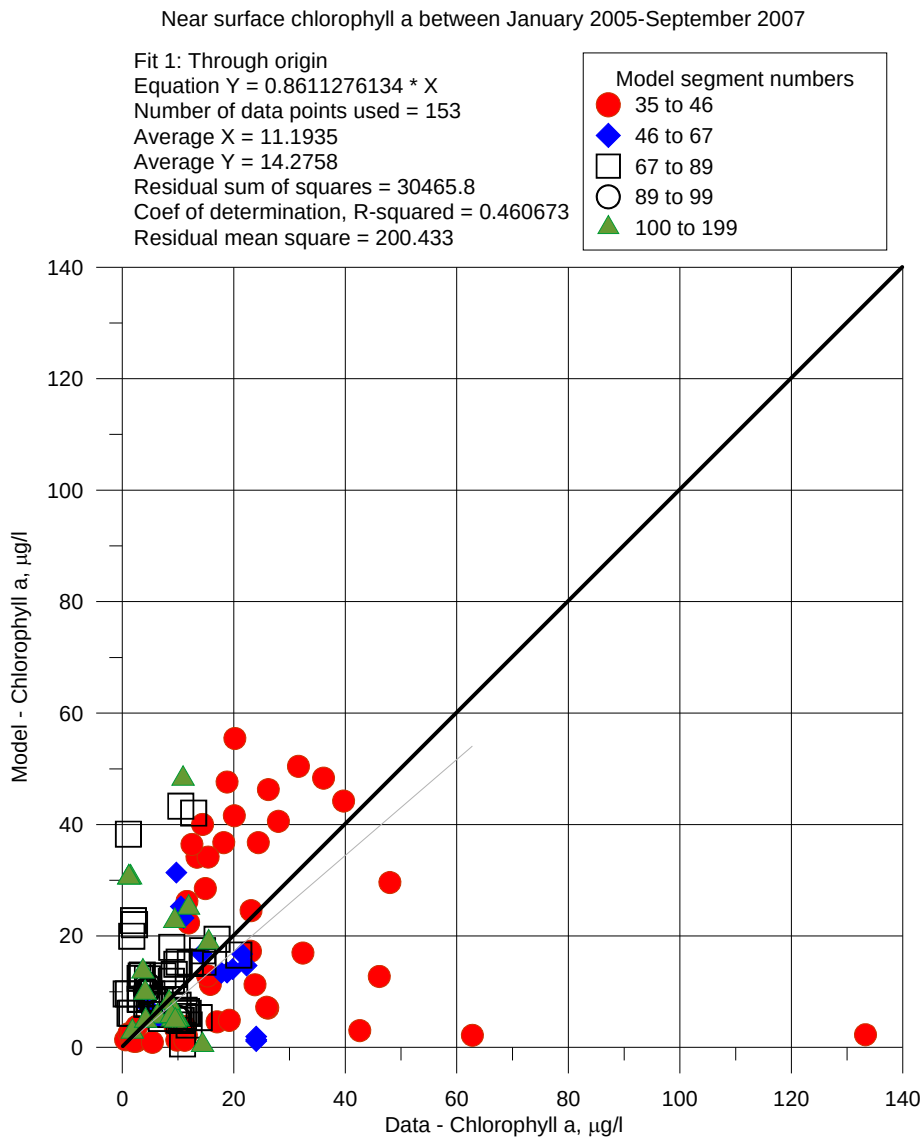

Figure 138. Model predictions of chlorophyll a compared to all field data during calibration period for all stations.

Total P. Comparisons of all the Total P field data compared to model predictions are shown in Figure 139. This is a comparison of measured Total P to model predicted Total P. Different sampling stations are differentiated by different symbols so that any bias along the length of the reservoir can be seen. The results are reasonable considering that daily values of Total P computed from a flow and date correlation were used to obtain the Total P in the inflow. Then the Total P was disaggregated into the state variables of the CE-QUAL-W2 model based on limited field data. Absolute mean error for Total P was 0.025 mg/l (mean error was 0.008 mg/l) while measurements for Total P were as high as 0.47 mg/l with a standard deviation of the field data of 0.058 mg/l. Absolute mean error for dissolved PO_4-P was 0.015 mg/l while measurements were as high as 0.093 mg/l and the standard deviation of the field data was 0.014 mg/l.

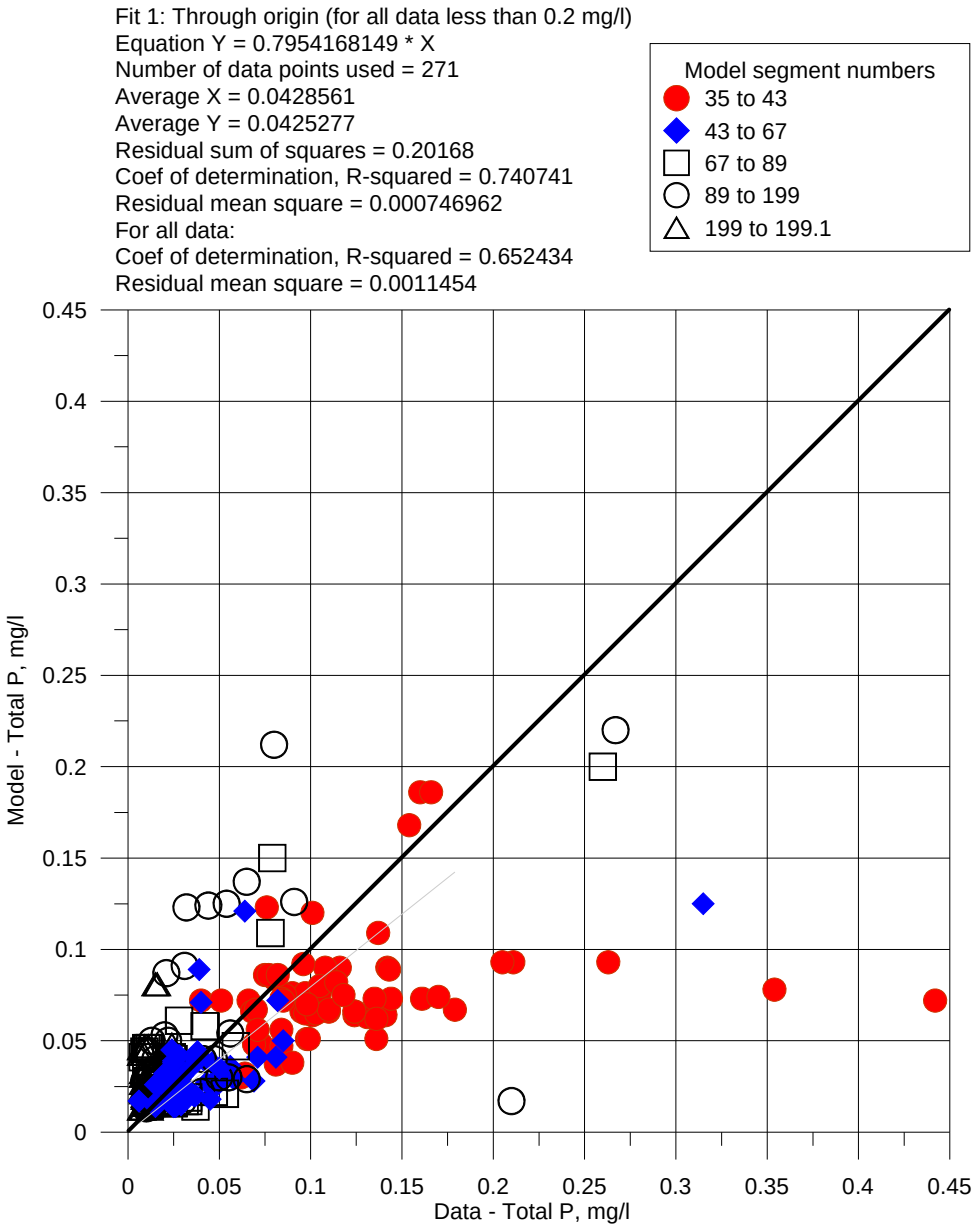

Figure 139. Model predicted Total P compared to field data for all stations during calibration period.

Model Set-up for Long-term Simulation

In order to evaluate the impact of phosphorus loading in the drainage basin on Tenkiller Reservoir, the model was set-up for a longer time period than the calibration period of January 1, 2005 to September 30, 2007. The hydrologic model of Engel (2008) was set-up and calibrated to field data between 1997 and 2006. In order to be compatible with the hydrologic model, the CE-QUAL-W2 model was also set-up for this same 10-year period. Since the impacts of loading from the drainage basin were to be evaluated over a longer period than 10 years, the hydrologic, water quality and meteorological data from 1997 to 2006 were repeated for a total of 50 years.

Various phosphorus loading scenarios were explored using hydrologic loading models providing daily Total P loads which were used to estimate inflow concentrations of Ortho P, ISS, and organics. These calculations were carried out using the methodology developed for the calibration run. The various model scenarios and their respective phosphorus loadings are discussed in Engel (2008). This section describes how the boundary conditions common to each of the 50–year model scenarios (excluding Historical flows) were developed.

Upstream Boundary Conditions

Illinois River Inflow

Flow

Figure 140 shows Illinois River total discharge over the base 10-year model period. An identical flow regime was repeated for each consecutive 10-year period of the 50-year model scenario.

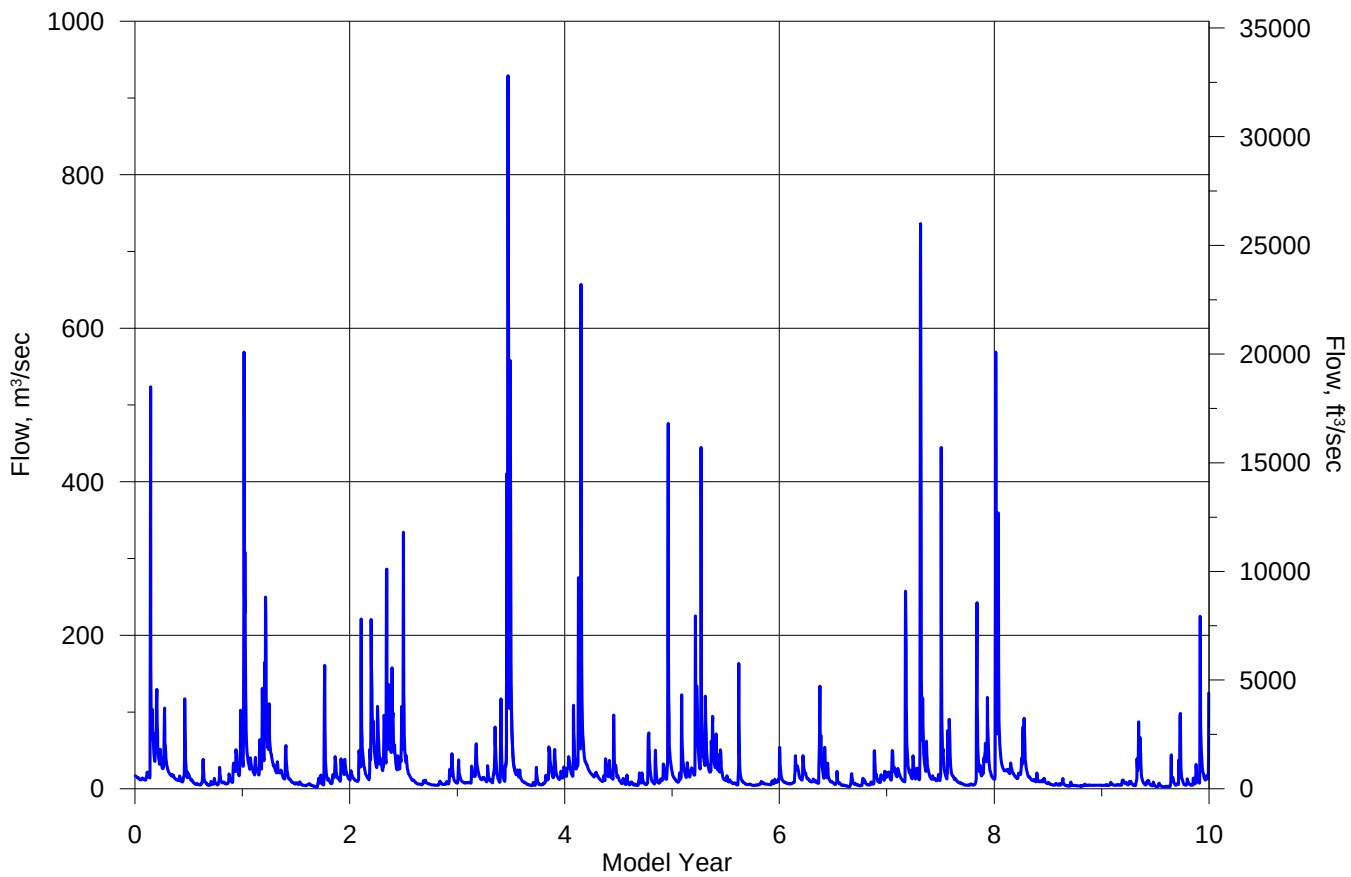

Figure 140. Illinois River discharge for the base 10-year period of the 50-year model scenario.

Temperature

The same procedure was used for constructing the inflow temperature sequence for the 10-year period from 1997-2006 as for the calibration period of 2005-September 30, 2007. A filtered equilibrium temperature (see Appendix B) was computed to approximate the inflow temperature. Figure 141 shows the estimated inflow temperatures and field data between 1997 and 2006. Figure 142 shows a comparison of the filtered equilibrium temperature and field data. Typical errors between measurements and predictions (data-estimated) were 0.2^{o}C mean error and 1.7^{o}C absolute mean error. A filtering interval of 200 hours and a depth of 2.5 m were used for the computation. Since these data were based on the Tulsa meteorological data and did not used measured solar radiation, the cloud cover correction factor of 0.0065 was adjusted to 0.0030 since the theoretical solar radiation model did not seem to have the same level of short-wave solar radiation.

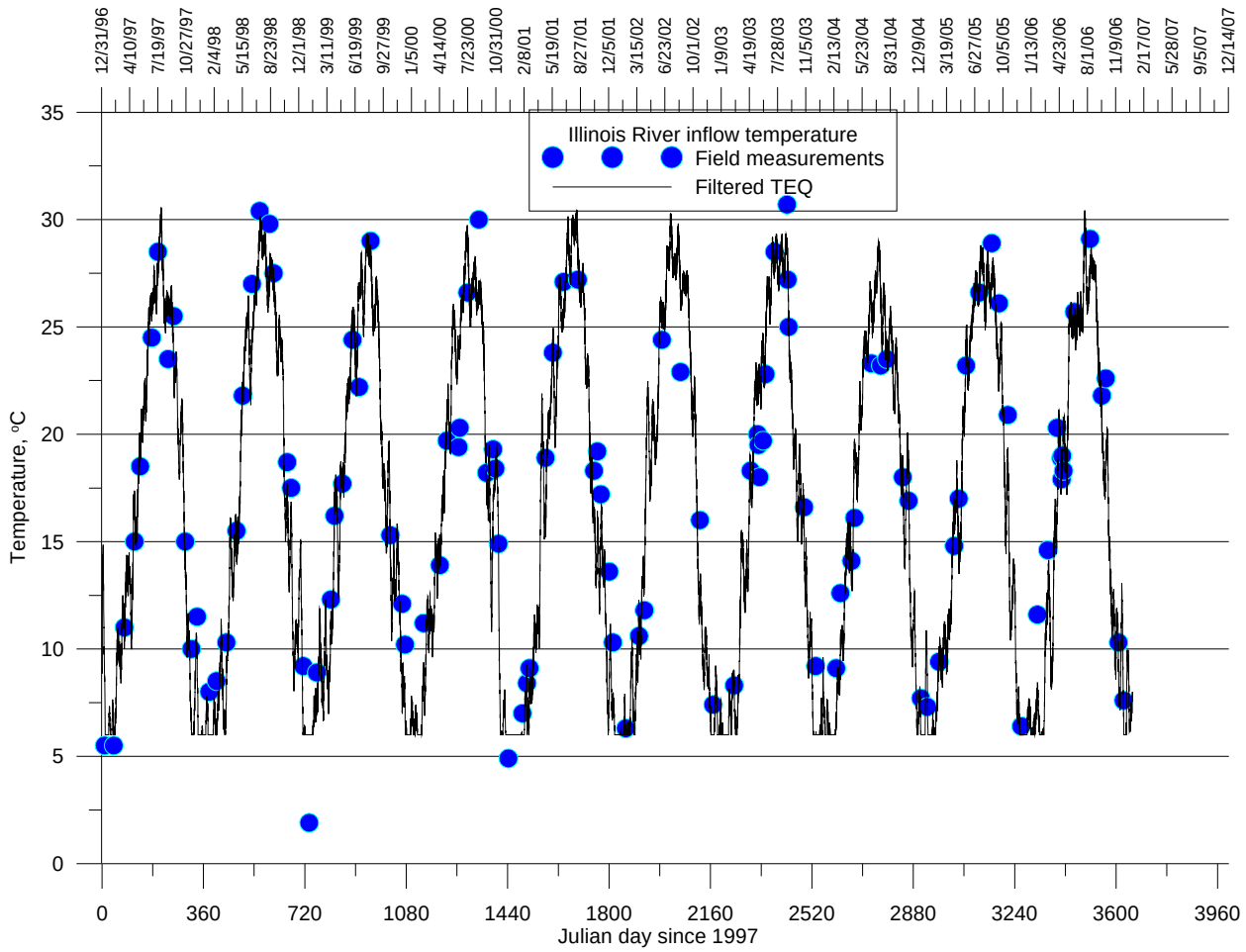

Figure 141. Measured temperature compared to filtered equilibrium temperature between 1997 and 2006.

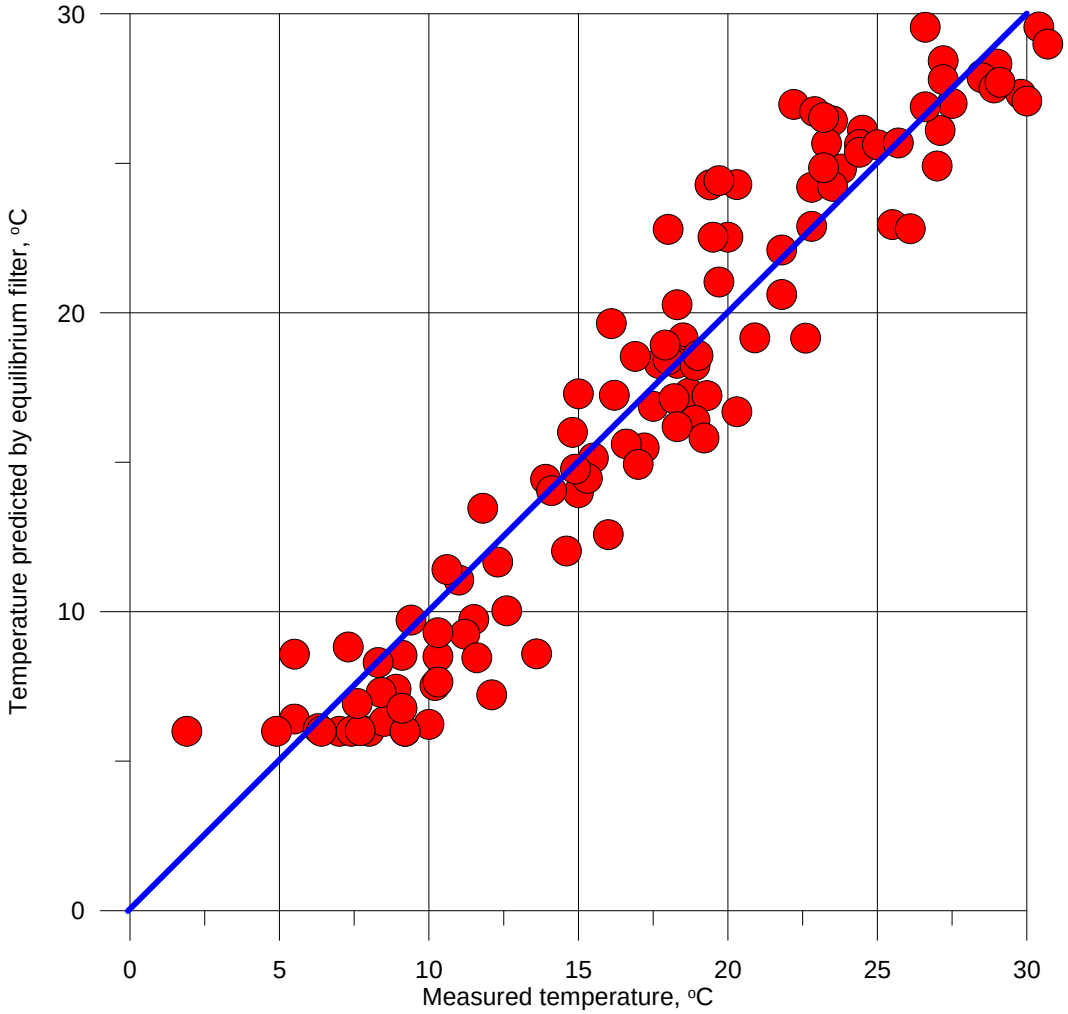

Figure 142. Comparison of measured and predicted inflow temperatures between 1997 and 2006.

Water Quality

Algae – Chlorophyll a data collected between 1997 and 2006 were used to estimate algae biomass inflow concentrations for the 10-year base model period. The conversion between chlorophyll a and the three algae groups used in the model was carried out using the methodology developed for the calibration model run (See page 20). Figure 143 shows the Illinois River algae concentrations for the 10-year base model period.

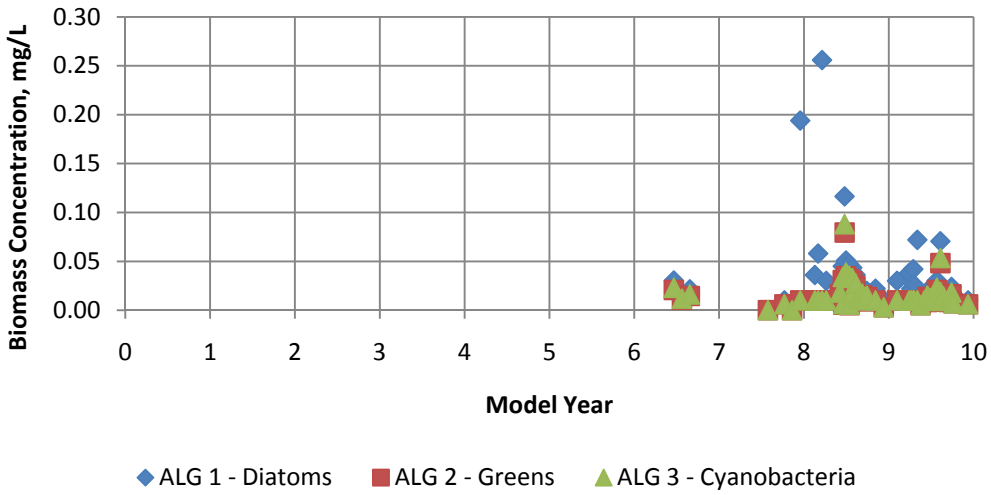

Figure 143. Illinois River algae group biomass concentrations for the base 10-year period of the 50-year model scenario.

Ammonia – (NH_4) Linear interpolation was used to estimate ammonia concentrations between available measured data for the years 1997 to 2006. Figure 144 shows ammonia data for the 10-year base model period. The ammonia in the inflow was unaffected by the model scenario since the inflow concentrations were based on field data from 1997 to 2006.

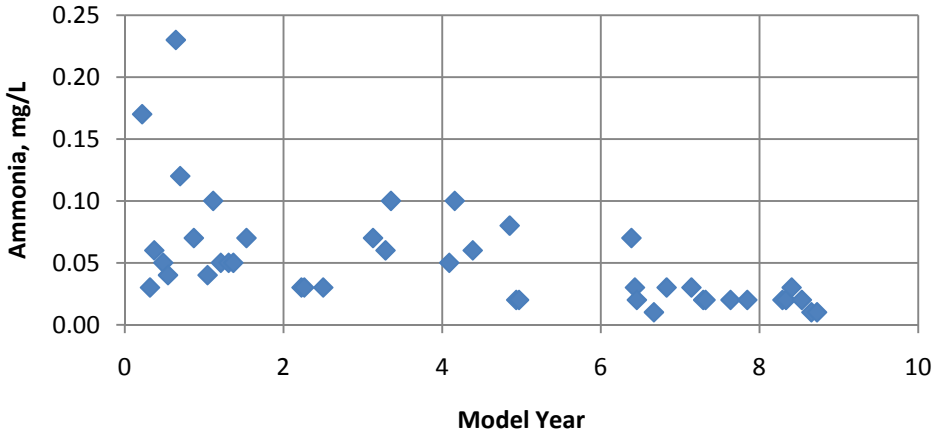

Figure 144. Illinois River ammonia data for the base 10-year period of the 50-year model scenario.

Dissolved Oxygen – Dissolved oxygen concentrations were estimated using the water temperature based DO saturation method described on page 22. Figure 145 shows the estimated DO values for the 10-year base model period.

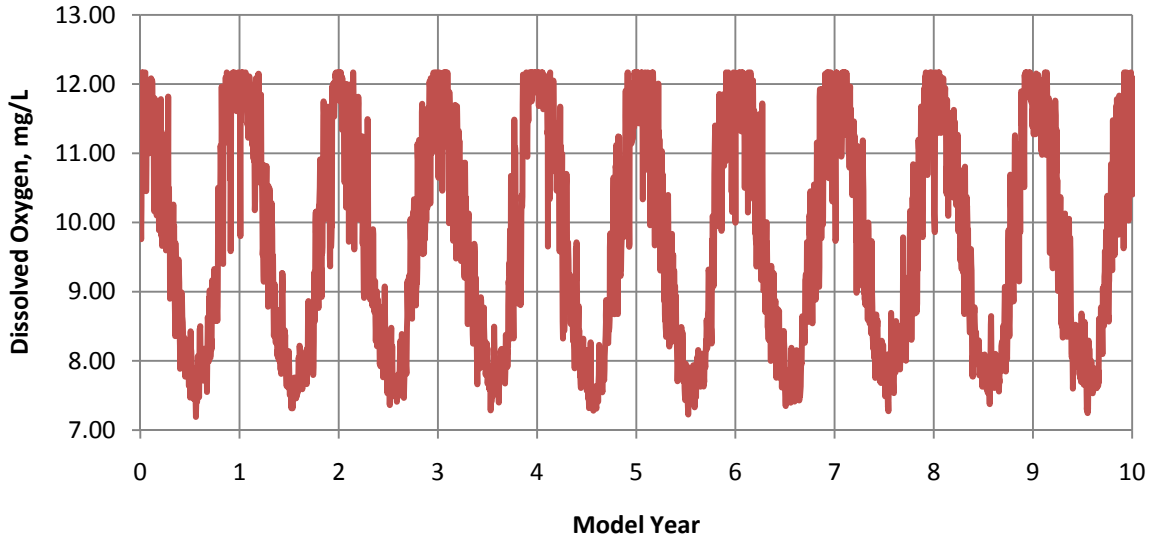

Figure 145. Illinois River dissolved oxygen for the base 10-year period of the 50-year model scenario.

Nitrate/Nitrites – Linear interpolation was used to estimate nitrate+ nitrite concentrations for the 10-year period between 1997 and 2006. Figure 146 shows Illinois River nitrate + nitrite data for the base 10- year model period. The nitrate + nitrite in the inflow was unaffected by the model scenario since the inflow concentrations were based on field data from 1997 to 2006.

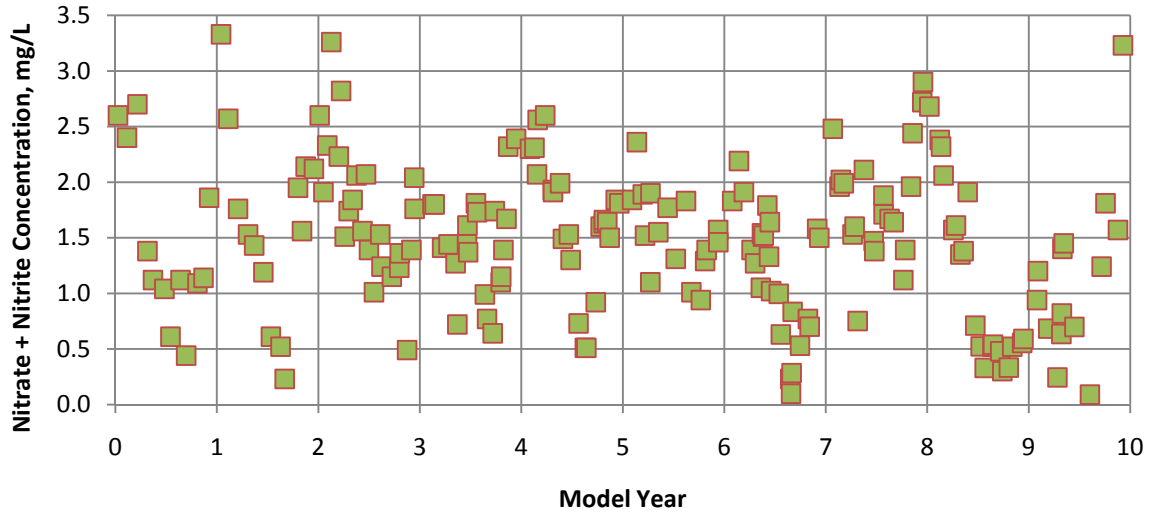

Figure 146. Illinois River nitrate + nitrite concentrations for the base 10-year period of the 50-year model scenario.

Baron Fork Inflow

Flow

Figure 147 shows Baron Fork Creek total discharge over the base 10-year model period. An identical flow regime was repeated for each consecutive 10-year period of the 50-year model scenario.

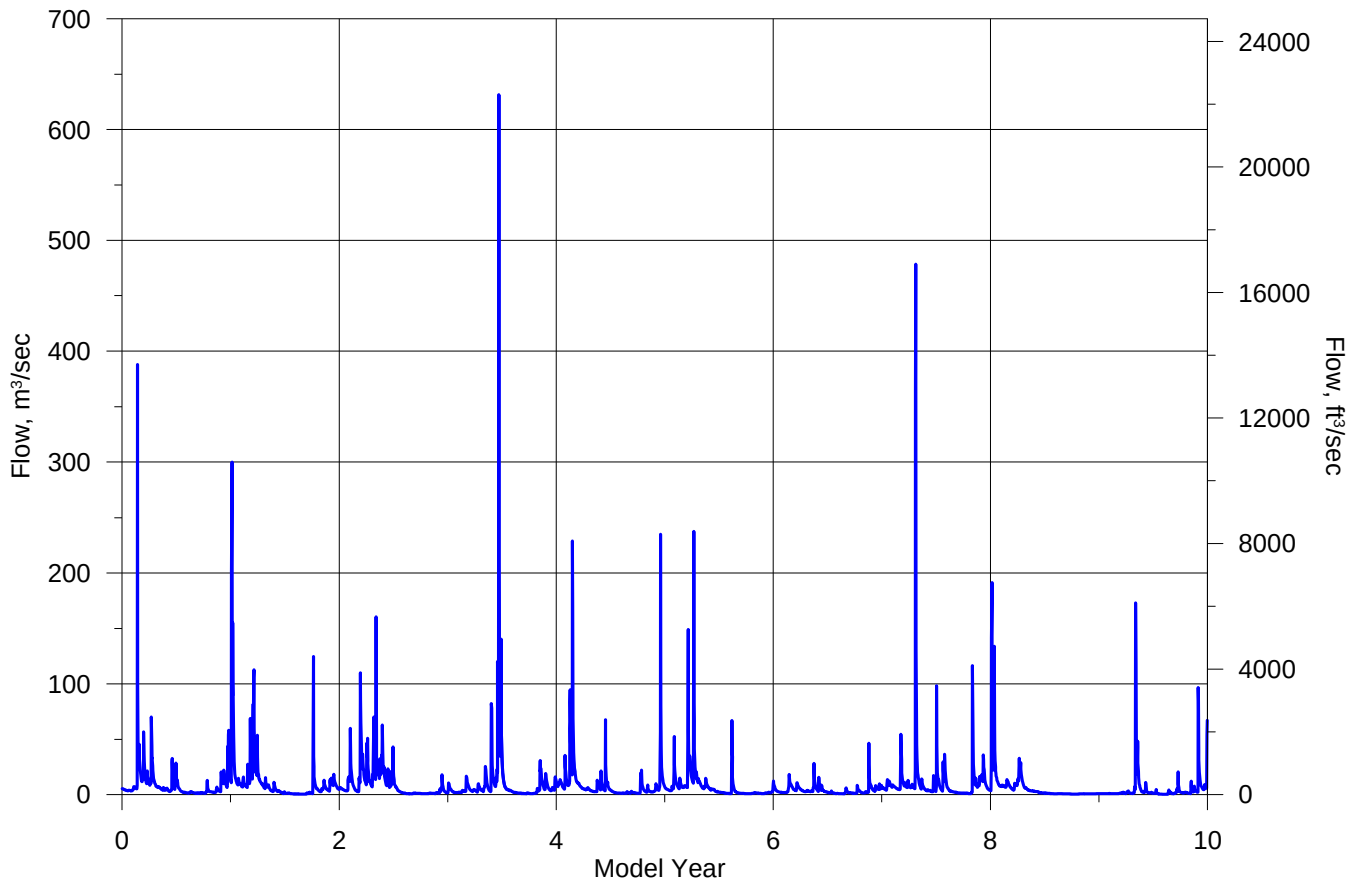

Figure 147. Baron Fork Creek discharge for the base 10-year period of the 50-year model scenario.

Temperature

The Illinois River filtered equilibrium water temperature (see Figure 141) was used to estimate temperatures for Baron Fork Creek for the 50-year scenario.

Water Quality

Algae – Chlorophyll a data collected between 1997 and 2006 were used to estimate algae biomass inflow concentrations for the 10-year base model period. The conversion between chlorophyll a and the three algae groups used in the model was carried out using the methodology developed for the calibration model run (See page 20). Figure 148 shows the Baron Fork Creek algae concentrations for the 10-year base model period.

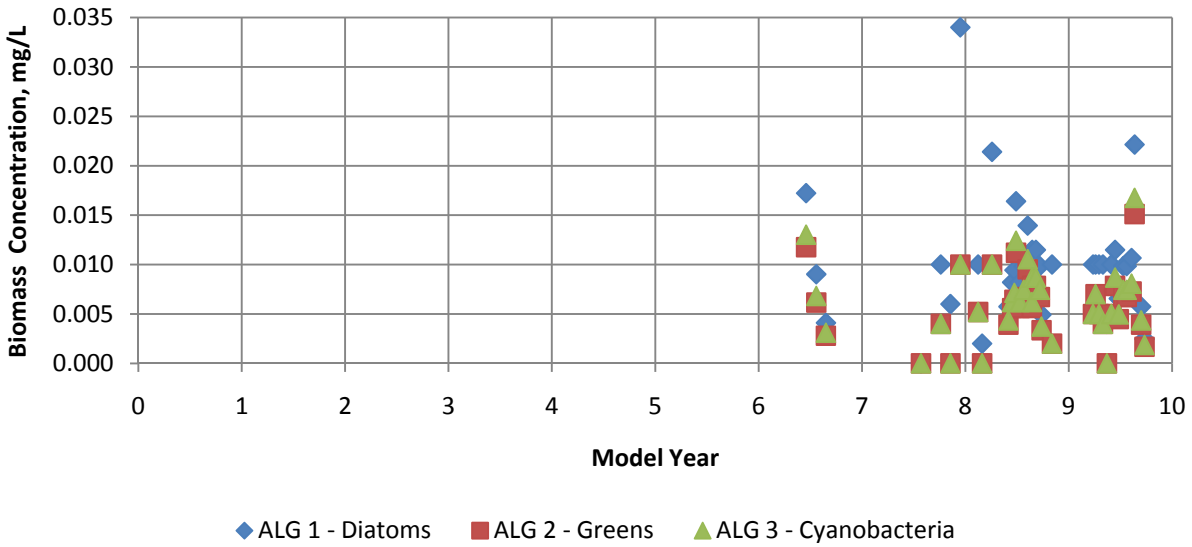

Figure 148. Baron Fork Creek algae group biomass concentrations for the base 10-year period of the 50-year model scenario.

Ammonia – (NH_4) All ammonia field data (with the exception of one sample) collected from Baron Fork Creek was below the detection limit of 0.05 mg/L.

Dissolved Oxygen – Illinois River DO levels were used to estimate DO levels for Baron Fork Creek for the 10-year base model period. (See page 125.)

Nitrate/Nitrites – Linear interpolation was used to estimate nitrate+ nitrite concentrations for the 10-year period between 1997 and 2006. Figure 149 shows Baron Fork Creek nitrate + nitrite data for the base 10-year model period.

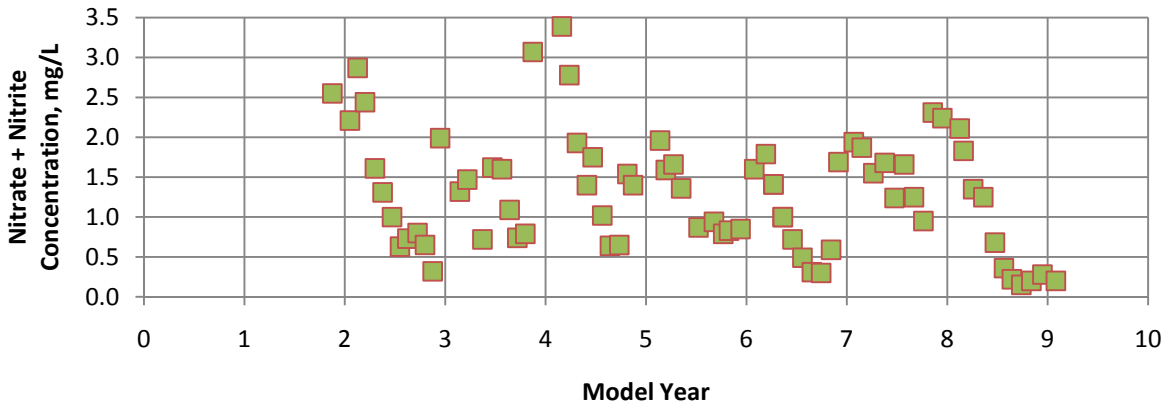

Figure 149. Baron Fork Creek nitrate + nitrite concentrations for the base 10-year period of the 50-year model scenario.

Caney Creek Inflow

Flow

Figure 150 shows Caney Creek total discharge over the base 10-year model period. An identical flow regime was repeated for each consecutive 10-year period of the 50-year model scenario.

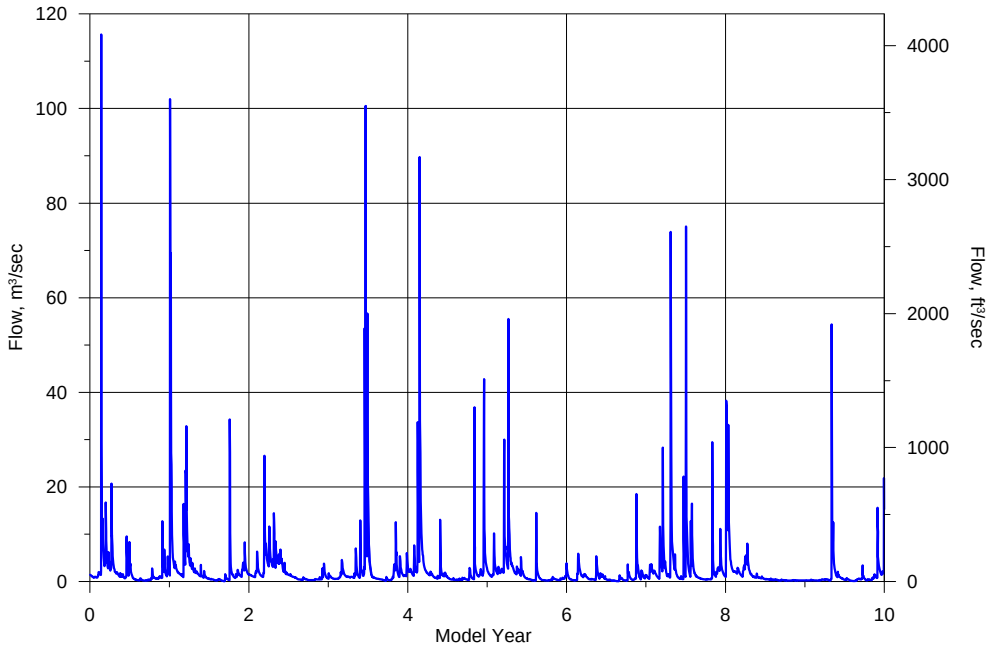

Figure 150. Caney Creek discharge for the base 10-year period of the 50-year model scenario.

Temperature

The Illinois River filtered equilibrium water temperature (see Figure 141) was used to estimate temperatures for Caney Creek for the 50-year scenario.

Water Quality

Algae – Chlorophyll a data collected between 1997 and 2006 were used to estimate algae biomass inflow concentrations for the 10-year base model period. The conversion between chlorophyll a and the three algae groups used in the model was carried out using the methodology developed for the calibration model run (See page 20). Figure 151 shows the Caney Creek algae concentrations for the 10-year base model period.

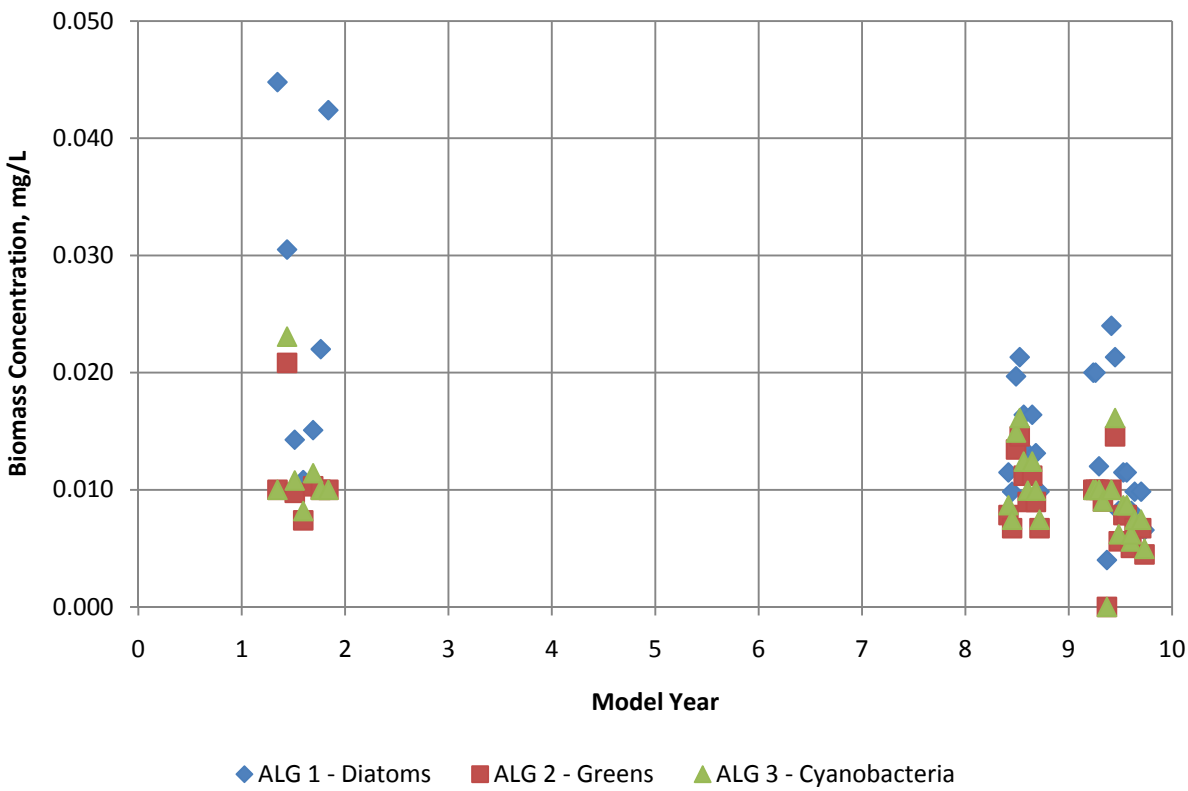

Figure 151. Caney Creek algae group biomass concentrations for the base 10-year period of the 50-year model scenario.

Ammonia – (NH_4) All ammonia field data (with the exception of one sample) collected from Baron Fork Creek were below the detection limit of 0.05 mg/L.

Dissolved Oxygen – Illinois River DO levels were used to estimate DO levels for Caney Creek for the 10-year base model period. (See page 125.)

Nitrate/Nitrites – Linear interpolation was used to estimate nitrate+ nitrite concentrations for the 10-year period between 1997 and 2006. Figure 152 shows Caney Creek nitrate + nitrite data for the base 10-year model period.

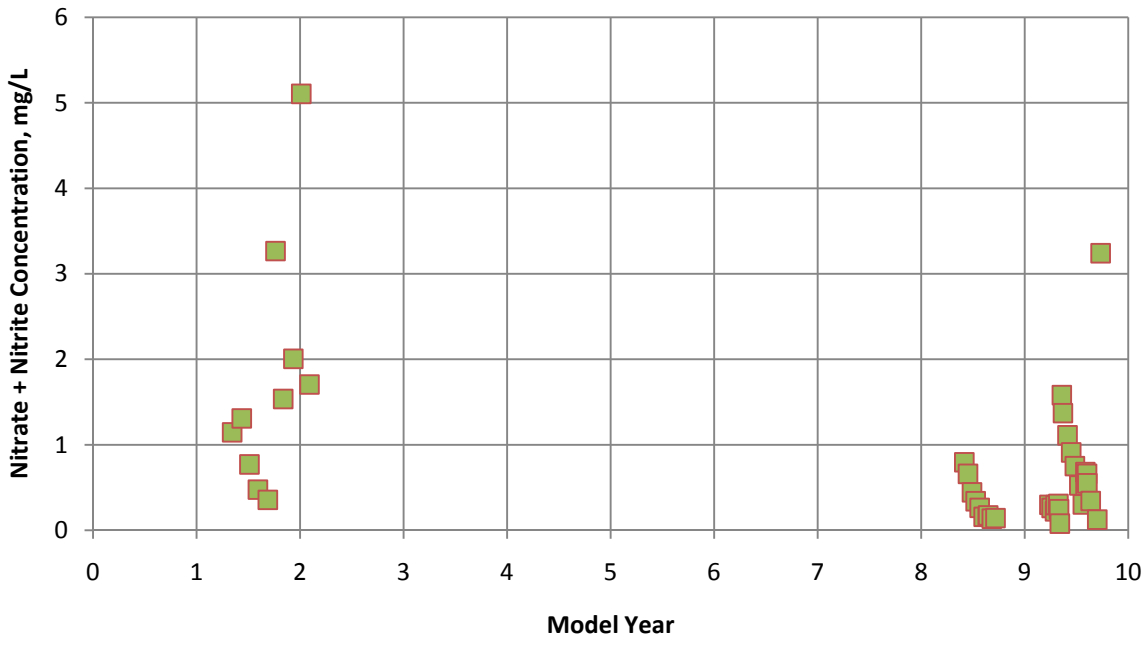

Figure 152. Caney Creek nitrate + nitrite concentrations for the base 10-year period of the 50-year model scenario.

Other Tributaries

Flow

Distributed inflow was calculated using the procedure developed for the calibration run, explained on page 43.

Figure 153 shows distributed inflows over the base 10-year model period. An identical flow regime was repeated for each consecutive 10-year period of the 50-year model scenario.

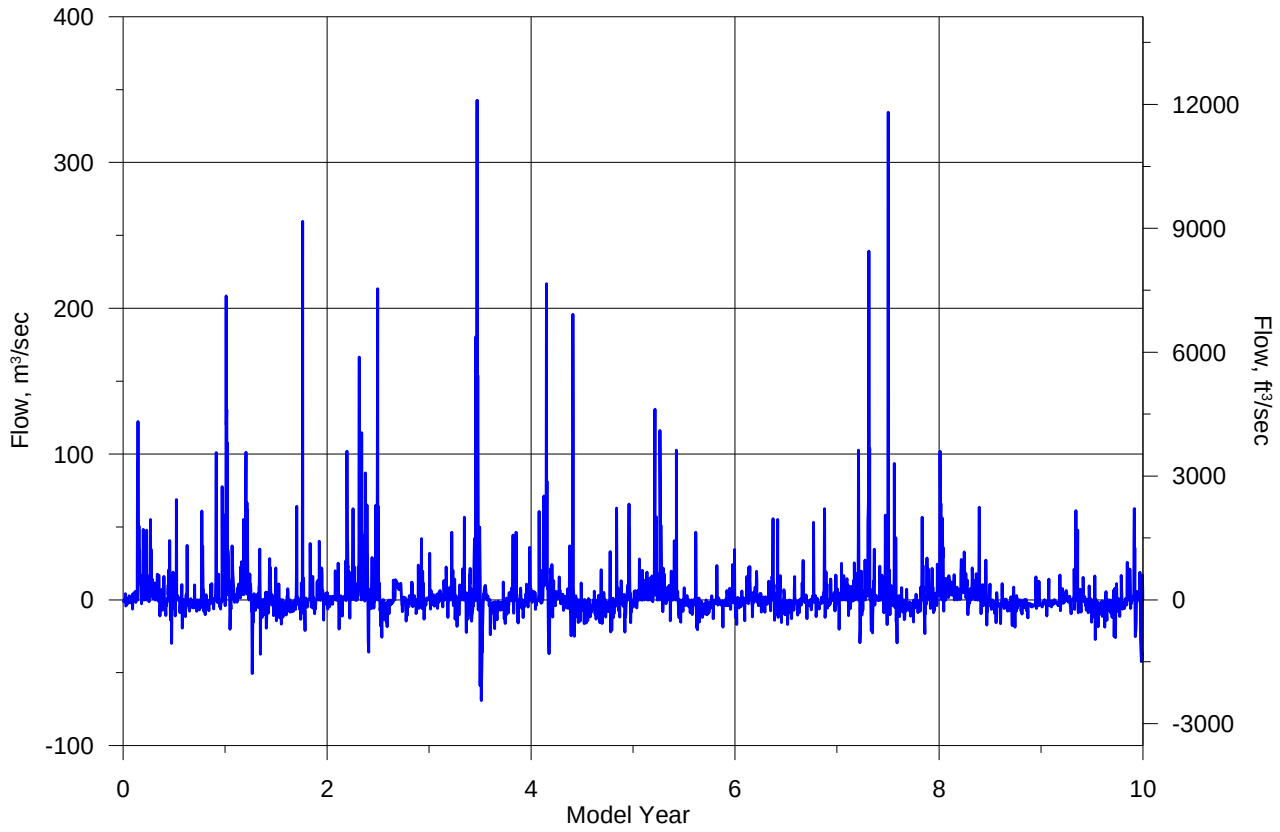

Figure 153. Distributed inflow for the base 10-year period of the 50-year model scenario.

Temperature

The Illinois River filtered equilibrium water temperature (see Figure 141) was used to estimate temperatures for distributed inflow for the 50-year scenario.

Water Quality

Water quality data from Caney Creek was used to estimate water quality parameters for the distributed tributary inflow.

Reservoir Water Level

Using an approach similar to the model calibration, model predictions of water level between January 1, 1997 and December 2006 were initially compared to the water level data. This assured that the representation of the hydrology and dam operations during the 10-year period agreed with measured water levels.

Since the model will be extended to 50 years by repeating this 10-year period five times, the ending water level at the end of 10 years had to match the beginning water level of the next period to avoid water level drift over the decades.

The daily average inflows for the Illinois River, Baron Fork, and Caney Creek were obtained from measurements as shown in the above sections. The Corps computed the outflow and total inflow based on a change of volume in the system (hence evaporation water loss was included in the flow computation). The change in the total inflow minus the flows from the 3 main inflow tributaries was added back to the model as a distributed inflow. In order to match water levels, another distributed inflow was added using the waterbalance program. The average water balance flow correction = -1.5 m^3/s (or about 50 cfs) for the 10-year period (Julian day 1.00 to 3652). Applying these corrections flows (shown in Figure 154), the resulting model prediction of water level compared to field data is shown in Figure 155. Errors in water level were very small as shown in Table 10.

Table 10. Water level errors between January 1997 and December 2006.

# of observations	Mean error	Absolute Mean error	RMS error
3590	-0.02 m	0.04 m	0.07 m

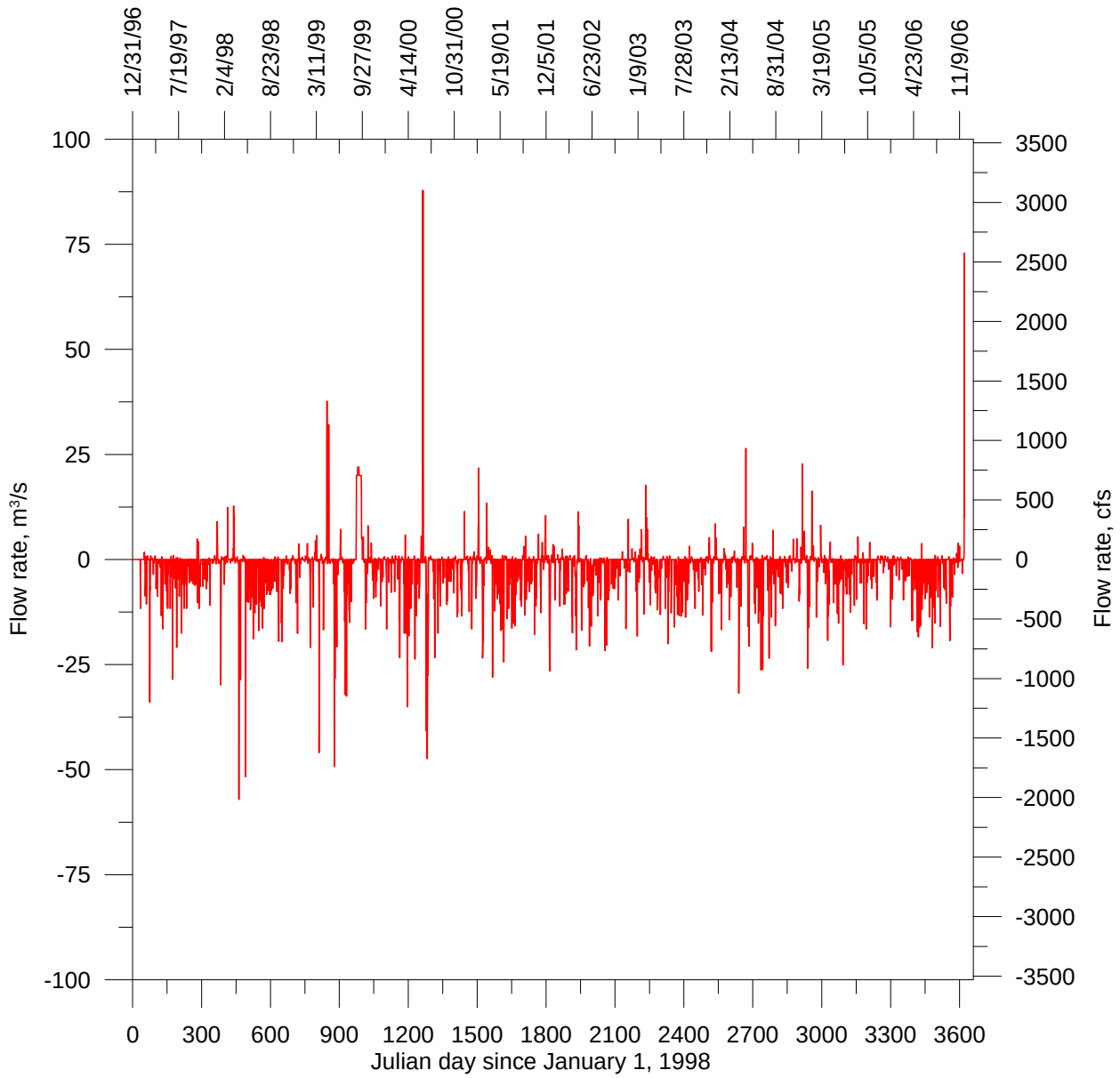

Figure 154. Computed water balance flows between January 1997 and December 2006.

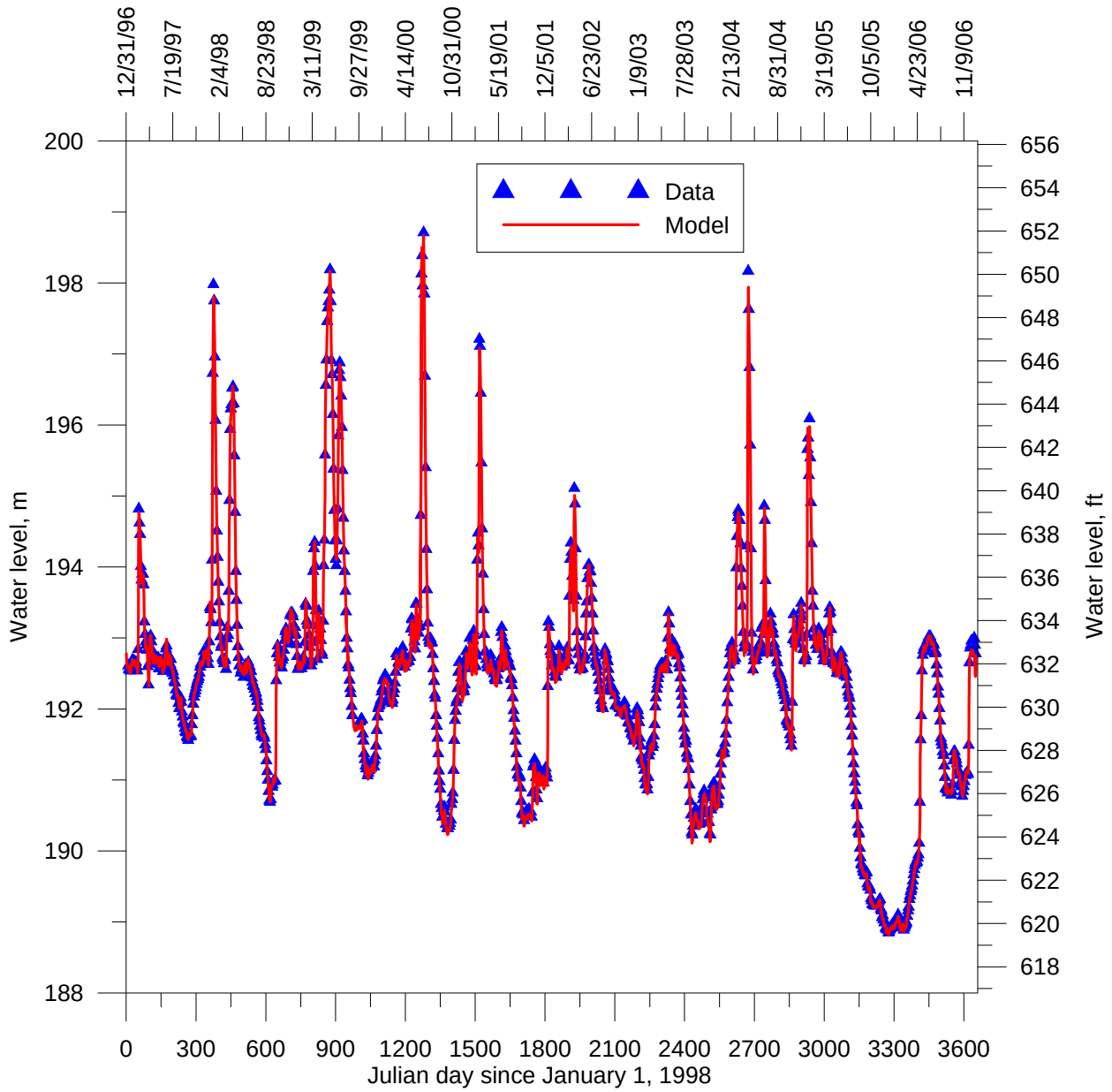

Figure 155. Water level data compared to model predictions between January 1997 and December 2006.

These water balance flows were then added to the already calculated distributed inflow/outflow file. This distributed inflow/outflow file was the difference between Corps calculated total inflow and the inflow from the 3 main tributaries of Tenkiller: Illinois, Baron Fork, and Caney Creek. These inflows are distributed equally around the first main branch of the lake.

Once the water balance flows were added to the distributed flows, these flows were smoothed such that oscillations of flow in on one day and flow out the next day were eliminated. Figure 156 shows the combined distributed inflows and the smoothed inflows. The combined distributed inflow file had an average flow of 2.9 m^3/s. The unsmoothed distributed inflow file had a standard deviation in the flow of 20.2 m^3/s, while the smoothed inflow file had a standard deviation of 18.8 m^3/s.

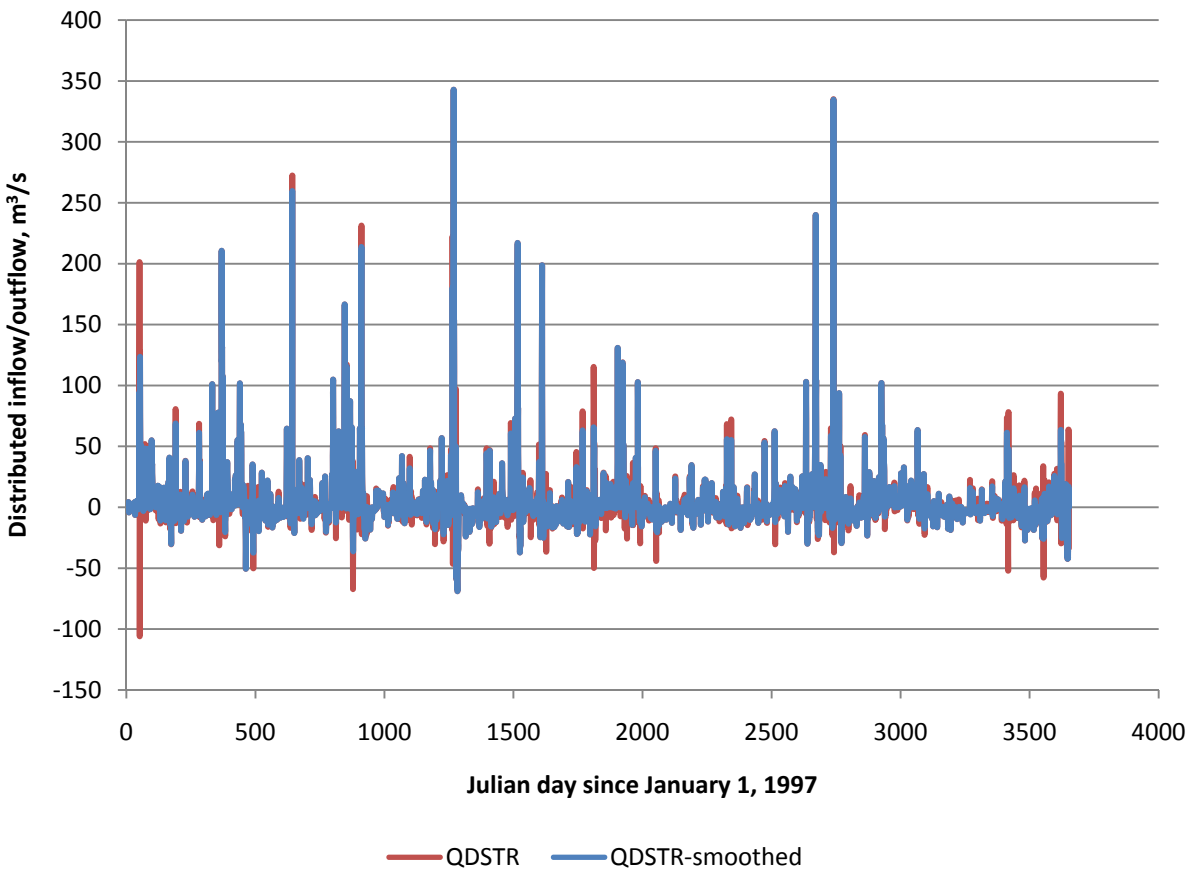

Figure 156. Distributed inflows from January 1997 to December 2006 combining the water balance flows showing the effect of smoothing.

Downstream Boundary Conditions

"Seepage" or minimum release flows were based upon observed minimum values in the dam outflow data provided by the Army Corps of Engineers. This average minimum flow rate varied with time as seen in Figure 157. Table 11 summarizes the base flow rates over the model period. This minimum flow rate was subtracted from the total release rate (when total release was at or above the minimum flow rate). When total release was below the seepage rate, the total flow was assumed to be base flow. Spillway release was calculated by subtracting powerhouse and base flow from total release. The final outflows from Tenkiller Reservoir are shown in Figure 158.

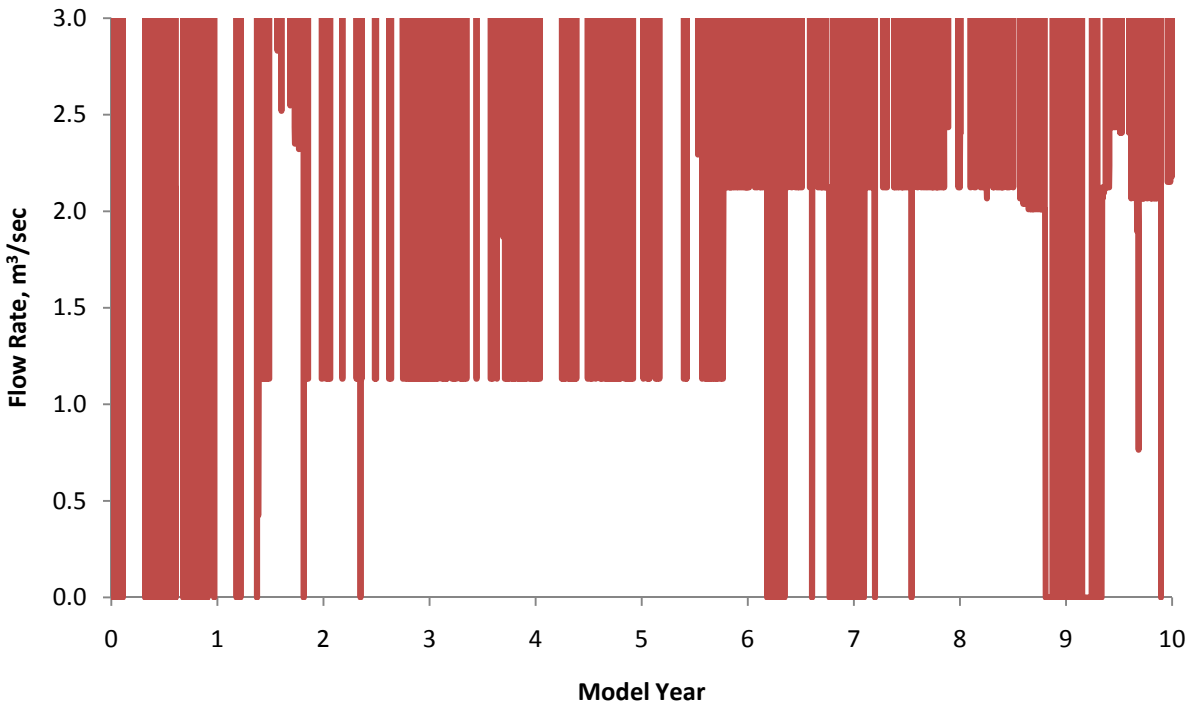

Figure 157. Minimum release flow from dam for the base 10-year period of the 50-year model scenario.

Table 11. Minimum base flows over time.

Date Range	Base Flow, m^3/sec
1/1/1997 - 5/20/1998	0
5/21/1998 - 10/7/2002	1.13
10/8/2002 - 11/3/2004	2.12
11/4/2004 - 12/31/2007	2.5

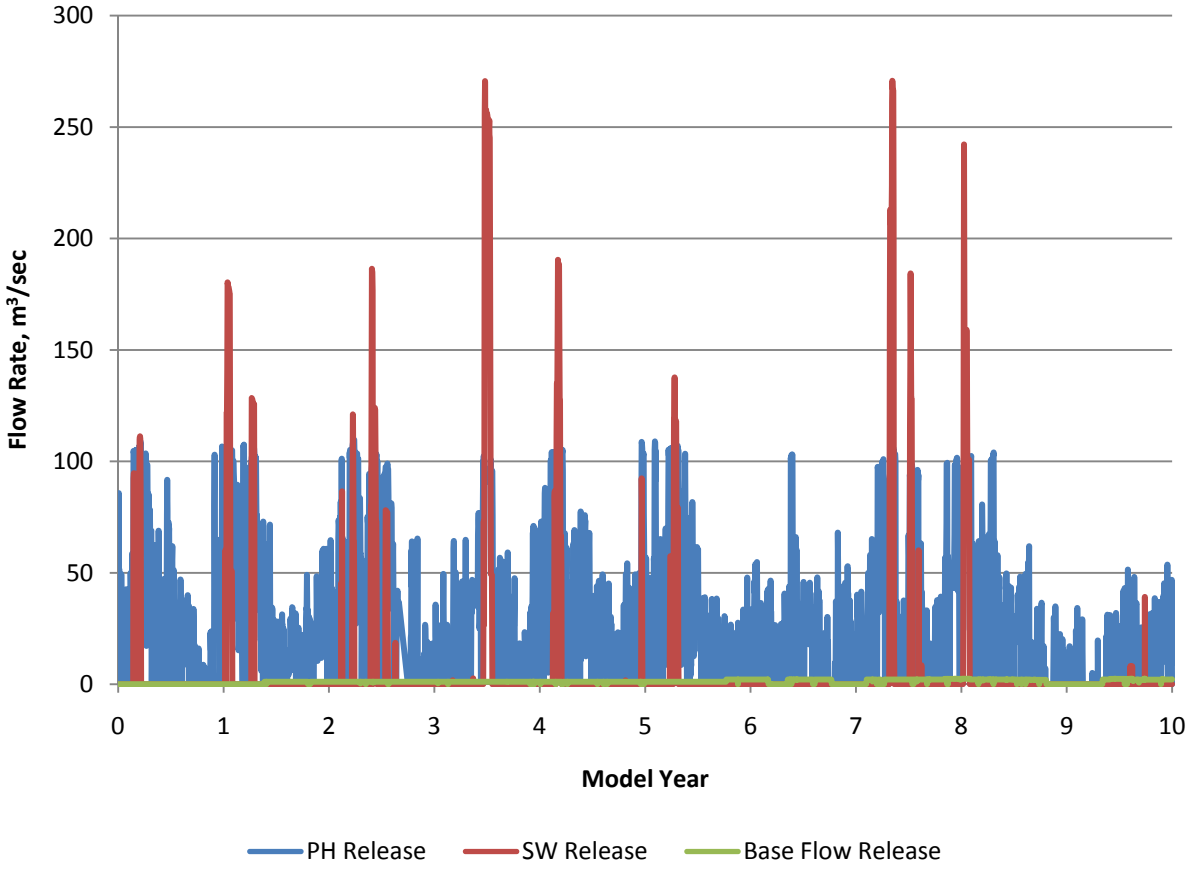

Figure 158. Outflows from Tenkiller Reservoir for the base 10-year period of the 50-year model scenario.

Meteorological Data

Data from Cookson, Oklahoma was not for the full ten year period. For this reason, meteorological data from Tulsa International Airport were used for the 10-year base period of 1997 to 2006. In order to better reproduce conditions at Tenkiller Lake, the relationships shown in Figure 52 and Figure 53 (see section entitled Air and Dew Point Temperature) were used to adjust the air temperature and dew point data collected at Tulsa. Tulsa wind speed and direction data were directly used for the 10-year model run. To create a 50-year meteorological data set, this base 10-year period of meteorological data was repeated 5 times.

Water Quality Management Scenarios

Model Scenarios

The model scenarios evaluated with the Tenkiller model are shown in Table 12. The prospective model scenarios were run for 50 years starting with a watershed representative of conditions at the end of 2006. The hydrology, meteorology, and dam operations were from January 1997 through December 2006 and repeated for every ten year period. Total P loadings were obtained from Engel (2008) for each of the scenarios. Boundary conditions for the other water quality constituents were estimated based on field data taken between 1997 and 2006. The historical model scenario though used inflow hydrology from 1950 to 1999 and a different dam operation than during the other simulations.

Table 12. Management scenarios considered with the Tenkiller Reservoir model.

Scenario #	Scenario name	Description	Dissolved PO_4-P	Sediment oxygen demand	Other water quality input parameters
1	Base	Existing loadings continued 'as is', status-quo	Data correlation to Total P based on 1997-2006 period	Internally computed sediment deposition, long-term or historical SOD from calibration model	Organic matter and inorganic suspended solids fractions were based on the Total P, N compounds based on field data, dissolved oxygen based on synthetic temperature sequence
2	Cessation-historical sediment oxygen demand reduction	Cessation of land application of poultry waste with gradual reduction in historical sediment oxygen demand	Data correlation to Total P based on 1997-2006 period	Internally computed sediment deposition, long-term SOD from calibration model reduced to 50% every 5 years (see discussion in next section)	Organic matter and inorganic suspended solids fractions were based on the Total P, N compounds based on field data, dissolved oxygen based on synthetic temperature sequence

Scenario #	Scenario name	Description	Dissolved PO_4-P	Sediment oxygen demand	Other water quality input parameters
3	Cessation-historical sediment oxygen demand immediate reduction	Cessation of land application of poultry waste with immediate reduction in historical sediment oxygen demand	Data correlation to Total P based on 1997-2006 period	Internally computed sediment deposition, long-term SOD from calibration model set to background levels of 0.1 $g/m^2/day$ from the beginning of the simulation	Organic matter and inorganic suspended solids fractions were based on the Total P, N compounds based on field data, dissolved oxygen based on synthetic temperature sequence
4	Natural conditions	All inflows at a flow-weighted average of 0.02 mg/l Total P	Data correlation to Total P based on 1997-2006 period	Internally computed sediment deposition and historical SOD set to 0.1 $g/m^2/day$	Same as base case
5	Growth conditions	Total P loadings in the watershed increase over time (see Engel, 2008)	Data correlation to Total P based on 1997-2006 period	Internally computed sediment deposition and historical SOD from calibration model	Same as base case
6	Historical conditions with hydrology from 1950-1999	Total P loadings in the watershed increase over time but from a time period before land application of poultry waste was significant in the watershed simulating conditions from 1950 to 1999 (see Engel, 2008)	Data correlation to Total P based on 1997-2006 period	Internally computed sediment deposition and historical SOD set to 0.1 $g/m^2/day$	Same as base case

Estimating sediment oxygen demand reduction over time for zero order sediment model

In general, the sediment in a reservoir or lake can be composed of an aerobic and an anaerobic layer, as shown in Figure 159. The primary variables governing changes in sediment would be:

- flux of particulate organic matter to the sediment (in CE-QUAL-W2 this would be algae and particulate organic matter, representing all non-living particulate organics)
- the rate at which the sediment is decayed (either aerobically and/or anaerboically)
- the rate of burial of the sediment.

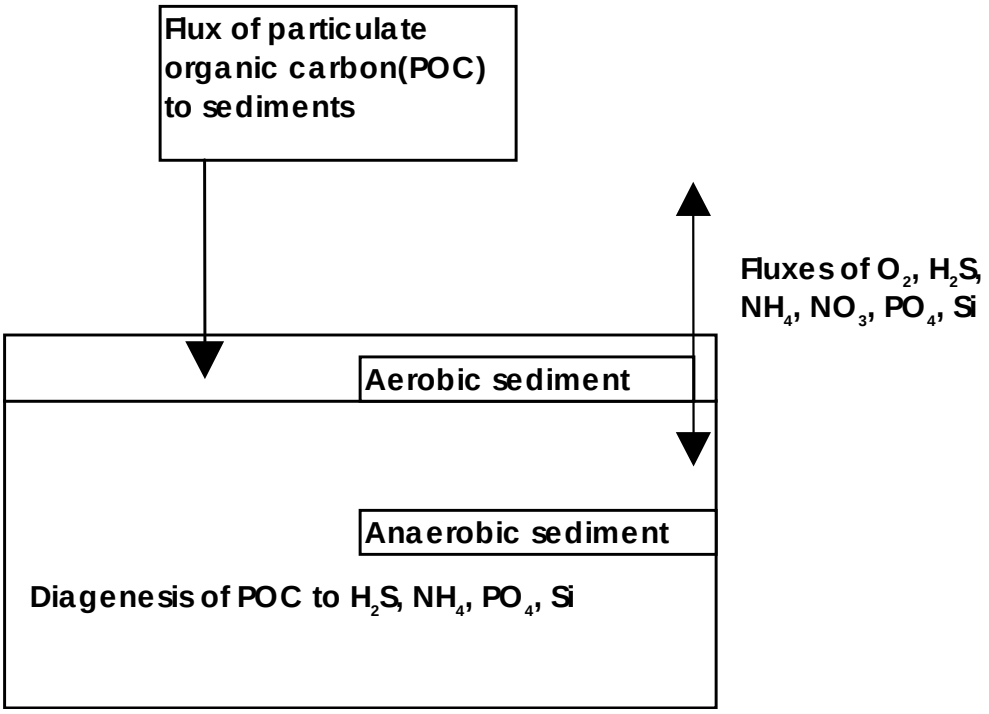

Figure 159. Schematic of sediment layers (after DiToro and Fitzpatrick, 1993).

The sediment oxygen demand in the CE-QUAL-W2 model is based on 2 different submodels:

1. A zero-order sediment oxygen demand based on aerobic decay of historical sediment accumulation (see Figure 160).
2. A first order, aerobic labile decay of deposited organics (see Figure 161).

CE-QUAL-W2 does not have an anaerobic digenesis submodel.

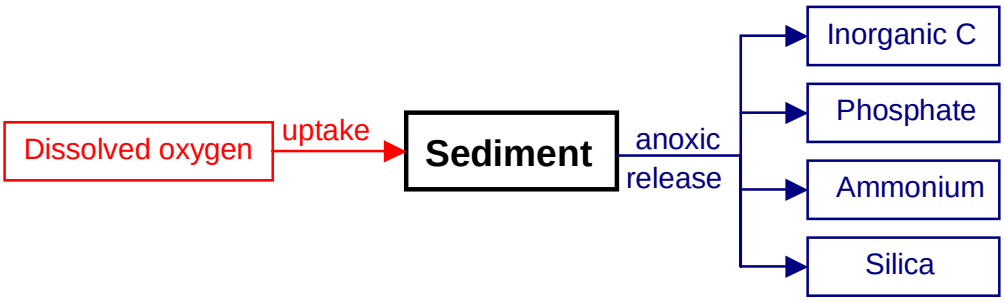

Figure 160. CE-QUAL-W2 zero order sediment oxygen demand model.

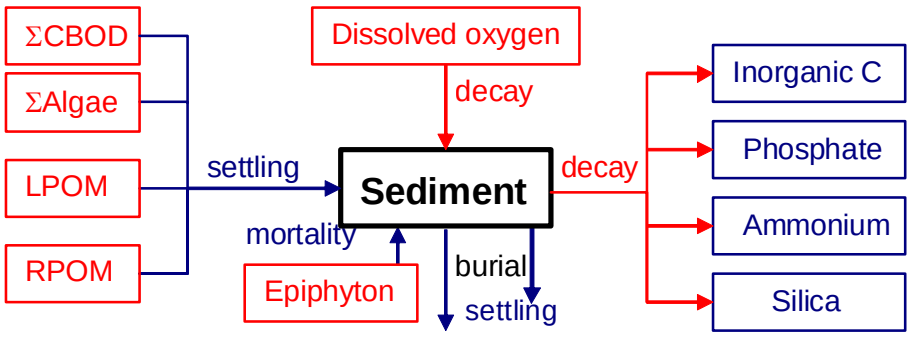

Figure 161. CE-QUAL-W2 first order predictive sediment oxygen demand.

In W2, the first order sediment model represents only the aerobic layer and decays sediment only when there is oxygen in the water above the sediment. Nutrients are released according to stoichiometry by the sediment compartment. If the water above the sediment goes anoxic, the sediment decay process is stopped. Nutrients are released under anoxic conditions in W2 with the zero order sediment compartment. Typical aerobic decay rates can be of the order of 0.01 to 0.1 day^{-1}.

In order to estimate the time for decay of organic sediment, the following information would be required:

- the amount of existing organics in the sediment as a function of location, in terms of g/m^2 (this would require understanding the "history" of loading and retention in the system since the reservoir's beginning; this is probably the largest unknown)
- the C, N, P content of those sediments (estimated from prior studies)
- the flux of POC to the sediments (currently modeled and historically estimated from prior field studies)
- the decay rate of the organic matter in the sediments under aerobic and anaerobic conditions (the aerobic degradation rate is used in the model, but the current model does not account for diagenesis in the sediment compartment; hence the model assumes an anaerobic decay rate of zero)
- the burial velocity of the sediment

If one assumes that the flux of POC to the sediments is stopped (which is overly conservative since nutrients can be recycled continuously in the reservoir even without nutrient inputs), then the rate of

decay is proportional to the assumed sediment decay rate. Most investigators have assumed a first order reaction rate of the form (ignoring any sources)

$$\frac{dC_s}{dt} = -KC_s \quad \textit{with the solution} \quad \frac{C_s(t)}{C_s(t=0)} = \exp(-Kt)$$

where C_s is the concentration of sediment in g/m^2 and K is the sediment decay rate in day^{-1}. In the Chesapeake Bay study of DiToro and Fitzpatrick (1993), anaerobic sediments were broken into 3 categories:

- rapidly reactive sediments (20 day half-life)
- slowly reactive sediments (1 year half-life)
- non-reactive sediments (no decay)

Table 13 shows typical percentage composition and typical decay rates for each of these sediment compartments. Figure 162 shows the fraction of sediment remaining in each fraction using parameter values from the table below and the simple model where no further sources of POM were present and no burial occurred.

Table 13. Sediment decay rates and assumed fraction sediment based on sediment type (DiToro and Fitzpatrick, 1993, and Cerco and Cole, 1994).

Sediment type	Assumed decay rate, K [day^{-1}]	Assumed percentage of total sediment
rapidly reactive	0.025-0.035	45-65%
slowly reactive	0.0013-0.0018	20-30%
non-reactive	0	15-25%

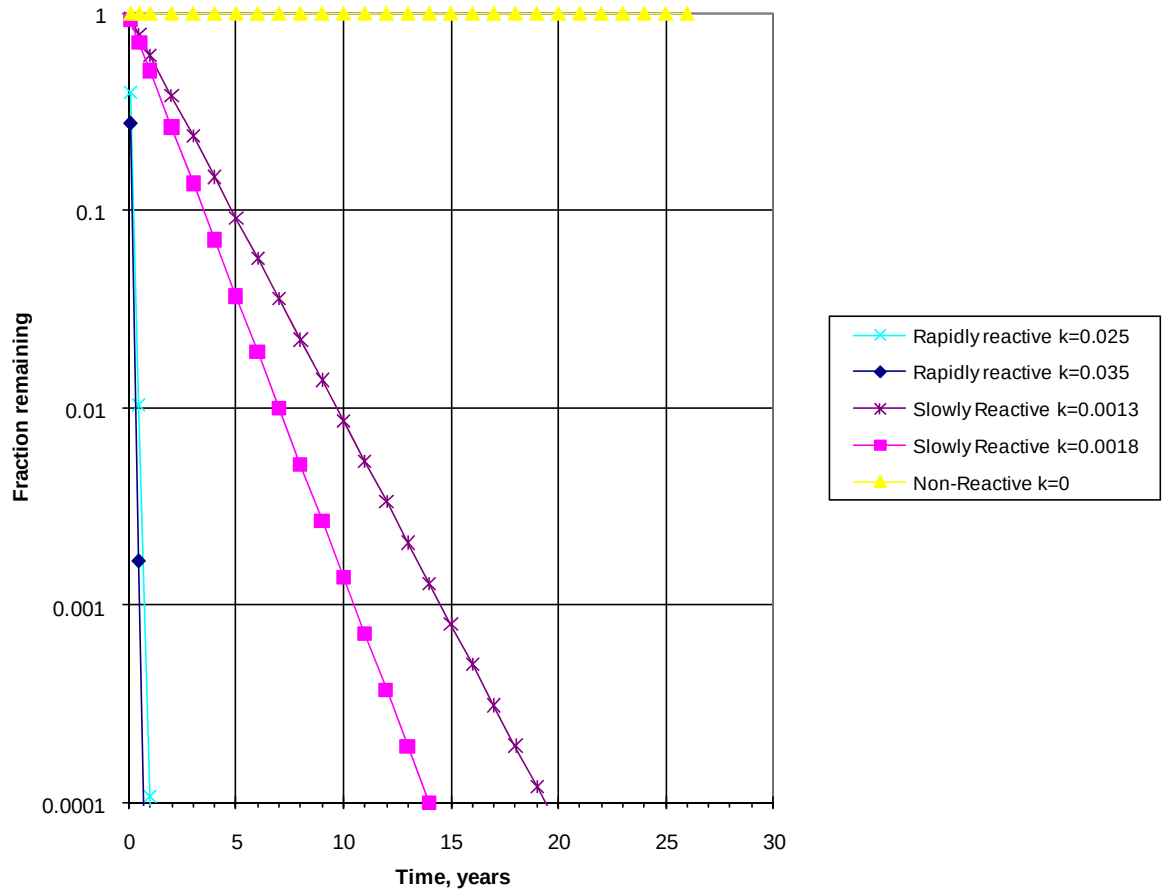

Figure 162. Variation of fraction of sediment remaining without any flux of organic matter to sediments as a function of decay rate range.

These results though may overpredict the speed of diagenesis since the flux of POC will rarely ever not be zero. A simple model with constant sediment flux, decay and burial would be:

$$\frac{dC_s}{dt} = -KC_s + Flux + Burial\,Rate$$

$$with\,Flux \neq f(t)$$

$$and$$

$$Burial\,Rate = -K_{burial}C_s,$$

$$the\,solution\,is$$

$$C_s = C_{st=0}\exp(-[K + K_{burial}]t) + \frac{(Flux)}{K + K_{burial}}\left(1 - \exp(-[K + K_{burial}]t)\right)$$

The flux to the sediments would be defined as

$$Flux = V_{s-algae} C_{algae} + V_{s-detritus} C_{detritus}$$

where V_s is the settling velocity of the algae or non-living particulate organic matter or detritus in m/d and C is the concentration of algae or detritus in the water column in mg/l. Unfortunately, this flux is quite dynamic and the above equation is only useful for order of magnitude estimates. The burial rate is the burial velocity over the sediment thickness. Cerco and Cole (1994) used a value of K_{burial} between 0.025 to 0.05 year^{-1} or between 7E-5 to 14E-5 day^{-1}. The above equation would predict that at steady-state the sediment would be in equilibrium with the water column such that $C_s = \frac{Flux}{K + K_{burial}}$.

Using the unsteady model with constant values for the flux, decay, and burial, the expected fractions of the 3 sediment types remaining as a function of time for a C_{so} of 1000 g/m^2 with K_{burial}=7E-5 day^{-1} are shown in Figure 163. In this example, all of the fast decaying organics are removed after the first year and the slowly reactive ones are decaying such that within 5 years only about 10% are remaining. Because of this uncertainty as to how the Tenkiller sediments will react to reductions in loading, the CE-QUAL-W2 model explored several different runs bracketing the expected sediment reduction.

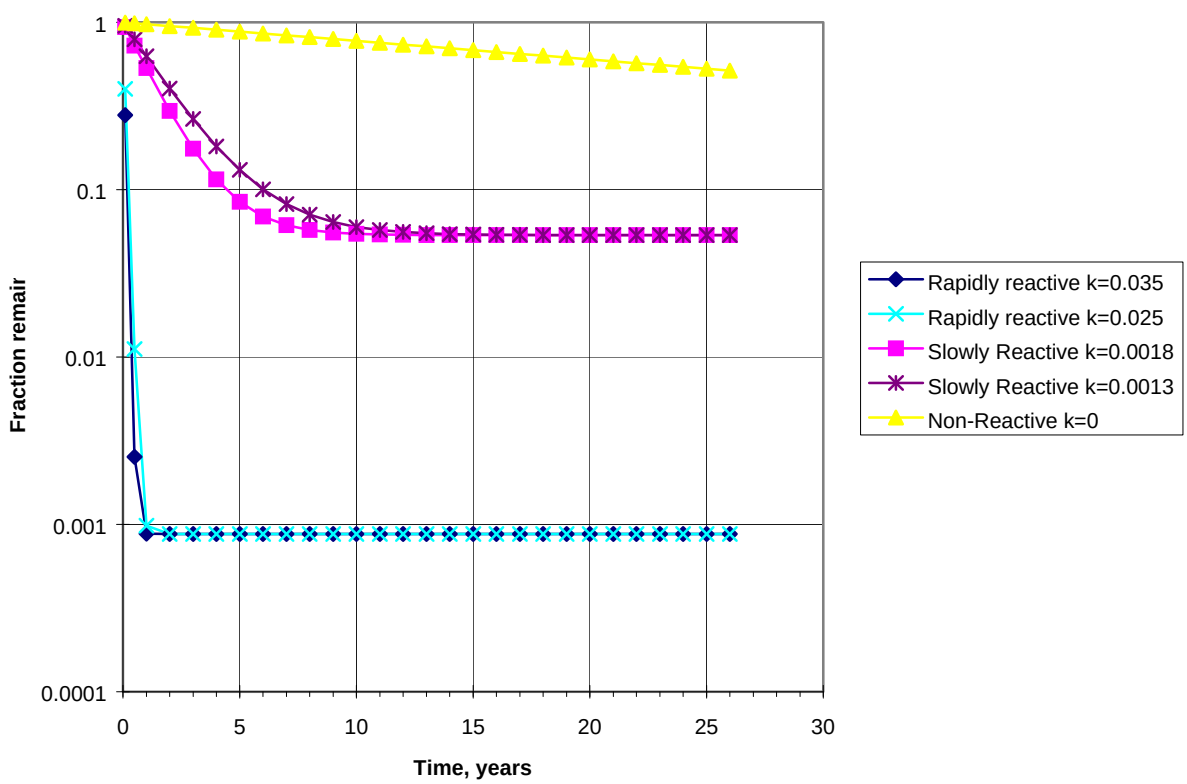

Figure 163. Fraction of sediment categories remaining assuming a constant sediment flux of 100 mg/m^2/day, C_{so} of 5000 g/m^2, and a burial rate of 7E-5 day^{-1}.

Hence, in the CE-QUAL-W2 scenarios, the 2 sediment compartments of CE-QUAL-W2 were treated as follows:

1. The dynamic accumulation of organics was computed based on the internal model dynamics driven by the boundary conditions. Hence reductions in Total P in the water shed would typically result in lower organic matter deposition to the sediment, thus reducing the oxygen demand.
2. The background sediment oxygen demand (the zero order model) was either kept the same as the calibration model (approximately 0.85 $g/m^2/day$), reduced using a decay rate half-life of about 5 years, which corresponds to a first order decay rate of 3.9E-4 day^{-1}, or immediately reduced to those found in low-productivity reservoirs/lakes of 0.1 $g/m^2/day$.

Testing of 50-year model

One of the model tests of the 50-year simulation was that the water level and hydrology was repeated correctly every 10 years and that there was no drift in water levels that would bias the long-term simulation. This test was run without simulating water quality. Figure 164 below shows the water level of the model over the 50-year period, with water level peaks and lows reproduced accurately every 10-year period showing no drift over time. Checks were also made on temperatures and other model predicted variables to ensure that the basic hydrodynamic model without water quality was stable over the 50-year period and would respond only to changes in water quality loadings once the water quality simulation was made.

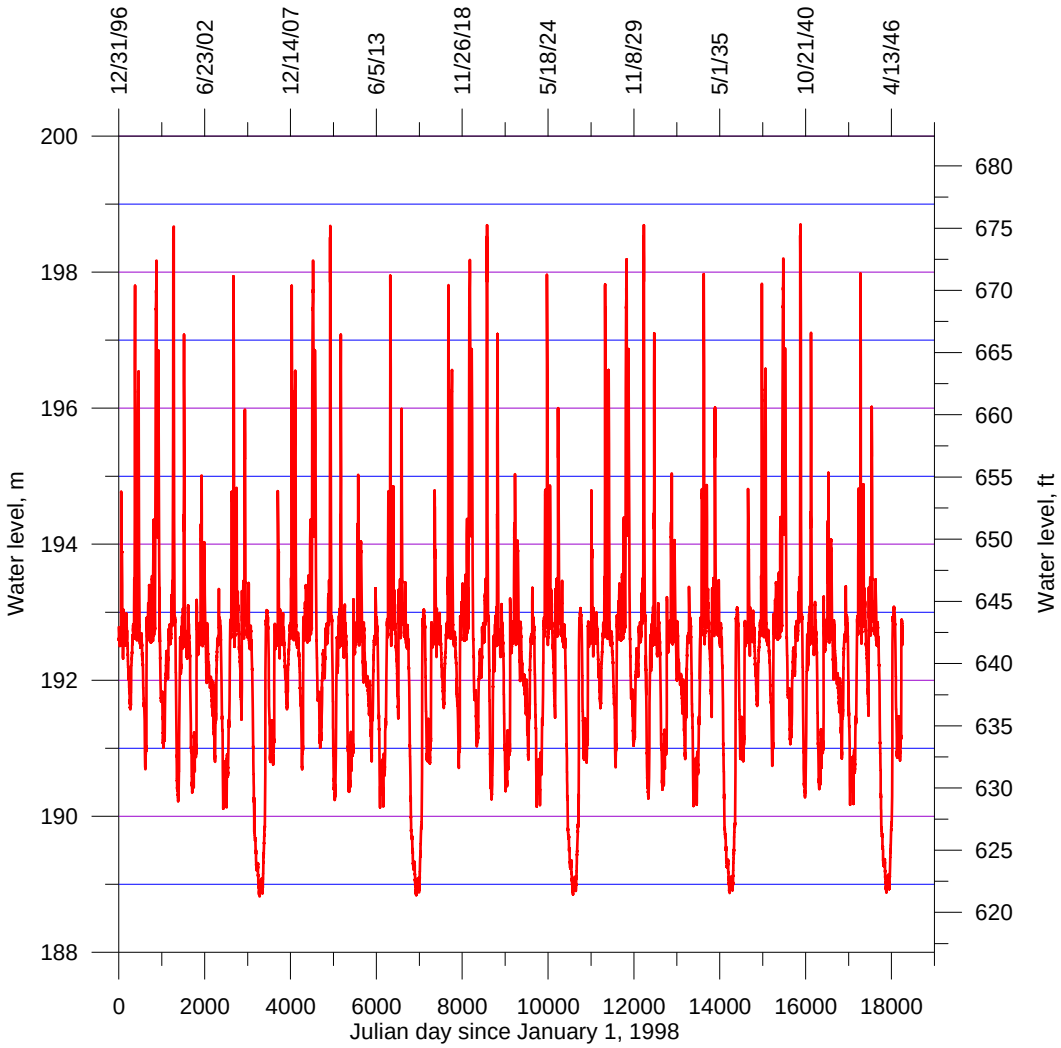

Figure 164. Water level for 50-year simulation showing no drift in water level after every 10-year period.

Model Scenario Results

The results of the model scenarios are described in this section. Note that these runs were based on the following assumptions:

1. The daily Total P loading from Engel (2008) was used to compute dissolved PO_4-P, particulate organic matter (both labile and refractory), dissolved organic matter (both labile and refractory), and algal biomass for the base case and cessation simulations..
2. NH_4-N, NO_2-N+NO_3-N, and algae biomass concentrations were unchanged between the scenarios and were based on field data from the 1997-2007 time period.

3. Dissolved oxygen and other water quality variables were also unchanged from the base case to the other scenarios and were based on field data from the 1997-2007 period.
4. Inflow temperatures, inflow rates and outflow rates were unchanged from the base case to the other cases.

The scenario runs were evaluated using several different approaches:

1. Computation of fish habitat volumes based on temperature and dissolved oxygen preferences of several species of fish, such as walleye and smallmouth bass.
2. Computation of volume-weighted surface values (upper 5-6 m) at the primary lake sampling stations (LK01, LK02, LK03, LK04) of chlorophyll a, Total-P, and dissolved oxygen.
3. Computation of dissolved oxygen in the discharge from Tenkiller Reservoir which is indicative of hypolimnetic anoxia in the summer.
4. Computation of P fluxes from sediment and all sources of sediment oxygen demand between model scenarios.

Surface Volume Weighted Averages

Volume weighted averages of the model predicted chlorophyll a and Total P dissolved were computed for the upper 5-6 m of the Tenkiller Reservoir at model segments 35, 59, 83, and 109 corresponding to lake sampling stations LK04, LK03, LK02, and LK01, respectively. Summer averages were computed between June 1 and September 30 of each year of the 50-year simulation.

Both time series and frequency distributions of these model results were compiled in this section.

Time Series of Summer Surface Volume Weighted Averages

Time series averages for chlorophyll a for the base, cessation and growth cases are shown in Figure 165, Figure 166, Figure 167, and Figure 168 for the 50-year simulation for lake sampling stations LK04, LK03, LK02, and LK01, respectively. The time series averages for chlorophyll a for the natural and historical cases are shown in Figure 169, Figure 170, Figure 171, and Figure 172 for the 50-year simulation for lake sampling stations LK04, LK03, LK02, and LK01, respectively. Linear trend lines were also shown for these simulations to assess overall trends for the 50 year period. The equations shown on the graphs are the linear trend equation where Y is the chlorophyll a concentration in µg/l and X is the year. The square root of the residual mean square provides an estimate of the standard error of the regression line, or the variability in chlorophyll a about the regression line. For the historical case, the chlorophyll a concentration was oftentimes very low at station LK04. This occurred because of changes in water level for the historical scenario for each year. In some years the upper reservoir was more

riverine causing little algae growth from the upper boundary condition to LK04. Hence, a regression line was not included for the historical simulation because of the large change in chlorophyll a between low-water summers to higher water summers.

Time series averages for chlorophyll a for the base, cessation and growth cases are shown in Figure 173, Figure 174, Figure 175, and Figure 176 for the 50-year simulation for lake sampling stations LK04, LK03, LK02, and LK01, respectively. The time series averages for chlorophyll a for the natural and historical cases are shown in Figure 177, Figure 178, Figure 179, and Figure 180 for the 50-year simulation for lake sampling stations LK04, LK03, LK02, and LK01, respectively. Linear trend lines were also shown for these simulations to assess overall trends for the 50 year period. The equations shown on the graphs are the linear trend equation where Y is the Total P concentration in mg/l and X is the year. The square root of the residual mean square provides an estimate of the standard error of the regression line, or the variability in Total P about the regression line.

Chlorophyll a

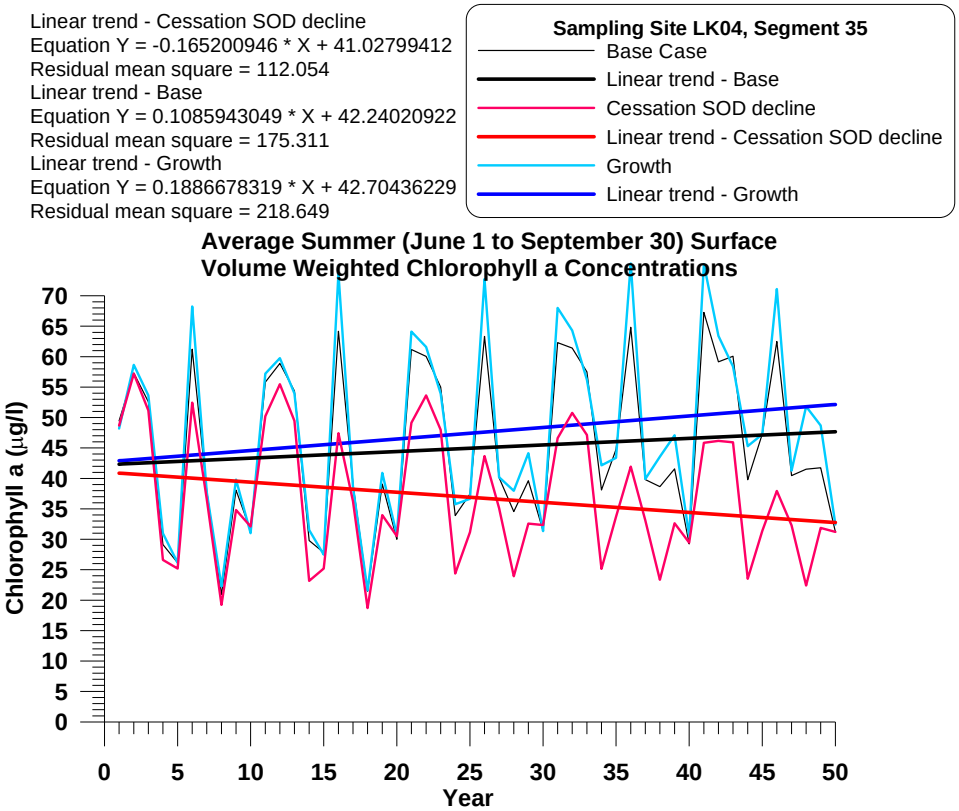

Figure 165. Volume weighted surface (5-6 m depth) average chlorophyll a at sampling site LK04, model segment 35 comparing cessation, growth and base case trends.

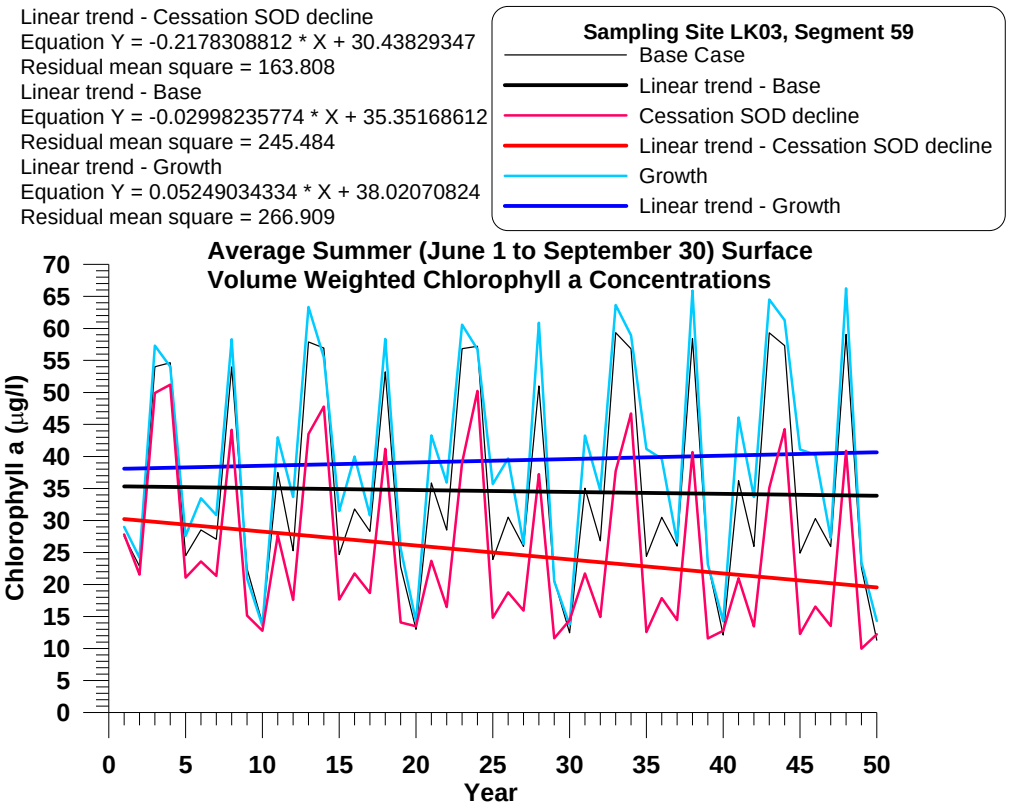

Figure 166. Volume weighted surface (5-6 m depth) average chlorophyll a at sampling site LK03, model segment 59 comparing cessation, growth and base case trends.

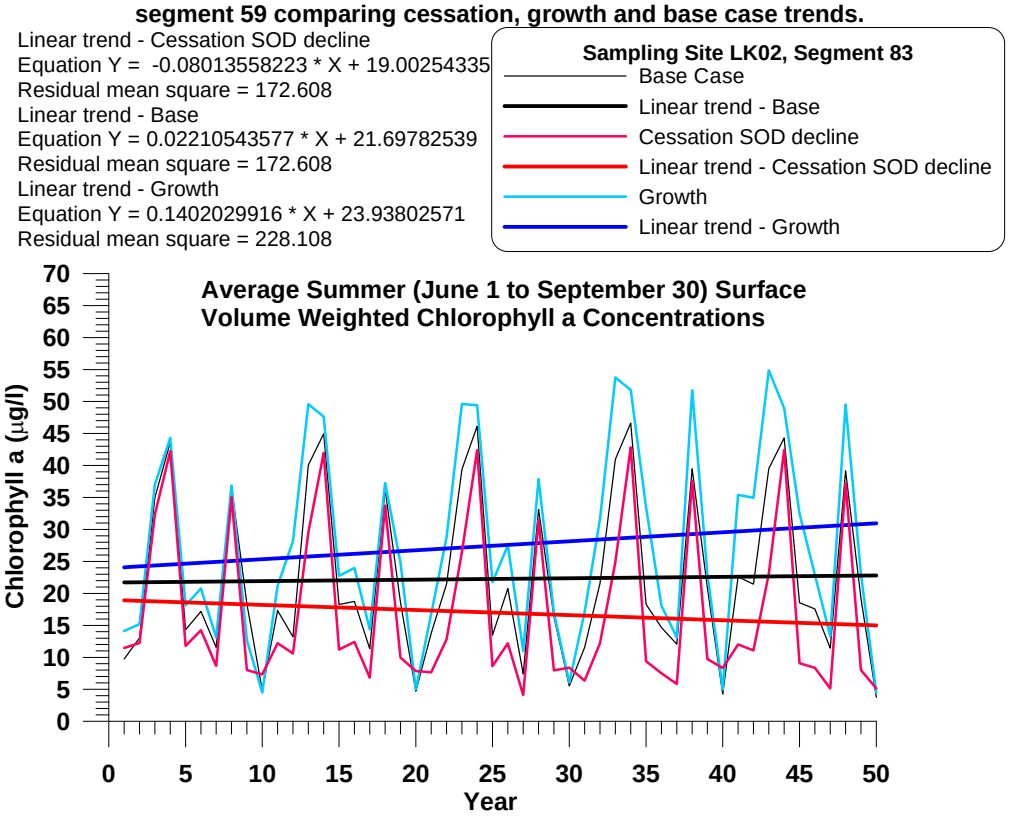

Figure 167. Volume weighted surface (5-6 m depth) average chlorophyll a at sampling site LK02, model segment 83 comparing cessation, growth and base case trends.

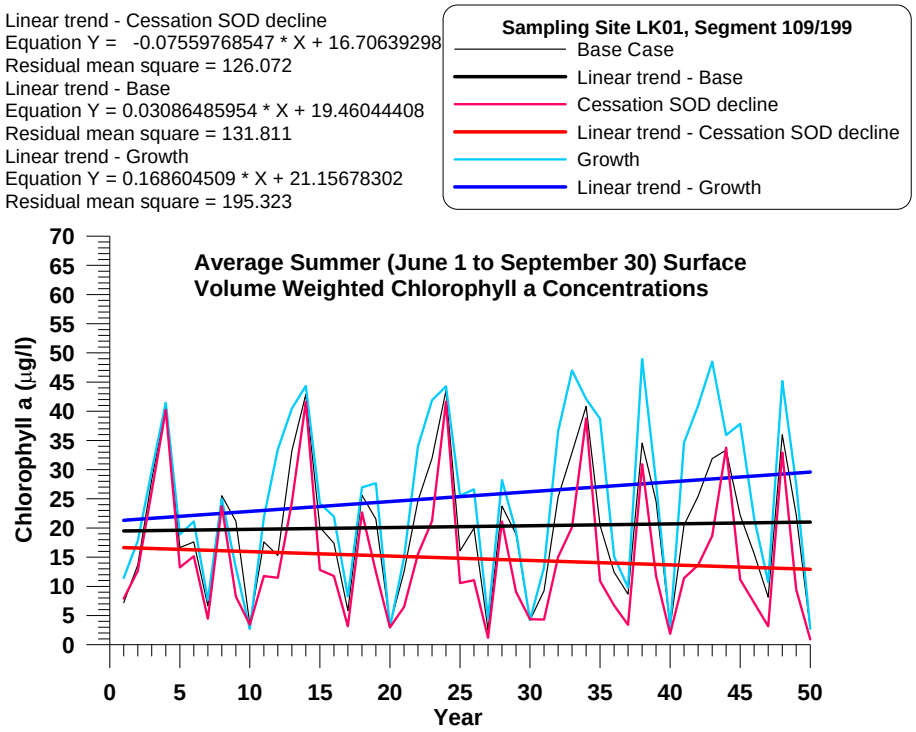

Figure 168. Volume weighted surface (5-6 m depth) average chlorophyll a at sampling site LK01, model segment 199 comparing cessation, growth and base case trends.

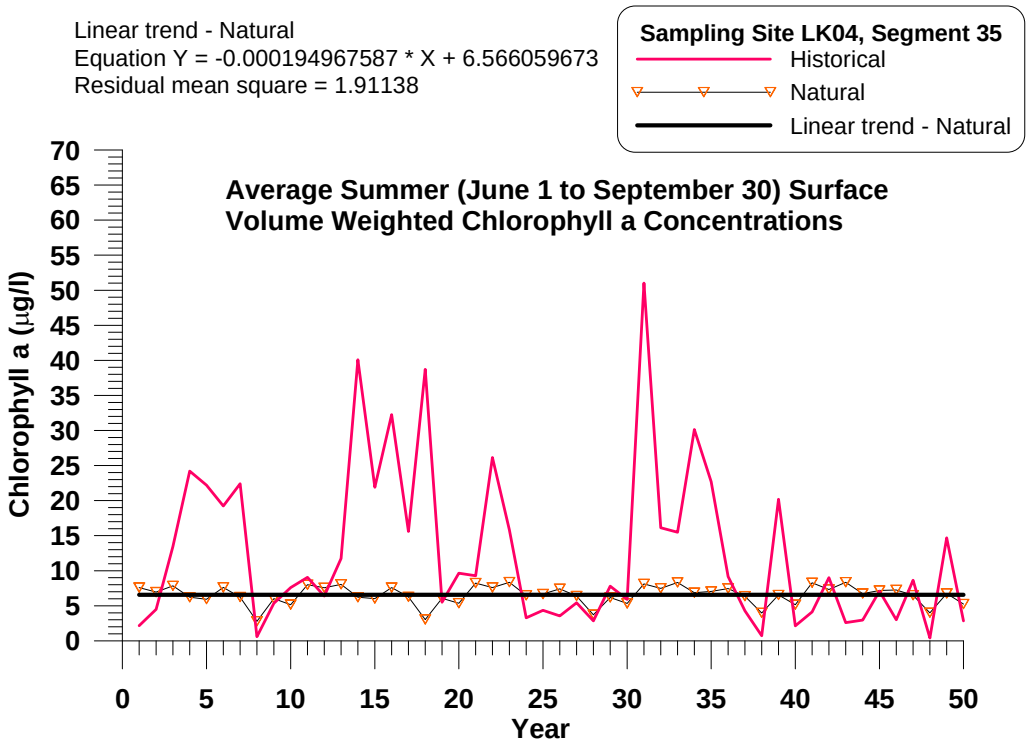

Figure 169. Volume weighted surface (5-6 m depth) average chlorophyll a at sampling site LK04, model segment 35 for historical and natural cases.

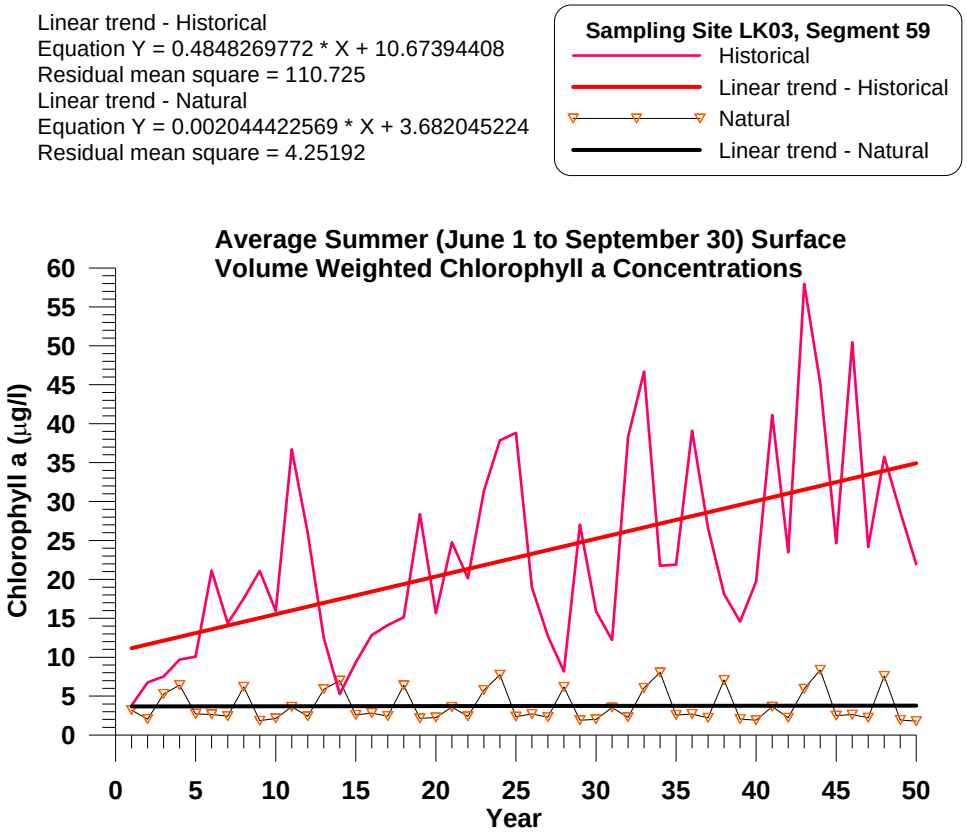

Figure 170. Volume weighted surface (5-6 m depth) average chlorophyll a at sampling site LK03, model segment 59 for historical and natural cases.

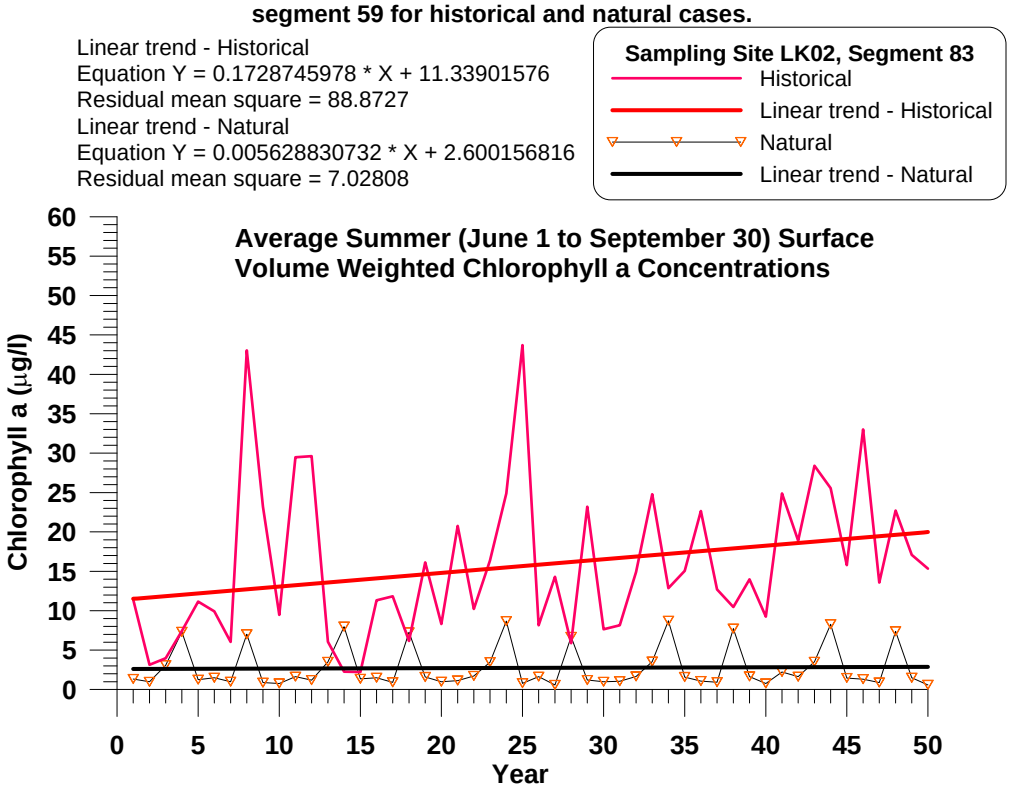

Figure 171. Volume weighted surface (5-6 m depth) average chlorophyll a at sampling site LK02, model segment 83 for historical and natural cases.

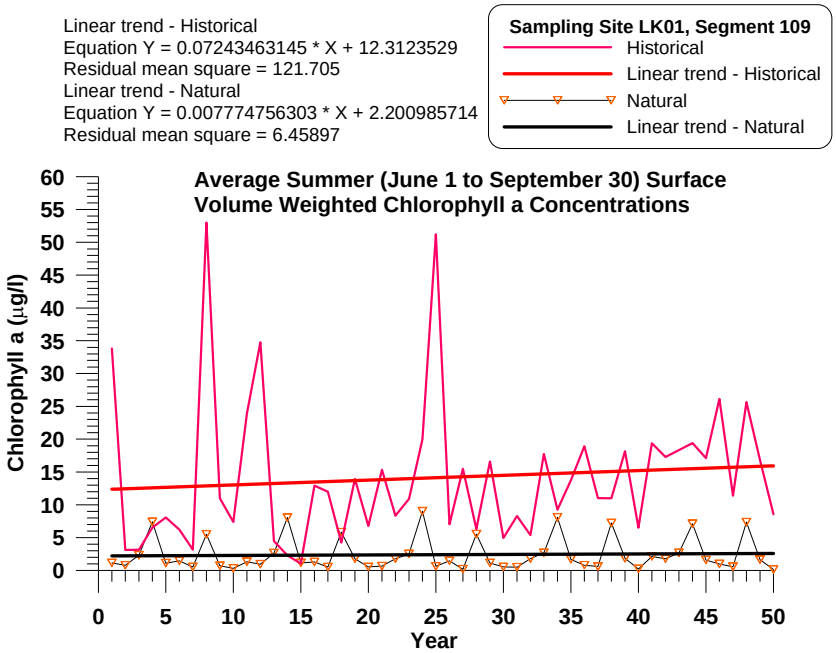

Figure 172. Volume weighted surface (5-6 m depth) average chlorophyll a at sampling site LK01, model segment 109 for historical and natural cases.

Total Phosphorus

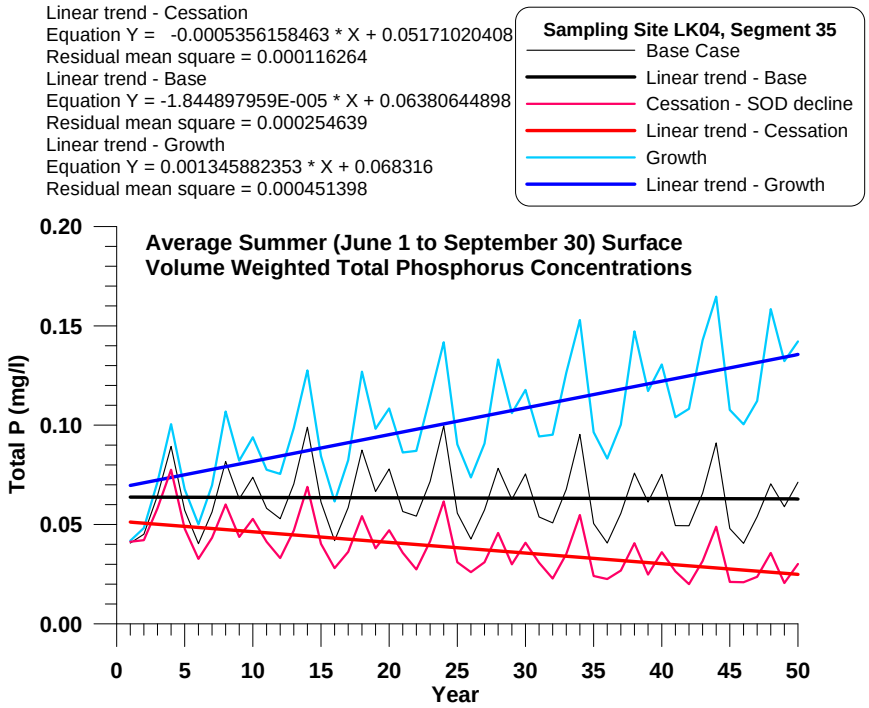

Figure 173. Volume weighted surface (5-6 m depth) average Total P at sampling site LK04, model segment 35 comparing cessation and base case trends.

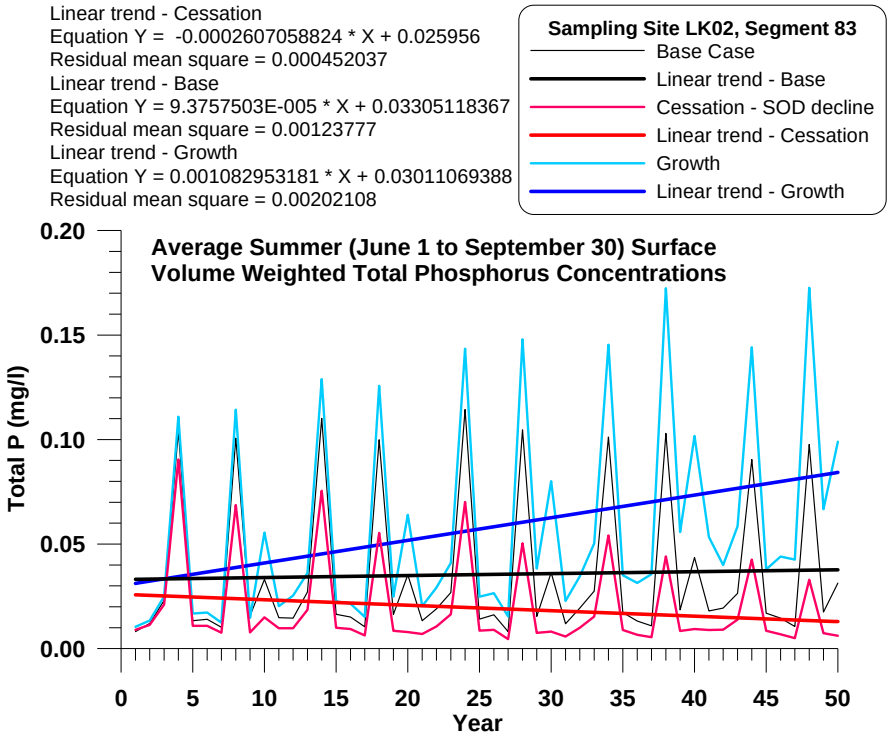

Figure 174. Volume weighted surface (5-6 m depth) average Total P at sampling site LK03, model segment 59 comparing cessation and base case trends.

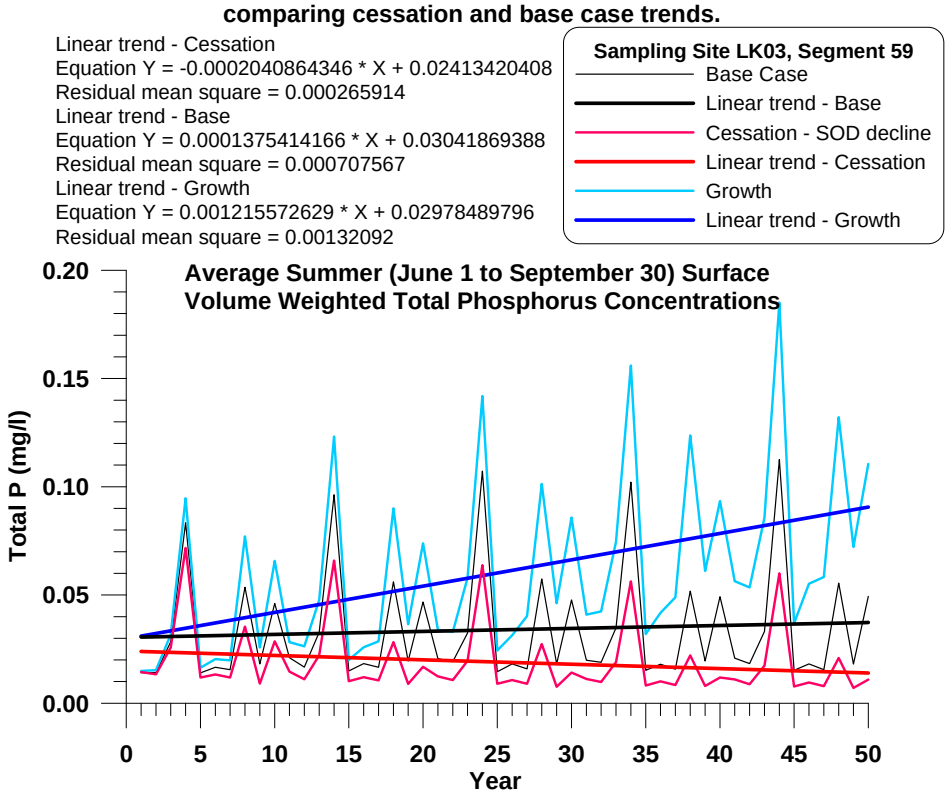

Figure 175. Volume weighted surface (5-6 m depth) average Total P at sampling site LK02, model segment 83 comparing cessation and base case trends.

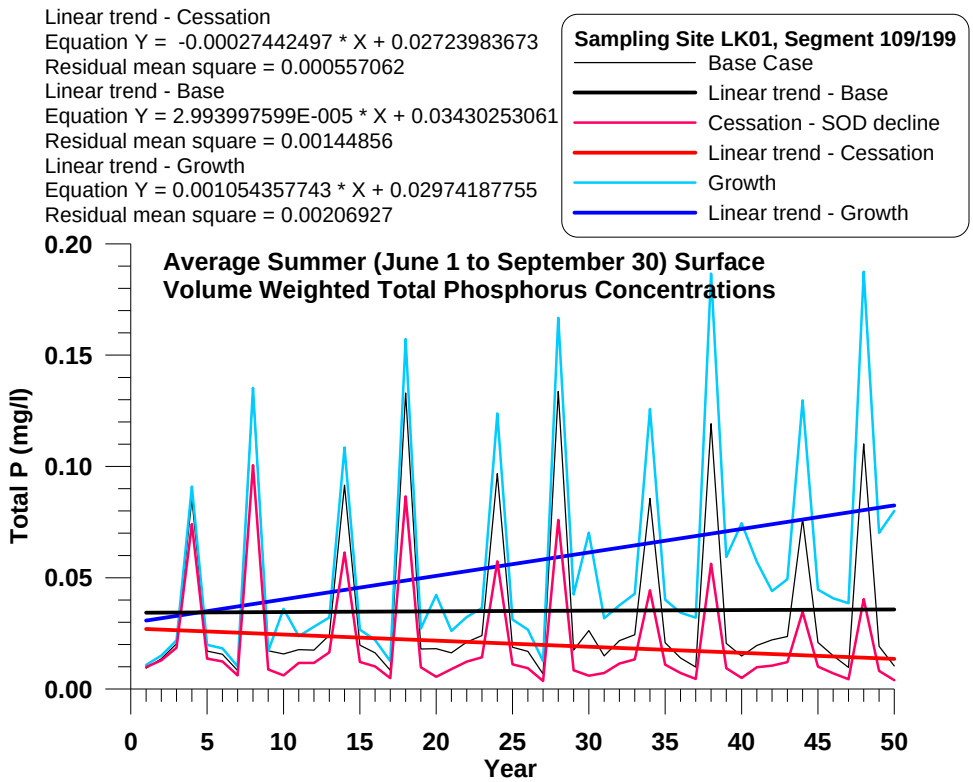

Figure 176. Volume weighted surface (5-6 m depth) average Total P at sampling site LK01, model segment 199 comparing cessation, growth and base case trends.

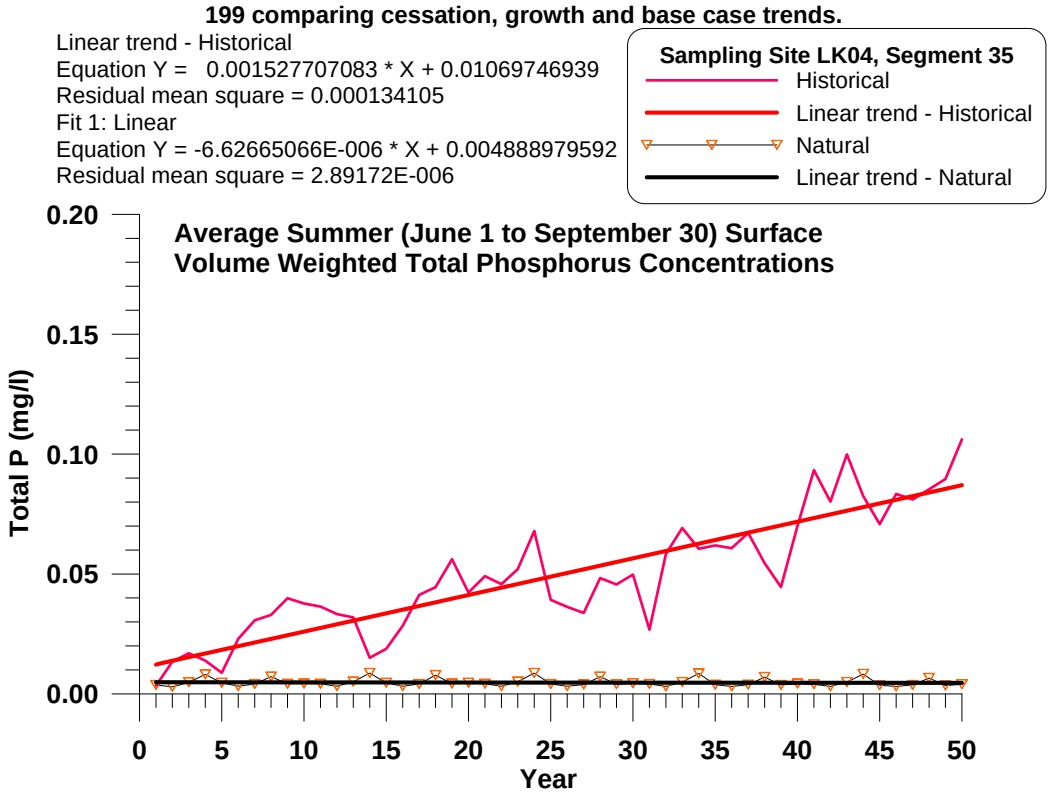

Figure 177. Volume weighted surface (5-6 m depth) average Total P at sampling site LK04, model segment 35 for historical and natural cases.

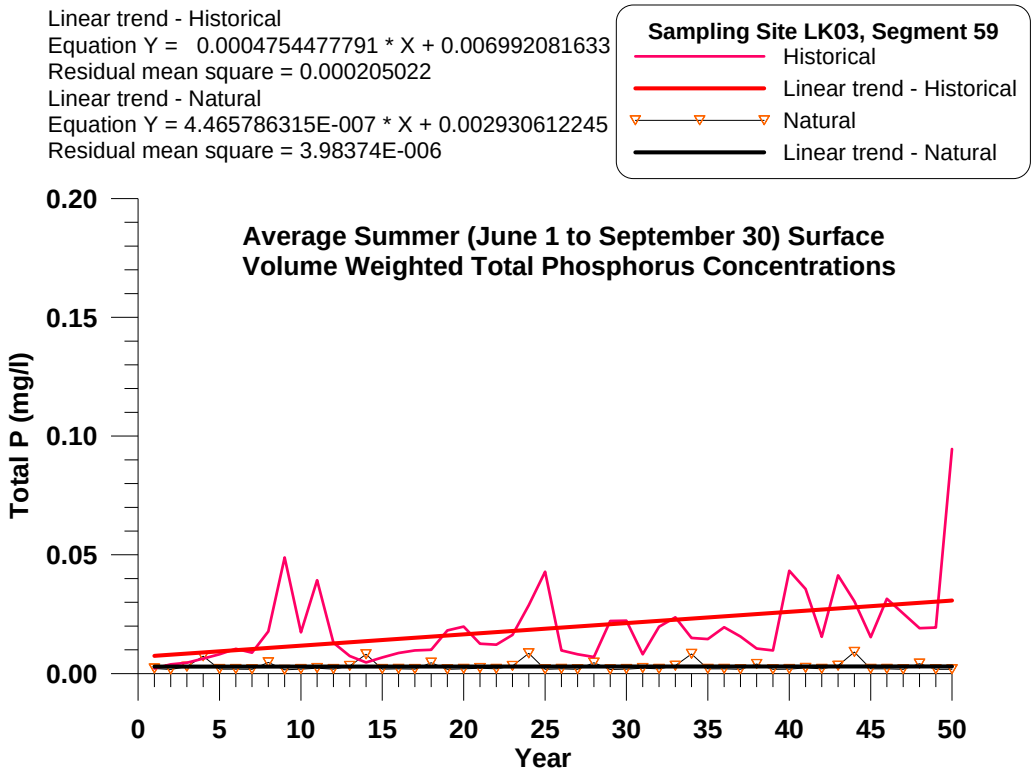

Figure 178. Volume weighted surface (5-6 m depth) average Total P at sampling site LK03, model segment 59 for historical and natural cases.

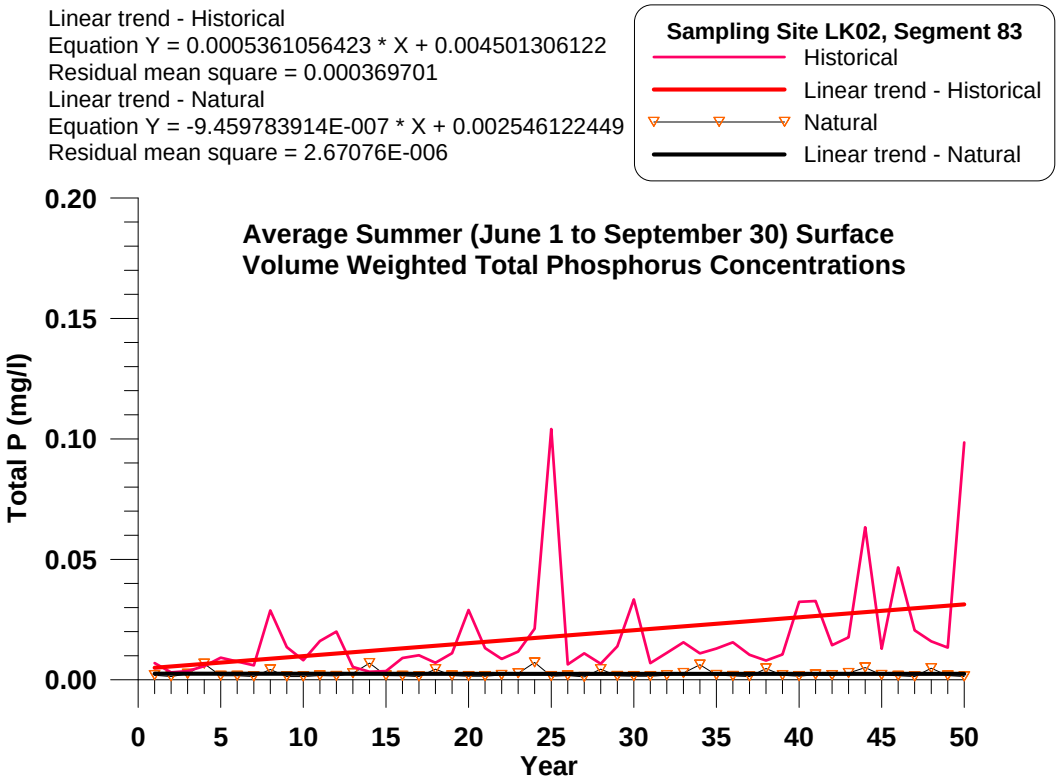

Figure 179. Volume weighted surface (5-6 m depth) average Total P at sampling site LK02, model segment 83 for historical and natural cases.

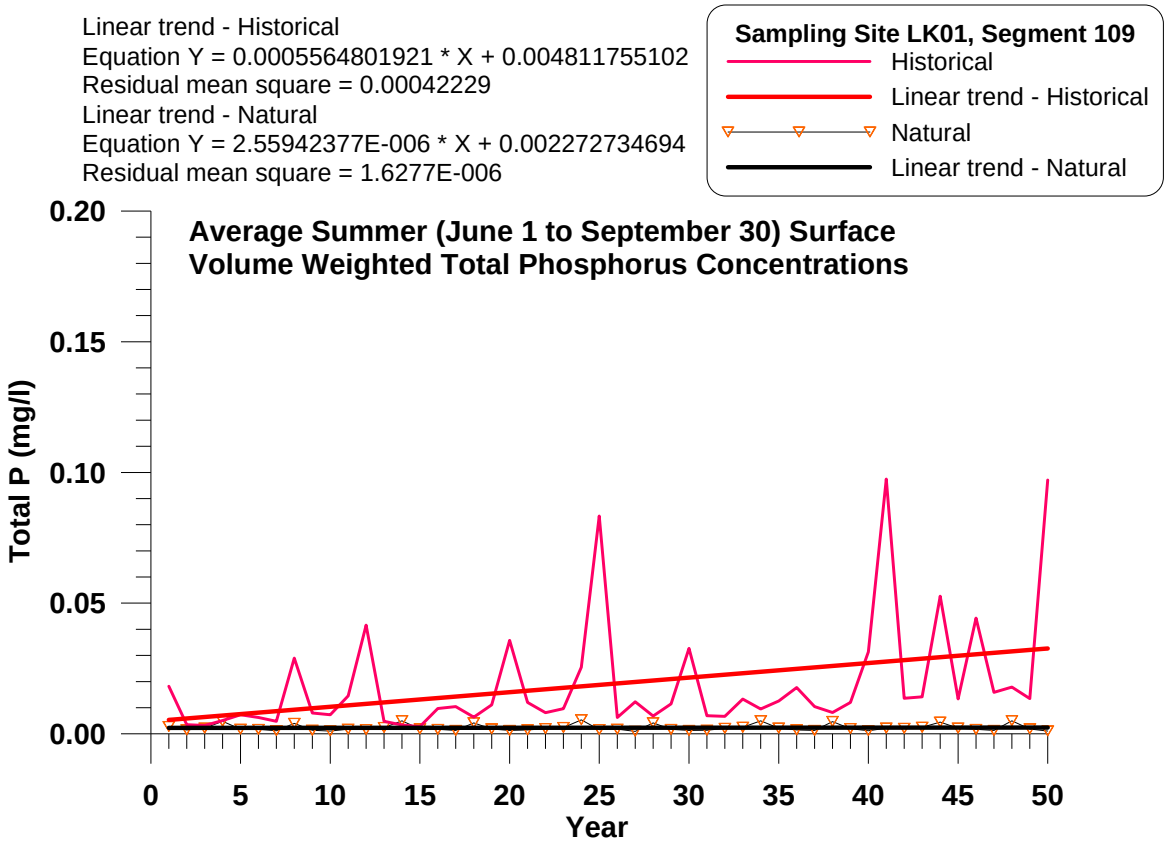

Figure 180. Volume weighted surface (5-6 m depth) average Total P at sampling site LK01, model segment 109(199) for growth, historical, and natural cases compared to base case.

Frequency Distributions of Surface Volume Weighted Concentrations

The frequency distributions of the model predictions of water quality were also compared between model scenarios. The following frequency distributions were for the period June 1 through September 30.

Figure 181, Figure 182, Figure 183, and Figure 184 show the frequency distributions for summer surface layer chlorophyll a for stations LK04 (segment 35), LK03 (segment 59), LK02 (segment 83), and LK01 (segment 109), respectively. Figure 185, Figure 186, Figure 187, and Figure 188 show the frequency distributions for summer surface layer Total P for stations LK04 (segment 35), LK03 (segment 59), LK02 (segment 83), and LK01 (segment 109), respectively.

Chlorophyll a

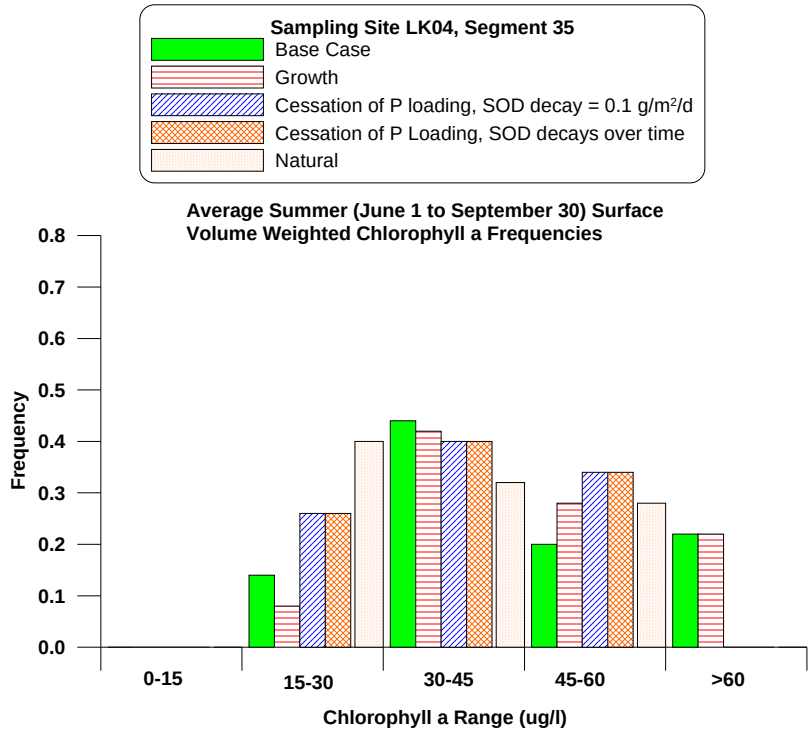

Figure 181. Frequency distribution for LK04 (segment 35) for chlorophyll a for summer surface layer over 50-year period.

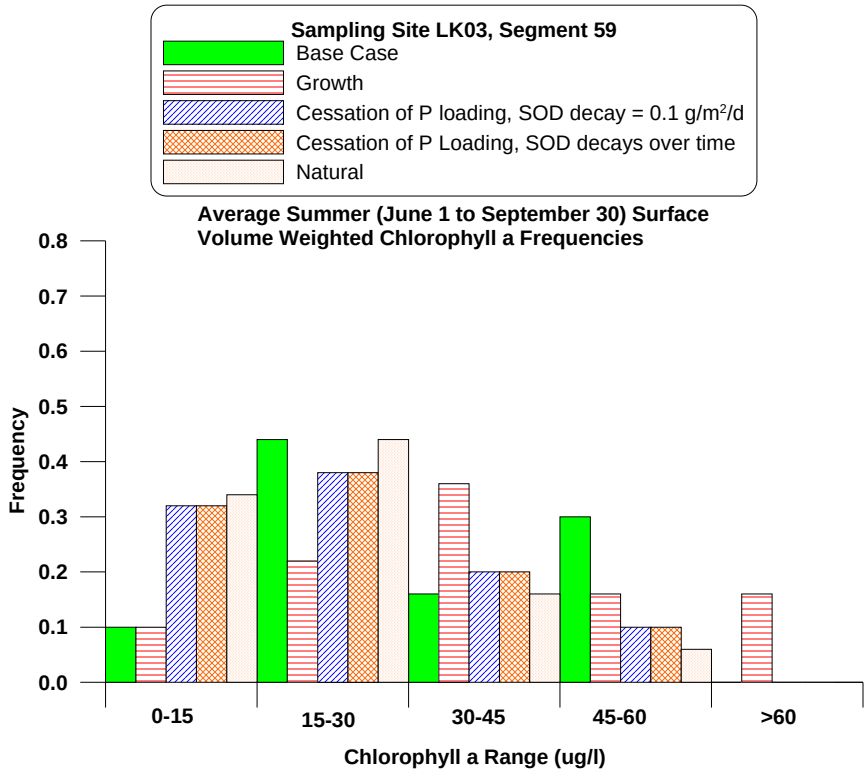

Figure 182. Frequency distribution for LK03 (segment 59) for chlorophyll a for summer surface layer over 50-year period.

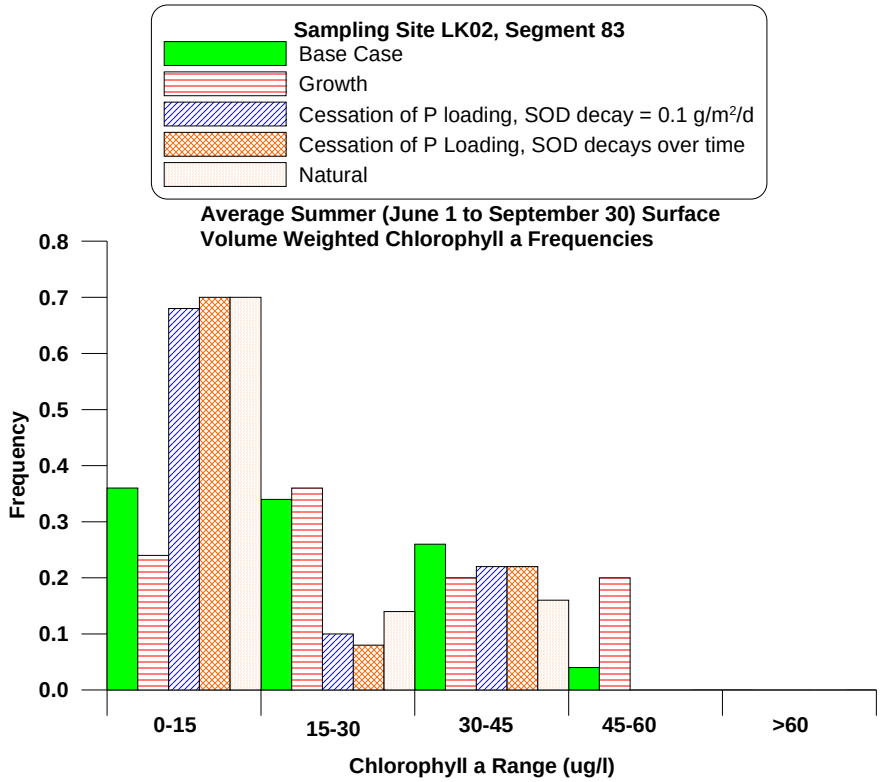

Figure 183. Frequency distribution for LK02 (segment 83) for chlorophyll a for summer surface layer over 50-year period.

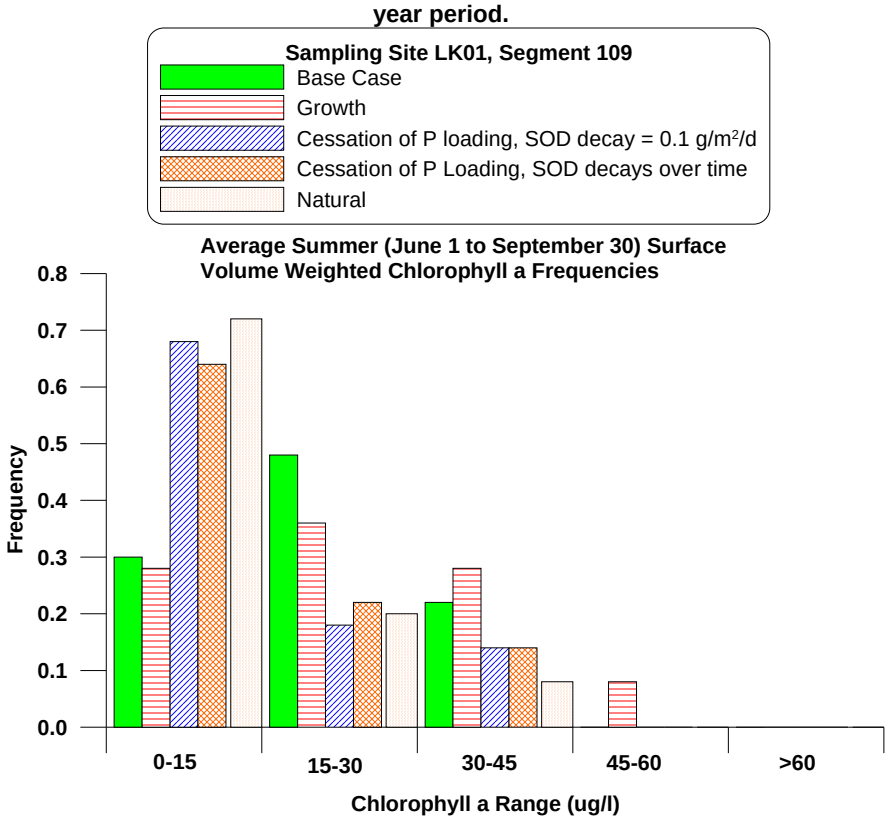

Figure 184. Frequency distribution for LK01 (segment 109) for chlorophyll a for summer surface layer over 50-year period.

Total Phosphorus

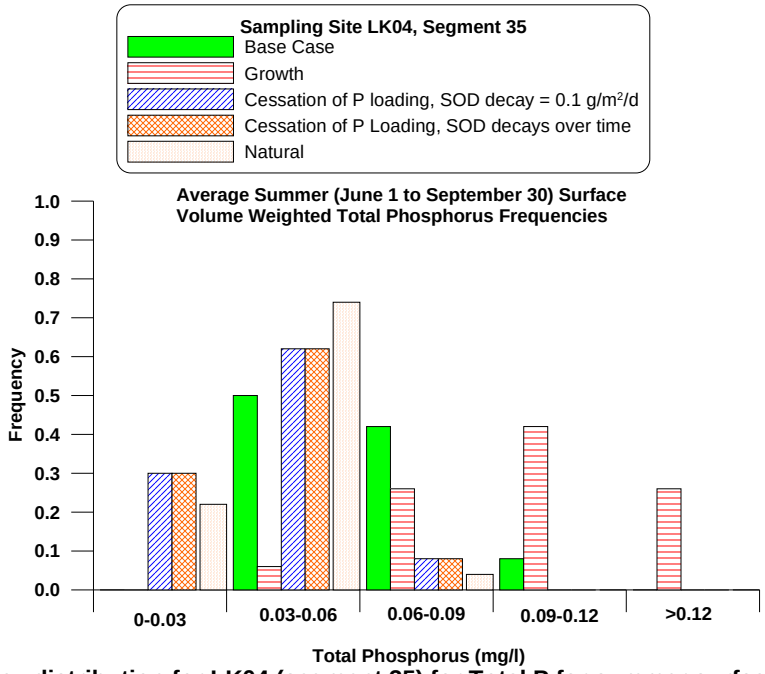

Figure 185. Frequency distribution for LK04 (segment 35) for Total P for summer surface layer over 50-year period.

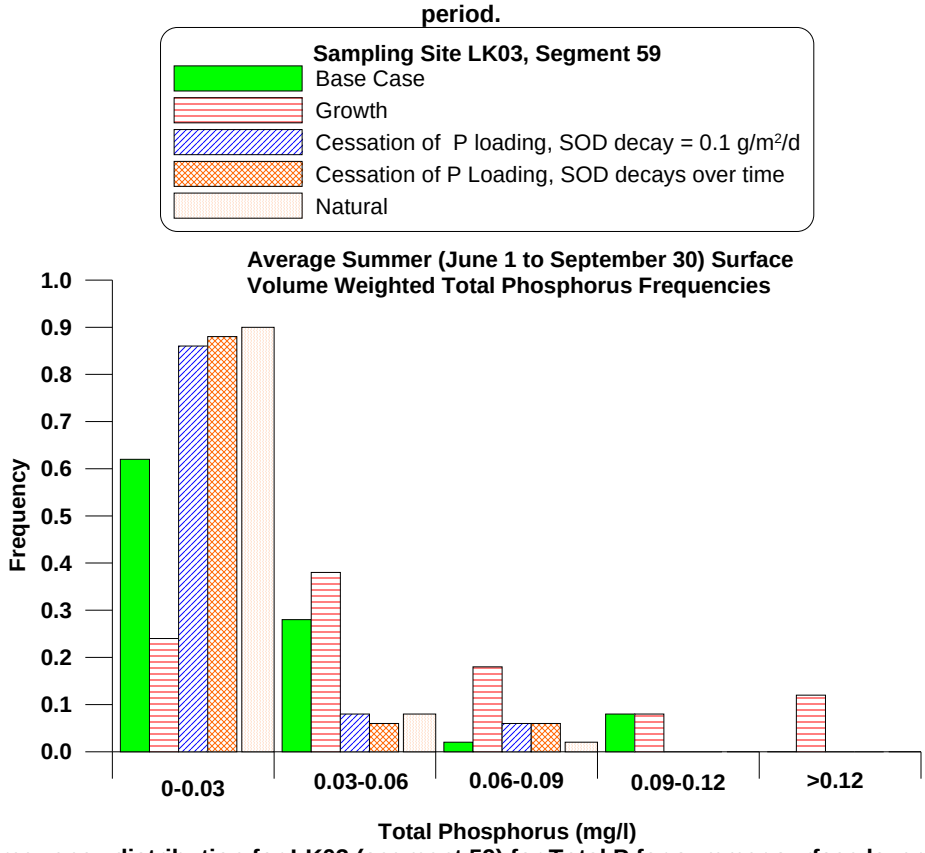

Figure 186. Frequency distribution for LK03 (segment 59) for Total P for summer surface layer over 50-year period.

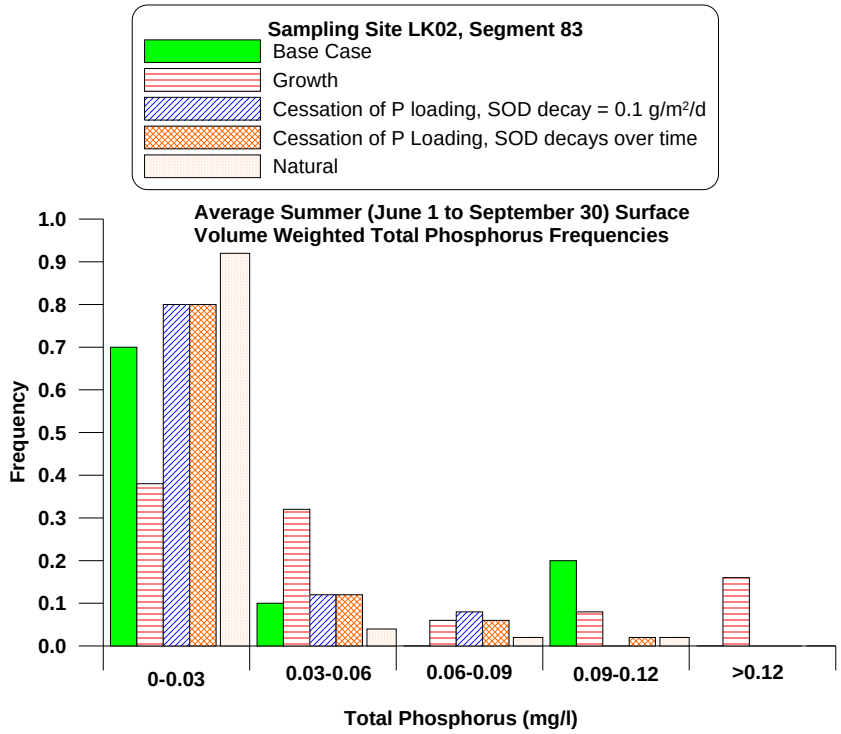

Figure 187. Frequency distribution for LK02 (segment 83) for Total P for summer surface layer over 50-year period.

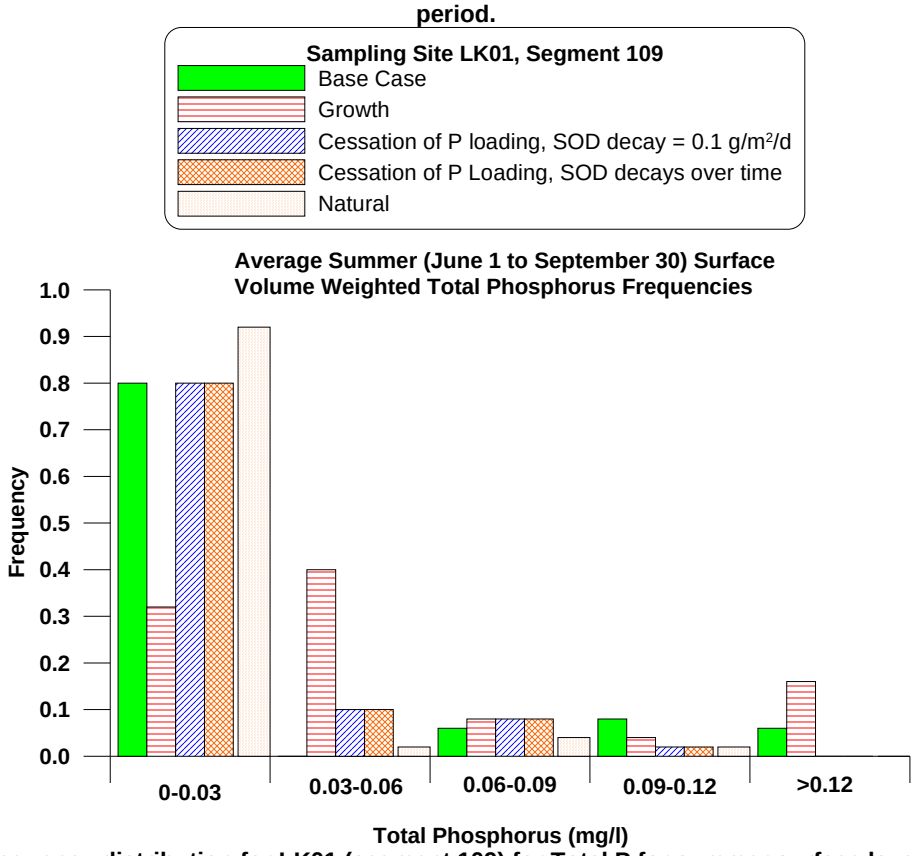

Figure 188. Frequency distribution for LK01 (segment 109) for Total P for summer surface layer over 50-year period.

Summary of Total P and chlorophyll a for summer volume weighted averages

The averages of the yearly Total P and chlorophyll a surface weighted concentrations were compared over the entire 50-year period and the last 10-year period.

Table 14, Table 15, Table 16 and Table 17 show the Total P averages and median values at the different sampling stations for the entire 50-year period and the last 10 years of that period, respectively. Table 18, Table 19 , Table 20 and Table 21 show the chlorophyll a averages and median values at the different sampling stations for the entire 50-year period and the last 10 years of that period, respectively. Note that these averages are not median values and may be influenced by high concentrations that only occur infrequently.

Table 14. Time averages of the Total P between model runs over the 50-year period.

Total P 50-year Average				
Scenario	Sampling Site LK04, segment 35	Sampling Site LK03, Segment 59	Sampling Site LK02, Segment 83	Sampling Site LK01, Segment 109
Base	0.063	0.034	0.035	0.035
Cessation of P loading SOD decay = 0.1 g/m2/d	0.038	0.019	0.019	0.020
Cessation of P Loading, SOD decays over time	0.038	0.019	0.019	0.020
Natural	0.005	0.003	0.003	0.002
Growth	0.102	0.061	0.058	0.057
Historical	0.050	0.019	0.018	0.019

Table 15. Median of the Total P between model runs over the 50-year period.

Total P 50-year Median				
Scenario	Sampling Site LK04, segment 35	Sampling Site LK03, Segment 59	Sampling Site LK02, Segment 83	Sampling Site LK01, Segment 109
Base	0.060	0.020	0.018	0.019
Cessation of P loading SOD decay = 0.1 g/m2/d	0.038	0.019	0.019	0.020
Cessation of P Loading, SOD decays over time	0.036	0.012	0.009	0.011
Natural	0.004	0.002	0.002	0.002
Growth	0.100	0.048	0.038	0.038
Historical	0.046	0.015	0.012	0.012

Table 16. Time averages of the Total P between model runs over the last 10-year period.

Total P years 41-50 Average				
Scenario	Sampling Site LK04, segment 35	Sampling Site LK03, Segment 59	Sampling Site LK02, Segment 83	Sampling Site LK01, Segment 109
Base	0.060	0.036	0.034	0.033
Cessation of P loading SOD decay = 0.1 g/m2/d	0.028	0.016	0.013	0.013
Cessation of P Loading, SOD decays over time	0.028	0.016	0.014	0.014
Natural	0.004	0.003	0.003	0.002
Growth	0.127	0.085	0.076	0.074
Historical	0.087	0.033	0.034	0.038

Table 17. Median of the Total P between model runs over the last 10-year period.

Total P years 41-50 Median				
Scenario	Sampling Site LK04, segment 35	Sampling Site LK03, Segment 59	Sampling Site LK02, Segment 83	Sampling Site LK01, Segment 109
Base	0.057	0.020	0.019	0.020
Cessation of P loading SOD decay = 0.1 g/m2/d	0.028	0.016	0.013	0.013
Cessation of P Loading, SOD decays over time	0.025	0.010	0.009	0.010
Natural	0.004	0.002	0.002	0.002
Growth	0.122	0.065	0.056	0.053
Historical	0.084	0.028	0.019	0.017

Table 18. Time averages of the chlorophyll a between model runs over the 50-year period.

Chlorophyll a 50-year Average				
Scenario	Sampling Site LK04, segment 35	Sampling Site LK03, Segment 59	Sampling Site LK02, Segment 83	Sampling Site LK01, Segment 109
Base	45.0	34.6	22.3	20.2
Cessation of P loading SOD decay = 0.1 g/m2/d	36.8	24.7	16.7	14.6
Cessation of P Loading, SOD decays over time	36.8	24.9	17.0	14.8
Natural	6.6	3.7	2.7	2.4
Growth	47.5	39.4	27.5	25.5
Historical	12.5	23.0	15.7	14.2

Table 19. Median of the chlorophyll a between model runs over the 50-year period.

Chlorophyll a 50-year Median				
Scenario	Sampling Site LK04, segment 35	Sampling Site LK03, Segment 59	Sampling Site LK02, Segment 83	Sampling Site LK01, Segment 109
Base	41.0	28.4	18.4	20.3
Cessation of P loading SOD decay = 0.1 g/m2/d	36.8	24.7	16.7	14.6
Cessation of P Loading, SOD decays over time	33.8	19.9	11.3	11.8
Natural	6.7	2.6	1.5	1.5
Growth	44.7	37.8	23.5	26.1
Historical	8.8	21.1	13.8	11.2

Table 20. Time averages of the chlorophyll a between model runs over the last 10-year period.

Chlorophyll a years 41-50 Average				
Scenario	Sampling Site LK04, segment 35	Sampling Site LK03, Segment 59	Sampling Site LK02, Segment 83	Sampling Site LK01, Segment 109
Base	49.1	35.3	23.8	21.8
Cessation of P loading SOD decay = 0.1 g/m2/d	34.7	21.7	15.4	13.8
Cessation of P Loading, SOD decays over time	34.9	21.9	16.2	14.2
Natural	6.8	3.9	2.9	2.6
Growth	53.5	41.8	32.0	30.6
Historical	5.5	35.3	21.5	18.0

Table 21. Median of the chlorophyll a between model runs over the last 10-year period.

Chlorophyll a years 41-50 Median				
Scenario	Sampling Site LK04, segment 35	Sampling Site LK03, Segment 59	Sampling Site LK02, Segment 83	Sampling Site LK01, Segment 109
Base	44.5	28.1	20.3	22.2
Cessation of P loading SOD decay = 0.1 g/m2/d	34.7	21.7	15.4	13.8
Cessation of P Loading, SOD decays over time	32.1	15.0	10.1	11.3
Natural	7.0	2.6	1.6	1.7
Growth	50.3	40.7	33.7	35.3
Historical	3.6	32.2	20.8	17.8

Dissolved oxygen concentration in release from Tenkiller Reservoir

The model predicts the dissolved oxygen concentration from the spillways and powerhouse released to the Illinois River below Tenkiller dam. This dissolved oxygen concentration in the dam release is an indication of hypolimnetic dissolved oxygen levels since most of the water is taken from the deep-level, powerhouse outlet. Occasionally, during the summer after a storm event well-oxygenated epilimnetic water is spilled from the surface gates. Hence, actual hypolimnetic dissolved oxygen levels would be lower than that shown in this analysis for those summers when spill occurred. Between May 1 and October 30 of each of the 50 years, Figure 189 shows the average (flow weighted) dissolved oxygen concentration for each summer for the base case and the cessation case. The trend in the cessation case is an improvement in hypolimnetic dissolved oxygen of almost 0.2 mg/l/year, while the base case continues to have lower dissolved oxygen in the release by about 0.006 mg/l less per year. Figure 190 shows the gradual decline in outlet dissolved oxygen for the historical scenario over the 50-year period with dissolved oxygen decreasing by about 0.08 mg/l per year. The growth scenario simulation for outlet dissolved oxygen is shown in Figure 191. The linear trend for the outlet dissolved oxygen was a reduction of about 0.002 mg/l per year for the growth scenario. In the trend lines included on the figures, Y is the dissolved oxygen in mg/l from the outlet to Tenkiller and X is the year.

Table 22 summarizes the change in average outlet dissolved oxygen over the 50-year period and during the last 10 years of that period.

Table 22. Average of May-October outlet dissolved oxygen concentrations.

Simulation	Average summer flow weighted DO between May 1 and October 31 *over entire 50 yr period*	Average summer flow weighted DO between May 1 and October 31 – *over last 10 years*
Base case – P loading as is	1.6 mg/l	1.5 mg/l
Cessation, SOD gradual decline to 0.1 $g/m^2/d$	2.9 mg/l	3.3 mg/l
Natural conditions	6.6 mg/l	6.3 mg/l
Growth	1.6 mg/l	1.5 mg/l
Historical	4.2 mg/l	3.1 mg/l

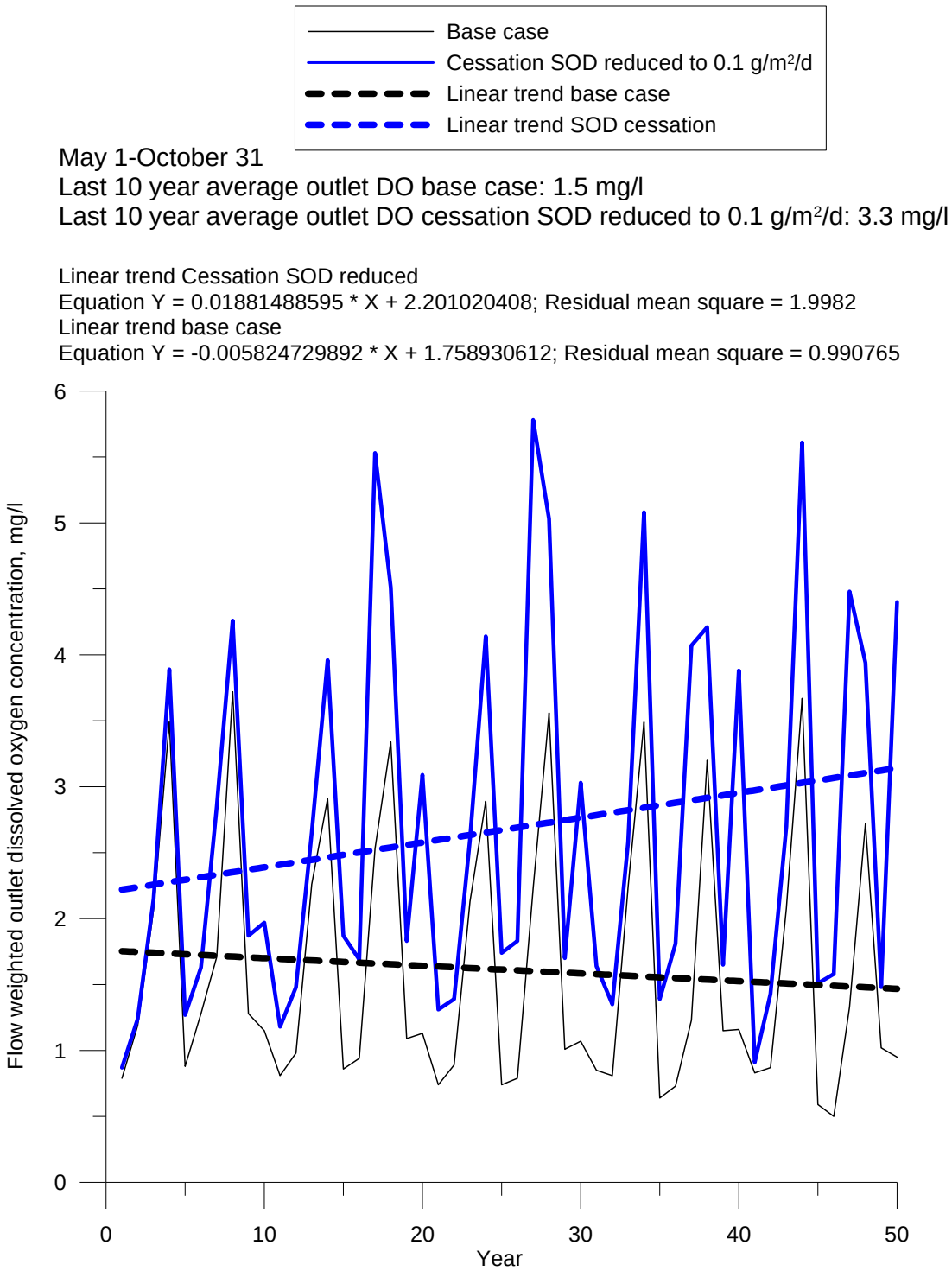

Figure 189. Average dissolved oxygen between May 1 and October 31 of each year for the base case and the cessation with SOD declining to 0.1 g/m^2/d. Running average is over 11 years.

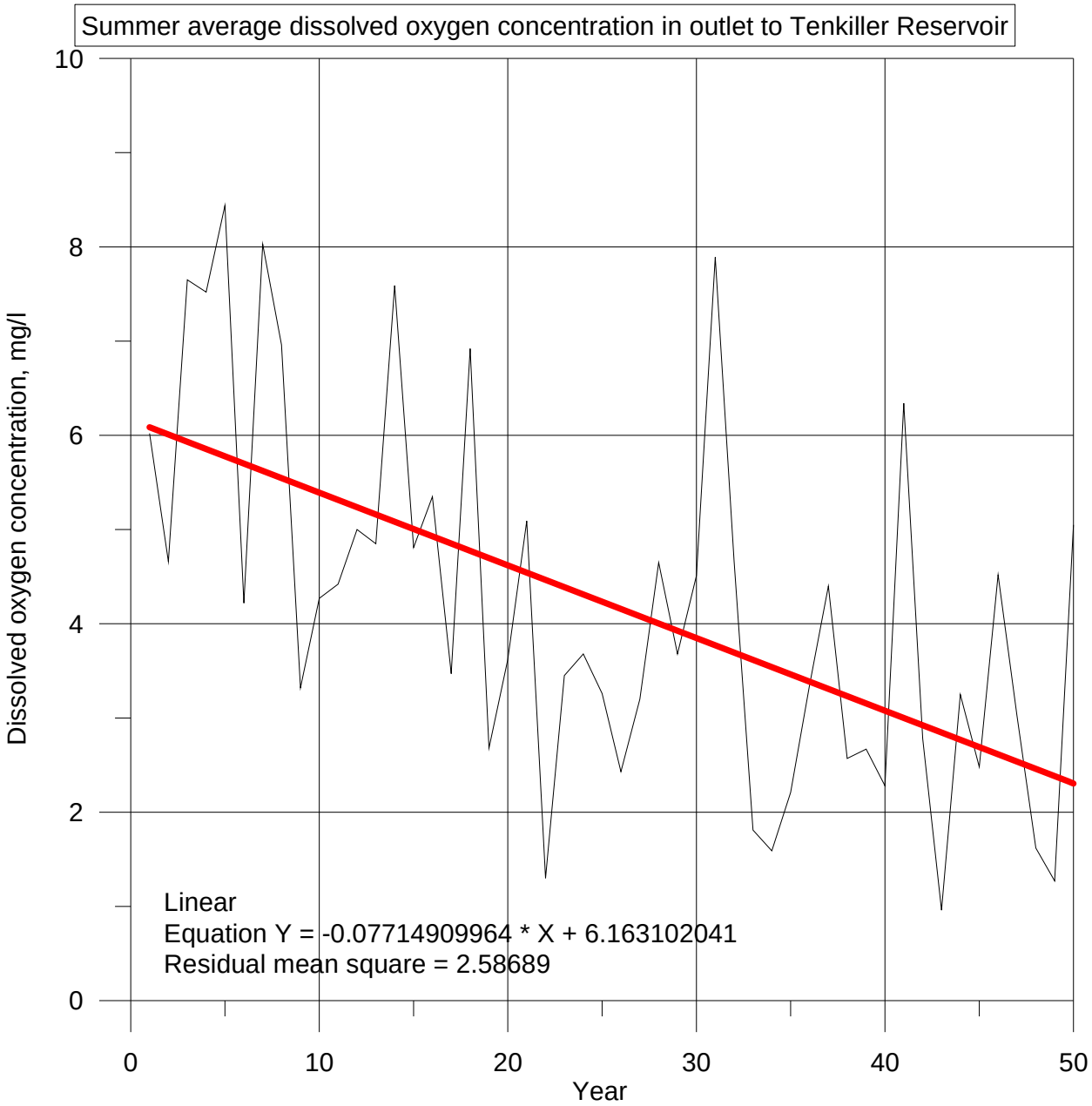

Figure 190. Historical scenario for summer outlet dissolved oxygen concentration each year for 50 years.

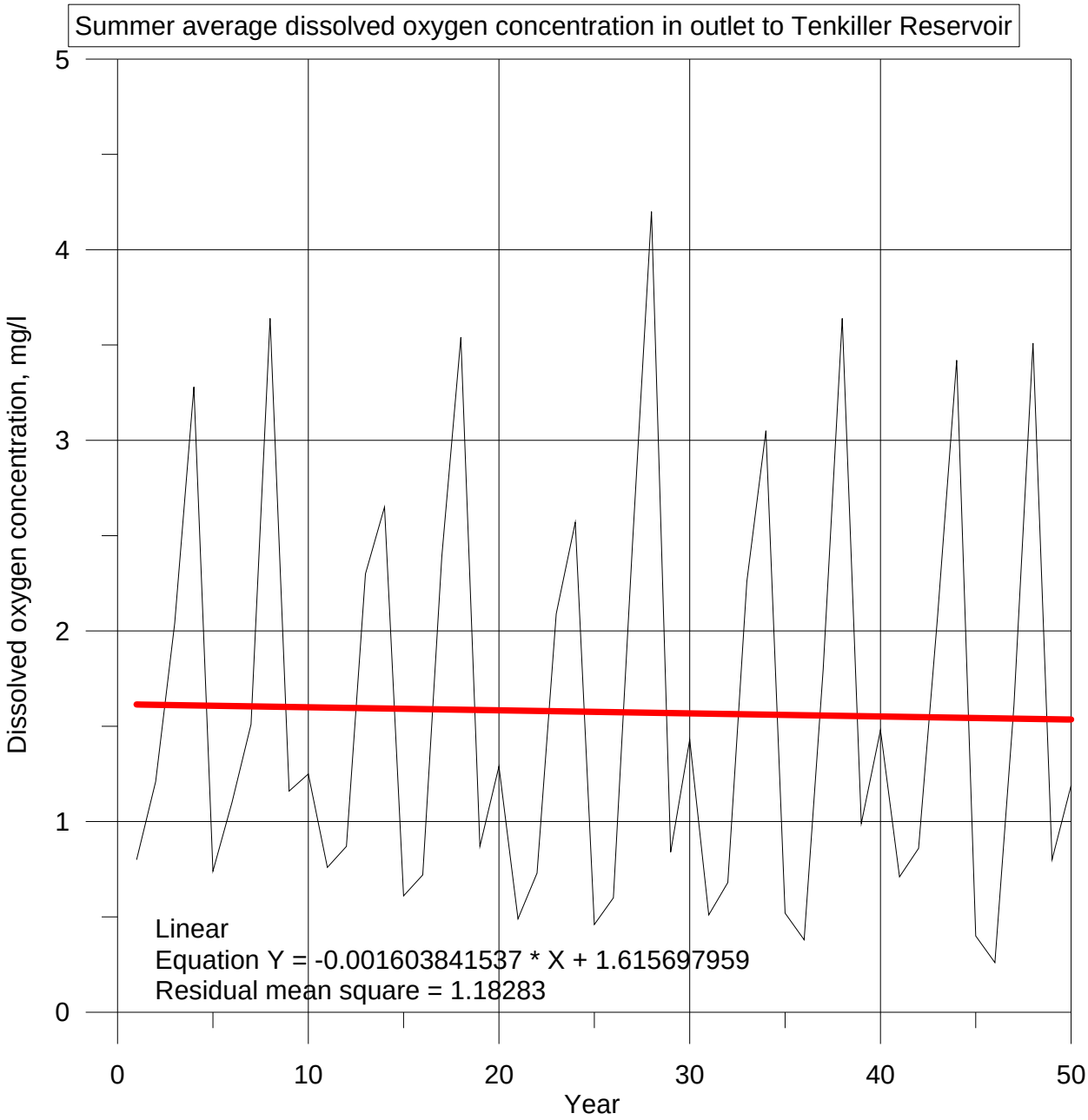

Figure 191. Growth scenario for summer outlet dissolved oxygen concentration each year for 50 years.

Dissolved Oxygen Dynamics

Dissolved oxygen demand from sediments

The model computed oxygen demand from all model segments were compared between model scenarios. The oxygen demand from sediments represents all the oxygen consumed by bacterial oxidation of organics at the sediment-water interface. In the CE-QUAL-W2 model this was represented as a background historical sediment oxygen demand (zero order model) and the demand from newly deposited organics (first order model). There were little differences between the 2 cessation runs where the zero order demand was reduced, except in the first few years. Figure 192 is a comparison between the base case P as is and the cessation scenario with SOD reduced to 0.1 g/m^2/day. Linear trend lines for the base case and the cessation scenarios are shown as straight lines in Figure 192. For the base case, the deposition of more organics from increased algae production increases overall sediment oxygen demand over the 50-year period. The reduction in Total P in the cessation scenario results in reduced algae growth and hence less deposition of organics to the sediments and consequent reduction in dissolved oxygen demand. In general, the reduction in oxygen demand in the lacustrine part of the reservoir is about 4E7 g/day over the last 10 years of the simulation.

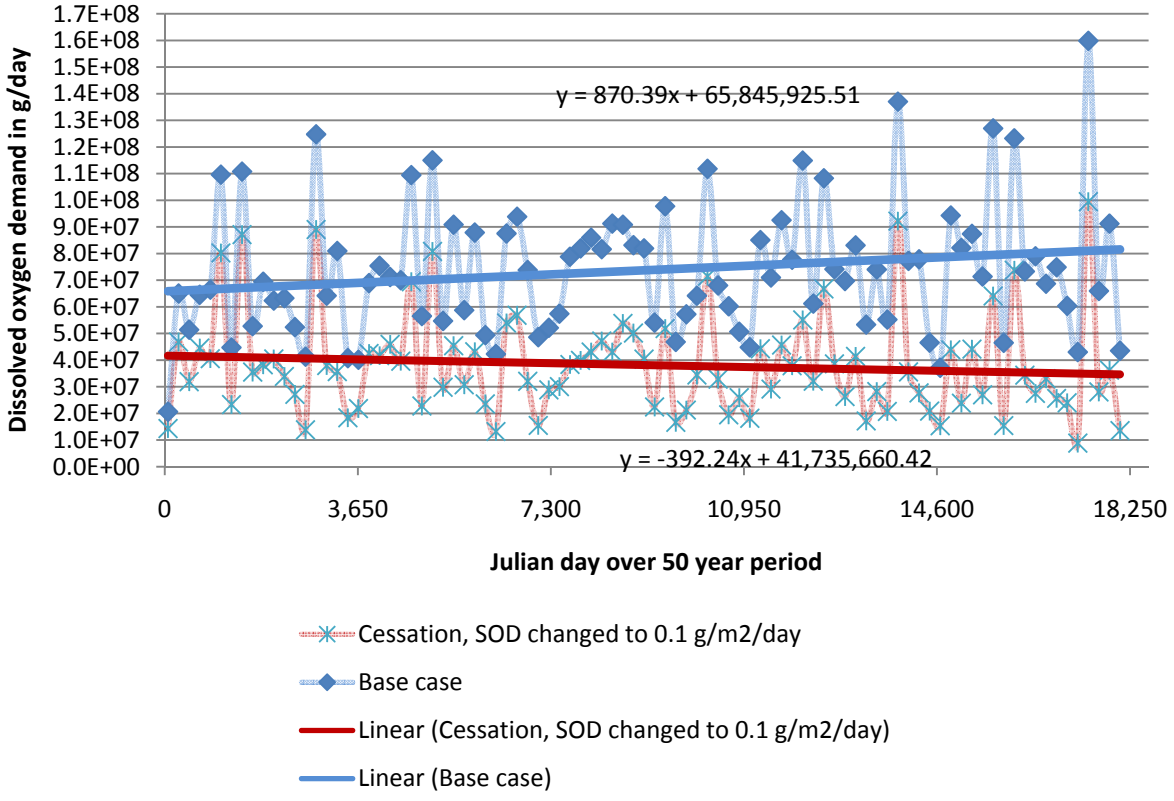

Figure 192. Difference between dissolved oxygen demand from zero order and first order sediment demand between base and cessation with SOD set to 0.1 g/m^2/d scenarios including linear trend lines over the 50-year period.

Dissolved oxygen water column demand from organic matter decomposition

The model computes the dissolved oxygen consumption in the water column as a result of particulate organic matter (both labile and refractory) and dissolved organic matter (both labile and refractory). This represents the amount of oxygen consumed by bacterial oxidation of organics in the water column. It does not account for algal respiration. Comparisons were made between the base 50-year simulation where the P loading was 'as is' and the different cessation cases. For a couple years the cessation run had more water column dissolved oxygen demand than the base case. This occurs as anoxia occurs later in the year and there is more opportunity to decay organics in an aerobic environment. Figure 193 shows a comparison of the base case and the cessation run with SOD set to 0.1 g/m^2/day. Linear trend lines for the base case and the cessation scenarios are shown as straight lines in Figure 193. Since the Total P load is used to compute organic matter, the cessation scenario results in a reduction in organic matter loading to Tenkiller and hence a reduction in water column oxygen demand. This comparison shows that over time the water column dissolved oxygen demand is reduced by about 3E7 g/day during the last 10-year period by enforcing the cessation scenario.

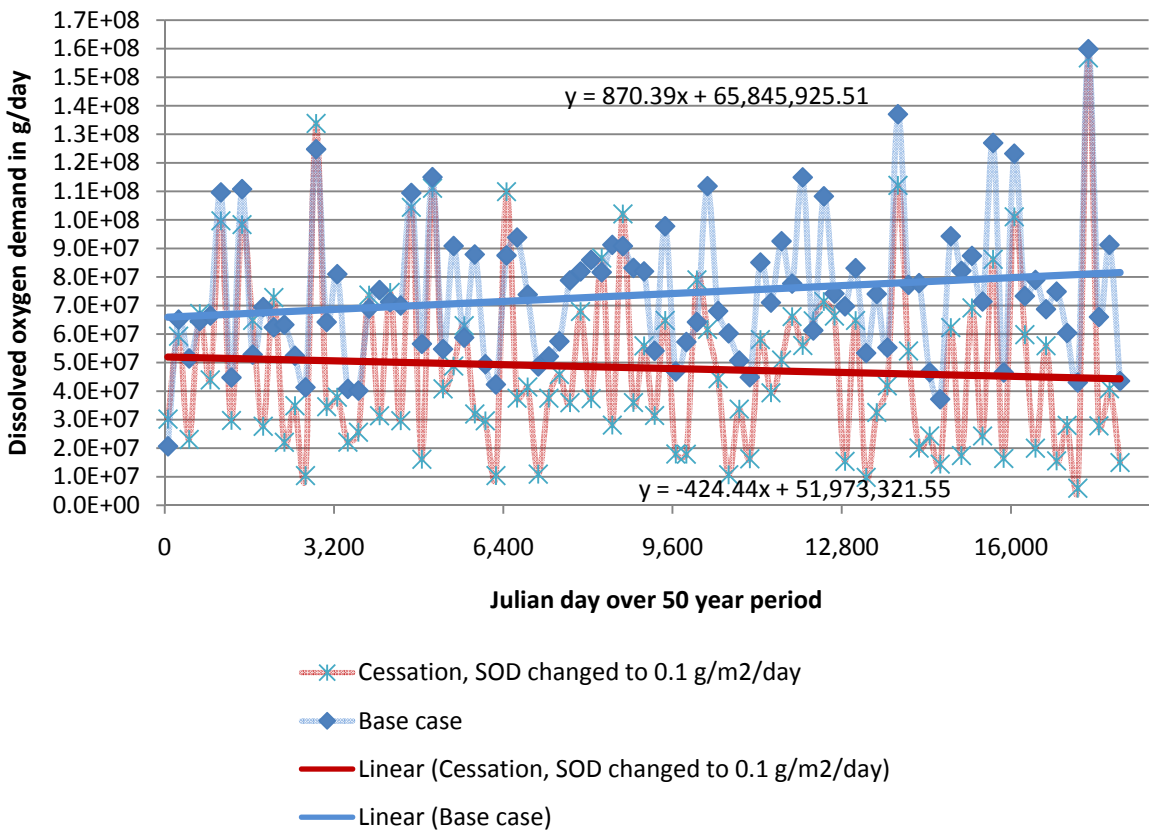

Figure 193. Dissolved oxygen demand from particulate and dissolved organic matter in the water column between base and cessation with SOD set to 0.1 g/m^2/d scenarios including linear trend lines over the 50-year period.

Dissolved oxygen net photosynthetic production

The model computes the overall photosynthetic production of dissolved oxygen for the entire reservoir as the sum of algae oxygen production minus the sum of algae oxygen respiration plus the sum of periphyton oxygen production minus the sum of periphyton oxygen respiration. Net photosynthetic production is usually a net source of oxygen to the photic zone of the reservoir. Increased photosynthetic production of oxygen is a result of increased algal growth. Figure 194 shows a comparison between the base case and the cessation case with SOD set to 0.1 g/m^2/d. Linear trend lines for the base case and the cessation scenarios are shown as straight lines in Figure 194. The base case shows a slight increase in net photosynthetic production while the cessation scenario shows a decrease. This indicates less algae growth for the cessation case as the Total P load to the reservoir is reduced. At the end of the 50-year period the rate of net oxygen production from algae declines by almost 2E8 g/day as P load from the watershed is reduced.

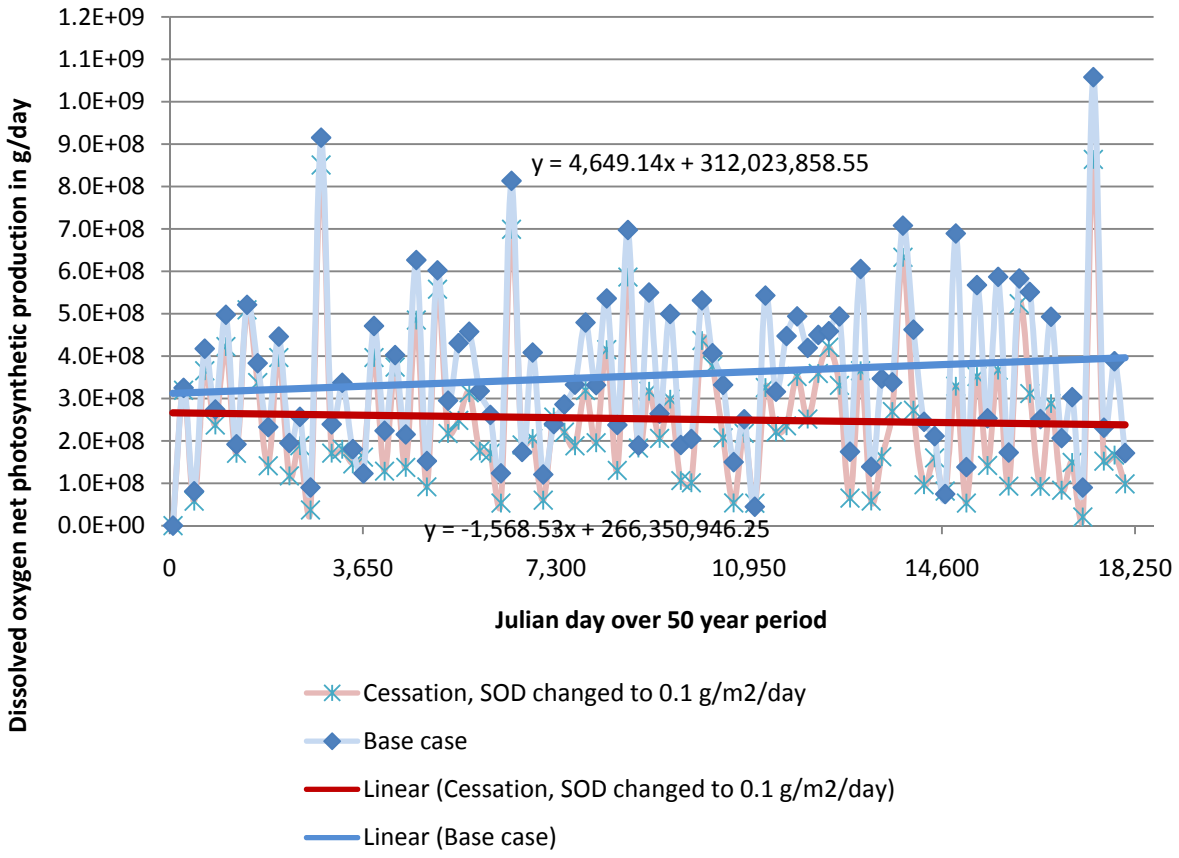

Figure 194. Dissolved oxygen net photosynthetic production from algae and periphyton between base and cessation scenarios with SOD set to 0.1 g/m^2/d including linear trend lines over the 50-year period.

Fish Habitat

The habitat preferences of fish were summarized by Cooke and Welch (2008) in Table 23. For the CE-QUAL-W2 model, the dissolved oxygen and temperature criteria used to compute habitat volume and % habitat volume are shown in Table 24.

Table 23. Fish habitat temperature and dissolved oxygen preferences (Cooke and Welch, 2008).

	Dissolved Oxygen (DO, mg/L)			Temperature (T, ^{o}C)			
Species	**Optimal DO**	**Mean of optimal DO**	**Highest EC, DO**	**Optimal T**	**Mean of optimal T**	**Lowest EC, high T**	**Lowest Lethal T**
rainbow trout	7.0 - 9.0	8.0	5.0	12-18	15	18	25
striped bass[2]	6.0	6.0	5.0	20-21	20.5	24	28
walleye	>5.0	7.0	<5.0	20-24	22	>24	29
white bass	>5.0	7.0	3.0	19-28	23.5	>28	27
smallmouth bass	6.0	6.0	4.0	21-27	24	29	32.3
spotted bass	6.0	6.0	<6.0	23.5-24.4	24	>24.4	34
gizzard shad	6.0	6.0	6.0	22-29	25.5	26.7	36.5
largemouth bass	8.0	8.0	5.0	24-30	27	30	35.0
channel catfish	7.0	7.0	5.0	26-29	27.5	21	33.5

EC - Effect Concentration (lowest of values of T> optimal and highest of values of DO <optimal)

Table 24. Fish habitat temperature and dissolved oxygen preferences used in the CE-QUAL-W2 model.

Species	DO criteria, mg/l	Temperature criteria, ^{o}C
Small mouth bass optimal	6.0	27
Small mouth bass suboptimal	5.0	29
Walleye suboptimal	5.0	24

The terms optimal and suboptimal are related to growth conditions for the fish. Optimal conditions are based on what fish prefer for growth and activity. Fish can still survive below suboptimal conditions, but sensitive fish may be under stress during these periods (Cooke and Welch, 2008).

The model evaluated whether the dissolved oxygen and temperature were acceptable for fish habitat based on 3 different fish criteria as shown in Table 24. Every model computational cell (model cells in the mainstem reservoir were typically 500 m in length by 1 m deep and of variable width) was evaluated every 3 hours to see if the volume in the model cell met the temperature and dissolved oxygen criteria. If the temperature and dissolved oxygen criteria were met, then the volume of that cell was deemed acceptable habitat volume. Then acceptable volumes were then summed up for all the model cells for the entire reservoir. Typical habitat volume and fraction of habitat volume for several years and for one

summer season for small mouth bass suboptimal conditions are shown in Figure 195 and Figure 196, respectively. Typical habitat volume and fraction of habitat volume for several years and for one summer season for walleye are shown in Figure 197 and Figure 198, respectively. These habitat volumes and fractions of total reservoir volume are based on having acceptable dissolved oxygen equal to or greater than the DO criteria and temperature equal to or less than the temperature criteria shown in Table 24. As shown during the yearly period, habitat becomes reduced considerably around mid-June through mid-September. This occurs as the heating occurs in the epilimnion (even though oxygen levels may be acceptable) and as dissolved oxygen depletion occurs in the hypolimnion (even though temperature levels may be acceptable). If the water level were at 192 m and the depth of the thermocline was 10 m below the surface, 53% of the reservoir volume is in the epilimnion where temperatures are high and only 47% of the volume is below the thermocline. Hence even though dissolved oxygen conditions may improve in the hypolimnion as a result of reducing deposition of oxygen demanding material, temperature is also a factor influencing fish habitat volume and can act as an upper limit to how much habitat volume can be affected by changes in watershed loading of Total P.

Table 25 shows the average and standard deviations of the habitat volumes and fractions averaged over the entire 50-year period and the last 10-year period of the 50-year sequence for the summer (June 15–September 15).

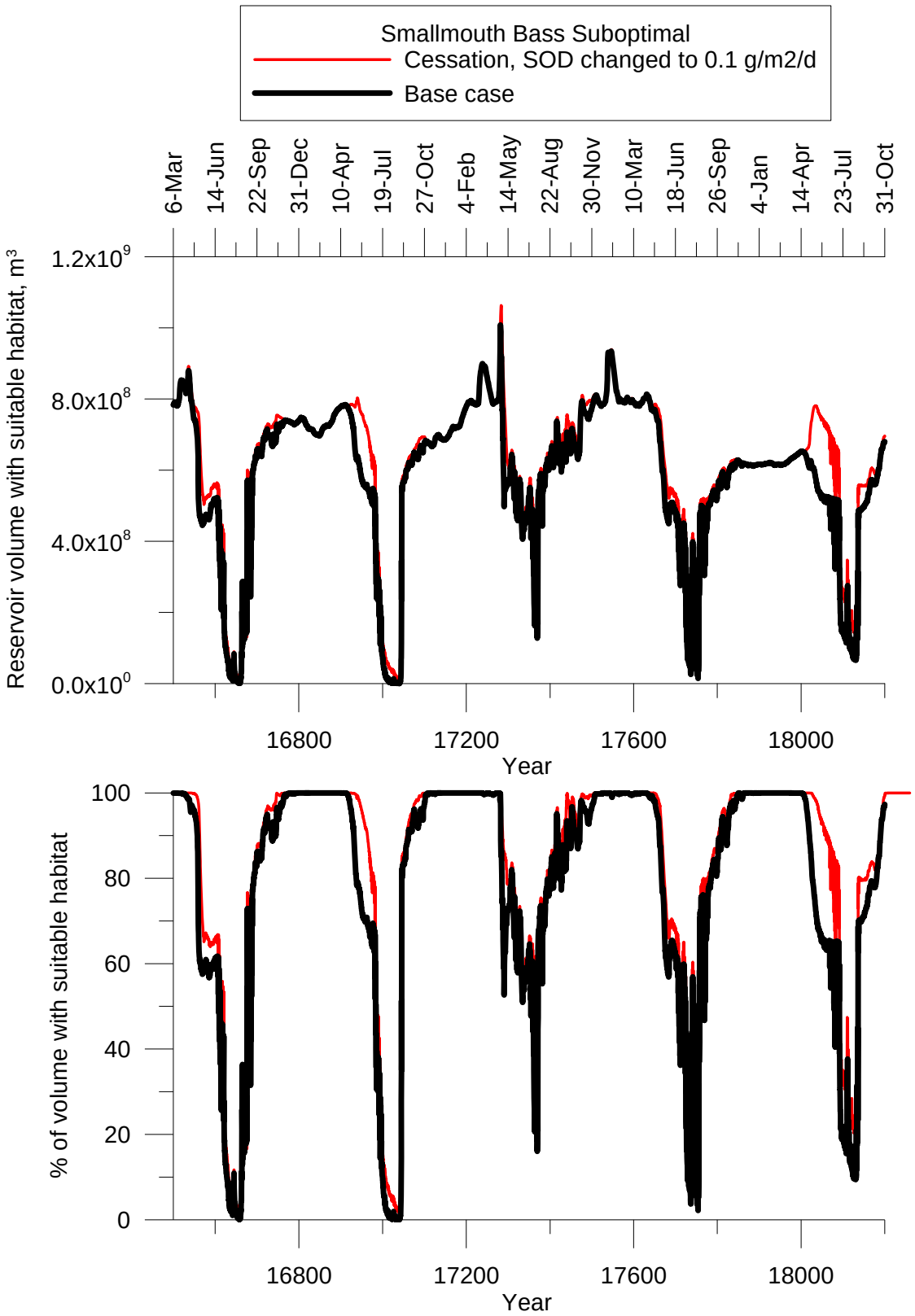

Figure 195. Smallmouth bass suboptimal habitat volume and fraction of volume over the last 5 years of the 50-year period.

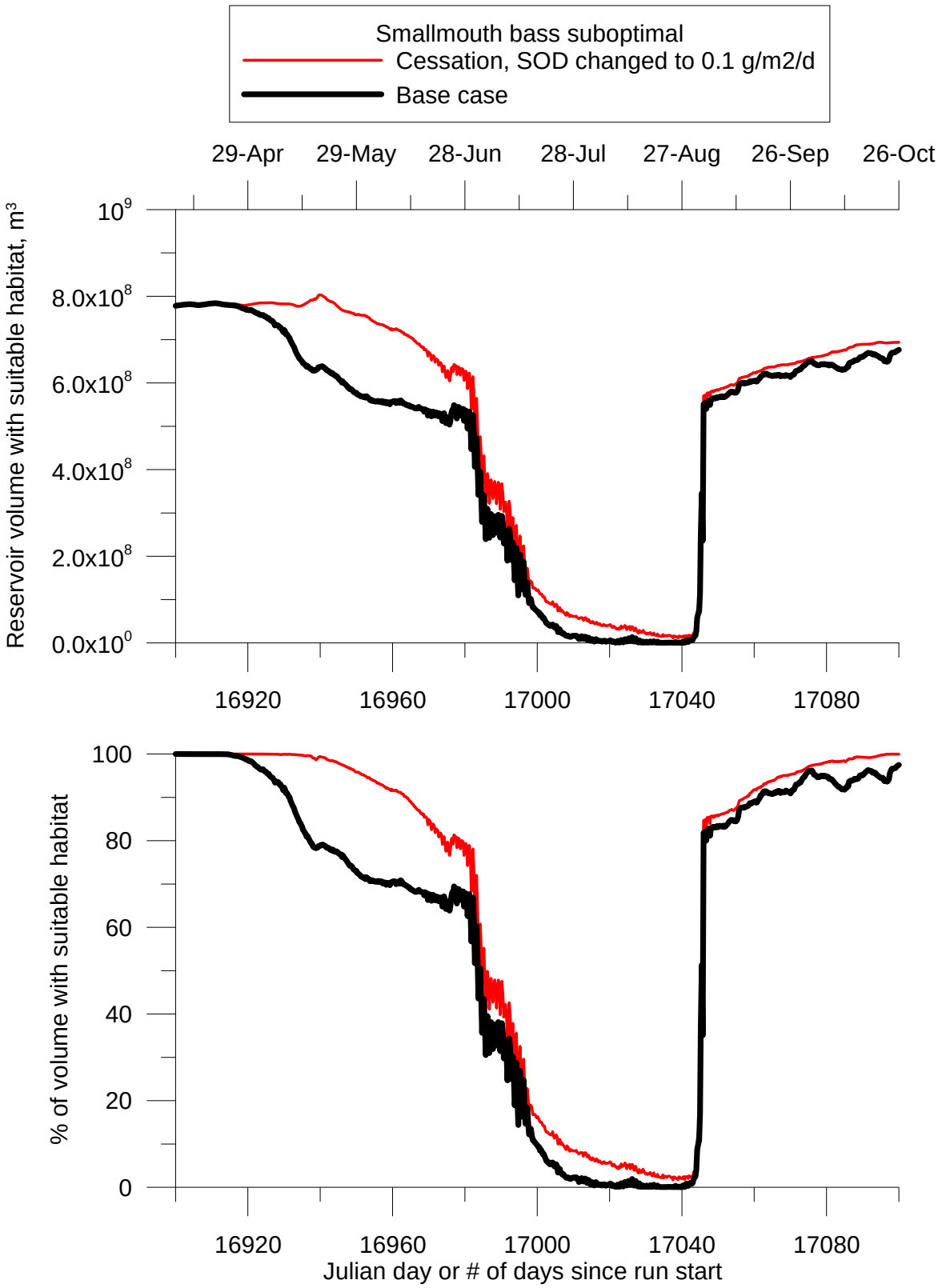

Figure 196. Smallmouth bass suboptimal habitat volume and fraction of volume over one of the last years of the 50-year period.

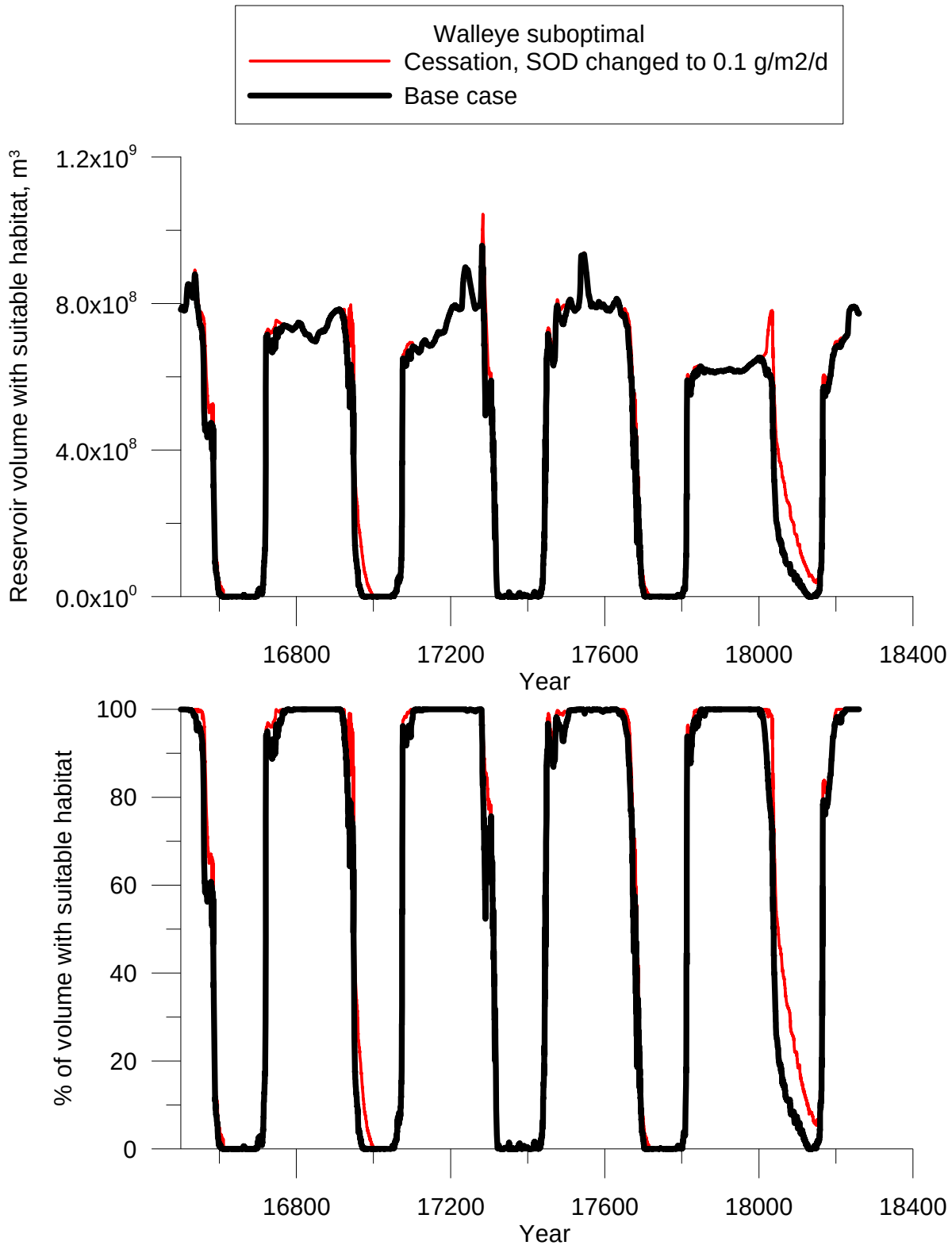

Figure 197. Walleye suboptimal habitat volume and fraction of volume over the last 5 years of the 50-year period.

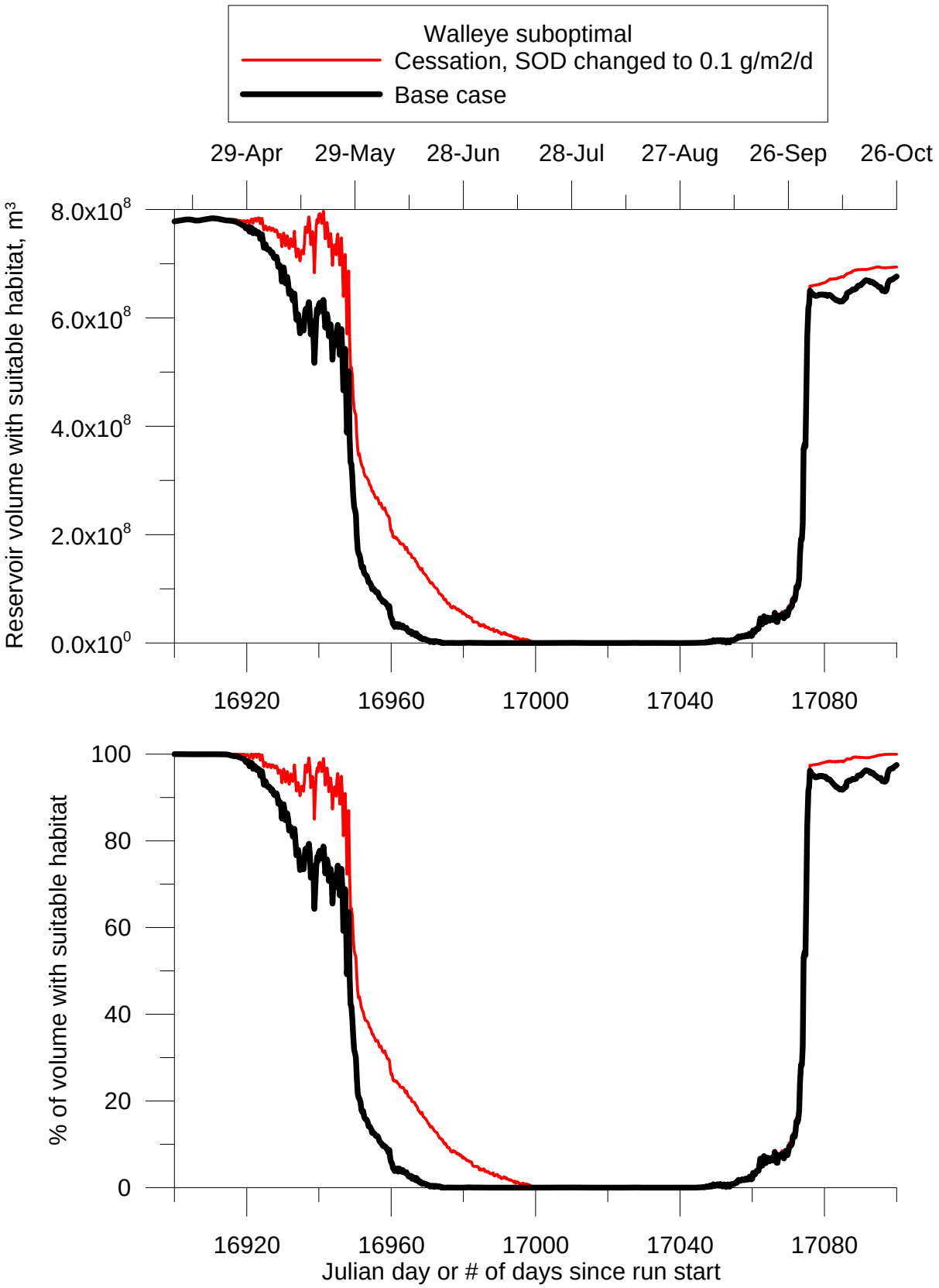

Figure 198. Walleye habitat volume and fraction of volume over one of the last years in the 50-year period.

Table 25. Habitat volume for small mouth bass and walleye for summer (June 15 through September 15) over the 50-year simulation.

Model run	% Total habitat volume - Small mouth bass optimal	Habitat volume (m^3)-Small mouth bass optimal	% Total habitat volume Small mouth bass suboptimal	Habitat volume (m^3)-Small mouth bass suboptimal	% Total habitat volume Walleye suboptimal	Habitat volume (m^3)-Walleye suboptimal
Base case - P loading as is – Mean 50 years	8.5	0.665E+08	33.5	0.255E+09	1.5	0.118E+08
Base case - P loading as is – Standard deviation 50 years	5.2	0.395E+08	13.3	0.101E+09	2.8	0.206E+08
Cessation, SOD changed to 0.1 g/m2/d – Mean 50 years	10.9	0.854E+08	37.7	0.287E+09	3.5	0.269E+08
Cessation, SOD changed to 0.1 g/m2/d – Standard deviation 50 years	6.8	0.509E+08	14.7	0.110E+09	5.2	0.387E+08
Natural Mean 50 years	24.1	0.187E+09	57.0	0.435E+09	14.3	0.108E+09
Natural Standard deviation 50 years	8.2	0.605E+08	13.6	0.103E+09	8.8	0.627E+08
Growth – Mean 50 years	8.2	0.637E+08	32.5	0.247E+09	1.5	0.111E+08
Growth – Standard deviation 50 years	5.0	0.383E+08	13.0	0.989E+08	2.7	0.202E+08
Historical - Mean 50 years	9.5	0.641E+08	37.1	0.247E+09	1.8	0.119E+08
Historical – standard deviation 50 years	6.0	0.393E+08	14.4	0.943E+08	3.2	0.221E+08

Total P loading, export, and sediment recycling

Inflows

Figure 199 shows the total phosphorus loading over the 50-year model period for two inflow scenarios, the base case and the cessation of land application of poultry waste. These represent the inflow Total P loading to the Tenkiller model from the model of Engle (2008) that were used to develop the boundary conditions for the CE-QUAL-W2 model.

Table 26 shows the summary of phosphorus inflow for each of the three main tributaries as well as for the distributed flows (in this case only positive inflows) which are ungaged runoff flows for the basin.

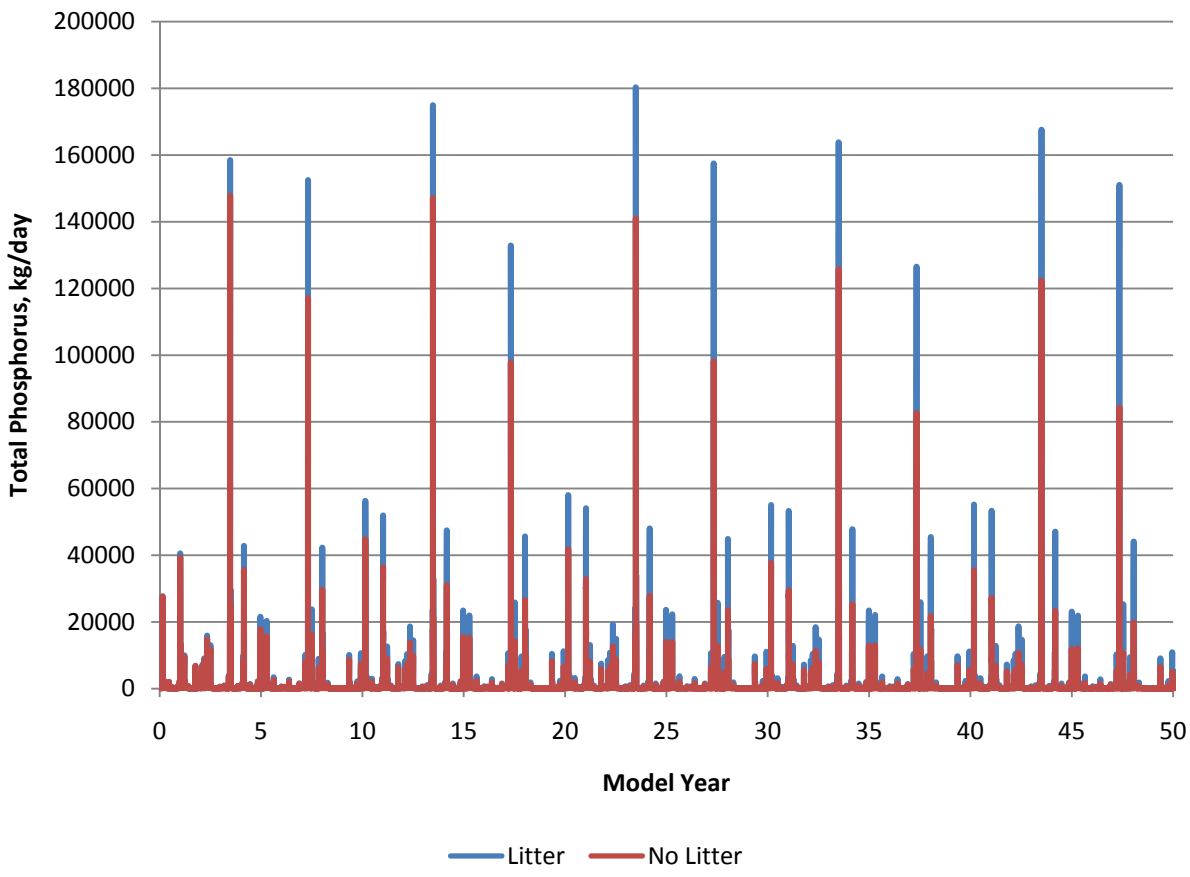

Figure 199: Total phosphorus inflow, two scenarios.

Table 26: Detailed summary of phosphorus inflows.

	Summary of Totals, kg/day		
	Base Case	Cessation	Percent Reduction:
Illinois River	543	320	41%
Baron Fork Creek	146	110	24%
Caney Creek	30	28	6%
Distributed Inflows	56	52	6%
Average	**775**	**510**	**34%**

The trends in the Total P inflow loading to Tenkiller reservoir for the cessation, growth and historical scenarios are shown in Figure 200, Figure 201, and Figure 202, respectively. Linear trend lines are shown in each of these figures for the Total P inflow load versus year. For the cessation case shown in Figure 200, the Total P loading decreases over time, whereas for the growth and historical simulations that the Total P loading increases over time.

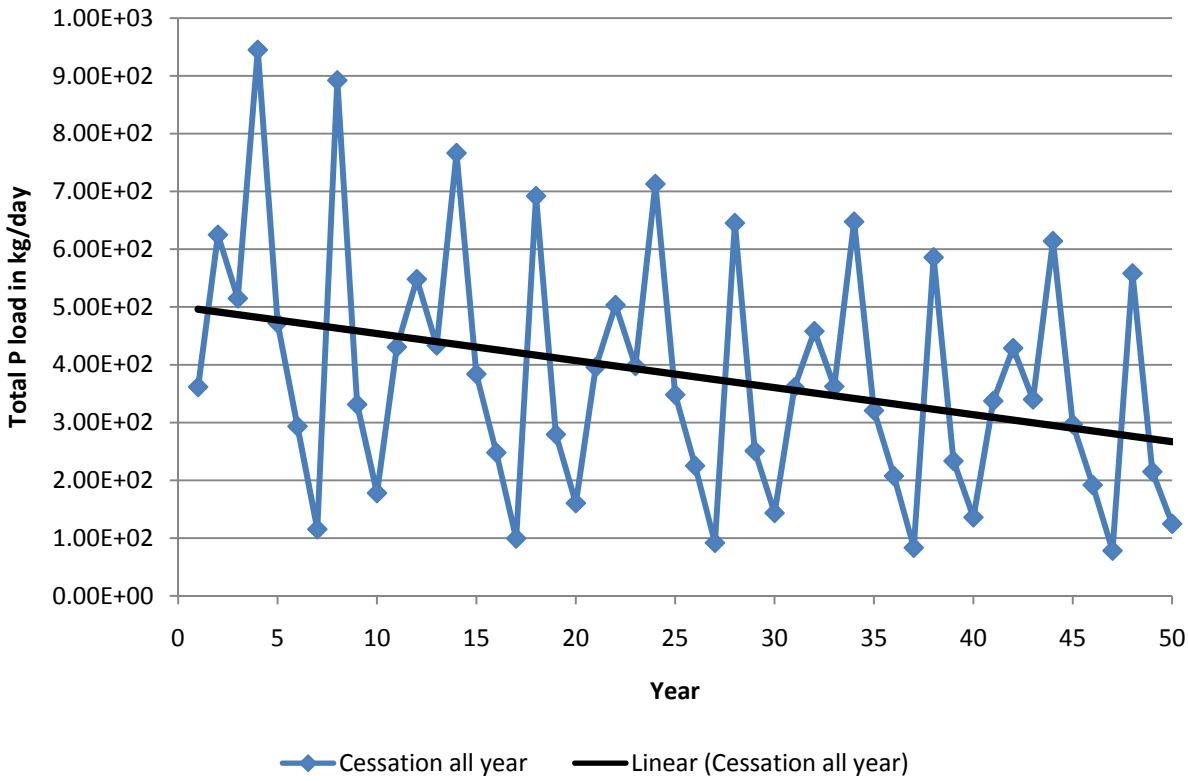

Figure 200. Yearly Total P inflow load to Tenkiller reservoir for the cessation scenario including linear trend line over 50-year period.

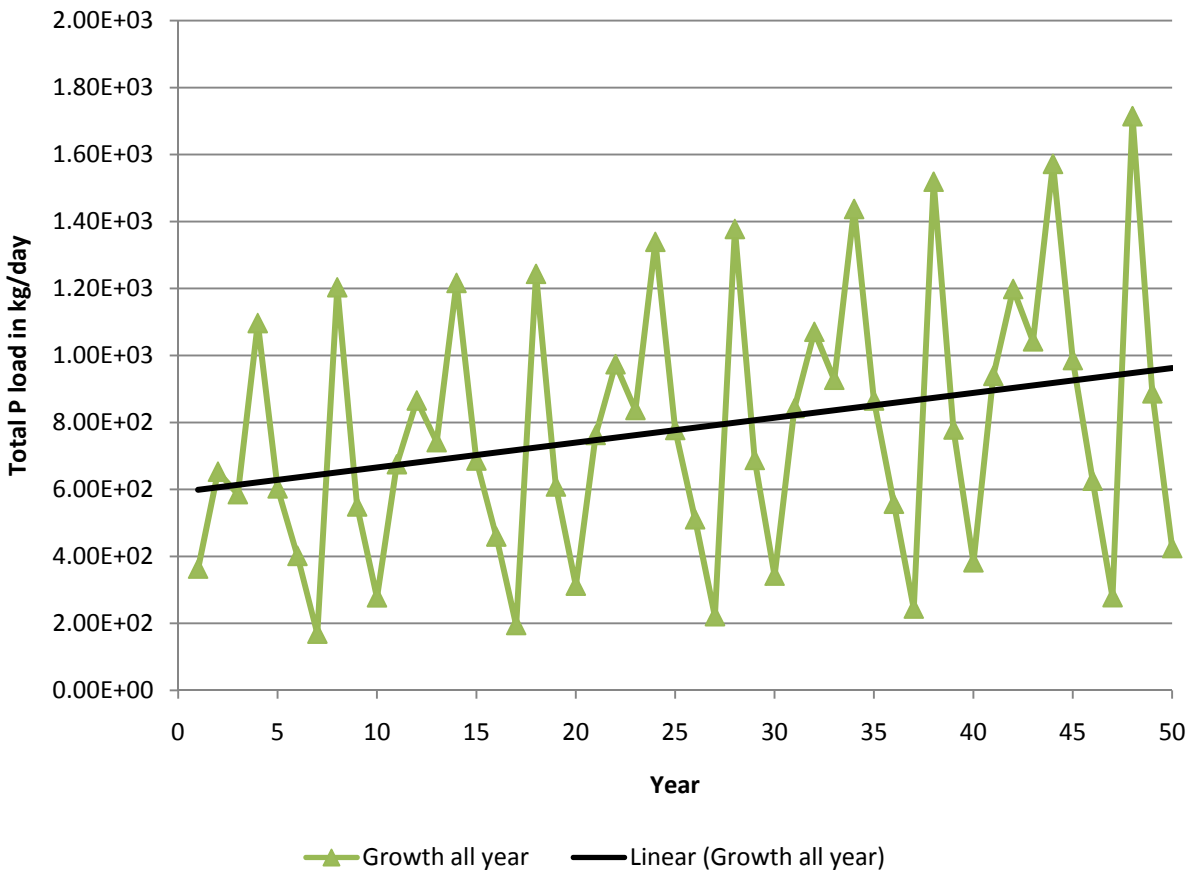

Figure 201. Yearly Total P inflow load to Tenkiller reservoir over for the growth scenario including linear trend line over 50-year period.

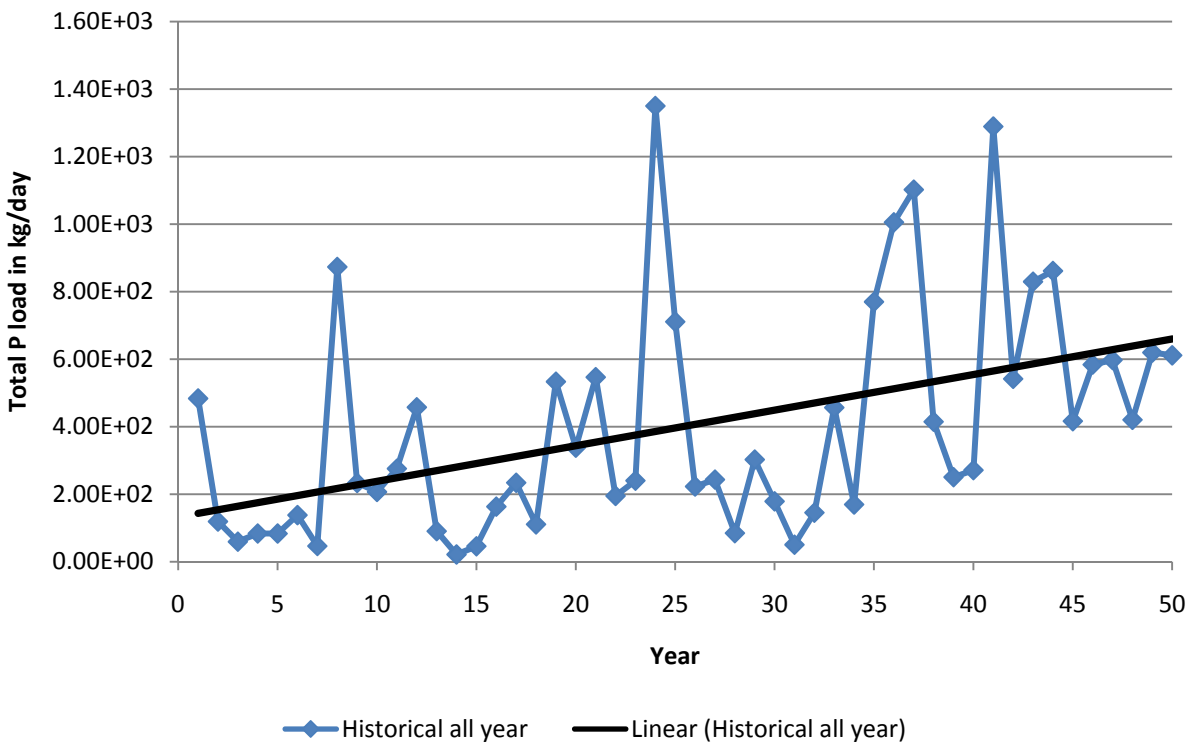

Figure 202. Yearly Total P inflow load to Tenkiller reservoir for the historical scenario including linear trend line over 50-year period.

Outflows

Phosphorus outflow from Tenkiller Lake was calculated by multiplying the average daily flow by the average daily Total P concentration. This Total P outflow includes phosphorus in the forms of Ortho P, Organic P, and P as a fraction of algae biomass. Table 27 summarizes the Total P outflows for each of the management scenarios. Total P in the outflows comparing the base case to the cessation case is shown in Figure 203, comparing the natural and growth scenario is shown in Figure 204, and the showing the historical scenario is shown in Figure 205. In each of these figures, the black line is the 50-year linear trend line and the equation on the figure is the linear equation for that trend line where X is the year and Y is the Total P in kg/d.

Table 27: Summary of Total P outflow from Tenkiller Reservoir.

	Average P Outflow from Dam, kg/day	P Outflow % of Base Case
Base Case	444	100%
Growth Scenario	598	135%
Cessation Scenario 1 - SOD=0.1 g/m2/day	274	62%
Cessation Scenario 2- SOD declines to 0.1 g/m2/day	223	50%
Historical Case	301	68%
Natural Case	40	9%

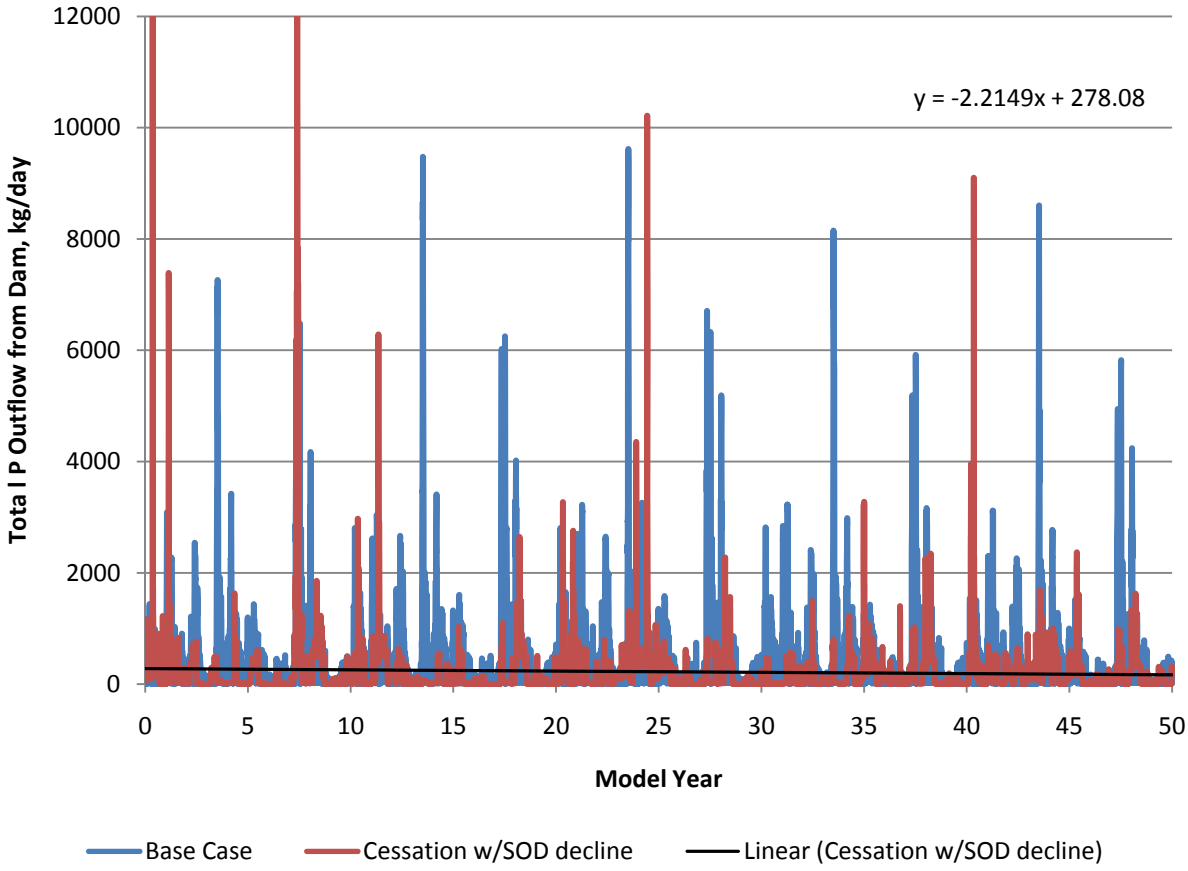

Figure 203. Total P outflow from Tenkiller reservoir for base and cessation scenarios, including linear cessation trend line over the 50-year period.

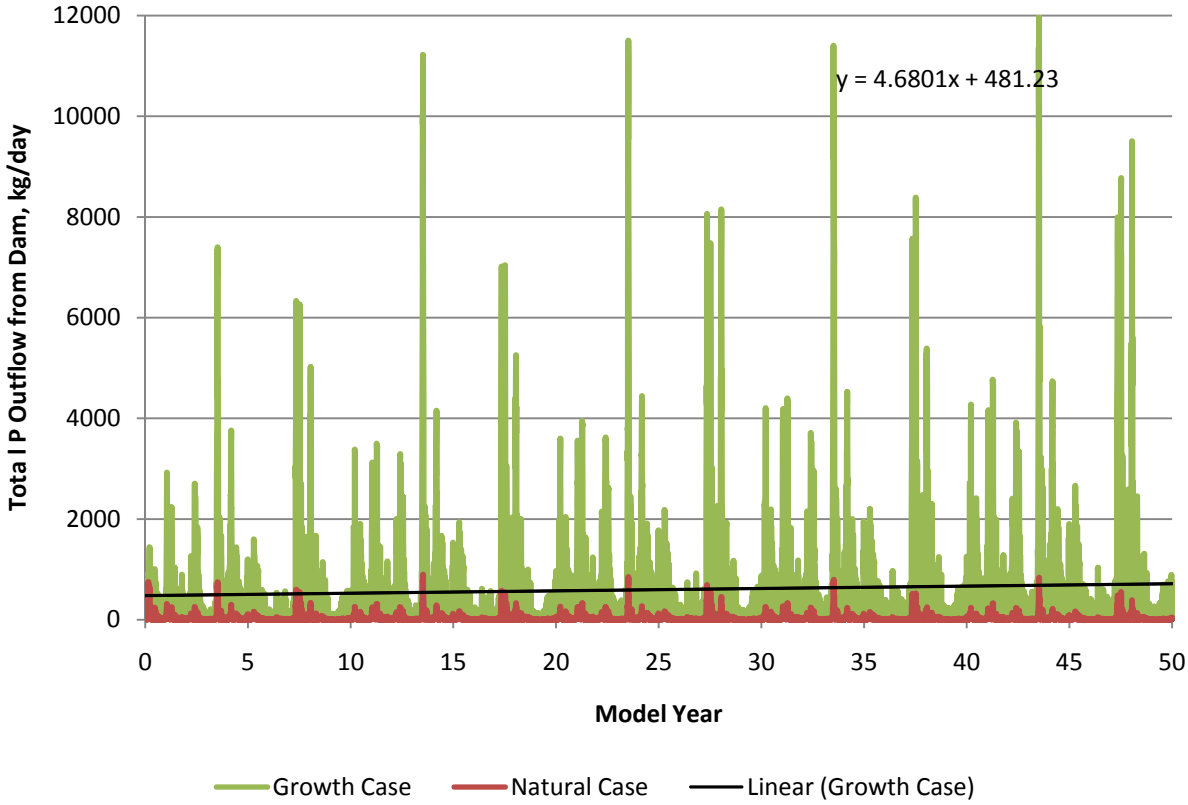

Figure 204. Total P outflow from Tenkiller reservoir for natural and growth scenarios, including linear growth trend line over the 50-year period.

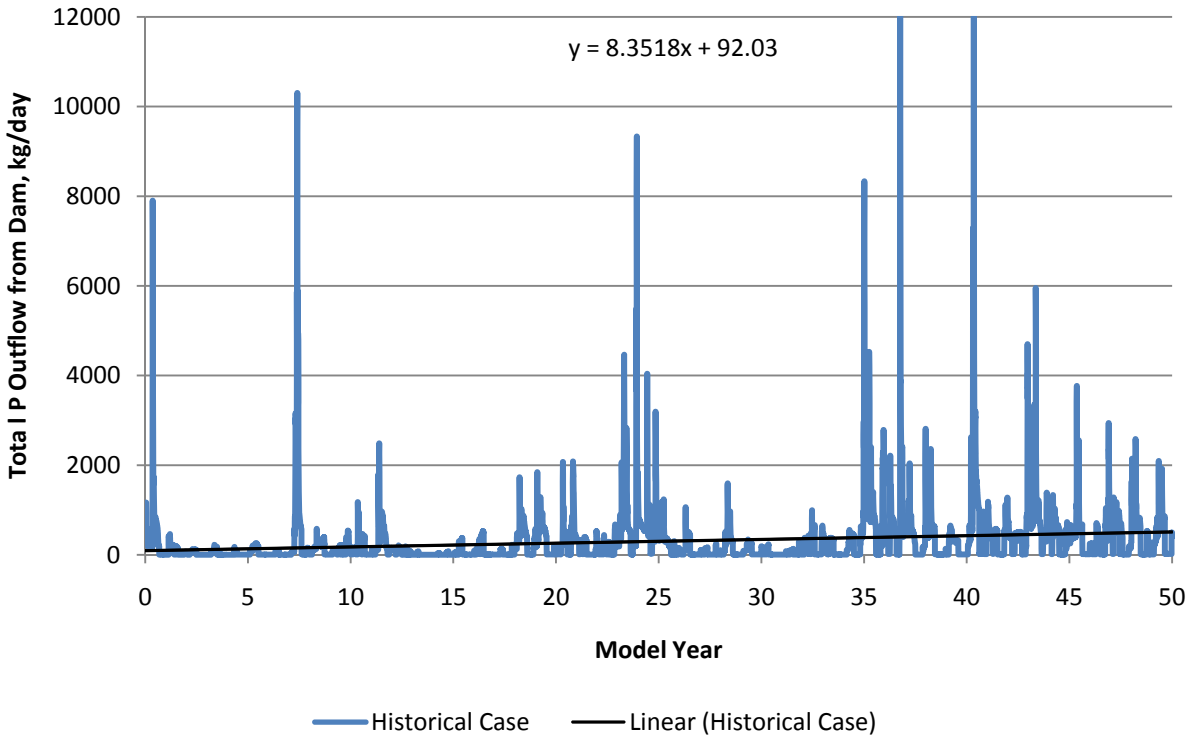

Figure 205. Total P outflow from Tenkiller reservoir for historical case, including linear historical trend line over the 50-year period.

Sediment P Flux

The flux of phosphorus from the sediments is summarized in Table 28 for each of the management scenarios. The sediment flux has been normalized on a per day basis for the entire 50-year period even though most of the flux occurs only during the summer periods.

Table 28: Summary of Total P sediment flux.

Scenario	SED, kg/50yr	SOD, kg/50yr	Total kg/50yr	Daily Average In Model Production, kg/day
Base Case	440899	1215698	1656597	91
Growth	380268	1308379	1688647	93
Cessation SOD = 0.1 g/m2/day	352048	109207	461256	25
Cessation SOD declines to 0.1 g/m2/day	359636	211223	570860	31
Historical	267432	96792	364225	20
Natural	65335	8671	74006	4

Summary and Conclusions

A water quality and hydrodynamic model of Tenkiller Reservoir was constructed in order to evaluate the response of the reservoir to changing Total P loadings in the watershed. The model was calibrated to field data taken between January 2005 and September 2007. The model was then used to simulate a 50-year period based on different model scenarios. These scenarios included no change in Total P loading in the watershed, growth of Total P loading in the watershed, a cessation of land application of poultry waste in the watershed, and a historical analysis of increased poultry waste land application in the watershed. These model results are one method of evaluating the impact of P loading to Tenkiller Reservoir.

Model Choice

The model chosen for Tenkiller Reservoir was the CE-QUAL-W2 Version 3.6 model (Cole and Wells, 2008). This model has been applied to over a thousand water bodies throughout the world and is well-suited for predicting water quality in stratified reservoir systems. The model and its source code can be downloaded from the following web site: http://www.cee.pdx.edu/w2.

Model Set Up

A water quality and hydrodynamic model was used to predict water level, velocities, temperature and water quality during the calibration period of 2005 to the Fall of 2007. The model was based on the following data sources:

1. Field measurements of bathymetry and historical bathymetric data
2. Water quality field data from the Illinois River, Baron Fork River, and Caney Creek taken by various sources (CDM, Oklahoma Water Resources, Corps of Engineers)
3. Meteorological data at Cookson and at Tulsa airport
4. Corps of Engineers water level, outflow and total inflow computations
5. USGS gauged inflow data

Using these data, calculations were made to generate the following boundary conditions:

1. Daily Total P for the Illinois River, Baron Fork River, and Caney Creek based on correlations based on LOADEST USGS model (Pickup, et. al, 2003; Tortorelli and Pickup, 2006) to time of year and flow rate. This Total P was then disaggregated into the state variables for the water quality model.
2. Hourly temperature in the inflow using a filtered equilibrium temperature approach (Adams and Wells, 1984)

3. Daily inflow dissolved oxygen concentrations used measured field data and interpolated between data points assuming saturation based on the filtered equilibrium temperature

Other water quality boundary conditions were interpolated to a daily values based on field measurements during the calibration period.

Model Calibration

The model predictions were compared to field data in the following sequence:

1. Water level
2. Temperature
3. Water quality variables

The predicted model water level was able to match measured data with a mean error of less than 5 mm and an absolute mean error of 2 cm.

The model accurately predicted temperature profiles within the reservoir with an absolute mean error of 0.77^{o}C, which is less than 1°C, the goal of a properly constructed temperature model. Being able to reproduce the stratification and water level dynamics of the reservoir are essential in order to be able to predict the water quality state variables.

Dissolved oxygen predicted by the model is a result of dynamics in the organic matter, nutrient and algae cycles. Dissolved oxygen profiles had an absolute mean error of less than 1.5 mg/l, with values less than 1.2 mg/l at several stations. The dissolved oxygen model was unable to predict supersaturation in the surface layer at some reservoir stations, but this was not deemed of importance in evaluating impacts of Total P loading even though it did affect the overall error statistics. One reason for this may be that the model results were compared always at 12 noon on the day of the field sampling even though some profiles may have been taken later in the day. Higher model error was evident at the riverine sampling station as a result of uncertainties in the inflow boundary conditions. Since the model was run continuously over 3 years, the historical sediment oxygen demand (SOD) was simplified to produce a reasonable profile over the 3 year period. In other words, the SOD was not tuned spatially and temporally to ensure perfect model-data agreement since this would bias long term simulations of the model. Organic matter deposition to the reservoir was also a significant additional source of SOD. The development of the metalimnetic minima and hypolimnetic depletion in the reservoir are reasonably reproduced with the model.

Total P is a derived variable in CE-QUAL-W2 and is the sum of organic matter P (dissolved and particulate, refractory and labile), algae, and dissolved PO_4-P. The Total P coming in the model is based on the USGS regression model LOADEST. This regression did particularly well matching overall yearly Total P loading, which is highly influenced by high flow events. Hence, one might expect that this approach may not be as accurate during lower flow periods. Even with these limitations, the model reasonably reproduced Total P at many of the sampling station locations. Dissolved ortho-P measurements are often below detection in the epilimnion during the summer as a result of algae uptake. The model accurately reflected this reduction in summer surface PO_4.

The Total N predicted by the model was also reasonably well reproduced at many of the sampling stations. Organic N was estimated from the organic matter load, which was estimated using the LOADEST regression for Total P. Both ammonia and nitrate were algae nutrients and were at times limiting the rate of algae growth because of inflows with very high P loads. The model absolute mean error for nitrate was about 7% of the overall range in the NO_3-N measurements; the model absolute mean error for ammonia was about 10% of the overall range in the NH_4-N measurements.

Algae were divided into 3 groups: diatoms, a mixed group including greens, and cyanobacteria. The CE-QUAL-W2 model uses dry weight biomass per liter for algae concentration. The model converts predicted algae biomass to chlorophyll a by using a chlorophyll a to algae ratio that is static. The ability to match cyanobacteria blooms often depends on having on-site wind data since they the buoyant algae can be transported by wind induced surface currents. The upstream boundary condition was based on limited inflow field data. Even with these limitations, the error in chlorophyll a model predictions was within about 15% of the range in measured chlorophyll a.

The model error in predicting an instantaneous sampling event for the other water quality state variables was usually less than 10% of the range of the measured variable and was less than the typical variability in the measurements.

In many cases improvements in the boundary conditions can result in lower model-data errors. Those refinements though will generally not affect the results of the scenarios runs, unless the model boundary conditions were changed. The model scenario runs are based on the same set of hydrologic and meteorological conditions (except the historical) and hence can be compared to one another in terms of changes in water quality as a result of differences in Total P loading.

Model Scenarios

The model was used to predict the response of the reservoir to changes in Total P loading in the watershed over a 50-year period. The 50-year period started with watershed conditions as they were at the end of 2006. Inflow and outflow hydrology and meteorological data for the 50 years were for the period 1997-2006 repeated every 10 years. Several scenarios were run with the model:

1. Base case, no change in the watershed
2. Cessation of further land application of poultry waste in the watershed
3. Natural case where the flow weighted average inflow concentrations of Total P were at 20 µg/l P for the 3 main tributaries: Illinois, Caney and Baron Fork.
4. Growth case where production of Total P increases over time.
5. Historical case where the P loading from the watershed grows over time starting with conditions as they existed before land application of poultry waste was significant in the watershed. (For this case only, the inflow and outflow hydrology is different from the other scenarios since it is based on inflow hydrology starting in the 1950 going through 1999.)

The Total P load from the Illinois River, Baron Fork River, and Caney Creek and the watershed conditions for each of these scenarios are described in Engel (2008).

Changing the Total P loading coming into Tenkiller Reservoir affects chlorophyll a, Total P, and outlet dissolved oxygen concentrations. The outlet dissolved oxygen concentrations are related to hypolimnetic anoxia since the main outflow is from the powerhouse which is close to the reservoir bottom. Note that this outflow also includes well-oxygenated, epilimnetic releases from the surface gates, hence it may not show how low dissolved oxygen concentrations are during summers when there is spill.

Table 29 shows the change in chlorophyll a for the cessation, historical and growth scenarios. The intercept shows the trend line chlorophyll a concentration in µg/l at the beginning of the simulation period (year 0) and the slope shows the change of that concentration over time. Changes in chlorophyll a as a result of the cessation scenario occur slower at the more lacustrine stations than in the riverine stations. Even though Total P is reduced by over 50% at the end of the 50 years, the chlorophyll a during the summer is only reduced from 20-36%. For the growth scenario, having a 42% increase in Total P loading resulted in increases in chlorophyll a from 21-43%.

Because the historical simulation has a different lake water level and different inflow hydrology to the other scenarios, this scenario is not meant to be compared to the other scenarios year-by-year. Often the chlorophyll a concentration predicted by the model at the LK04 station (model segment 35) was very low. This occurred because of high inflows when the lake level was low, making the upper part of the reservoir more riverine and creating algae growth further downstream.

Table 30 shows the changes in surface summer Total P for the cessation, growth, and historical runs at several lake stations in Tenkiller Reservoir. The intercept shows the trend line Total P concentration in mg/l at the beginning of the simulation period (year 0) and the slope shows the change of that concentration over time.

Table 31 shows the changes in outlet dissolved oxygen concentrations for the base, cessation, growth, and historical scenarios for the summer period June 1 through September 30. The intercept shows the trend line dissolved oxygen concentration in mg/l at the beginning of the simulation period (year 0) and the slope shows the change of that concentration over time. The dissolved oxygen in the outlet from Tenkiller Reservoir reflects the hypolimnetic oxygen conditions since the powerhouse outlet is near the reservoir bottom. The average outlet dissolved oxygen is improved by over 1 mg/l as a result of the cessation scenario. Even though the Growth scenario had a lower average dissolved oxygen than the base scenario, for some of the years during the summer the growth case had higher outlet dissolved oxygen concentrations than the base case. This occurred because high summer flow events sent highly oxygenated epilimnetic water (from increased algae growth) over the spillway, thus affecting the outlet dissolved oxygen.

Table 29. Change in chlorophyll a over time during the 50-year period for the cessation, growth, and historical runs. Trends are only for summer periods between June 1 and September 30.

Scenario	Lake Station	Slope, chlor a µg/l/year	Intercept, chlor a in µg/l	% change over 50 years	Standard error of estimate, µg/l chlor a
Cessation	LK04	-0.1652	41.03	-20.1	10.6
Cessation	LK03	-0.2178	30.44	-35.8	12.8
Cessation	LK02	-0.080135	19.00	-21.1	13.1
Cessation	LK01	-0.075597	16.70	-22.6	11.2
Historical	LK03	0.484827	10.67	227.2	10.5
Historical	LK02	0.1729	11.34	76.2	9.4
Historical	LK01	0.07243	12.31	29.4	11.0
Growth	LK04	0.1886678	42.70	22.1	14.8
Growth	LK03	0.0525	10.67	24.6	16.3
Growth	LK02	0.1402	23.94	29.3	15.1
Growth	LK01	0.1686	21.16	39.8	14.0

Table 30. Change in Total P over time during the 50-year period for the cessation, growth, and historical runs. Trends are only for summer periods between June 1 and September 30.

Scenario	Lake Station	Slope, Total P in mg/l/year	Intercept, Total P in mg/l	% change over 50 years	Standard error of estimate, Total P in mg/l
Cessation	LK04	-0.0005356	0.05171	-51.8	0.011
Cessation	LK03	-0.000204	0.02413	-42.3	0.016
Cessation	LK02	-0.00026	0.025956	-50.1	0.021
Cessation	LK01	-0.000274	0.0272398	-50.3	0.024
Historical	LK04	0.0015277	0.0107	713.9	0.012
Historical	LK03	0.00047544	0.006992	340.0	0.014
Historical	LK02	0.0005361	0.0045	595.7	0.019
Historical	LK01	0.000556	0.0048	579.2	0.020
Growth	LK04	0.00134588	0.068316	98.5	0.021
Growth	LK03	0.00121557	0.02978	204.1	0.036
Growth	LK02	0.00108	0.03	180.0	0.045
Growth	LK01	0.001054	0.02974	177.2	0.045

Table 31. Change in outlet dissolved oxygen over time during the 50-year period for the base, cessation, growth, and historical runs between June 1 and September 30.

Scenario	Average outlet dissolved oxygen, mg/l	Slope, DO in mg/l/year	Intercept, DO in mg/l	% change over 50 years	Standard error of estimate, in mg/l dissolved oxygen
Base	1.61	-0.00582	1.76	-17	1.0
Cessation	2.78	0.018815	2.20	43	1.4
Growth	1.57	-0.0016	1.62	-5	1.1
Historical	4.20	-0.07715	6.16	-63	1.6

Changes in fish habitat were also shown as a result of changes in Total P loading. For example, the suboptimal habitat volume for Walleye over a 50-year period doubled as a result of implementing the cessation scenario during June 15-September 15. Even though the Walleye habitat volume improved, it was still only 4% of the lake volume on average over the 50-year period between June 15 and September 15. The natural scenario approached an average of 14% of the lake volume during the same period. Since the fish habitat volumes also include temperature criteria, changes in Total P loading in the watershed did little to affect surface epilimnetic temperatures. Since the epilimnetic volume is greater than the hypolimnetic volume, during the summer period there are practical limits as to how far optimal fish habitat can be improved. Improvements in fish habitat were a result of improving hypolimnetic oxygen conditions. These oxygen conditions were improved by reducing the amount of algae grown in the reservoir and thus reducing the amount of algae deposited to the sediments which consume oxygen.

The model results show that the impacts of P loading in the watershed extend over a longer period than 50 years even if a cessation is in-place and that even after 50 years the reservoir still has not approached a pristine condition (such as the 'natural' scenario). The historical simulation shows that after about 50 years of increased P loading from the watershed, hypolimnetic anoxia has reached similar conditions to that at the beginning of the base scenario or no change in P loading (conditions in the watershed at the end of 2006). Further increase in P loading from the watershed will continue to have deleterious effects on the reservoir, but not in proportion to the increased load since other factors start playing a role – such as N limitation. Since the model simulations did not account for any N limitation apart from existing conditions, any changes in N loading as a result of these scenarios were not evaluated.

Based on this modeling study, the final conclusions can be made:

1. The model was able to reproduce to a reasonable degree field data during model calibration in 2005 through 2007.
2. The model was therefore useful in assessing the response of the reservoir to changes in loading of Total P as a result of changes in poultry waste land application in the basin.
3. Algae growth is largely dependent on P loading to the reservoir. The algae contribute to hypolimnetic depletion of dissolved oxygen thereby impairing habitat for fish that are sensitive to high temperatures and low dissolved oxygen.
4. The model scenarios were able to predict trends in Total P in the lake as a result of changes in Total P loading from the watershed.

   a. For the Base scenario, Total P concentrations remained approximately constant over the 50-year period.
   b. For the Cessation scenario, Total P concentrations were reduced by 20% to 35% (depending on the lake station) over the 50-year period.
   c. For the Growth scenario, Total P concentrations increased by about 100% to 200% by the end of the 50-year period
   d. For the Historical scenario, Total P concentrations increased by about 300% to 700% by the end of the 50-year period.
5. The Base scenario showed that water quality conditions in Tenkiller Reservoir would continue to be unacceptable for fish habitat due to low hypolimnetic dissolved oxygen concentrations.
6. The Growth scenario showed continued degradation of water quality in Tenkiller Reservoir further reducing fish habitat.
7. The Cessation scenario showed that after 50 years, the reservoir would not have recovered to a natural pristine state. High Total P loading in the basin would continue to degrade water quality.
8. The Historical scenario started with acceptable levels of oxygen in the hypolimnion but gradually over the 50 year period approached the current levels predicted by the base case.
9. The Natural scenario showed that better fish habitat and more pristine conditions in the reservoir can be obtained by significantly reducing Total P loading to Tenkiller Reservoir.

References

Adams, E. E. and Wells, S. A. (1984) "Field Measurements on Side Arms of Lake Anna, Virginia," Journal of Hydraulic Engineering, ASCE, Vol. 110, No. 6, 773-793.

Annear, R., Berger, C., Wells, S. (2006) “Idaho Pend Oreille River Model Model Development and Calibration,” Technical Report EWR-02-06, Department of Civil and Environmental Engineering, Portland State University, Portland, Oregon.

Annear, R. L., and S. A. Wells (2007), A comparison of five models for estimating clear-sky solar radiation, Water Resources Research, 43, W10415, doi:10.1029/2006WR005055.

Berger, C., Annear, R. L., and Wells, S. A. (2001)”Lower Willamette River Model: Model Calibration,” Technical Report EWR-2-01, Department of Civil Engineering, Portland State University, Portland, Oregon, 100 pages.

Berger, C., Annear, R., Wells, S., and Cole, T. (2003) “Upper Spokane River Model: Model Calibration 2001,” Technical Report EWR-1-03, Department of Civil and Environmental Engineering, Portland State University, Portland, Oregon.

Berger, C., Wells, S. (2005) “Lake Whatcom Water Quality Model,” Technical Report EWR-03-05, Department of Civil and Environmental Engineering, Portland State University, Portland, Oregon.

Boegman, L. (2006) A model of the stratification and hypoxia in central Lake Erie, Proceedings Sixth International Symposium on Stratified Flows Dec. 11-14, University of Western Australia, Perth, 6 pp.

Boegman, L., Loewen, M. R., Hamblin, P. F., and Culver, D. A. (2001) Application of a two-dimensional hydrodynamic reservoir model to Lake Erie. Can. J. Fish. Aquat. Sci., 58:859–869.

Brady, D.K., Graves, W.L., and Geyer, J.C. (1969) "Surface Heat Exchange at Power Plant Cooling Lakes", Cooling Water 2, Discharge Project No. 5, Publication No. 69-901, Edison Electric Institute, New York, NY.

Cerco, C. and Cole, T. (1994) “Three-Dimensional Eutrophication Model of Chesapeake Bay,” Paper No. E-94-4, Waterways Experiment Station, Corps of Engineers, Vicksburg, Ms.

Chapra, S. (1997) Surface Water Quality Modeling, McGraw-Hill, N.Y.

Cole, T. and Buchak, E. (1995) CE-QUAL-W2: A Two-Dimensional, Laterally Averaged, Hydrodynamic and Water Quality Model, Version 2.0, Instruction Report EL-95-, US Army Waterways Experiment Station, Vicksburg, MS.

Cole, T. and Wells, S.A. (2008) “CE-QUAL-W2: A Two-Dimensional, Laterally Averaged, Hydrodynamic and Water Quality Model, Version 3.6,” Instruction Report EL-2006-, USA Engineering and Research Development Center, Waterways Experiment Station, Vicksburg, MS.

Cooke, G. D. and Welch, E. B. (2008) Eutrophication of Tenkiller Reservoir, Oklahoma and Effects on Water Quality and Fisheries, expert report for State of Oklahoma.

Corps of Engineers (2008) http://www.swt.usace.army.mil/PROJECTS/civil/civil_projects.cfm?number=33

Craig, P. (2004) User's Manual for EFDC_Explorer: A Pre/Post Processor for the Environmental Fluid Dynamics Code, Dynamic Solutions, Knoxville, TN.

DeGasperi, C. (2007) Development of 2-D and 3-D Hydrodynamic Models of Lake Sammamish, King Co. DNRP, Washington, 2007 CE-QUAL-W2 Seminar Day Portland, Oregon June 22, 2007.

DiToro, D. M., and Fitzpatrick, J. J. (1993) "Chesapeake Bay Sediment Flux Model", Corps of Engineers, Paper No. EL-93-2, U. S. Army Engineer District, Baltimore, Maryland.

Edinger, J. E. and E. M. Buchak (1978). "Numerical hydrodynamics of estuaries." *Estuarine and Wetland Processes with Special Emphasis on Modeling*, edited by P. Hamilton and K. B. MacDonald, Plenum Press, NY, 115-146.

Engel, B. (2008) Expert report for State of Oklahoma.

Gavrieli, I., Lensky, N., Dvorkin, Y., Lyakhovsky, V., and Gertman, I. (2006) "A Multi-Component Chemistry-Based Model for the Dead Sea: Modifications to the 1D Princeton Oceanographic Model," Geologic Survey of Israel, Report GIS/24/2006, Jerusalem.

Hanna, B. and Campbell, S. (2000) Water Quality Modeling in the Systems Impact Assessment Model for the Klamath River Basin- Keno, Oregon to Seiad Valley, California, Open-File Report 99-113 U.S. Department Of The Interior, U.S. Geological Survey.

National Research Council (2001) Assessing the TMDL Approach to Water Quality Management, Committee to Assess the Scientific Basis of the Total Maximum Daily Load Approach to Water Pollution Reduction, Water Science and Technology Board, Division on Earth and Life Studies, National Academy Press, Washington, D.C.

Park, K., Kuo, A., Shen, J. and Hamrick, J. (1995) A Three-Dimensional Hydrodynamic-Eutrophication Model (Hem-3d): Description Of Water Quality And Sediment Process Submodels (EFDC Water Quality Model), School of Marine Science, Virginia Institute of Marine Science, College of William and Mary, Gloucester Point, VA.

Pickup, B. E., Andrews, W. J., Haggard, B., E., and Green, W. R. (2003) "Phosphorus Concentrations, Loads, and Yields in the Illinois River Basin, Arkansas and Oklahoma, 1997-2001," Water-Resources Investigations Report 2003-4168, USGS, U.S. Department of the Interior.

Sullivan, A. and Rounds, S. (2005) Modeling Hydrodynamics, Temperature, and Water Quality in Henry Hagg Lake, Oregon, 2000–03,Prepared in cooperation with Clean Water Services, Scientific Investigations Report 2004–5261, Department of the Interior, Geological Survey.

Tortorelli, R. L. and Pickup, B. E. (2006) "Phosphorus Concentrations, Loads, and Yields in the Illinois River Basin, Arkansas and Oklahoma, 2000-2004," Water-Resources Investigations Report 2006-5174, USGS, U.S. Department of the Interior.

Wells, S. A. and Gordon, J. A. (1982) "Geometric Variations in Reservoir Water Quality," Water Resources Bulletin, Vol. 18, No. 4, 661-670.

Wells, S. A.; Annear, R.; Berger, C.; and Sytsma, M. (2000) "Modeling and Analysis of Cooper Creek Reservoir Water Quality," prepared for the City of Sutherlin, OR, March 2000, 75 pages.

Williams, D.T.; Drummond, G.R.; Ford, D.E.; and Robey, D.L. (1980) "Determination of Light Extinction Coefficients in Lakes and Reservoirs", *Surface Water Impoundments*, *Proceedings of the Symposium on Surface Water Impoundments*, American Society of Civil Engineers, H.G. Stefan, ed.

Appendix A: Bathymetry in Tenkiller Reservoir

Because of uncertainty in processing sonar data made of Tenkiller Reservoir, 2 possible approaches were used to process the sonar data. These approaches are discussed below.

Approach 1: Sonar Elevation Data and Contour Lines – Variable Correction Factor

The main assumption in this approach was that the sonar data were reported as "depth-from-sonar-tow fish". Tow fish lengths (if unaccounted for in the data) were unlikely to be consistent. To address this issue and to determine the variable length of the tow fish, a comparison was carried out between the available contour data and the sonar depth/elevation measurements. The comparison was carried out by locating sonar elevation data that fell within 2 to 10 m of each contour line and comparing the elevations of the two data sets.

Figure 206 illustrates this method for one contour line. The yellow line indicates the 171.0 meter contour line and the light blue line indicates the location of sonar elevation data. Each red dot shows the location at which the sonar data is within a minimum of a 10 m radius of this contour line. The elevation of each point is labeled in white. The average difference between the sonar elevation and contour elevation was calculated to determine the appropriate sonar data correction. Significant outliers (over 4 meter elevation difference) were excluded from this calculation. It was assumed that these data points were indicative of finer resolution in the sonar data rather than a systematic "tow fish" length. A similar process was followed for each contour line. The results of this analysis are summarized in Table 32. This data are shown in Figure 207.

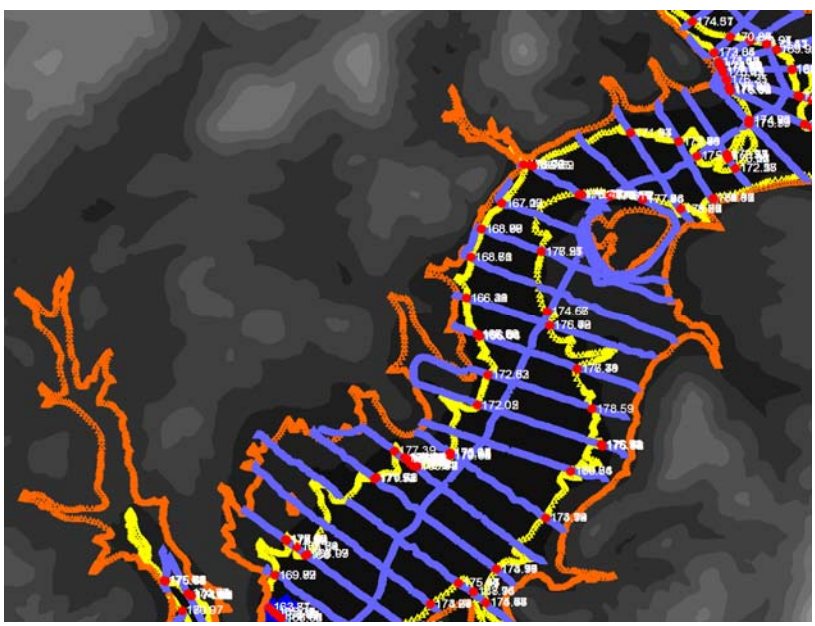

Figure 206. Sonar elevation vs. contour line comparison

Table 32. Sonar elevation vs. contour line comparison

10 Meter Radius (± 4 meter vertical outliers removed)

Contour Line, m	Average Sonar Reading, m	Average Difference, m
153.4	155.55	2.11
159.5	161.75	2.22
165.6	167.52	1.89
171.7	173.30	1.58
177.8	178.59	0.77
183.9	185.35	1.40
190	189.73	-0.28
193.06	191.32	-1.74

5 Meter Radius (± 4 meter vertical outliers removed)

Contour Line, m	Average Sonar Reading, m	Average Difference, m
153.4	155.48	2.04
159.5	162.18	2.65
165.6	167.53	1.90
171.7	173.26	1.54
177.8	178.63	0.81
183.9	185.32	1.41
190	189.70	-0.31
193.06	190.87	-2.19

2 Meter Radius (± 4 meter vertical outliers removed)

Contour Line, m	Average Sonar Reading, m	Average Difference, m
153.4	155.84	2.40
159.5	162.86	3.33
165.6	167.08	1.45
171.7	173.59	1.86
177.8	178.92	1.10
183.9	185.23	1.32
190	189.61	-0.40

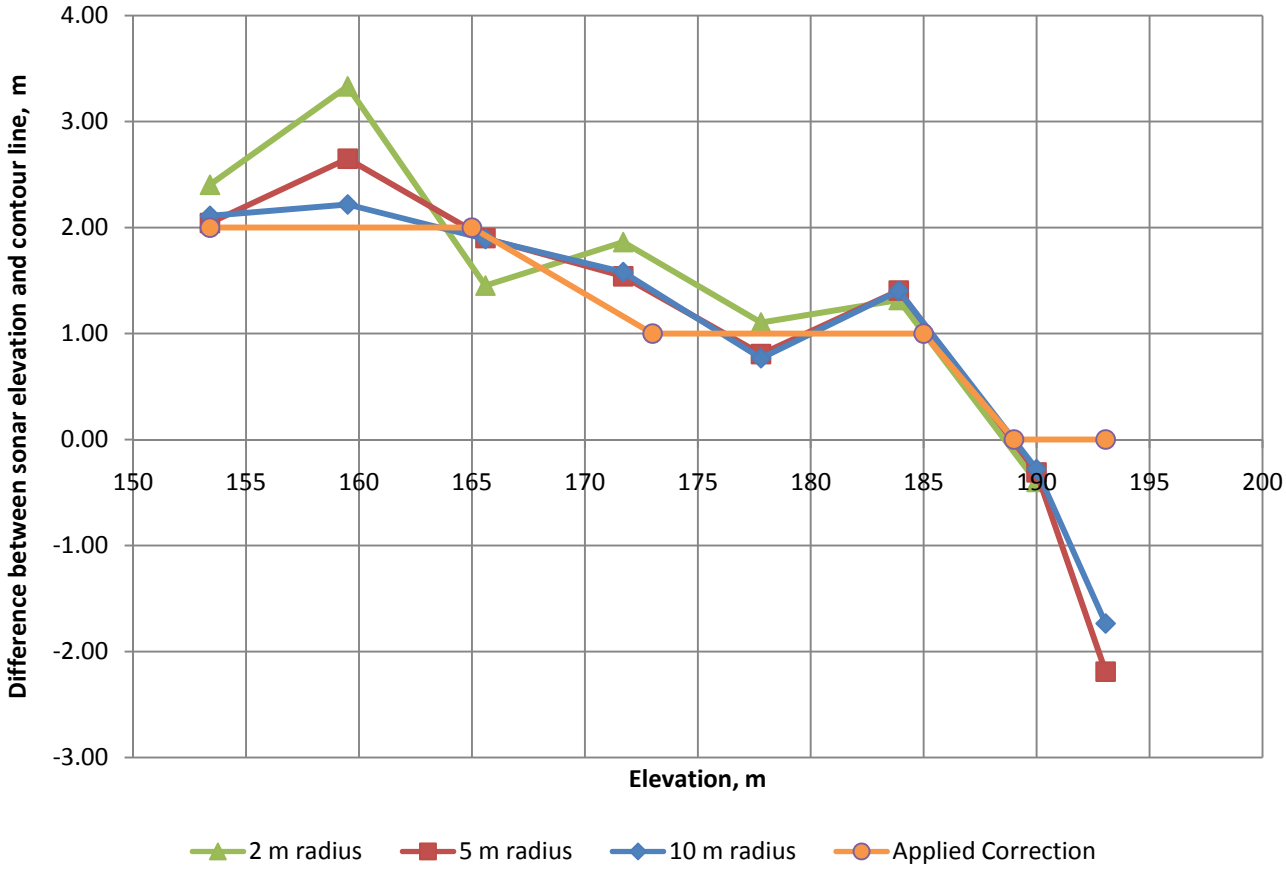

Figure 207. Plot of difference between sonar elevation and contour lines

The results of the above comparison suggested the corrections itemized in Table 33 be applied to the sonar elevation data to account for variable tow fish length:

Table 33. Variable sonar elevation corrections

Range, m	Elevation Correction, m
150 – 165	$Z_c = Z_o - 2$
165 – 173	$Z_c = Z_o - (2.0 + (1.0/8.0) * (- Z_o + 165.0))$
173 – 185	$Z_c = Z_o - 1$
185 – 189	$Z_c = Z_o - (1.0 + (1.0/4.0) * (- Z_o + 185.0))$
189 – 193	$Z_c = Z_o$

Note: Z_o = Original Sonar Elevation Z_c = Corrected Sonar Elevation

Approach 2: Sonar Elevation Data and Contour Lines - Consistent Correction factor

The main assumption of this approach was that the sonar data were reported as "depth-from-water-surface".

Assuming that the length of the tow fish was already factored in to the elevation measurements, the only uncertainty that remained was whether or not the water level on the days of the survey had been correctly accounted for in the processed elevation data. An analysis of the data showed that a water level of 193.05 m had been assumed for calculating elevation from sonar depth measurements.

Table 34 shows the actual water levels recorded over the six days during which the sonar survey was conducted. No data were available as to what sonar data had been collected on which day of the survey.

Table 34. Water level on days of sonar survey.

Date	Water Level, m
July 13, 2005	191.88
July 14, 2005	191.83
July 15, 2005	191.76
July 16, 2005	191.76
July 17, 2005	191.67
July 18, 2005	191.62
Average Water Level:	**191.75**

According to the above information, the water level used to convert sonar depth measurements to elevation data was an average of 1.3 meters higher than actual conditions during the data collection period. This would result in an average systematic error of elevations calculated to be 1.3 meters above actual elevations. Figure 208 illustrates this concept.

Figure 208. Consistent sonar elevation error scenario.

Processing of Corrected Sonar Elevation Data and Contour Line Elevation Data

Upon completion of the sonar elevation corrections discussed above, each sonar dataset was merged with the contour line elevation data. Using SURFER software, these two merged datasets were then processed by the Kriging gridding method. The final result was two similar Tenkiller Reservoir bathymetry grids, based upon approaches 1 and 2. It was then necessary to determine which version was best to use in the model.

Comparison of Approaches 1 and 2

Approaches 1 and 2 were compared by plotting their respective volume elevation curves, shown in Figure 209 and surface area elevation curves, shown in Figure 210. An analysis of the volume and surface-area elevation curves indicated that both methods resulted in very similar bathymetry grids.

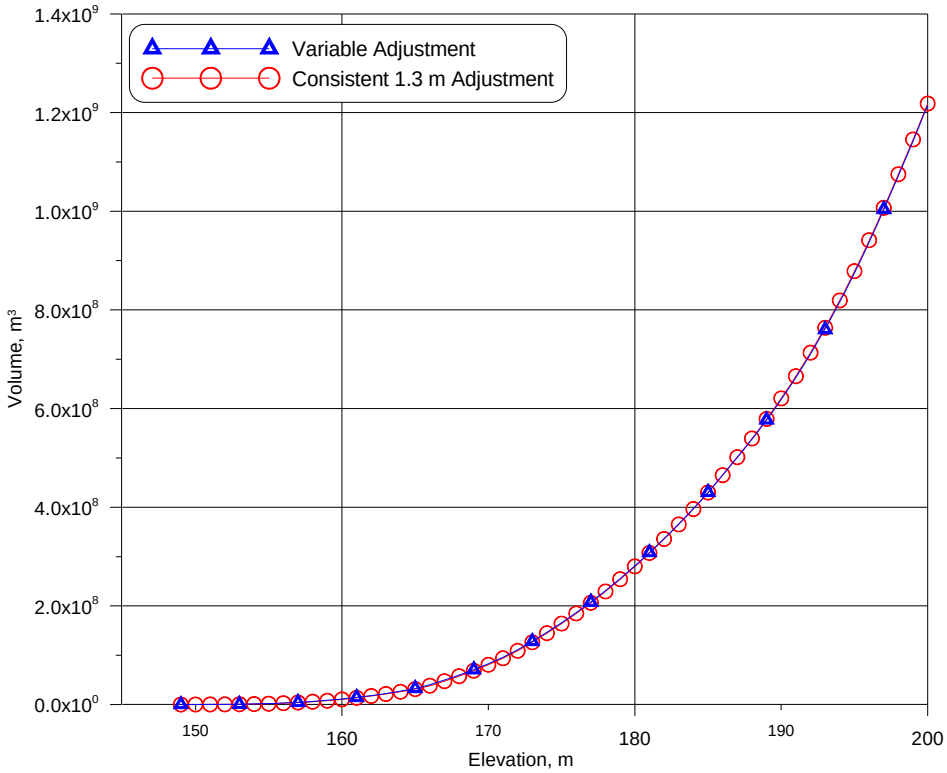

Figure 209. Volume-elevation curve for approaches 1 and 2.

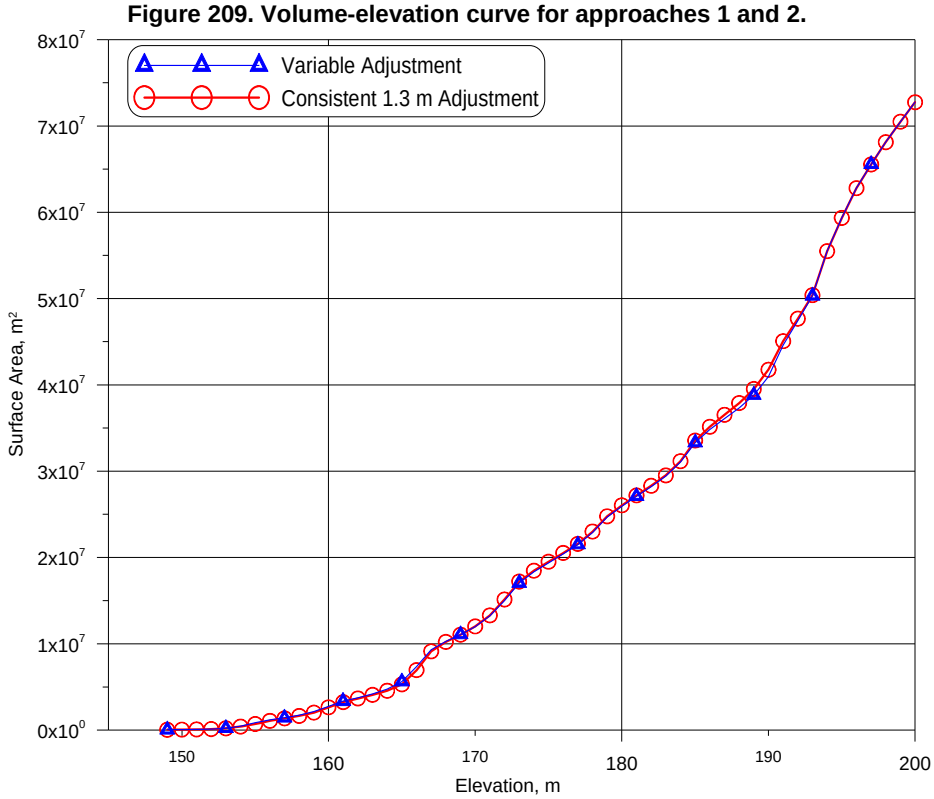

Figure 210. Surface area-elevation curve for approaches 1 and 2.

Appendix B: Estimating inflow temperatures based on meteorological conditions

The inflow temperature records from field data were sparse over the calibration (January 2005-September 2007) and management scenario period (January 1997-December 2006). In order to fill in data gaps in the inflow temperatures for all the tributaries a filtered equilibrium temperature approach was used based on a technique of Adams and Wells (1984). This section discusses background information on the equilibrium temperature and the filtered equilibrium estimation technique based only on meteorological data, the approximate depth of the stream and the averaging period.

The equilibrium temperature

The net heat flux entering or leaving the water surface is a function of the incoming short wave solar radiation, the incoming long wave radiation, evaporation, conduction and back radiation. One equation incorporating all of these processes is the following heat balance equation (assuming Ryan-Harleman evaporation equation):

$$\varphi_n[W/m^2] = 0.94\varphi_{sc}\left(1-0.65C^2\right) + 5.15\cdot 10^{-13}\left(T_{air}+273\right)^6\left(1+0.17C^2\right) - 5.51\cdot 10^{-8}\left(T_s+273\right)^4 - \left[2.7\left(T_{sv}-T_{av}\right)^{1/3}+3.2W_2\right]\left(e_s-e_2\right)\left[1+0.61\frac{T_s-T_2}{e_s-e_2}\right]$$

where T_{air} is the air temp in deg C, T_s is the surface temp in deg C, e_s is the saturated vapor pressure at water surface temp, T_{sv} and T_{av} are the virtual surface and air temperatures in deg K, C is cloud cover fraction from 0 to 1. The equilibrium temperature is defines as that value of T_s (surface temperature) for which the net heat flux, ϕ_n, is zero. Since the equation cannot be solved for explicitly for that temperature, a root finding bi-section technique is used to determine Teq. This is illustrated below in Figure 211.

The equilibrium temperature concept was a mathematical approach to surface heat transfer that linearized the Φ_n term which was a function of $T_{surface}$ to the 4th power to a function of $T_{surface}$ to the 1st power. This allowed analytical solutions to temperature models to be used and introduced another term, K called the surface heat transfer coefficient. This term dictates the speed at which the water body responds to the temperature.

$$\Phi_n = -K\left(T_s - T_E\right)$$

Another approach for computing T_E is to use an approximate technique from Brady et al. (1969):

$$T_E = \frac{\phi_{sn}}{23 + f(W)(\beta + 0.255)} + T_d$$

where φ_{sn}: net short wave solar in Btu/ft^2/day
T_d: dew point temperature ^{o}F

f(W): wind speed function = 17W_2 Lake Hefner model , in Btu/ft^2/day/mm Hg

$$\beta = 0.255 - 0.0085T^* + 0.000204T^{*2}$$

$T^*=0.5(T_w+T_d)$

T_w: water surface temperature
T_d: dew point temperature

W_2: wind speed at 2 m in mph

K can be computed from the slope of net flux vs temperature or can be obtained using an approximate formula (Brady et al., 1969):

$$K = 23 + (\beta_w + 0.255)17W_2$$

Where $\beta_w = 0.255 - 0.0085T_w + 0.000204T_w^{\ 2}$

units of K are in Btu/ft^2/day/^{o}F

This approximate approach was used to compute T_E and K for each hour of the meteorological record.

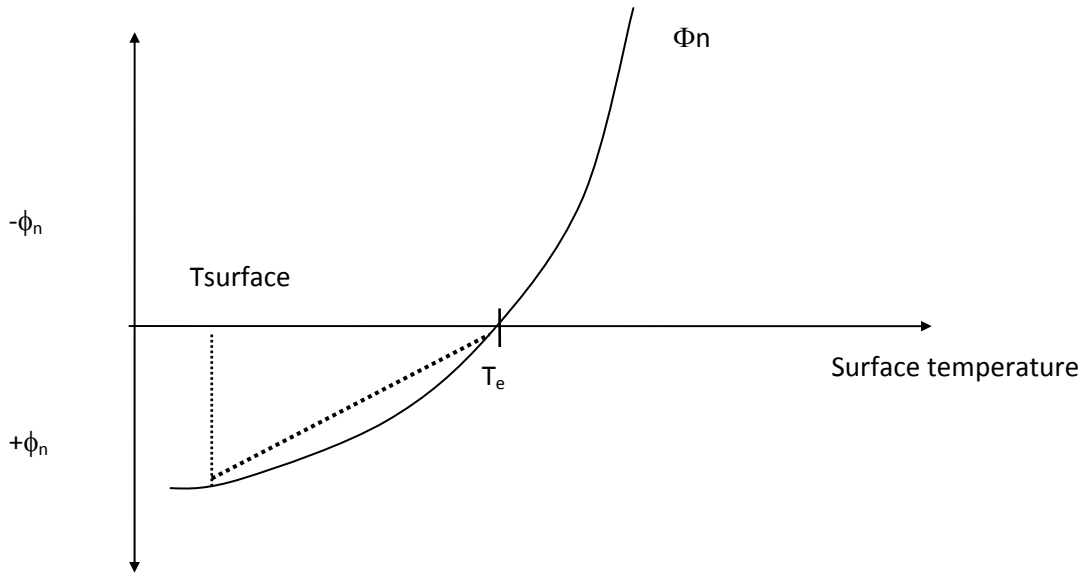

Figure 211. The definition of equilibrium temperature.

The filtered equilibrium temperature

An approach described in Adams and Wells (1984) was used to predict inflow tributary temperatures. This approach consisted of an exponential filter based on the equilibrium temperature and surface heat exchange coefficient. For example, the temperature of the tributary, $T_{tributary}$, at a particular hour computing using the following equation:

$$T_{tributary} = \frac{\sum_{n=1}^{t_{residence}/\Delta t} T_e(t - n\Delta t)\exp(-(n-1)\bar{k}\Delta t)}{\sum_{n=1}^{t_{residence}/\Delta t} \exp(-(n-1)\bar{k}\Delta t)}$$

where T_e: equilibrium temperature (defined as the value of temperature for which the net surface heat flux is zero)

Δt: time step (usually one hour)

$\bar{k}$: kinematic surface heat exchange coefficient (average over preceding residence time)

$= \frac{\overline{K}}{\rho c_p h}$ where K is the surface heat exchange coefficient, ρ is the density, c_p is the specific heat at constant pressure, h is the average depth of the water

$t_{residence}$: residence time of fluid exposed to meteorological conditions

n: number of time steps to "average" the meteorological conditions

The kinematic heat exchange coefficient was calculated using the meteorological file for the basin.

Appendix C: Error statistics

Model-data comparisons in the model calibration involved times series plots and vertical profile plots, where available. Model-data error statistics were also developed to evaluate how well the model matched with data. Mean error, absolute mean error and root mean square error statistics were used for evaluating flow, water level, and stream temperature. The equation used for the mean error is:

$$Mean_Error(ME) = \frac{\sum_{1}^{n}(\text{model} - \text{data})}{n}$$

where 'n' is the number of observations, 'model' is the model predicted state variable and 'data' is the field data variable. The absolute mean error between model and data is defined as:

$$Absolute_Mean_Error(AME) = \frac{\sum_{1}^{n} abs(\text{model} - \text{data})}{n}$$

The root mean square error between the model and data is defined as:

$$Root_Mean_Square_Error(RMS) = \sqrt{\frac{\sum_{1}^{n}(\text{model} - \text{data})^2}{n}}$$

Appendix D: Temperature Profile Comparisons

Figure 212 through Figure 221 show comparisons between the CE-QUAL-W2 temperature model predictions and field data collected between January 2005 and September 2007 at Lake stations LK01 (model segment 199), LK02 (model segment 83), LK03 (model segment 59), LK04 (model segment 35), and LK05 (model segment 109).

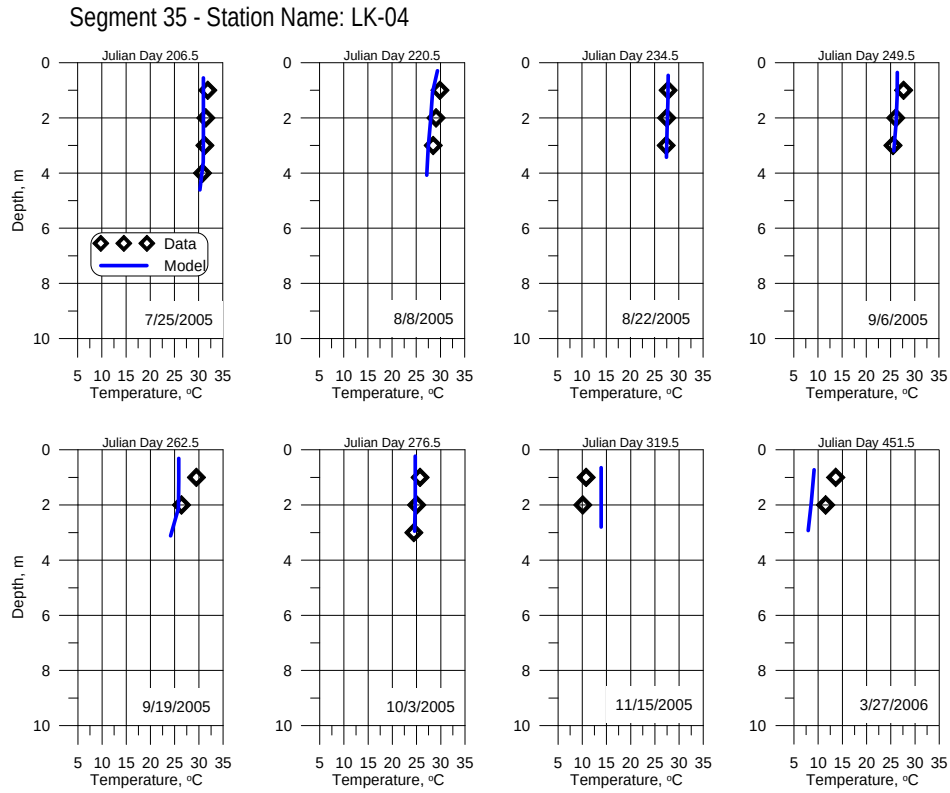

Figure 212. Temperature profiles segment 35 Part 1.

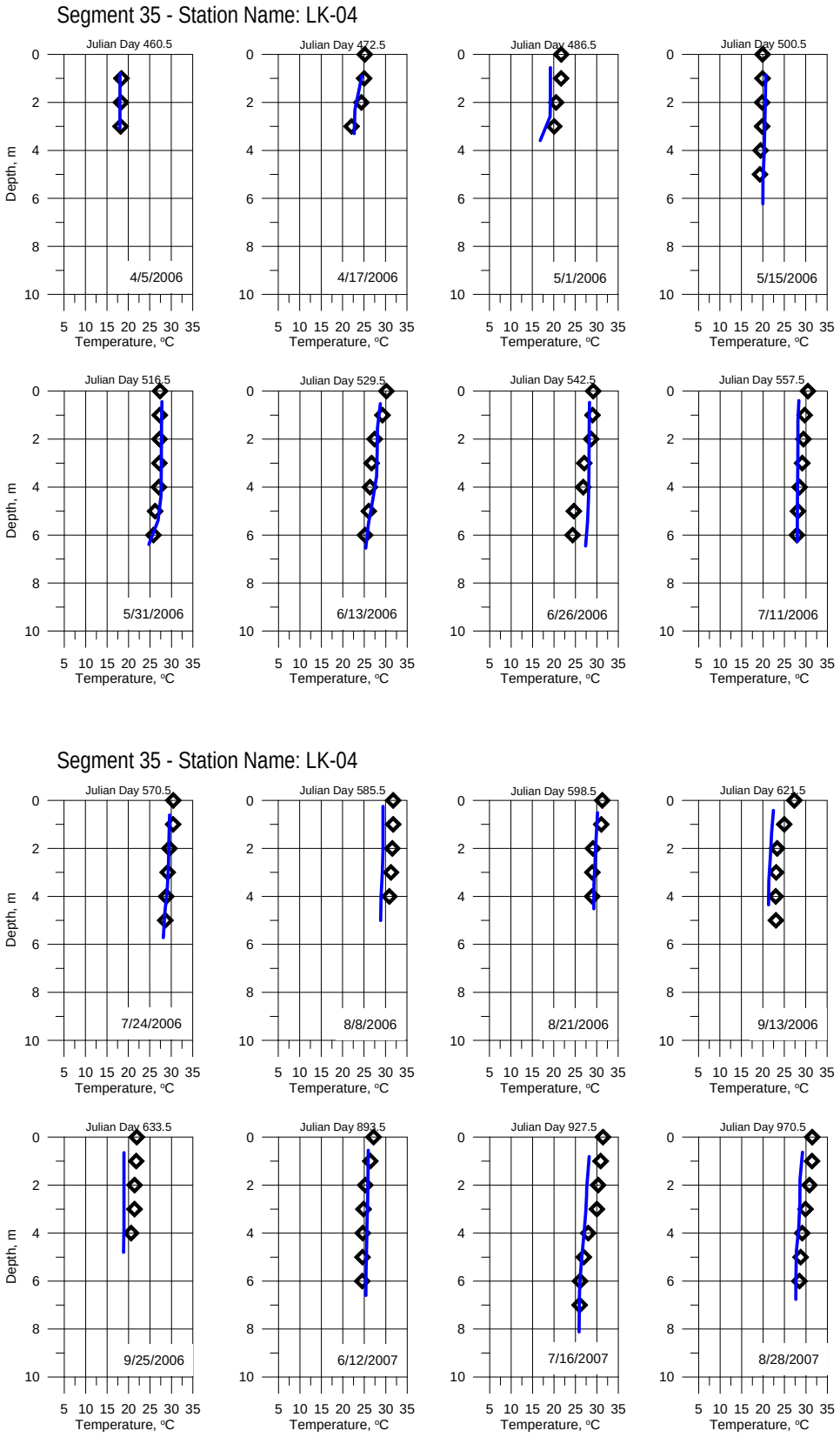

Figure 213. Temperature profiles segment 35 Parts 2 & 3.

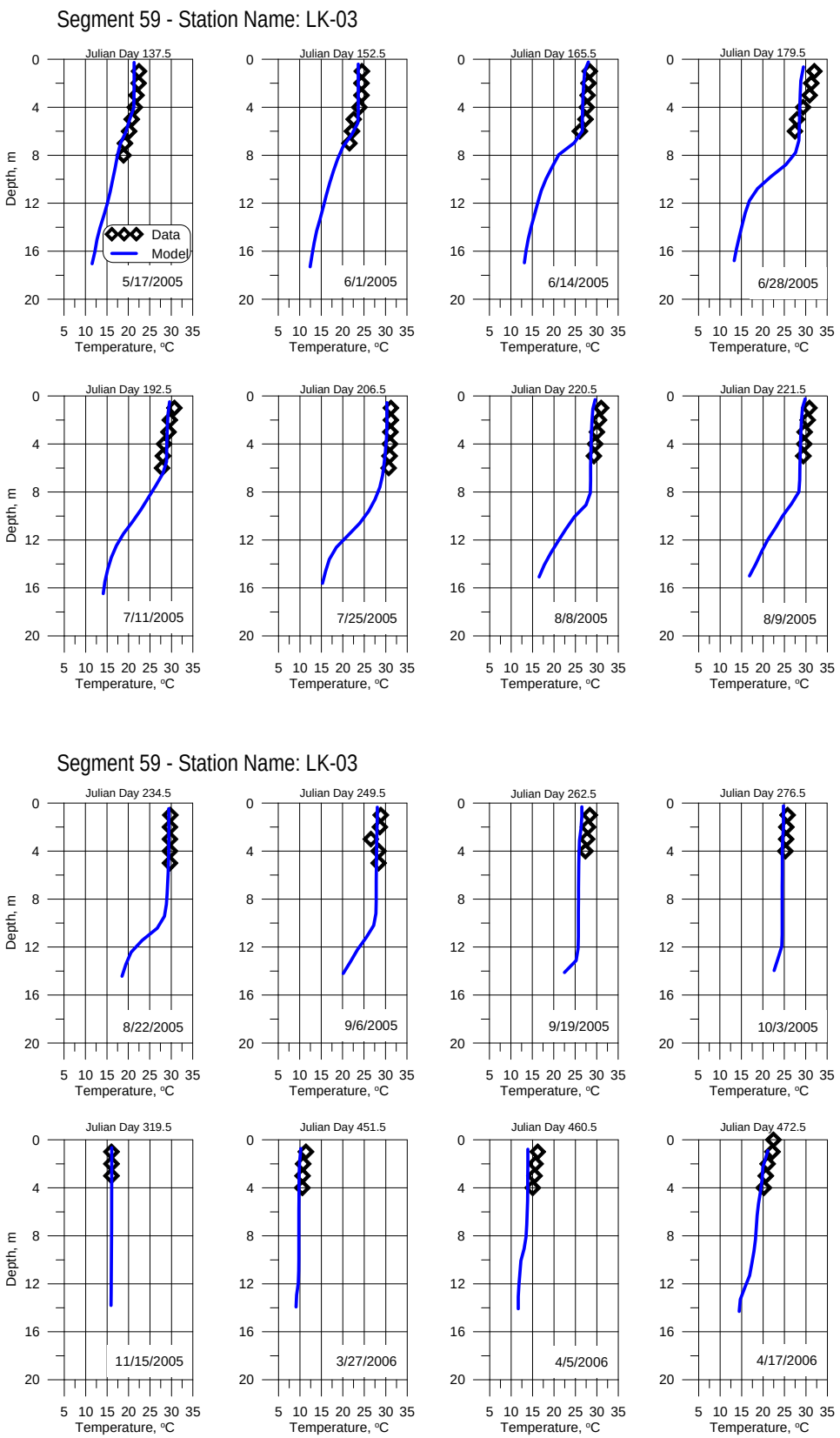

Figure 214. Temperature profiles segment 59 Parts 1 & 2.

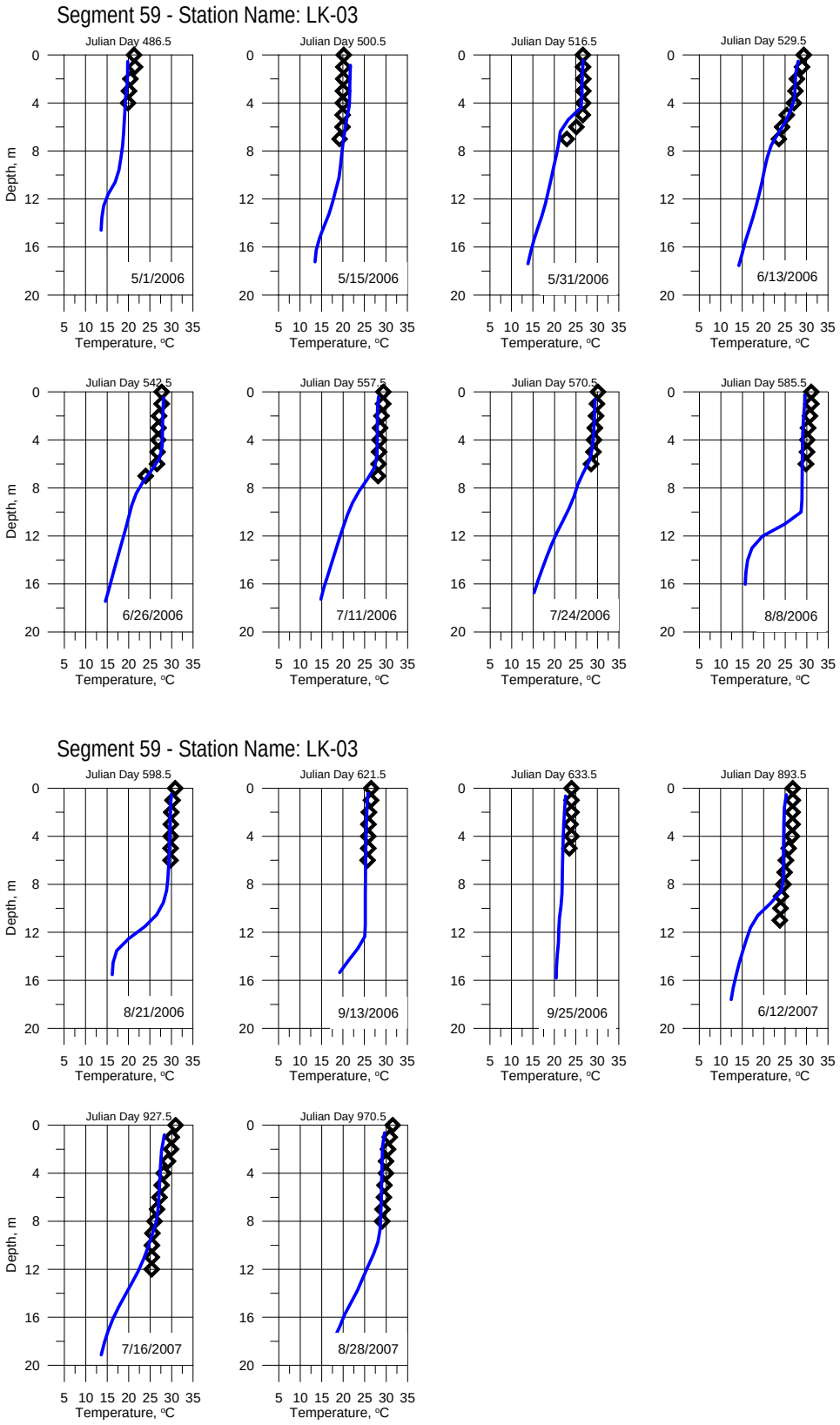

Figure 215. Temperature profiles segment 59 Parts 3 & 4.

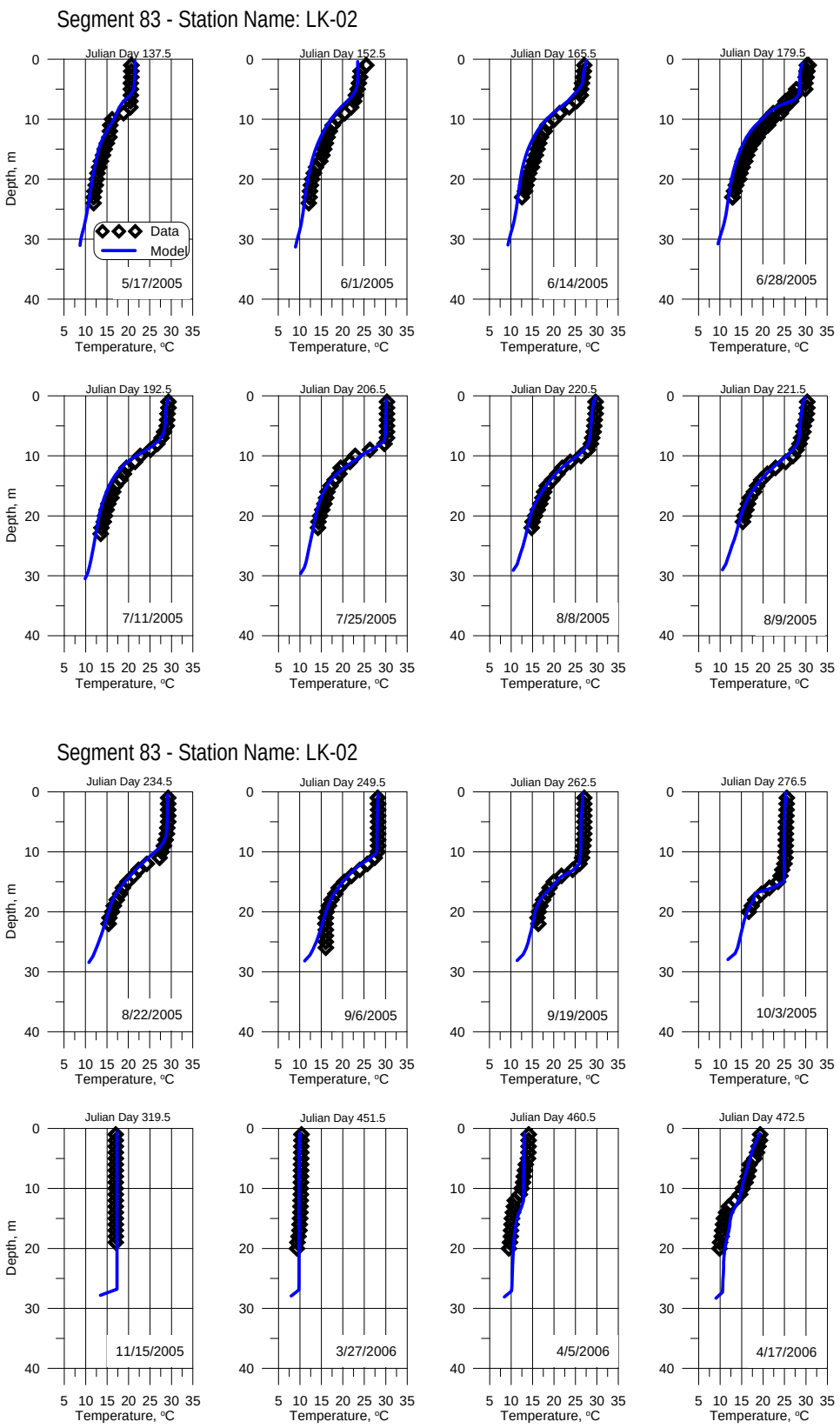

Figure 216. Temperature profiles segment 83 Parts 1 & 2.

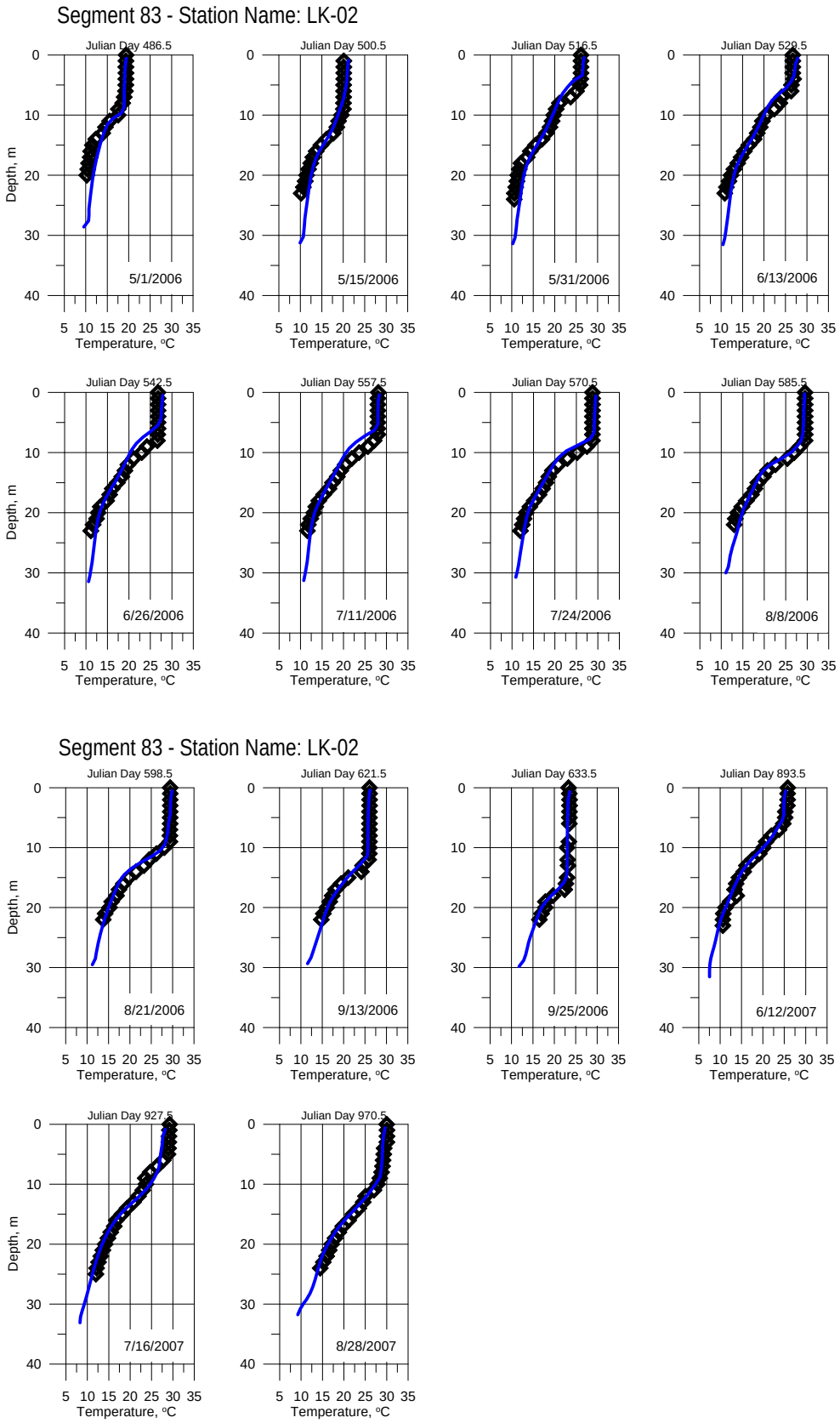

Figure 217. Temperature profiles segment 83 Parts 3 & 4.

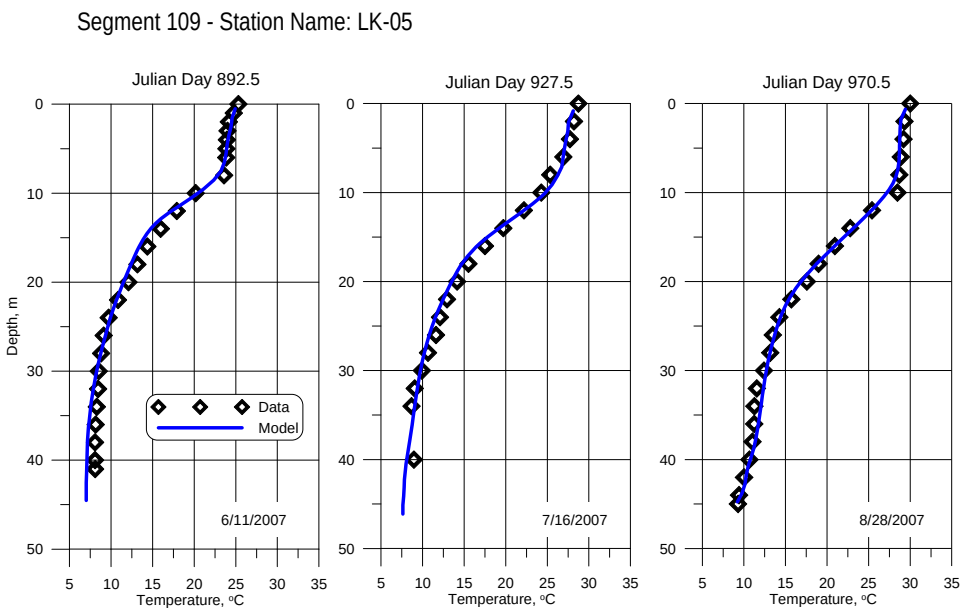

Figure 218. Temperature profiles segment 109.

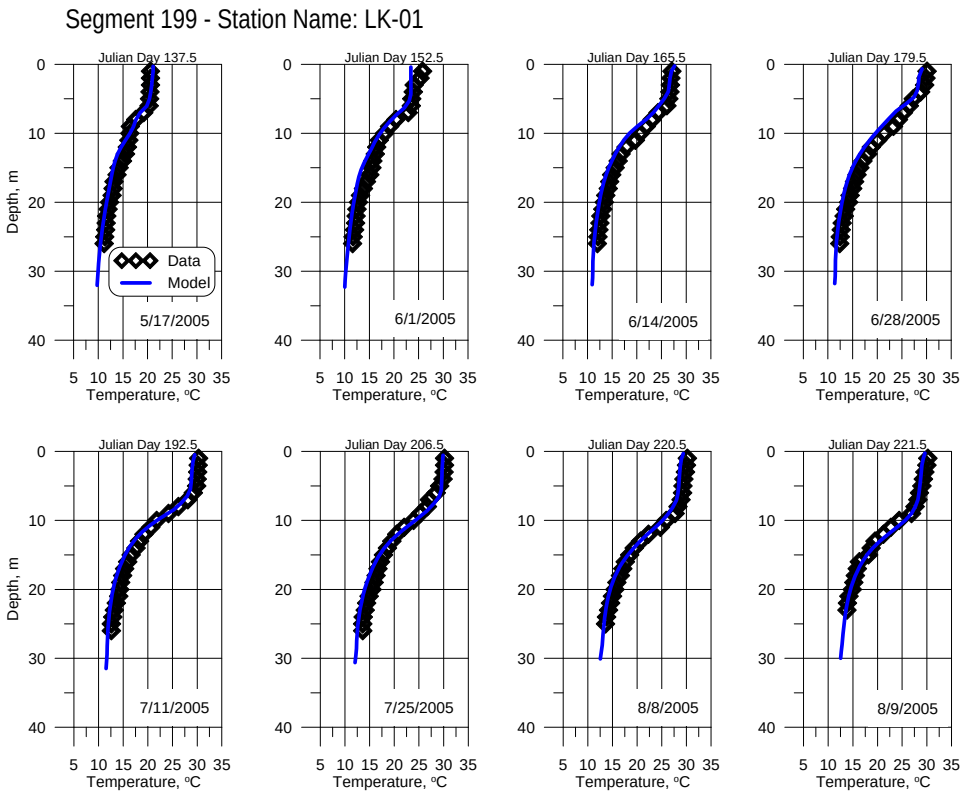

Figure 219. Temperature profiles segment 199 Part 1.

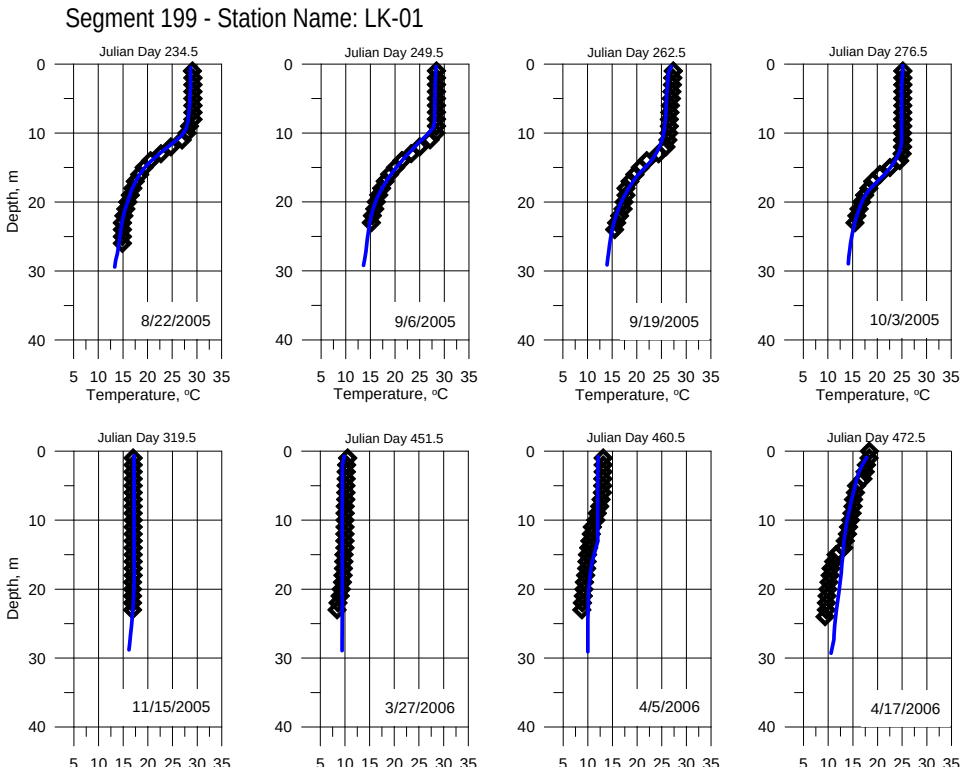

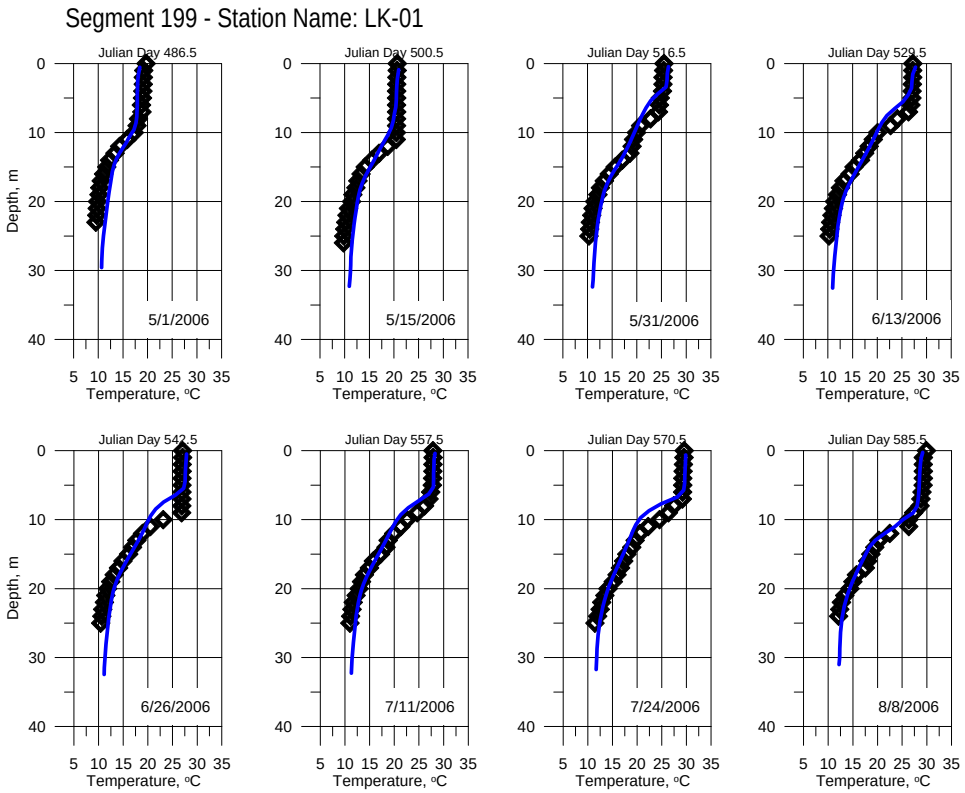

Figure 220. Temperature profiles segment 199 Parts 2 & 3.

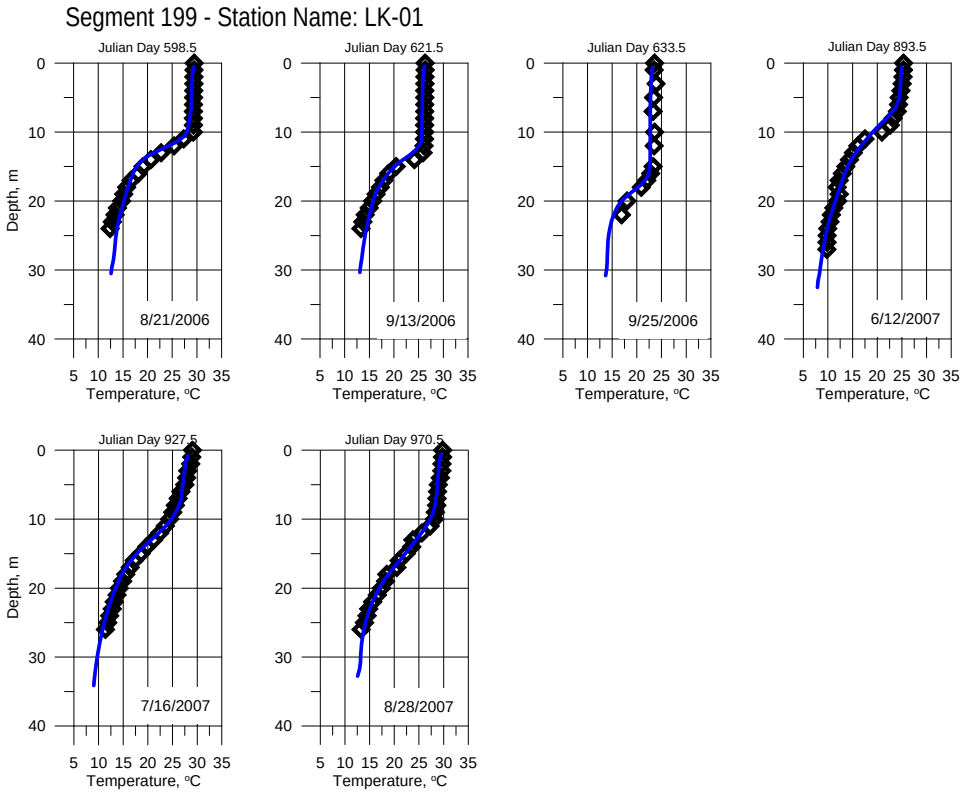

Figure 221. Temperature profiles segment 199 Part 4.

Appendix E: Dissolved Oxygen Profile Comparisons

Figure 222 through Figure 232 show comparisons between the CE-QUAL-W2 dissolved oxygen model predictions and field data collected between January 2005 and September 2007 at Lake stations LK01 (model segment 199), LK02 (model segment 83), LK03 (model segment 59), LK04 (model segment 35), LK05 (model segment 109), as well as RWI-SUMWCI (model segment 43), Cherokee (model segment 46), and Carlile (model segment 67).

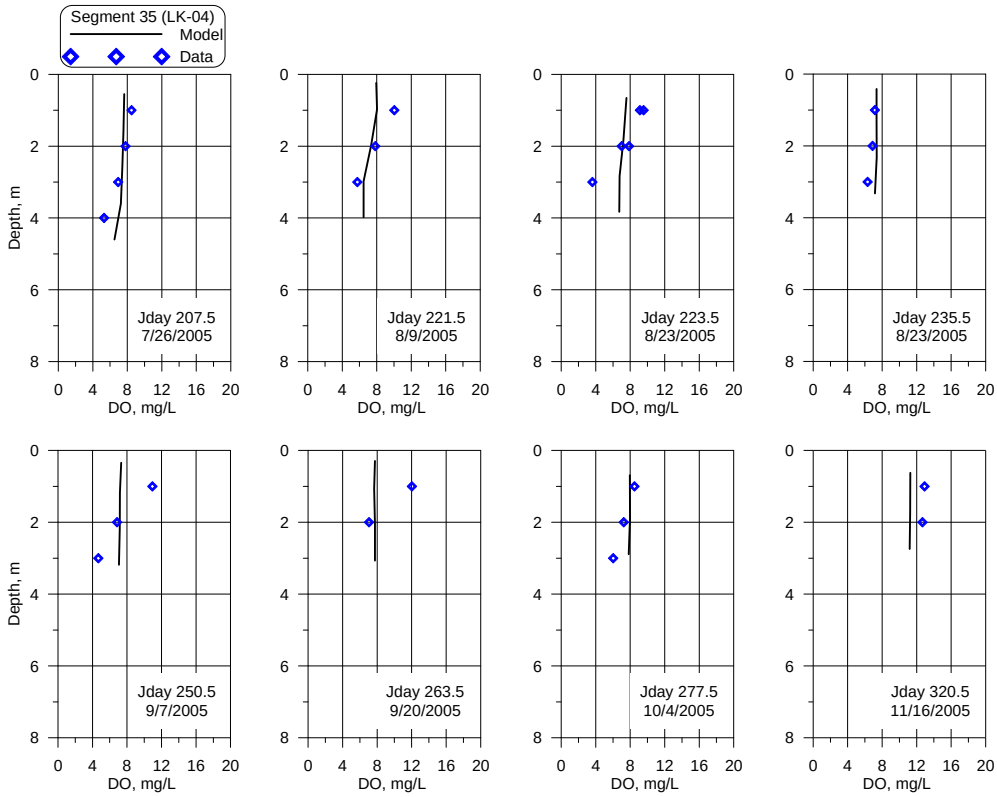

Figure 222. Dissolved oxygen profiles segment 35 Part 1.

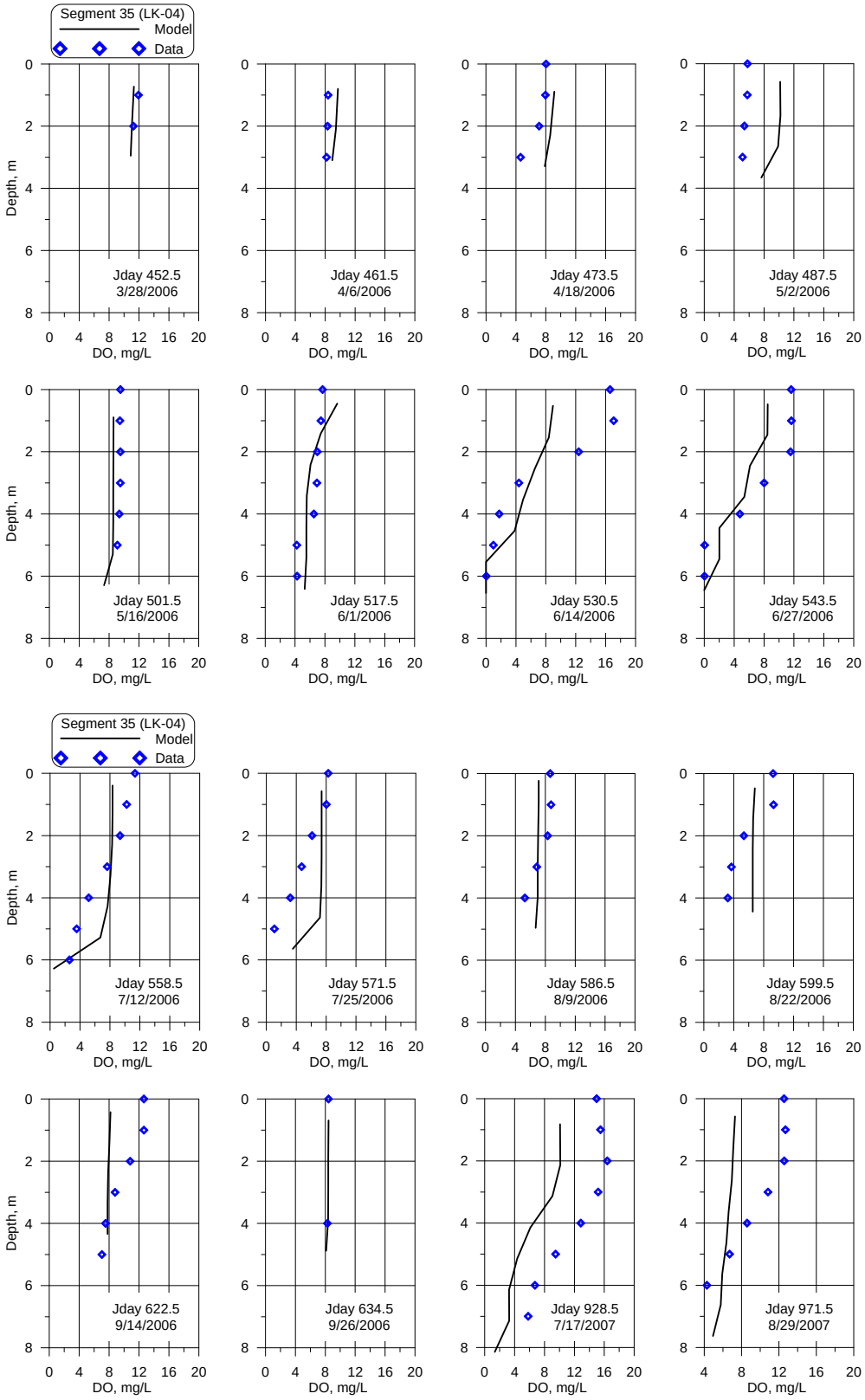

Figure 223. Dissolved oxygen profiles segment 35 Parts 2 & 3.

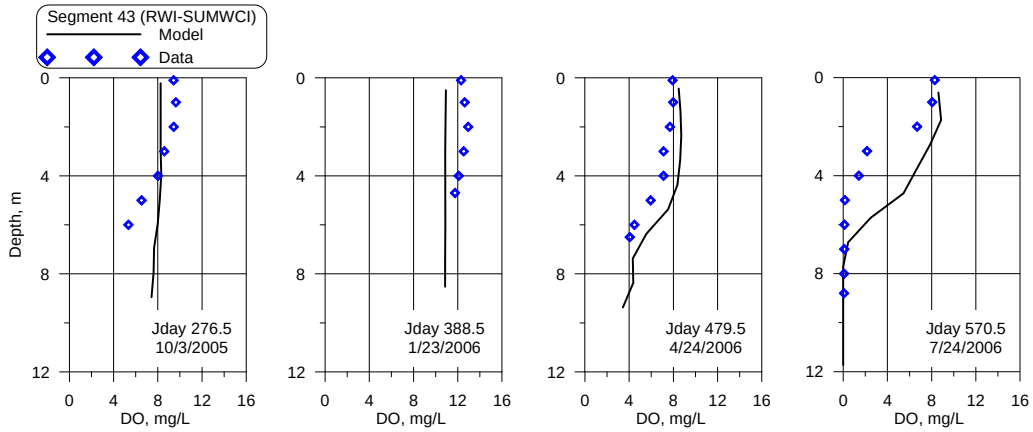

Figure 224. Dissolved oxygen profiles segment 43.

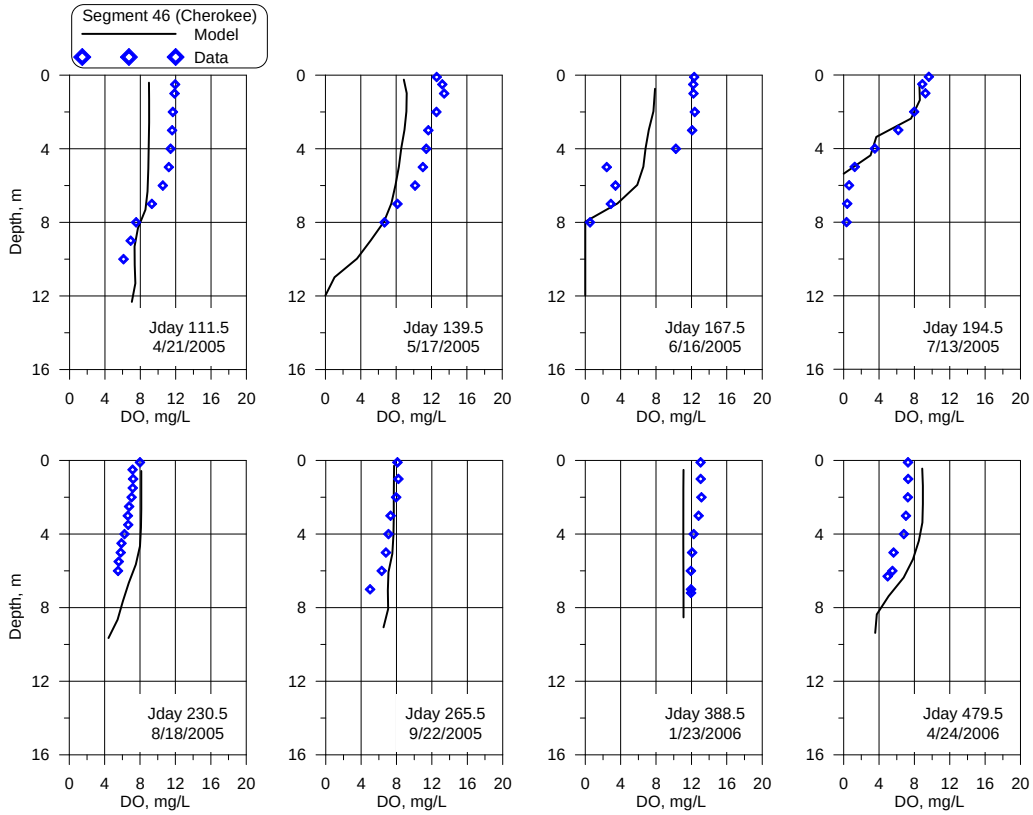

Figure 225. Dissolved oxygen profiles segment 46.

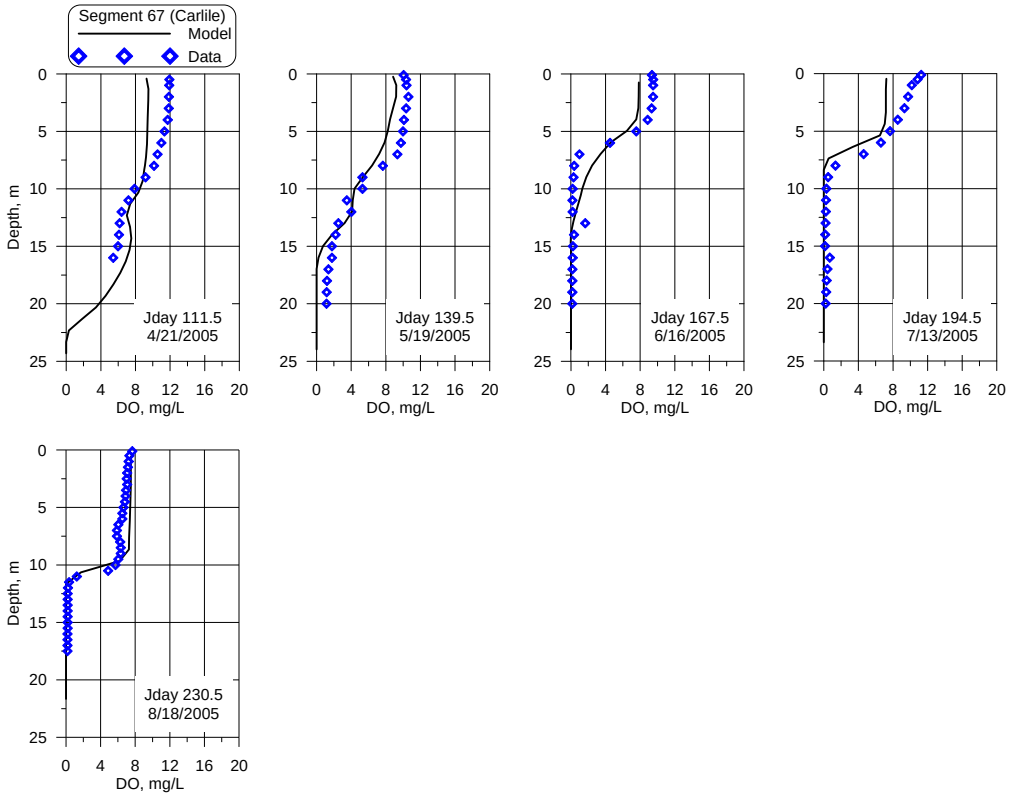

Figure 226. Dissolved oxygen profiles segment 67.

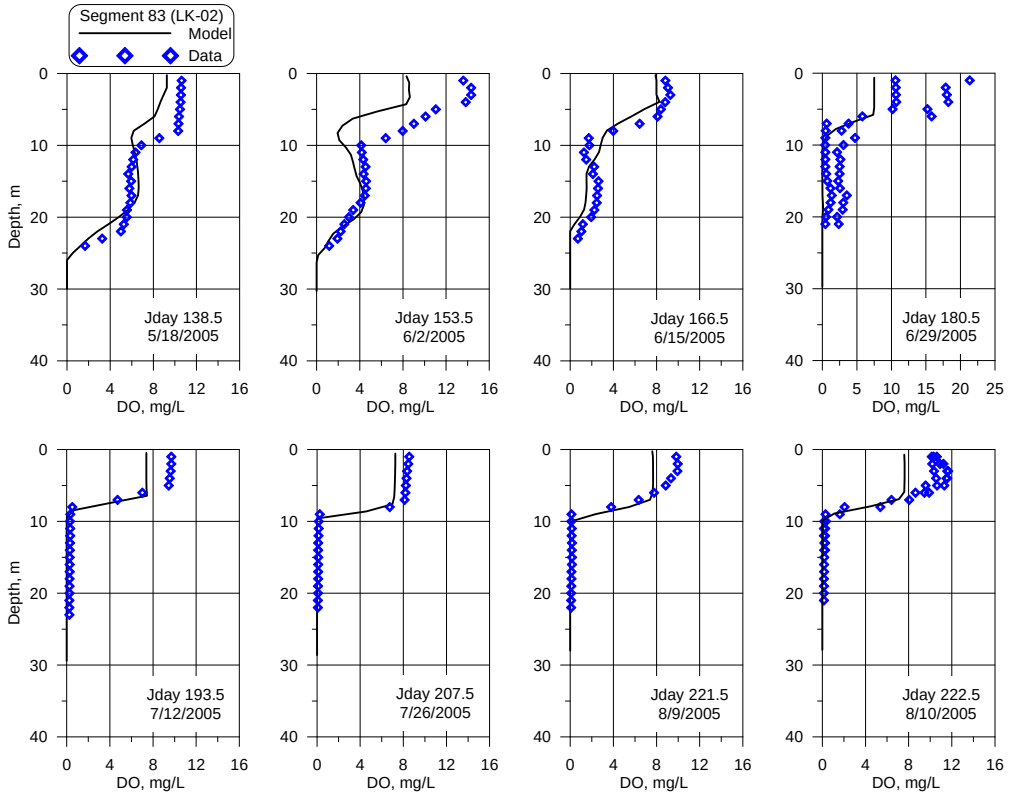

Figure 227. Dissolved oxygen profiles segment 83 Part 1.

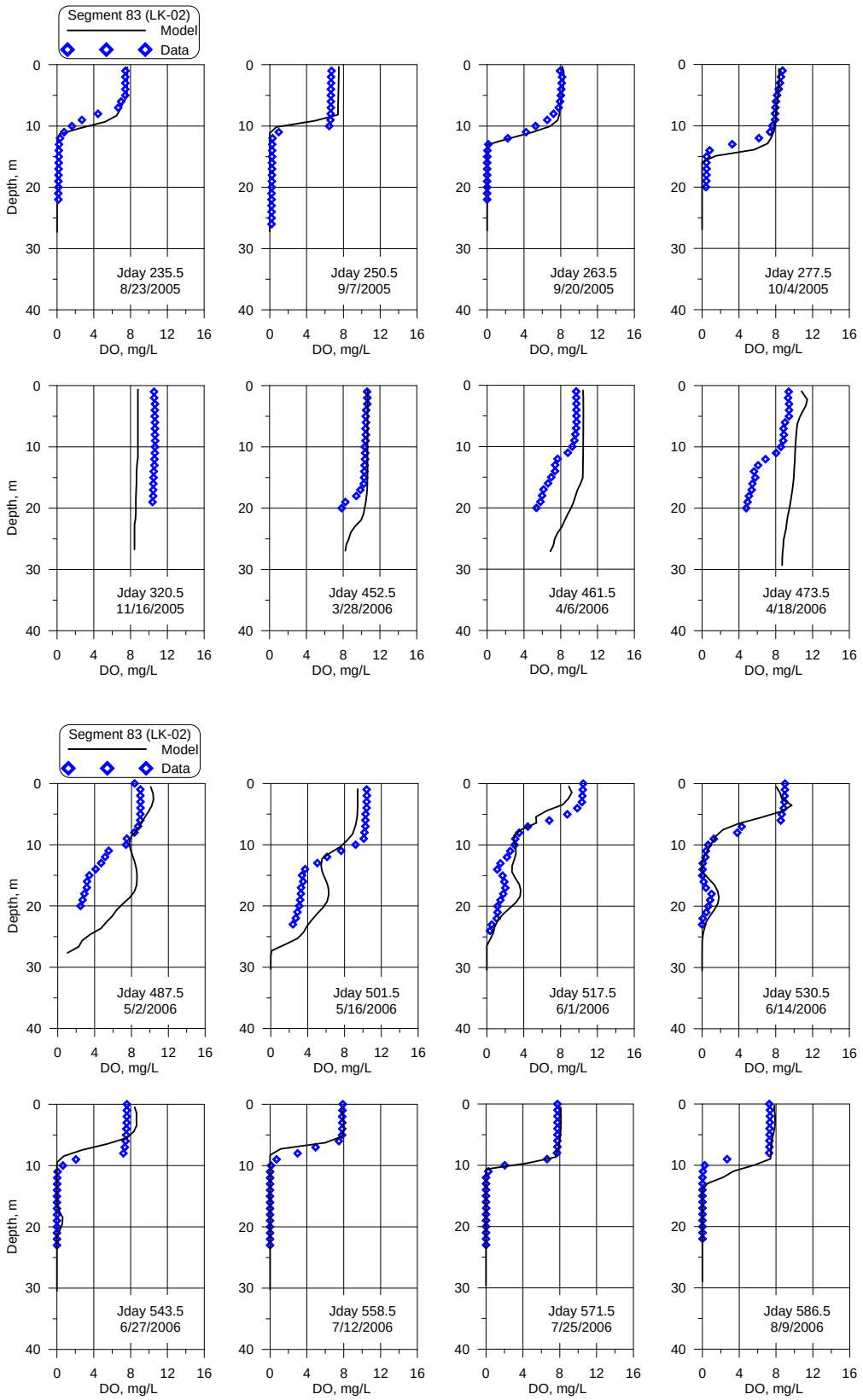

Figure 228. Dissolved oxygen profiles segment 83 Parts 2 & 3.

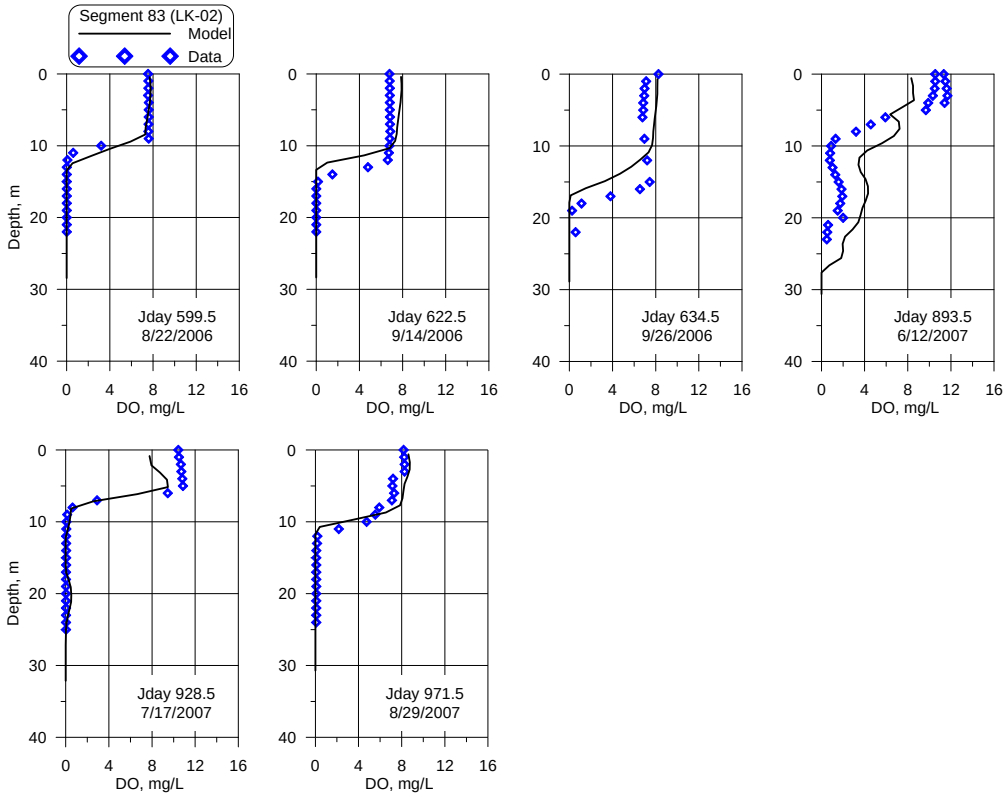

Figure 229. Dissolved oxygen profiles segment 83 Part 4.

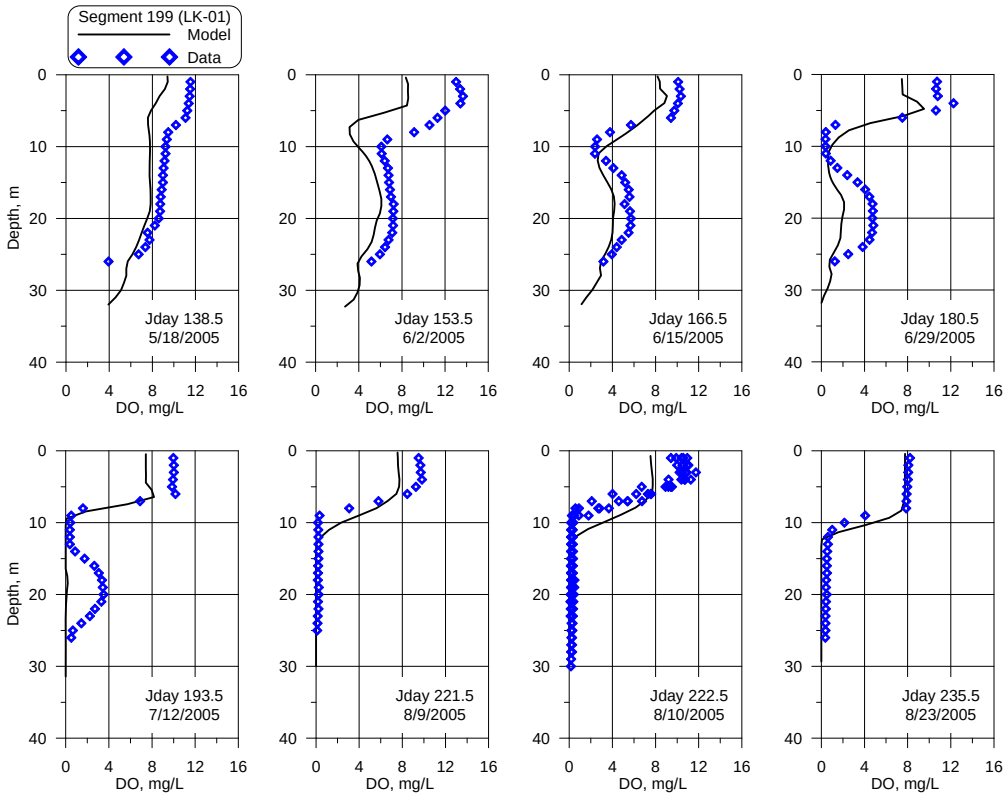

Figure 230. Dissolved oxygen profiles segment 199 Part 1.

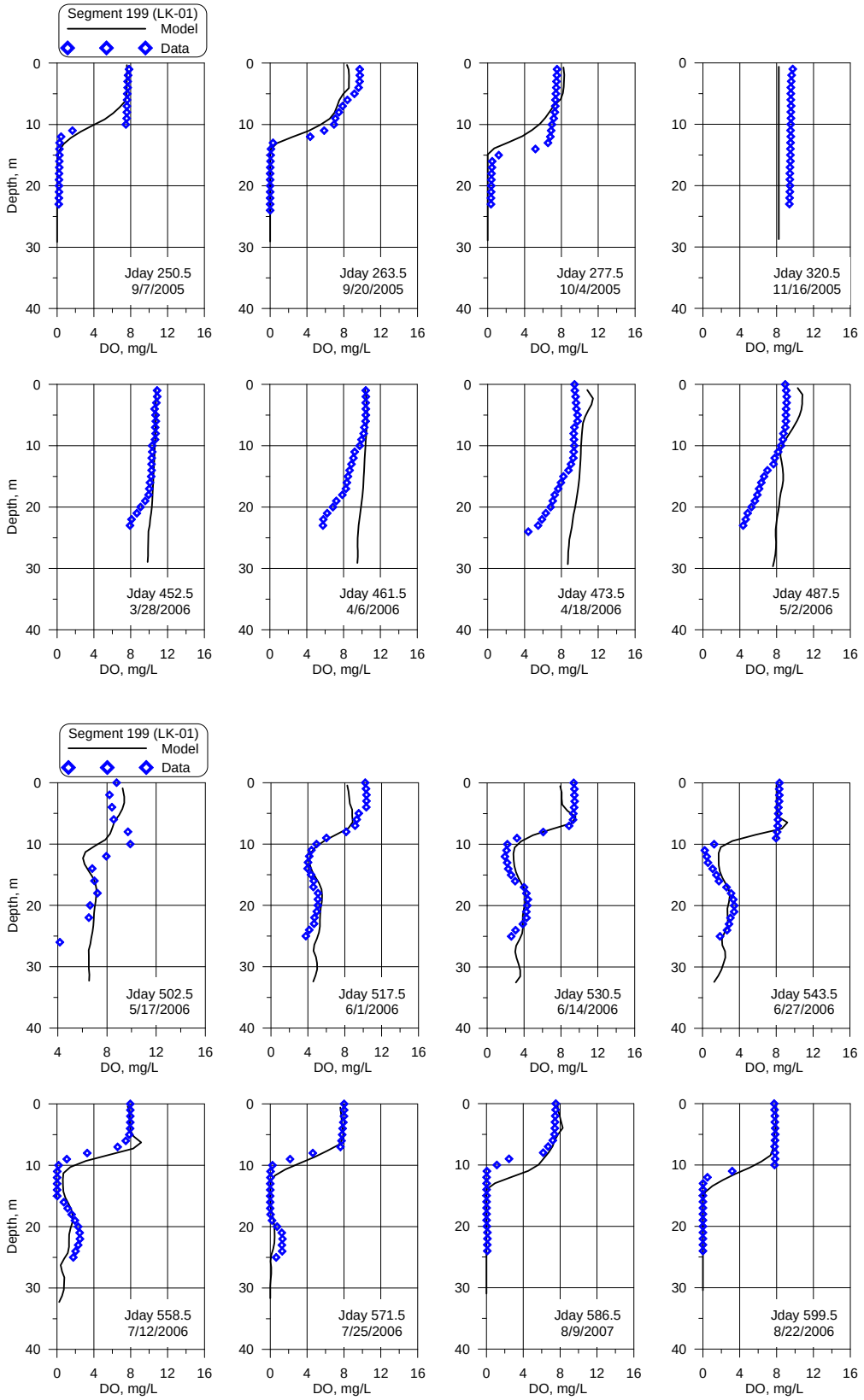

Figure 231. Dissolved oxygen profiles segment 199 Parts 2 & 3.

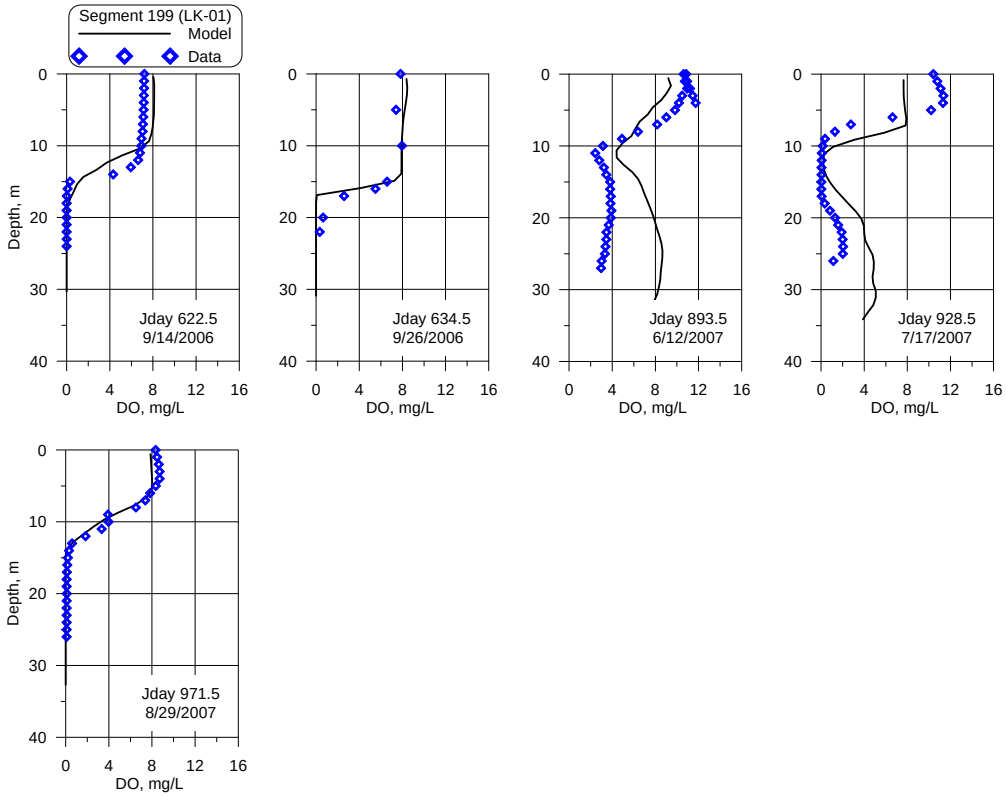

Figure 232. Dissolved oxygen profiles segment 199 Part 4.

Appendix F: Chlorophyll a Profile Comparisons

Profiles of chlorophyll a field data compared to profiles of model predictions are shown in Figure 233, Figure 234, Figure 235, Figure 236, Figure 237, Figure 238, Figure 239, Figure 240, Figure 241, and Figure 242 for model segments 35 [LK04], 46, 59 [LK03],67, 83 [LK02], 89, 199 [LK01], and 108/109 [LK05], respectively. The solid line represents model predictions and the discrete points represent field measurements.

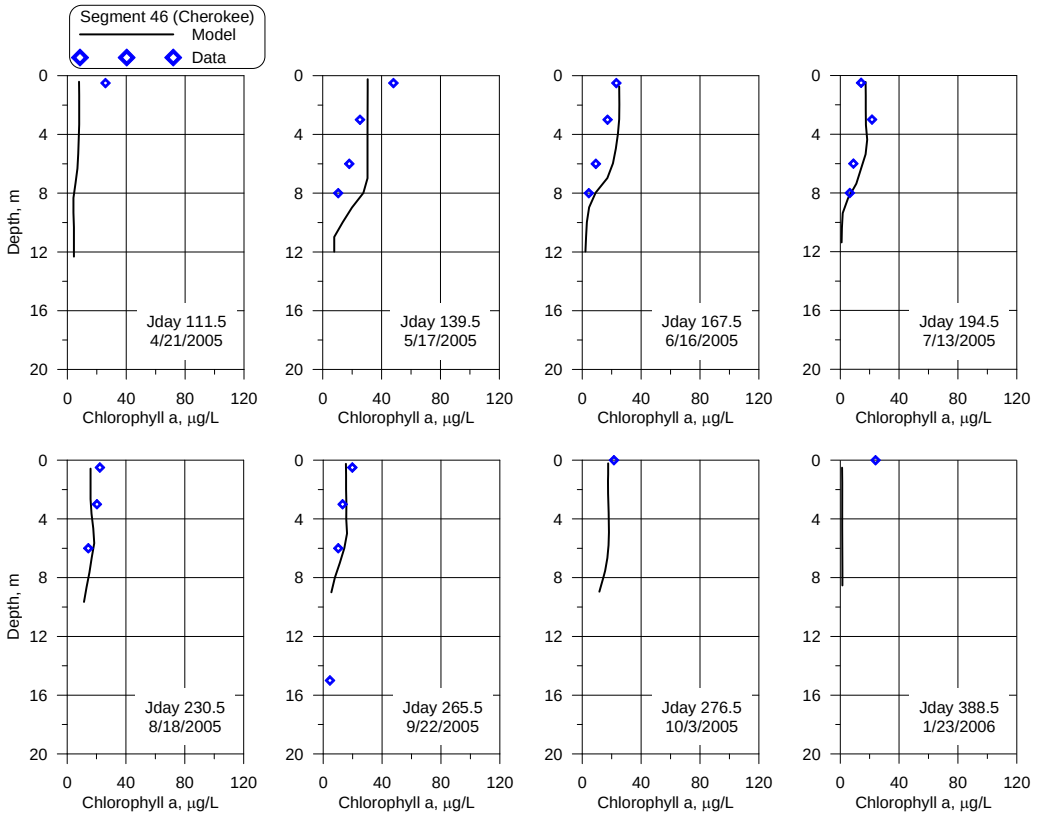

Figure 233. Chlorophyll a model vs. data profile – segment 46 during calibration period.

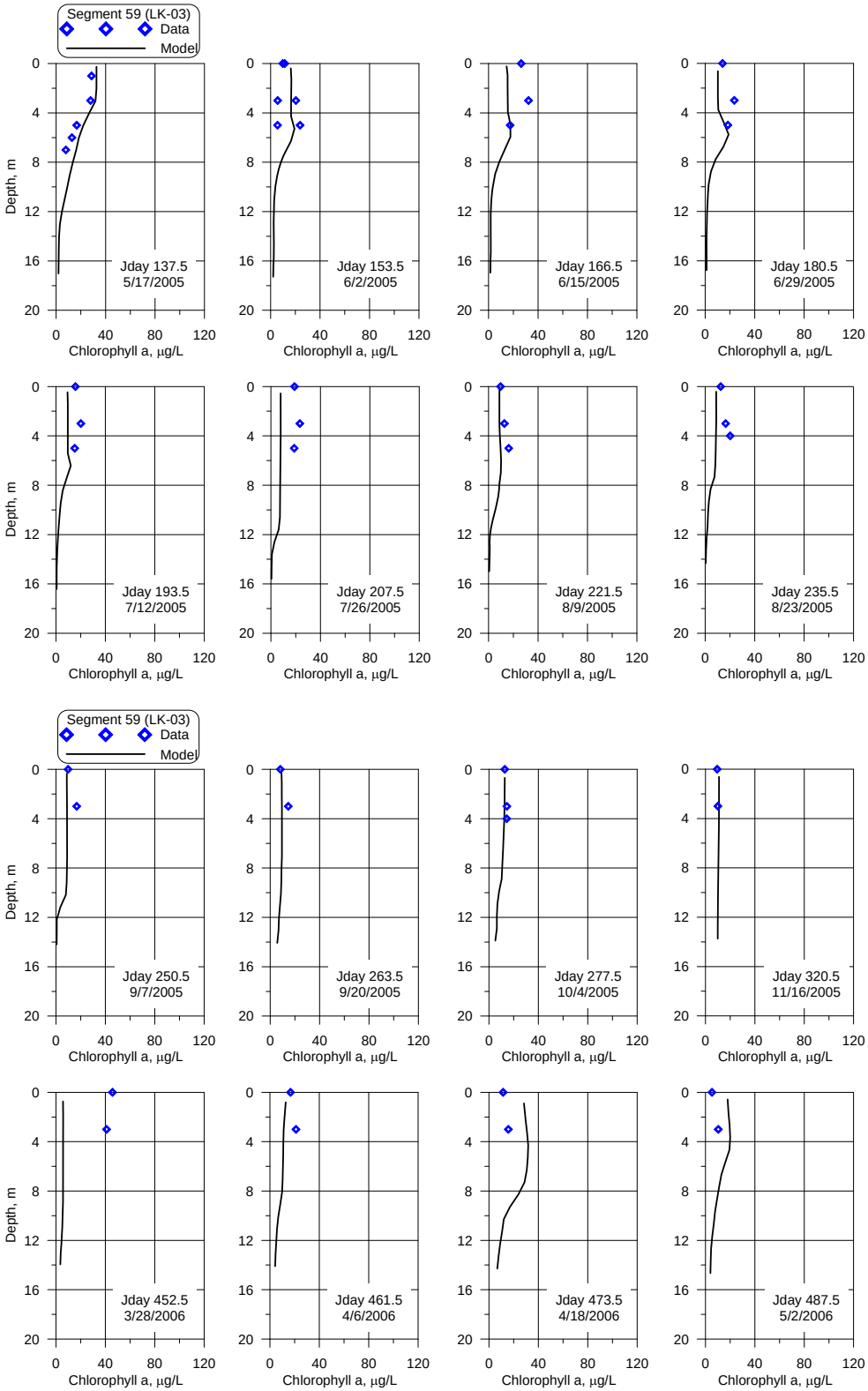

Figure 234. Chlorophyll a model vs. data profile – segment 59 Parts 1 & 2 during calibration period.

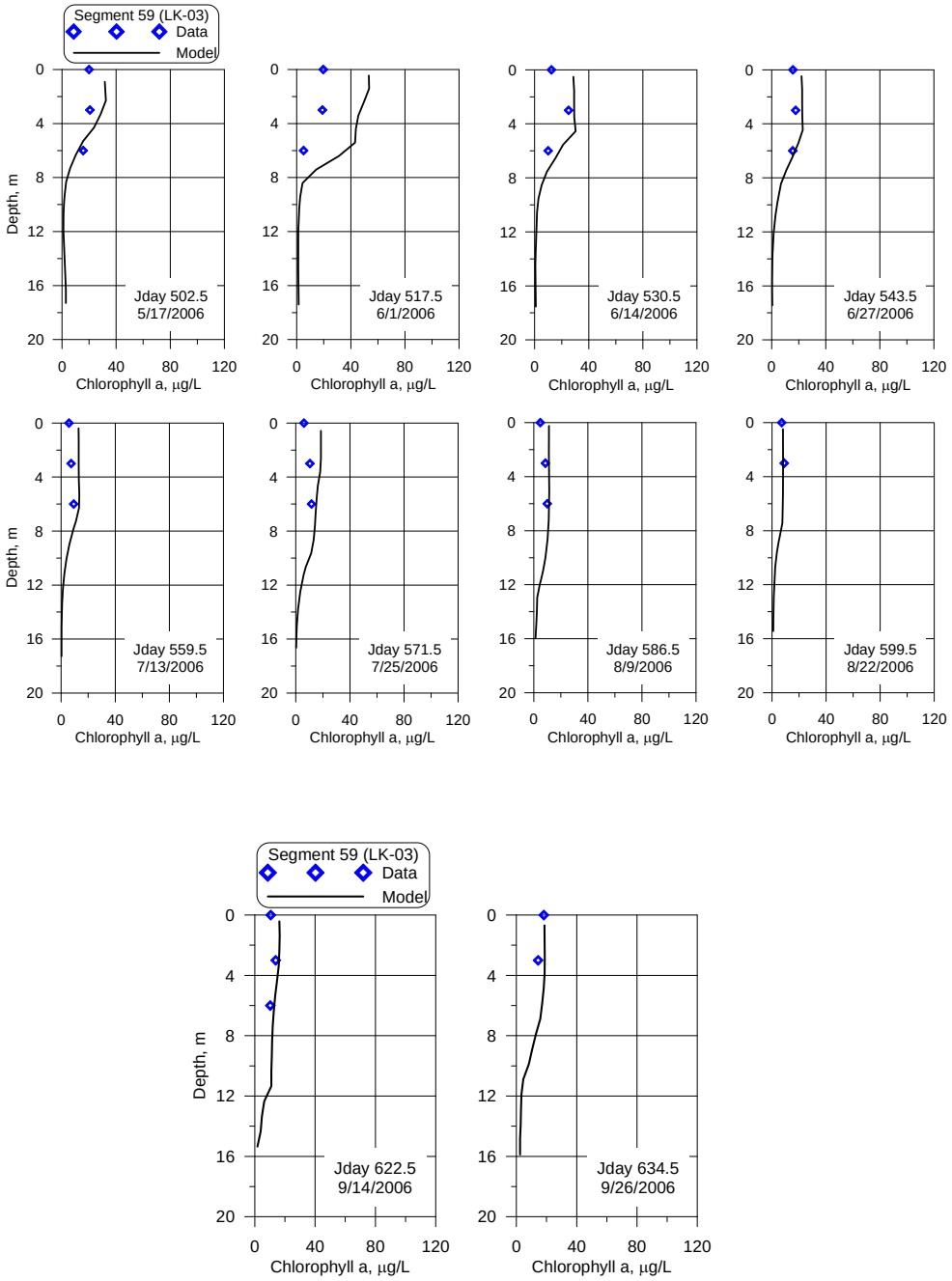

Figure 235. Chlorophyll a model vs. data profile – segment 59 Parts 3 & 4 during calibration period.

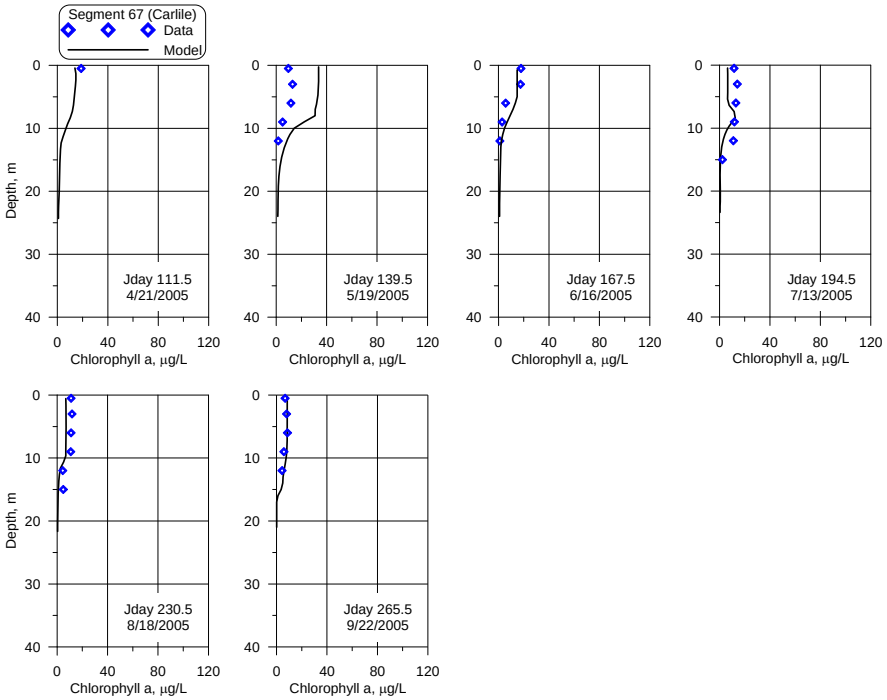

Figure 236. Chlorophyll a model vs. data profile – segment 67 during calibration period.

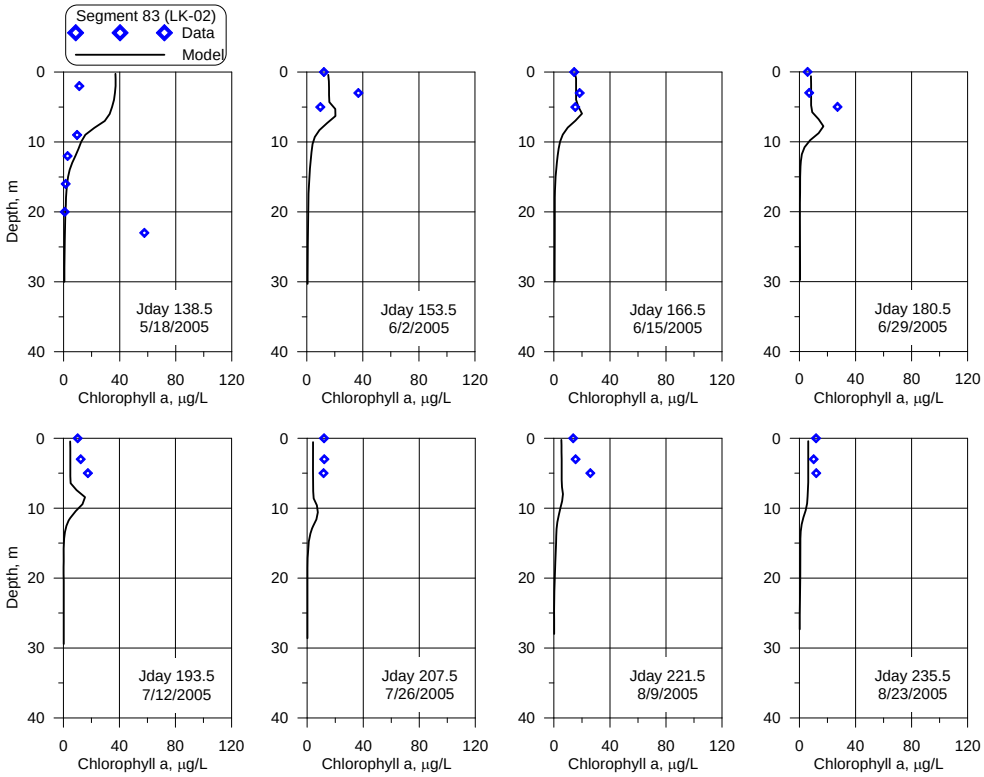

Figure 237. Chlorophyll a model vs. data profile – segment 83, Part 1 during calibration period.

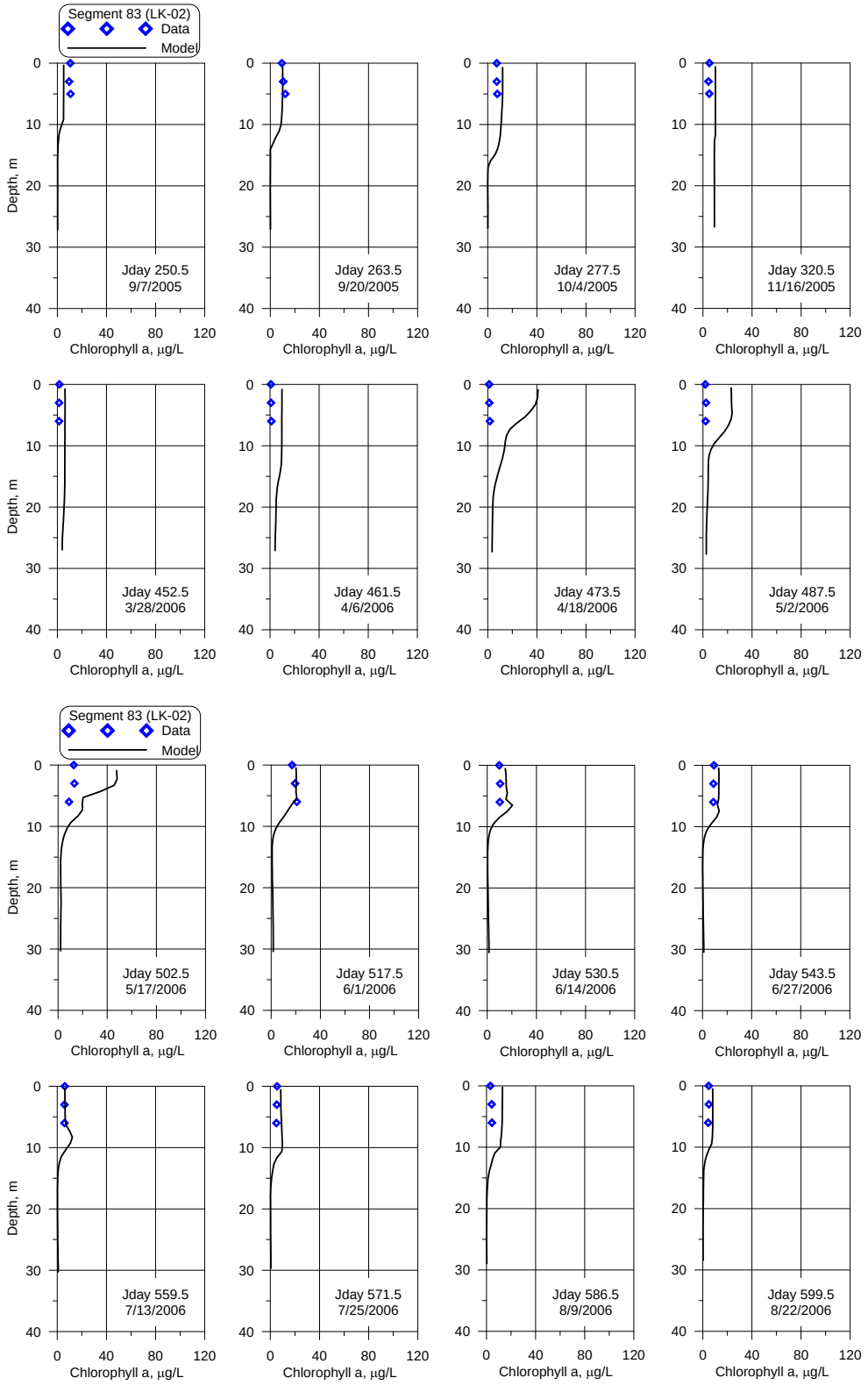

Figure 238. Chlorophyll a model vs. data profile – segment 83 Parts 2 & 3 during calibration period.

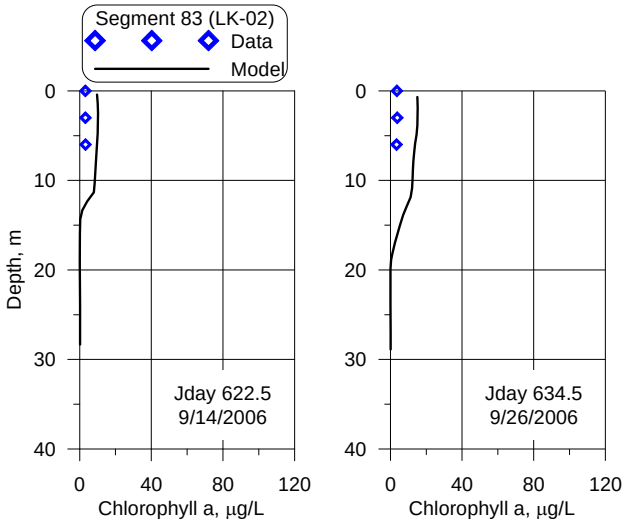

Figure 239. Chlorophyll a model vs. data profile – segment 83 Part 4 during calibration period.

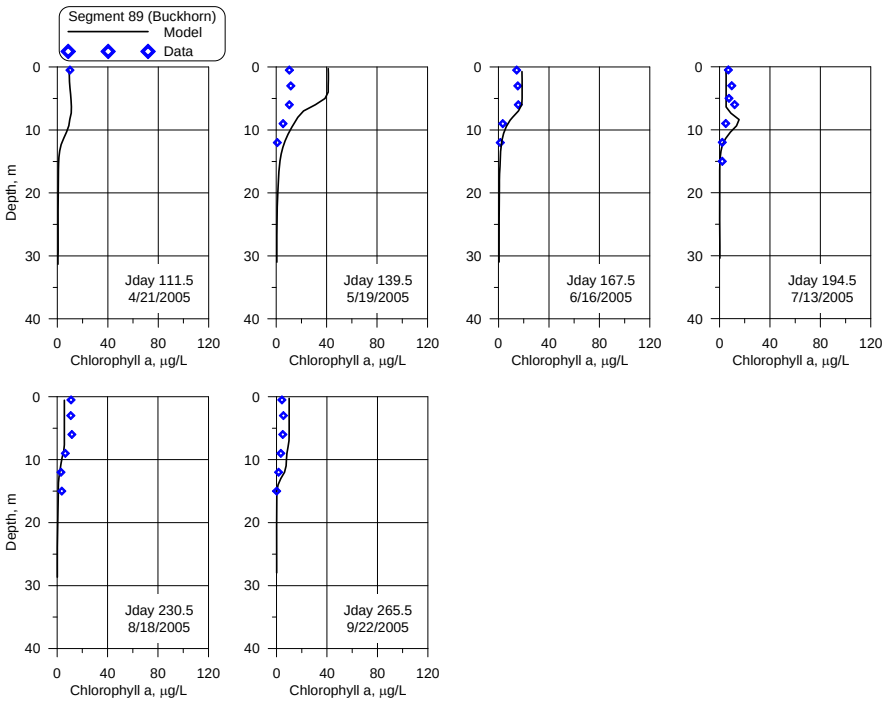

Figure 240. Chlorophyll a model vs. data profile – segment 89 during calibration period.

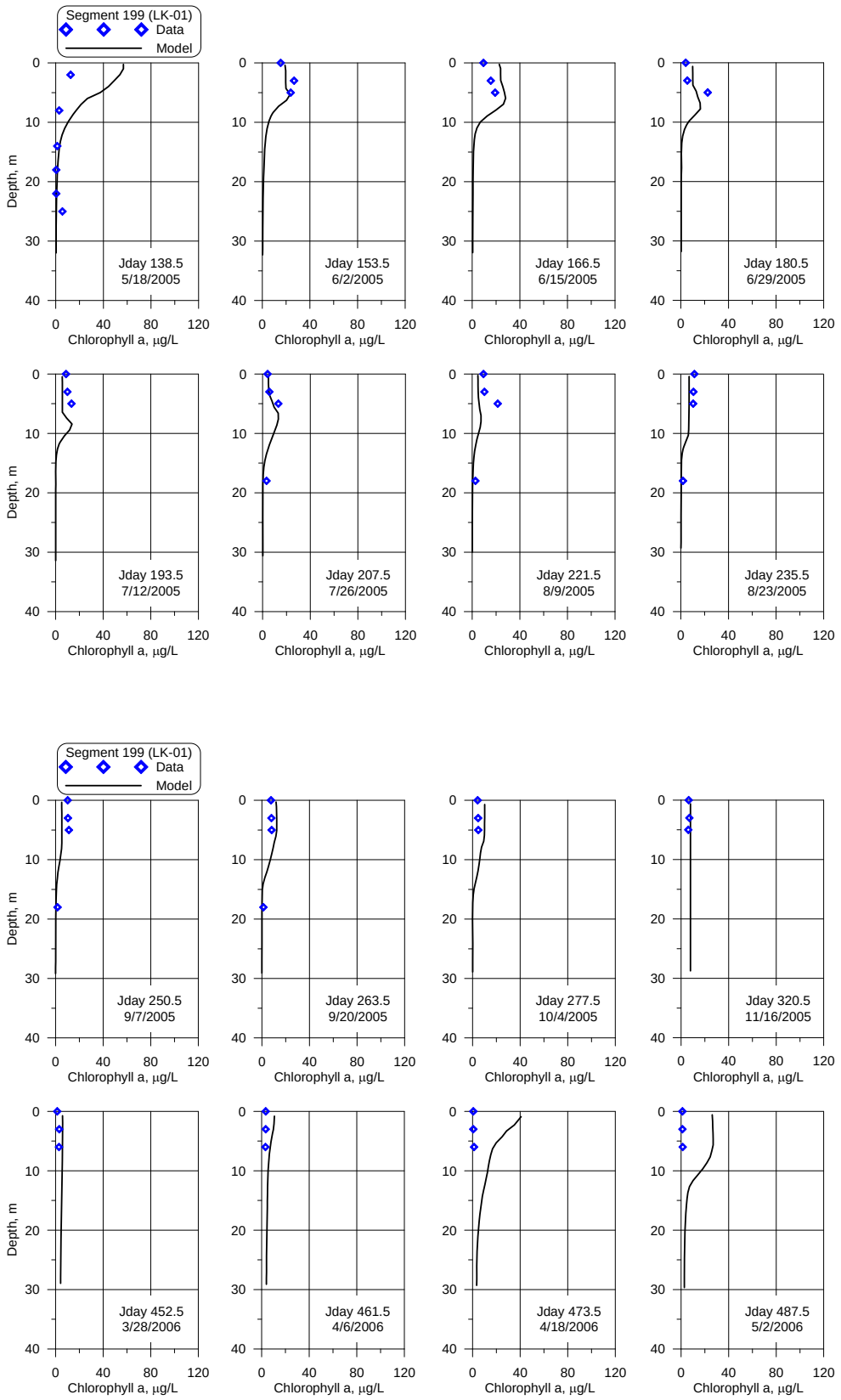

Figure 241. Chlorophyll a model vs. data profile – segment 199 Parts 1 & 2 during calibration period.

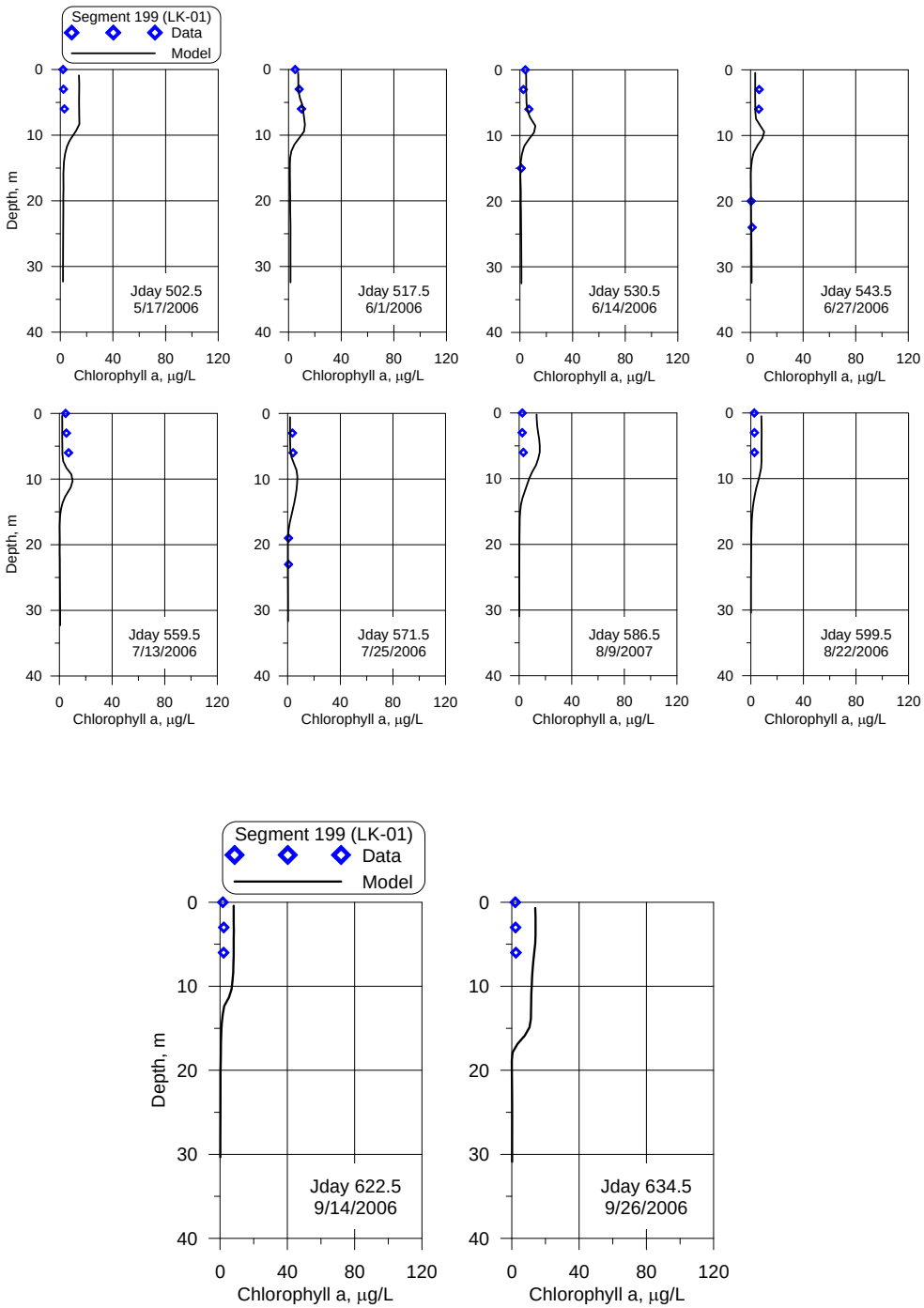

Figure 242. Chlorophyll a model vs. data profile – segment 199 Parts 3 & 4 during calibration period.

Appendix G: Appropriateness of Model Calibration

What criteria are used to judge the adequacy of water quality models? There are no generally accepted global criteria on how good is good enough for model calibration. Typical criteria that our research group uses are the following for average absolute mean error over all model stations:

- Water level within 10 cm
- Temperature within 1°C
- Dissolved oxygen in eutrophic system less than 2 mg/l
- Nutrient and algae concentrations within 10-20% of the range of the field data

These are criteria that we have developed over the years in doing water quality modeling studies. Models at times will exceed these calibration criteria, but on average the model should be able to meet these if the boundary condition data are adequate. Often reported model error is a function of the range in the field data. For example, when measured chlorophyll a values range 2-5 µg/l, an error of 1 µg/l seems low, but can be from 20-50% of the measured value. In order to provide guidance in how well other models have been able to predict field data, Table 35 shows typical calibration errors for studies of lakes, reservoirs and river systems.

Table 35. Typical model-data calibration errors.

Water quality variable	Calibration absolute mean error	Reference	Waterbody	Comments
Ammonia	0.02-0.04 mg/l	Berger et al. (2003)	Long Lake Spokane River	
Ammonia	0.02 mg/l	Sullivan and Rounds (2005)	Hagg Lake	
Ammonia-N	7-39 µg/l	Berger et al. (2001)	Willamette River	
Chlorophyll a	24.1% of measurement value with a standard deviation of 19% (most values were between 2 and 5 ug/l)	Schladow and Hamilton (1997)	Prospect Reservoir	
Chlorophyll a	0.6 µg/l (in terms of fraction of measurement: 0.3-0.6)	Annear et al. (2006)	Pend Oreille	Range of chlorophyll a values was from 1-2 µg/l
Chlorophyll a	2.2-25 µg/l	Berger et al. (2001)	Willamette River	

Water quality variable	Calibration absolute mean error	Reference	Waterbody	Comments
Chlorophyll a	2.4 µg/l	Sullivan and Rounds (2005)	Hagg Lake	Algae concentrations were typically less than 5 µg/l
Dissolved oxygen	9.9% of measurement value with a standard deviation of 13.9%	Schladow and Hamilton (1997)	Prospect Reservoir	
Dissolved oxygen	0.9 mg/l	Wells et al. (2000)	Cooper Creek Reservoir Sutherlin	Limited profiles
Dissolved oxygen	1.6-2.1 mg/l	Berger et al. (2003)	Long Lake Spokane River	
Dissolved oxygen	0.6-1.1 mg/l	Berger and Wells (2005)	Lake Whatcom	
Dissolved oxygen	0.2 mg/l	Annear et al. (2006)	Pend Oreille	
Dissolved oxygen	0.2-2.2 mg/l	Berger et al. (2001)	Willamette River	
Dissolved oxygen	0.4-0.73 mg/l	Sullivan and Rounds (2005)	Hagg Lake	
Dissolved Oxygen	0.53 -1.46 mg/l	Hanna and Campbell (2000)	Klamath River	R^2=0.468 - 0.342
Dissolved PO4-P	5-12 µg/l	Berger et al. (2001)	Willamette River	
Nitrate+Nitrite	0.1-0.52 mg/l	Berger et al. (2003)	Long Lake Spokane River	
Nitrate+Nitrite	68-234 µg/l	Berger et al. (2001)	Willamette River	
Temperature	Less than 1°C	Cole and Wells (2006)	70 different reservoirs around the world	

Water quality variable	Calibration absolute mean error	Reference	Waterbody	Comments
Temperature	5.2% of measurement value with a standard deviation of 3.6%, or about 1°C at 20°c	Schladow and Hamilton (1997)	Prospect Reservoir	Defined as (measured – simulated)/measured value)
Temperature	0.9 ^{o}C	Wells et al. (2000)	Cooper Creek Reservoir Sutherlin	
Temperature	0.7-1.01^{o}C	Berger et al. (2003)	Long Lake Spokane River	
Temperature	0.44-0.67^{o}C	Berger and Wells (2005)	Lake Whatcom	
Temperature	0.4^{o}C (range from 0.2-0.6^{o}C)	Annear et al. (2006)	Pend Oreille	
Temperature	0.4^{o}C – 2.1 ^{o}C (typical less than 0.75^{o}C)	Berger et al. (2001)	Willamette River	
Temperature	0.68^{o}C	Sullivan and Rounds (2005)	Hagg Lake	
Temperature	0.5 - 2.29 ^{o}C	Hanna and Campbell (2000)	Klamath River	R^2=0.972 - 0.853
Total P	7.8-25 µg/l	Berger et al. (2001)	Willamette River	
Total P	6-12 µg/l	Sullivan and Rounds (2005)	Hagg Lake	